

Electronic Thesis and Dissertation Repository

---

11-30-2012 12:00 AM

## Protection and Control of Active Distribution Networks and Microgrids

Mohammad Amin Zamani  
*The University of Western Ontario*

Supervisor

Dr. Amirnaser Yazdani  
*The University of Western Ontario* Joint Supervisor

Dr. Tarlochan Singh Sidhu  
*The University of Western Ontario*

Graduate Program in Electrical and Computer Engineering  
A thesis submitted in partial fulfillment of the requirements for the degree in Doctor of Philosophy  
© Mohammad Amin Zamani 2012

Follow this and additional works at: <https://ir.lib.uwo.ca/etd>



Part of the [Power and Energy Commons](#)

---

### Recommended Citation

Zamani, Mohammad Amin, "Protection and Control of Active Distribution Networks and Microgrids" (2012). *Electronic Thesis and Dissertation Repository*. 1046.  
<https://ir.lib.uwo.ca/etd/1046>

This Dissertation/Thesis is brought to you for free and open access by Scholarship@Western. It has been accepted for inclusion in Electronic Thesis and Dissertation Repository by an authorized administrator of Scholarship@Western. For more information, please contact [wlsadmin@uwo.ca](mailto:wlsadmin@uwo.ca).

PROTECTION AND CONTROL OF ACTIVE DISTRIBUTION  
NETWORKS AND MICROGRIDS

(Spine title: Protection and Control of Microgrids)

(Thesis format: Monograph)

by

Mohammad Amin Zamani

Graduate Program in Electrical and Computer Engineering

A thesis submitted in partial fulfillment  
of the requirements for the degree of  
Doctor of Philosophy

The School of Graduate and Postdoctoral Studies  
The University of Western Ontario  
London, Ontario, Canada

© Mohammad Amin Zamani 2012

THE UNIVERSITY OF WESTERN ONTARIO  
School of Graduate and Postdoctoral Studies  
**CERTIFICATE OF EXAMINATION**

Examiners:

Supervisors:

.....  
Dr. Amirnaser Yazdani

.....  
Dr. Tarlochan S. Sidhu

Supervisory Committee:

.....

Dr. Peter W. Lehn

.....

Dr. Ken McIsaac

.....

Dr. Mohammad R. Dadash Zadeh

.....

Dr. George K. Knopf

The thesis by

**Mohammad Amin Zamani**

entitled:

**Protection and Control of Active Distribution Networks and Microgrids**

is accepted in partial fulfillment of the  
requirements for the degree of  
Doctor of Philosophy

.....  
Date

.....  
Chair of the Thesis Examination Board

# Abstract

This thesis is mainly focused on (i) modeling and control of Electronically Coupled Distributed Energy Resources (EC-DERs) under severe network imbalances and transient incidents, and (ii) protection of active distribution networks and microgrids against different types of faults. In the first part, an enhanced control strategy is proposed to improve the performance of EC-DERs under faults and transient disturbances, in a multi-unit microgrid setting. With the use of proposed control strategy, the host microgrid can ride through network faults, irrespective of whether they take place within the microgrid jurisdiction or impact the upstream grid, and quickly reclaim its pre-fault operating conditions to improve post-fault recovery. Further, the proposed control scheme enables the host microgrid to retain its power quality for the duration of the faults, in both modes of operation, which is a desirable property for detection of certain classes of faults, as well as for sensitive loads.

In the second part of the thesis, appropriate strategies are proposed for protection of low- and medium-voltage microgrids in the islanded mode as well as the grid-connected mode of operation. The proposed protection strategies aim to detect and isolate the faults that impact the microgrid, in a selective manner. The proposed strategies can be implemented through programmable logic tools which are commercially available; hence, the structures of new relays that enable the proposed protection strategies are also discussed in the thesis. In addition, the thesis investigates the operation of an existing distribution network as a microgrid. Thus, practical control and protection strategies that enable off-grid operation of the distribution network (considering the system constraints) are discussed. The effectiveness of the proposed control and protection strategies are demonstrated through time-domain simulation studies conducted in the PSCAD/EMTDC software environment.

**Keywords:** Distributed Energy Resources, Fault, Grid-Connected Mode, Islanded Mode, Microgrid, Microprocessor-Based Relays, Power Electronics, Power System Protection, Voltage-Sourced Converter, Voltage and Frequency Regulation.

To my parents and my wife, who have supported me each step of the way.

# Acknowledgement

I would like to express my sincere gratitude to Dr. Amirnaser Yazdani and Dr. Tarlochan Singh Sidhu for their excellent supervision, bright ideas, and continuous encouragement throughout the course of this research. It has been a great privilege to pursue my higher education under their supervision.

Also, the financial support provided by the University of Western Ontario and Dr. T. S. Sidhu is gratefully acknowledged.

# Contents

<b>Certificate of Examination</b>	<b>ii</b>
<b>Abstract</b>	<b>iii</b>
<b>Dedication</b>	<b>iv</b>
<b>Acknowledgements</b>	<b>v</b>
<b>List of Figures</b>	<b>xi</b>
<b>List of Tables</b>	<b>xvi</b>
<b>List of Appendices</b>	<b>xviii</b>
<b>List of Abbreviations</b>	<b>xix</b>
<b>List of Nomenclature</b>	<b>xxi</b>
<b>1 Introduction</b>	<b>1</b>
1.1 Statement of Problem and Research Objectives . . . . .	1
1.2 Microgrids . . . . .	2
1.2.1 Motivations and Advantages . . . . .	2
1.2.2 Architecture . . . . .	4
1.3 Control of Microgrids . . . . .	6
1.3.1 Supervisory Control . . . . .	6
1) Centralized Control . . . . .	7
2) Decentralized Control . . . . .	8
1.3.2 Control of DERs . . . . .	10
1) Grid-Connected-Mode Control . . . . .	10
2) Islanded-Mode Control . . . . .	14

1.4	Protection of Microgrids . . . . .	15
1.4.1	Traditional Protection Coordination . . . . .	15
1.4.2	Grid-Connected-Mode Protection . . . . .	17
1.4.3	Islanded-Mode Protection . . . . .	18
1.5	Thesis Contributions . . . . .	18
1.6	Thesis Outline and Related Literature Review . . . . .	20
1.7	Summary and Conclusion . . . . .	23
<b>2</b>	<b>Control of EC-DETs</b>	<b>24</b>
2.1	Introduction . . . . .	24
2.2	Network Faults and Their Implications on the Control of EC-DETs . . . . .	25
2.3	Structure of the EC-DEt . . . . .	26
2.4	Basic Control Strategy for EC-DEt . . . . .	26
2.4.1	Current-Control Scheme of the VSC . . . . .	26
2.4.2	Voltage Magnitude Regulation Scheme . . . . .	29
2.4.3	Phase-Locked Loop (PLL) . . . . .	30
2.4.4	Frequency Regulation Scheme . . . . .	32
2.5	Enhanced Control Strategy for EC-DETs . . . . .	33
2.5.1	Modifications to the Voltage Magnitude Regulation Scheme . . . . .	33
2.5.2	Modifications to the Phased-Locked Loop . . . . .	34
2.5.3	Proposed Phase-Angle Restoration Scheme . . . . .	36
2.5.4	Network-Wide and Local Synchronization Processes . . . . .	37
2.6	Generic Model of Single-Phase EC-DETs . . . . .	39
2.7	Test Microgrid and Study Cases . . . . .	40
2.7.1	Grid-Connected Mode of Operation . . . . .	42
2.7.2	Islanded Mode of Operation . . . . .	46
2.7.3	Response to Operation Mode Switching Incidents . . . . .	49
2.8	Summary and Conclusion . . . . .	51
<b>3</b>	<b>Protection of a Typical Distribution Network Embedding DEts</b>	<b>52</b>
3.1	Introduction . . . . .	52
3.2	Impact of DEts on Traditional Coordination and the Proposed Solution . . . . .	53
3.3	Design Example . . . . .	54
3.3.1	Distribution Network Structure . . . . .	54
3.3.2	Coordination of Protection . . . . .	57



3.3.3	The Use of Directional Elements . . . . .	59
3.3.4	Impact of a new DER on the Protection Coordination . . . . .	61
3.3.5	Retrieval of protection Coordination after System Alterations . . . . .	64
3.4	Simulation Results . . . . .	65
3.5	Summary and Conclusion . . . . .	69
<b>4</b>	<b>Protection of Low-Voltage Microgrids</b>	<b>70</b>
4.1	Introduction . . . . .	70
4.2	Characteristics of Low-Voltage Distribution Networks and Assumptions Made . . . . .	71
4.2.1	Structure . . . . .	71
4.2.2	Conventional Protection . . . . .	71
4.2.3	Grounding Practices . . . . .	72
4.2.4	DER Interface Mechanisms . . . . .	73
4.2.5	DER Control Strategies . . . . .	73
4.3	Proposed Protection for the Islanded Mode of Operation . . . . .	73
4.3.1	Household Consumer Protection . . . . .	73
4.3.2	Network Protection . . . . .	74
4.3.3	Fault Detection . . . . .	75
4.3.4	Protection Coordination . . . . .	76
4.3.5	Protection Scheme Extension . . . . .	79
4.4	Proposed Protection for the Grid-Connected Mode of Operation . . . . .	81
4.4.1	External Faults . . . . .	82
4.4.2	Neutral Voltage Displacement (NVD) Protection . . . . .	82
4.5	Proposed Microgrid Protection Relay (MPR) . . . . .	83
4.5.1	Special Case . . . . .	85
4.6	Simulation Results . . . . .	85
4.6.1	Study Microgrid . . . . .	86
4.6.2	Study Cases . . . . .	87
1)	Islanded Mode of Operation . . . . .	87
2)	Grid-Connected Mode of Operation . . . . .	88
4.7	Summary and Conclusion . . . . .	88
<b>5</b>	<b>Protection of Medium-Voltage Microgrids</b>	<b>93</b>
5.1	Introduction . . . . .	93

5.2	Typical Medium-Voltage Distribution Networks . . . . .	94
5.3	Medium-Voltage Microgrids . . . . .	94
5.4	Structure of the Relay Enabling the Proposed Protection Strategy . . . .	95
5.4.1	Strategy for High-Impedance Fault Detection . . . . .	98
5.4.2	Directional Decision Making . . . . .	101
5.5	Proposed Protection Strategy . . . . .	101
5.5.1	Main Protection . . . . .	102
5.5.2	Backup Protection . . . . .	106
5.6	Design Example . . . . .	107
5.7	Study Cases and Simulation Results . . . . .	111
5.7.1	Islanded Mode of Operation . . . . .	111
5.7.2	Grid-Connected Mode of Operation . . . . .	112
5.8	Summary and Conclusion . . . . .	112
<b>6</b>	<b>Operation of an Existing Distribution Network as a Microgrid</b>	<b>117</b>
6.1	Introduction . . . . .	117
6.2	Study System . . . . .	118
6.3	Microgrid Formation due to Islanding . . . . .	118
6.4	Operation as a Microgrid: Control . . . . .	120
6.4.1	Scenario 1: Conventional DER(s) . . . . .	120
6.4.2	Scenario 2: Electronically Coupled DER(s) . . . . .	121
	1) Control of the EC-DER (Wind-Power Units) . . . . .	122
	2) Control of the BESS . . . . .	124
	3) Pitch-Angle Control . . . . .	126
6.5	Operation as a Microgrid: Protection . . . . .	128
6.5.1	Grid-Connected Mode of Operation . . . . .	129
6.5.2	Islanded Mode of Operation . . . . .	130
6.6	Simulation Results . . . . .	133
6.6.1	Control Schemes . . . . .	134
6.6.2	Protection Schemes . . . . .	140
6.7	Summary and Conclusion . . . . .	143
<b>7</b>	<b>Summary, Conclusions, and FutureWork</b>	<b>146</b>
7.1	Summary . . . . .	146
7.2	Conclusion . . . . .	147

7.3	Future Works . . . . .	149
<b>A</b>	<b>Specifications of the EC-DERs of Chapter 2</b>	<b>150</b>
A.1	EC-DER Controllers . . . . .	150
A.2	EC-DER Parameters . . . . .	151
<b>B</b>	<b>Modeling of Protective Devices</b>	<b>152</b>
B.1	Analytical Equations of Protective Devices . . . . .	152
B.1.1	Fuse . . . . .	152
B.1.2	Recloser and Relay . . . . .	153
B.1.3	Directional Characteristic . . . . .	153
<b>C</b>	<b>Relay Settings and Device Numbers for Chapter 4</b>	<b>155</b>
C.1	Relay Settings . . . . .	155
C.2	Device/Function Numbers . . . . .	155
<b>D</b>	<b>Load and Relay Parameters for Chapter 5</b>	<b>158</b>
D.1	Network Loads . . . . .	158
D.2	Relay Signals . . . . .	158
<b>E</b>	<b>DER Parameters for Chapter 6</b>	<b>160</b>
E.1	Parameters of the DFIG and Wind Turbine . . . . .	160
E.2	Parameters of the Synchronous Machine . . . . .	160
	<b>Bibliography</b>	<b>162</b>
	<b>Curriculum Vitae</b>	<b>173</b>

# List of Figures

1.1	Single-line schematic diagram of a typical microgrid. . . . .	5
1.2	A schematic illustrating centralized control of a typical microgrid. . . .	8
1.3	(a) Real power versus frequency ( $P-\omega$ ) droop characteristic and (b) reactive power versus voltage ( $Q-V$ ) droop characteristic. . . . .	10
1.4	Voltage-mode control of the real- and reactive-power outputs of a grid-connected EC-DER. . . . .	12
1.5	Current-mode control of the real- and reactive-power outputs of a grid-connected EC-DER. . . . .	13
1.6	Current-mode control of the real- and reactive-power outputs of a nondispatchable grid-connected EC-DER. . . . .	14
1.7	Typical characteristic curves, their coordination, and the margin remaining after the addition of a DER. . . . .	16
2.1	Schematic diagram of the three-phase EC-DER and its control architecture. . . . .	27
2.2	Block diagram of the current-control scheme of the three-phase EC-DER.	28
2.3	Block diagram of the voltage magnitude regulation scheme of the three-phase EC-DER. . . . .	31
2.4	Block diagrams of the equivalent decoupled loops for regulation of $v_{sd}$ and $v_{sq}$ . . . . .	31
2.5	Schematic diagram of the PLL. . . . .	32
2.6	Block diagram of the frequency regulation loop. . . . .	33
2.7	Block diagram of the enhanced voltage magnitude regulation scheme for the three-phase EC-DER. . . . .	34
2.8	Block diagram of the frequency regulation loop, augmented with the proposed phase-angle restoration loop. . . . .	37

2.9	Block diagram of the scheme for network-wide and local synchronization processes: calculation of the (a) frequency setpoint, (b) voltage magnitude setpoint, and (c) $d$ - and $q$ -axis components of the voltage across the MMS.	38
2.10	Generic model of single-phase EC-DERs.	40
2.11	Single-line schematic diagram of the study low-voltage microgrid.	41
2.12	Waveforms of Bus1 voltage under a transient grid fault at point F1; (a) basic control and (b) enhanced control.	43
2.13	Real-power output waveforms of the three-phase EC-DERs under a transient grid fault at point F1; (a) basic control and (b) enhanced control.	43
2.14	Waveforms of the (a) converter output current and (b) DER output current under a transient grid fault at point F1 (EC-DER1).	44
2.15	Real-power output waveforms of the three-phase EC-DERs during and subsequent to successful reclosure of the 11-kV line at $t=2.5$ s; (a) basic control and (b) enhanced control.	45
2.16	Waveforms of the magnitude of Bus1 voltage in response to successful reclosure of the 11-kV line at $t=2.5$ s; (a) basic control and (b) enhanced control.	45
2.17	Waveforms of the voltage drop across MMS during the dead time of the reclosing process; (a) basic control and (b) enhanced control.	46
2.18	Real-power output waveforms of the three-phase EC-DERs under a temporary fault at point F2 of the islanded microgrid; (a) basic control and (b) enhanced control.	47
2.19	Waveforms of the phase-angle error for the three-phase EC-DERs under a temporary fault at point F2 of the islanded microgrid; (a) basic control and (b) enhanced control.	47
2.20	Waveforms of Bus1 voltage under a temporary fault at point F2 of the islanded microgrid; (a) basic control and (b) enhanced control.	48
2.21	Real-power output waveforms of the three-phase EC-DERs under a permanent fault at point F3 of the islanded microgrid; (a) basic control and (b) enhanced control.	48
2.22	Waveforms of the substation bus voltage under a permanent fault at point F3 of the islanded microgrid; (a) basic control and (b) enhanced control.	49

2.23	Real-power output waveforms of the three-phase EC-DETs under a permanent grid fault at point F1 and successive reclosing; (a) basic control and (b) enhanced control. . . . .	50
2.24	Waveform of the voltage across MMS (phase a) during the synchronization process. . . . .	50
2.25	Real- and reactive-power output waveforms of the three-phase DETs during the synchronization process. . . . .	51
3.1	Flowchart of the proposed coordination method. . . . .	55
3.2	Single-line schematic diagram of the studied test system. . . . .	56
3.3	Equivalent circuit for ( $I_R/I_F$ ) calculation. . . . .	58
3.4	Coordination of protective devices of Feeder 1 for phase unit. . . . .	59
3.5	Coordination of protective devices of Feeder 1 for ground unit. . . . .	59
3.6	Diagrams showing (a) forward and reverse definite times for relays, and (b) logics of implementation. . . . .	60
3.7	Symbolic logic circuit for substation protection. . . . .	61
3.8	Curves characterizing the recloser-fuse grading time as a function of (the inverse of) $Z_{DER2}$ . . . . .	62
3.9	Curves characterizing the fuse-fuse grading time as a function of (the inverse of) $Z_{DER2}$ . . . . .	63
3.10	Coordination of protective devices of Feeder 2 for phase unit. . . . .	64
3.11	Coordination of protective devices of Feeder 2 for ground unit. . . . .	65
3.12	Coordination of devices when DER2 is not in place. . . . .	66
3.13	Tripping times of the recloser and fuse when DER2 is not in place. . . . .	66
3.14	Coordination loss when DER2 is added to the test system. . . . .	67
3.15	Tripping times of the recloser and fuse when DER2 is in place. . . . .	67
3.16	Retrieval of coordination after the addition of DER2. . . . .	68
3.17	Operation of the recloser in the slow mode when the fuse fails to operate. . . . .	68
4.1	The TN-C-S grounding configuration in an LV network. . . . .	72
4.2	Diagram showing the coordination of MPRs in the islanded mode of operation. . . . .	77
4.3	Symbolic logic circuit for substation bus protection. . . . .	79
4.4	Extending the protection scheme for SMs including four MPRs. . . . .	80

4.5	Traditional coordination of fuses and relays in a typical distribution network. . . . .	81
4.6	Coordination of the IMPR and MPRs for an external (grid) fault. . . .	83
4.7	Simplified schematic diagram of the proposed MPR (or IMPR). . . . .	84
4.8	Single-line diagram of the study LV microgrid. . . . .	86
5.1	Single-line diagram of a typical medium-voltage distribution network and its conventional protection devices. . . . .	95
5.2	The network of Fig. 5.1 that is equipped with DERs and can be operated as an MV microgrid. . . . .	96
5.3	Simplified schematic diagram of an MPR/CMPR. . . . .	97
5.4	Concept of a Delta-Filter for a time-varying waveform: (a) continuous-time form, and (b) discrete-time form. . . . .	99
5.5	Flowchart of the proposed protection scheme. . . . .	104
5.6	Schematic Diagram of the WLAN communication protocol, augmented with wireless Ethernet Bridges, for the proposed protection strategy implemented in an example microgrid. . . . .	106
5.7	Single-line diagram of the study microgrid with the embedded MPRs and CMPRs. . . . .	108
5.8	Grading scheme of the study microgrid relays for the backup protection strategy. . . . .	110
6.1	Single-line schematic diagram of the study system. . . . .	119
6.2	Schematic diagram of a DFIG wind-power unit. . . . .	123
6.3	Single-line schematic diagram of the study system with the wind farm and the BESS. . . . .	125
6.4	Droop-based power management strategy; (a) real power compensator with synchronization function and (b) reactive power compensator with synchronization function. . . . .	127
6.5	(a) Conventional pitch-angle control scheme and (b) proposed pitch-angle control scheme, for the wind-power units. . . . .	128
6.6	Simplified schematic diagram of the MPR employed in this chapter. . .	133
6.7	Case 1: operation in the grid-connected mode; (a) with synchronous DER and (b) with EC-DER. . . . .	134

6.8	Case 2: operation in the islanded mode; (a) with synchronous DER and (b) with EC-DER. . . . .	135
6.9	Case 3: system response to a temporary fault in the islanded mode; (a) with synchronous DER and (b) with EC-DER. . . . .	136
6.10	Case 3: system response to a permanent fault in the islanded mode; (a) with synchronous DER and (b) with EC-DER. . . . .	137
6.11	Case 4: synchronization process; (a) with synchronous DER and (b) with EC-DER. . . . .	138
6.12	Case 5: system response under environmental changes in the islanded mode of operation (Scenario 2 of Section 6.4). . . . .	139
6.13	Case 5: system response when the pitch-angle control takes action in the islanded mode of operation (Scenario 2 of Section 6.4). . . . .	139
6.14	Coordination of the recloser and fuse of the study system in the grid-connected mode; (a) phase element and (b) ground element. . . . .	141
6.15	Diagram showing the coordination of digital relays within the study system. . . . .	142
B.1	Characteristic of the directional element (phase comparison). . . . .	154



# List of Tables

1.1	Classification of Control Strategies for DERs . . . . .	11
3.1	Fault Calculation Results for the Test System . . . . .	58
4.1	Currents Required for Safe Operation of Household Fuses in 5 Cycles (83 ms) from the Fault Inception . . . . .	74
4.2	Operating Times of Primary and Backup Protection for Selected Solid Fault Scenarios in the Islanded Mode of Operation . . . . .	89
4.3	Operating Times of Primary and Backup Protection for Selected High-Impedance Fault Scenarios in the Islanded Mode of Operation . . . . .	90
4.4	Operating Times of Primary and Backup Protection for Selected Solid Fault Scenarios in the Grid-Connected Mode of Operation . . . . .	91
4.5	Operating Times of Primary and Backup Protection for Selected High-Impedance Fault Scenarios in the Grid-Connected Mode of Operation . . . . .	92
5.1	Logics for Detecting and Isolating a Fault within the Study Microgrid . . . . .	109
5.2	Operating Times of Main and Backup Protections for Selected Solid Fault Scenarios in the Islanded Mode of Operation . . . . .	113
5.3	Operating Times of Main and Backup Protections for Selected High-Impedance Fault Scenarios in the Islanded Mode of Operation . . . . .	114
5.4	Operating Times of Main and Backup Protections for Selected Solid Fault Scenarios in the Grid-Connected Mode of Operation . . . . .	115
5.5	Operating Times of Main and Backup Protections for Selected High-Impedance Fault Scenarios in the Grid-Connected Mode of Operation . . . . .	116
6.1	Operating Times of the Main and Backup Protection for Selected Fault Scenarios in the Grid-Connected Mode of Operation (with OCRs) . . . . .	144
6.2	Operating Times of the Main and Backup Protection for Selected Fault Scenarios in the Grid-Connected Mode of Operation (with MPRs) . . . . .	144

6.3	Operating Times of the Main and Backup Protection for Selected Fault Scenarios in the Islanded Mode of Operation (with OCRs) . . . . .	145
6.4	Operating Times of the Main and Backup Protection for Selected Fault Scenarios in the Islanded Mode of Operation (with MPRs) . . . . .	145
A.1	Parameters of the Three-Phase EC-DETs . . . . .	151
B.1	Coefficients of Fuse Characteristic Curves . . . . .	153
C.1	Time Delays for MPRs . . . . .	156
C.2	Time Delays for the IMPR . . . . .	156
C.3	Inverse-Time Overcurrent Relay Parameters for MPRs and the IMPR . .	156
C.4	Three-Phase Protection Module Parameters for MPRs and the IMPR . .	157
C.5	Device/Function Numbers . . . . .	157
D.1	Bus Loads for the Distribution Network of Fig. 5.1. . . . .	159
D.2	Relay Signals . . . . .	159
E.1	Parameters of the Wind Turbine. . . . .	160
E.2	Parameters of the DFIG Unit. . . . .	161
E.3	Parameters of the Synchronous DER. . . . .	161

# List of Appendices

Appendix A Specifications of the EC-DETs of Chapter 2 . . . . .	150
Appendix B Modeling of Protective Devices . . . . .	152
Appendix C Relay Settings and Device Numbers for Chapter 4 . . . . .	155
Appendix D Load and Relay Parameters for Chapter 5 . . . . .	158
Appendix E DER Parameters for Chapter 6 . . . . .	160

## Abbreviations and Symbols

AC	Alternating Current
BESS	Battery Energy Storage System
CB	Circuit Breaker
CHP	Combined Heat and Power
CMPR	Communication-Assisted Microgrid Protection Relay
D	fault Direction signal
DC	Direct Current
DER	Distributed Energy Resource
DES	Distributed Energy Storage devices
DFIG	Doubly-Fed Induction Generator
DG	Distributed Generator
DMS	Distribution Management System
DNO	Distribution Network Operator
EC-DER	Electronically Coupled Distributed Energy Resource
ES	Ethernet Switch
FCL	Fault Current Limiter
FD	Fault Detection signal
GSC	Grid-Side Converter
GY	Grounded Wye (grounded star)
HIF	High-Impedance Fault
IMPR	Interface Microgrid Protection Relay
LANP	Local Area Network Port
LC	Local Controller
LDRC	Local Distributed energy Resource Controllers
LLC	Local Load Controllers
LV	Low Voltage
MCC	Microgrid Central Controller
MMS	Main Microgrid Switch
MMT	Minimum Melting Time
MO	Market Operator
MPC	Microgrid Protection Commander
MPPT	Maximum Power Point Tracking
MPR	Microgrid Protection Relay

MV	Medium Voltage
NVD	Neutral Voltage Displacement
OC	OverCurrent
OCR	OverCurrent Relay
PI	Proportional-Integral
PLL	Phase-Locked Loop
PCC	Point of Common Coupling
PSCAD	Power System Computer-Aided Design
PV	Photovoltaic
PWM	Pulse-Width Modulation
RSC	Rotor-Side Converter
RTDS	Real-Time Digital Simulator
SM	Secondary Main
TCT	Total Clearing Time
VCO	Voltage-Controlled Oscillator
VSC	Voltage-Sourced Converter
WEB	Wireless Ethernet Bridge
WLAN	Wireless Local Area Network

# Nomenclature

$i_{tabc}$	VSC AC-side current
$i_{sabc}$	DER output current
$i_{ext}$	Output current of the DER input source
$v_{tabc}$	VSC AC-side terminal voltage
$v_{sabc}$	DER terminal voltage
$v_{dc}$	DC-link voltage
$v_{Mabc}$	Microgrid-side voltage of the MMS
$v_{Gabc}$	Grid-side voltage of the MMS
$v_{MMS}$	Voltage across the MMS
$P_s$	Output real power of the DER
$Q_s$	Output reactive power of the DER
$P_{ext}$	Exogenous input power to the single-phase DER
$C_{dc}$	DC-link capacitance
$C_s$	Capacitance of the DER LC filter
$L_s$	Inductance of the DER LC filter
$R_s$	Parasitic resistance of $L_s$ (including on-state resistance of VSC switches)
$D_P$	Real power droop coefficient
$D_Q$	Reactive power droop coefficient
$I_{fmax}$	Maximum fault current of the feeder
$I_{fmin}$	Minimum fault current of the feeder
$T_e$	Machine electrical torque
$v_W$	Wind speed
$V_0$	Nominal network voltage magnitude
$\omega_0$	Nominal power system frequency
$\omega_r$	Machine rotor angular speed
$\beta$	Blade pitch angle
$\rho$	$dq$ -frame reference angle
$T_s$	Sampling period
$f_s$	Sampling/switching frequency

# Chapter 1

## Introduction

### 1.1 Statement of Problem and Research Objectives

A microgrid is broadly referred to as a well-defined area of an electric distribution network which embeds an appreciable number of distributed energy resources, in addition to local loads; it is managed and controlled by an intelligence and would be capable of operating in isolation from the host utility grid (islanded mode of operation), as well as in conjunction with the grid (grid-connected mode of operation). A microgrid can be a residential neighborhood, an industrial or commercial facility, a university campus, a hospital, an off-grid remote community, etc. The microgrid could be forced to switch to the islanded mode of operation, for example, due to the occurrence of a fault in the host grid, or it could intentionally disconnect itself from the grid, for example, if economics warrant the islanded mode of operation [1]. Regardless, the microgrid is expected to ensure efficient service to the microgrid loads, with superior quality and reliability, in addition to economical benefit for the microgrid owner, as well as ancillary services to the host grid.

Despite their perceived advantages, microgrids introduce new and serious challenges to distribution networks. However, the economical and environmental benefits of microgrids have motivated extensive research and development efforts towards resolving the technical issues associated with this new and fast-growing technology. The distributed energy resources are required to collectively control the network voltage and frequency, properly share the network power demand, ride through faults and disturbances, and enable seamless transitions of the microgrid from the grid-connected mode of operation to the islanded mode of operation, and vice versa. These requirements present a challenge

to the control of microgrids and their constituent distributed energy resources [2]. In addition, adoption of the microgrid concept results in a cellular structure within distribution networks; thus, it warrants a revision of the traditional philosophy of protection which assumes a radial network structure with a unidirectional flow of power [3], [4].

The objectives of the thesis are:

- To introduce a mathematical model for electronically coupled distributed energy resources and to develop a control strategy for the regulation of the amplitude and frequency of their terminal voltages in the islanded mode of operation such that the quality of power is preserved under network faults, transient disturbances, and severe imbalances.
- To enhance the aforementioned control strategy with algorithms that enable fast post-fault recovery of the microgrid, local synchronization<sup>1</sup>, and network synchronization<sup>2</sup>.
- To develop a protection strategy and microprocessor-based relay for low-voltage microgrids, in order to ensure safe operation of the microgrids in both modes of operation, without any need for communications or adaptive protective devices.
- To develop a communication-assisted protection strategy using microprocessor-based relays, in order to protect large medium-voltage microgrids in both their operational modes, even in case of the communication failure.
- To investigate the control and protection of an existing distribution network to operate as a microgrid, when the need arises.

## 1.2 Microgrids

### 1.2.1 Motivations and Advantages

One of the most drastic changes that the electric power system is undergoing is the integration of Distributed Energy Resources (DERs) into distribution networks [5]. DERs are relatively small-scale generators or energy storage devices that are interfaced with

---

<sup>1</sup>In this thesis, synchronization of a distributed energy resource with the network is referred to as the “*local synchronization*”.

<sup>2</sup>In this thesis, synchronization of the entire islanded microgrid with the host utility grid is referred to as the “*network synchronization*”.



low-/medium-voltage distribution networks and can offset the local power consumption, or even export power to the upstream network if their generation surpasses the local consumption. Most modern DERs employ non-conventional energy resources and are interfaced with the host utility grid through power-electronic converters, as efforts are made to utilize renewable or sustainable energy sources. The increasing proliferation of Electronically Coupled DERs (EC-DERs), such as photovoltaic systems, micro-gas turbines, wind power systems, and battery energy systems, is expected to inevitably challenge the operating principles of the traditional power systems.

An emerging and promising philosophy of operation to mitigate the technical issues associated with widespread proliferation of DERs, and to offer additional value, is to designate relatively small areas of a distribution network that embed DERs and loads, and to operate them in a deliberate and controlled way. Such subnetworks, referred to as microgrids, should be able to operate independently (under emergency conditions or as planned), as well as in parallel with the rest of the distribution network. The concept of microgrid has attracted considerable attention due to its potential to integrate large amounts of renewable energy resources into the electric power system, without compromising the power quality, while promising to maintain supply reliability, to enhance energy conversion efficiency, and to provide ancillary services to the power system [6].

One of the main benefits of microgrids is the use of Combined Heat and Power (CHP) equipment that makes the microgrid an integrated energy system with high energy efficiency. The waste heat from the conversion of fuel to electrical power in small generators can be used by local consumers, through the CHP technology, to raise the DER efficiency [6], [7]. In addition, most DERs of a microgrid are of electronically coupled type which can rapidly correct voltage sags, harmonics, etc., even in the presence of nonlinear and/or unbalanced loads; this, in turn, leads to an improved power quality. Moreover, the proximity between generation and consumption can improve the reliability of service to sensitive loads. Reliability is further enhanced by diversification and decentralization of the supply; thus, loss of one unit can be compensated for by the other units [1].

As mentioned earlier, microgrids are envisioned to embed a great deal of EC-DERs to play a significant role in the electric power systems of the future for cleaner air, reduced transmission and distribution costs, and enablement of energy efficiency enhancement initiatives. The use of clean and renewable energy resources can substantially reduce greenhouse gas emissions. The environmental issues have become exceedingly important in developed countries. For example, according to a 2005 study prepared for the govern-

ment of Canada, the health-related damages of coal-fired plants could exceed 3 billion dollars a year [8]. Therefore, building clean and sustainable sources of electricity is a top priority for the Canadian government. Smaller generators have also economical benefits such as shorter construction times and transmission lines [9].

## 1.2.2 Architecture

The main components of a microgrid are distributed generators (wind turbines, photovoltaic arrays, rotating machines, fuel cells, etc.), distributed energy storage devices (flywheels, batteries, supercapacitors, compressed-air systems, etc.), and local critical/non-critical loads. Distributed Generators (DGs) can generally be classified into two main groups, based on their interfacing media: (i) traditional rotating-machine-based DGs and (ii) electronically interfaced DGs. The first group are those that consist of direct-coupled rotating machines and are directly interfaced to the network through interconnection transformers (e.g., a synchronous generator driven by a reciprocating engine or an induction generator driven by a fixed-speed wind turbine). The second group, however, utilizes DC/AC or AC/DC/AC power-electronic converters as their coupling media with the host grid (e.g., photovoltaic systems or variable-speed wind energy conversion systems). The control techniques and characteristics of power-electronic converters are significantly different than those of the conventional rotating machines [10]. Moreover, due to the limited current rating of silicon devices, the fault current of electronically interfaced DGs should be limited to a maximum of about two times their nominal current [4].

Distributed Energy Storage devices (DESSs) are mainly employed as energy-backup systems to compensate for the power shortage within the microgrid, particularly in the islanded mode of operation when the generators may not be able to satisfy the entire load power demand. They can also be employed in the grid-connected mode of operation to smooth out the intermittent power of renewable energy resources and/or to incorporate significant load changes [11]. Since, due to their inherent large time constants, traditional rotating-machine-based DGs cannot rapidly respond to power intermittencies, instability may occur in transient situations. Thus, the use of DESSs is necessary to prevent such an issue. A DES is modeled in this thesis as a constant DC voltage source interfaced with the utility grid through a power-electronic converter. It acts as a controllable AC voltage sources (with very fast output characteristics) to face sudden system changes such as load or operational mode switchings. It should be noted that all DESSs have a finite capacity for storing energy and, thus, can be in service for a limited period of time.

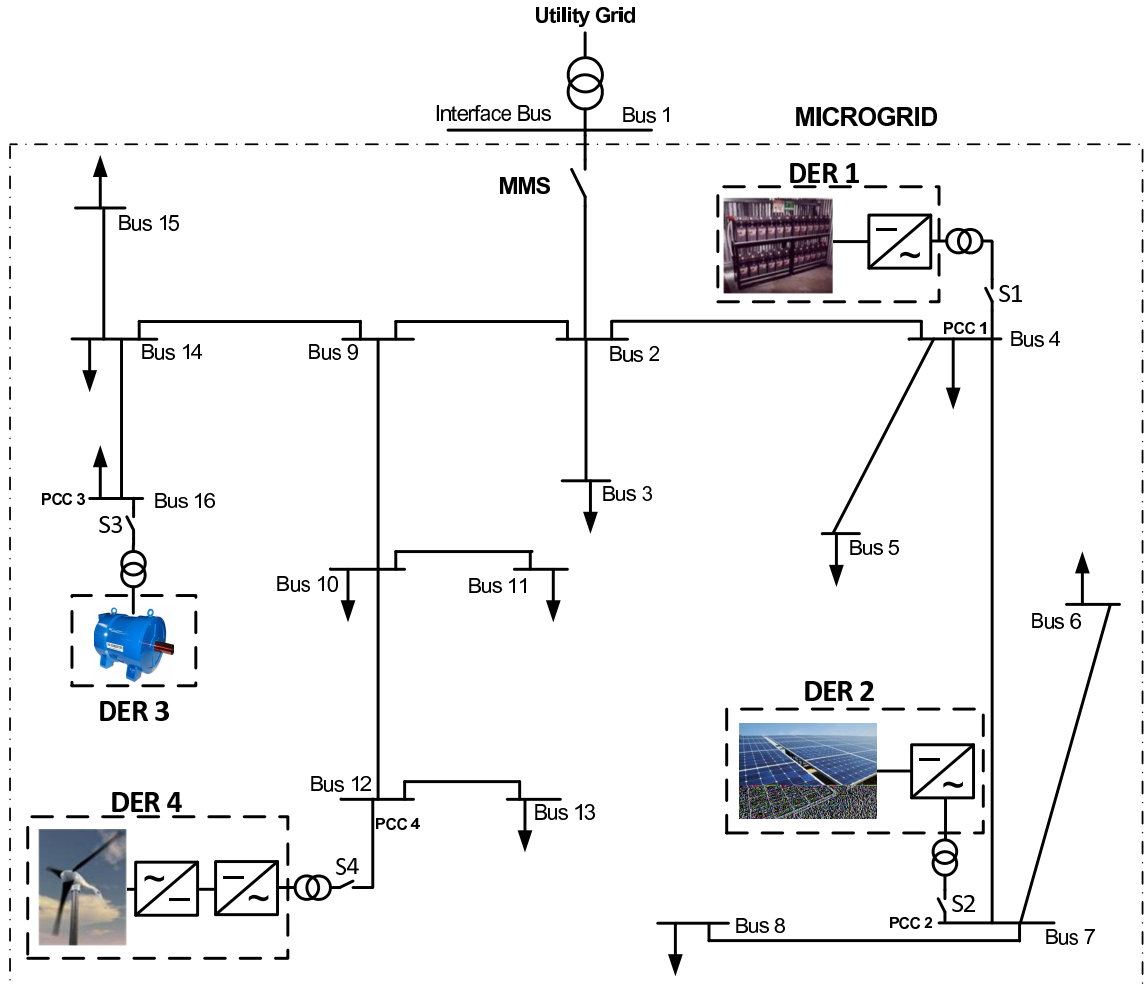


Figure 1.1: Single-line schematic diagram of a typical microgrid.

Fig. 1.1 illustrates a single-line schematic diagram of an example microgrid that embeds a Photovoltaic (PV) system, a variable-speed wind turbine, a battery energy storage unit, and a traditional rotating-machine-based generator. EC-DERs are interfaced with the point of common coupling of their corresponding bus through a power-electronic converter and a transformer. However, the rotating-machine-based DER is directly interfaced with its corresponding host bus through an interconnection transformer. The microgrid is connected to the interface bus (Bus 1) where it is interfaced with the host utility grid through the Main Microgrid Switch (MMS); Bus 1, in turn, is energized from a high-voltage transmission grid, through a substation transformer.

The microgrid of Fig. 1.1 normally operates in the grid-connected mode where it is connected to the main utility grid. In this mode, DERs deliver constant real and reactive powers to the distribution network; the net difference between the aggregate power of

DERs and local loads is balanced by the upstream host grid. In case of an unplanned event, e.g., a network fault, the MMS is expected to disconnect the microgrid from the utility grid. Subsequently, the microgrid can continue to operate in the so-called islanded mode. While islanded operation is mainly to enhance the system reliability and is caused by unexpected incidents, it can also be intentional, e.g., for maintenance requirements, effective and optimized utilization of a system, and/or electrification of remote off-grid communities. The microgrid shall also be able to resynchronize itself to the host grid and smoothly switch back to the grid-connected mode.

## 1.3 Control of Microgrids

As explained in Section 1.1, adoption of the microgrid concept results in a cellular structure within distribution networks and, thus, it is no longer possible to control the network using the basic control strategies of conventional distribution systems. The control scheme of a microgrid should be designed in a way that the system can safely operate in both the grid-connected and the islanded modes. In the grid-connected mode of operation, DERs operate in a constant real- and reactive-power control mode meaning that they exchange a pre-specified power with the distribution network, e.g., to minimize the power import from the main grid [12]. In the islanded mode of operation, however, the control algorithm must control the local network voltage and frequency and provide the instantaneous real and reactive power of the loads. Thus, appropriate voltage and frequency regulation schemes are necessary to enhance the network reliability and to preserve the system stability. Otherwise, microgrids with a high penetration of DERs can experience reactive and/or real-power oscillations. Unlike a large power system, the impedances between DERs in a microgrid are not significant. Therefore, small errors in voltage setpoints of DERs may cause large circulating currents that exceed the DER ratings [13]. Control of microgrids can be broadly divided into (i) supervisory control and (ii) control of DERs. These are described below.

### 1.3.1 Supervisory Control

Supervisory control schemes of microgrids, which are also known as *network* or *overall* control schemes, can be categorized into two groups: (1) centralized control schemes [14], [15] and (2) decentralized control schemes [12], [16], [17]. In the following subsections, the two aforementioned control schemes are briefly described.

### 1) Centralized Control

For the overall control of a microgrid, three control levels are typically defined:

- Local Controllers (LCs), which could be either Local DER Controllers (LDRCs) or Local Load Controllers (LLCs);
- Microgrid Central Controller (MCC);
- Distribution Management System (DMS).

The LCs are assumed to control DERs and controllable loads within a microgrid, by tracking desired commands. In a centralized mode of control, the LCs receive their commands from the MCC; thus, the MCC issues control setpoints to DERs and controllable loads through a communication link. The commands are determined based on a variety of criteria, such as market signals and economy of the microgrid; optimal operation of the microgrid; host grid conditions and requirements; and microgrid internal conditions and requirements [14]. Therefore, the MCC is assumed to take different roles ranging from the optimization of the microgrid key parameters to coordination of LCs. It should be noted that, depending on the control approach, each LC may also have a certain level of intelligence.

In the grid-connected mode of operation, the microgrid voltage is imposed by the host utility grid and, thus, the function of the supervisory control is to issue the real- and reactive-power commands to the LDRCs. By contrast, in the islanded mode of operation, the DERs are mainly controlled to regulate the microgrid voltage magnitude and frequency. Consequently, the supervisory control can specify the commands for steady-state voltage magnitude and frequencies of the DERs, ensuring well being of the loads or safe reconnection of the microgrid to the host grid once the operating mode is to be switched to the grid-connected mode. Further, the supervisory control can shed loads in the islanded mode of operation, depending on load criteria, microgrid energy reserves, or other considerations. Finally, the DMS<sup>1</sup> is a higher level of controller responsible for the technical operation in a medium- and low-voltage area, in which more than one microgrid exist [7]. Thus, the DMS does not belong to one microgrid and is interfaced with the microgrid through its corresponding MCC. Fig. 1.2 illustrates the hierarchical control system architecture of the microgrid of Fig. 1.1.

---

<sup>1</sup>This high-level controller is also referred to as the “*Distribution Network Operator (DNO)*” or “*Market Operator (MO)*”, in some references [15].

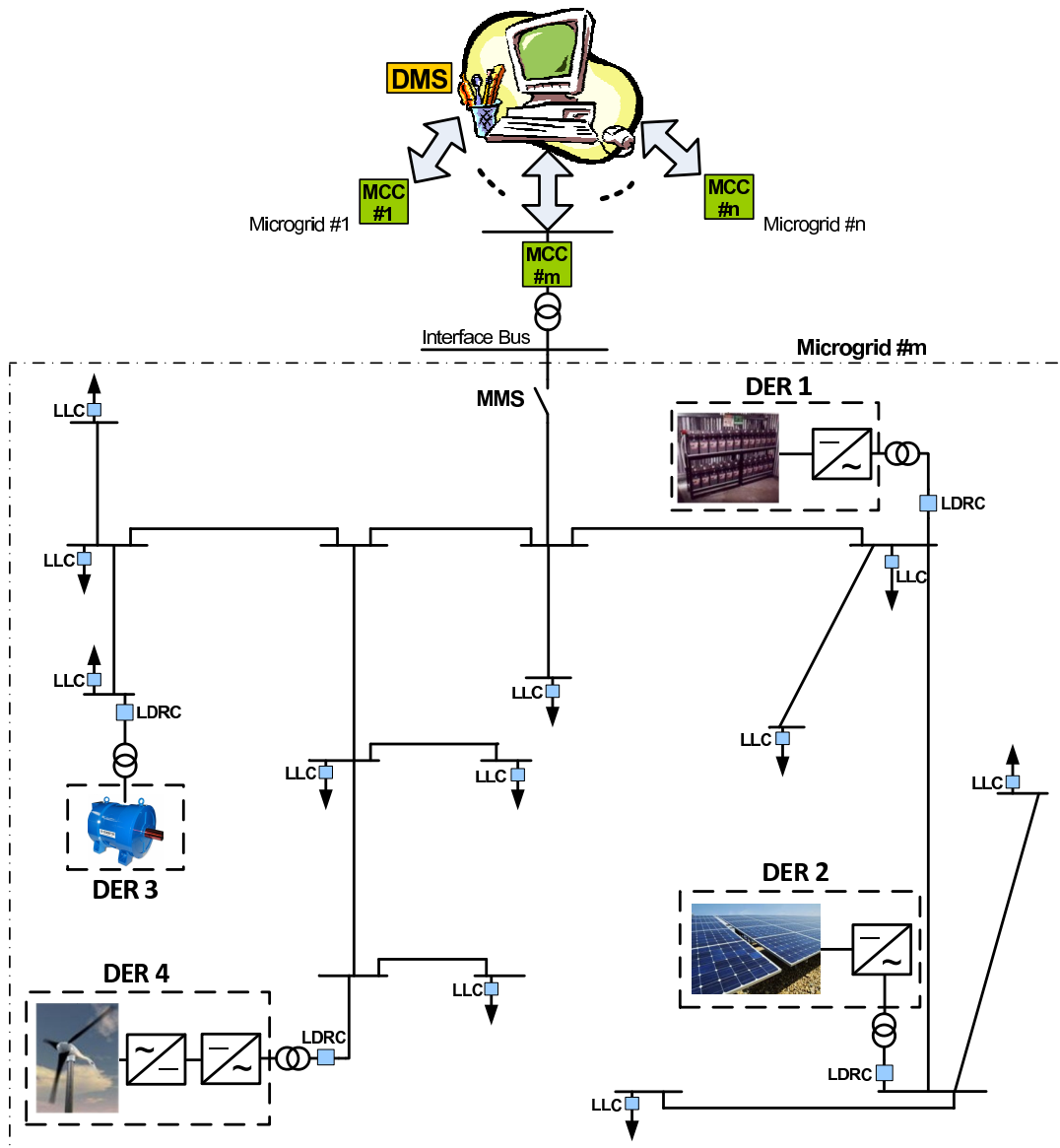


Figure 1.2: A schematic illustrating centralized control of a typical microgrid.

## 2) Decentralized Control

Reliability issues of the centralized control approach might counteract the enhanced reliability obtained by the concept of the microgrids [16]. Further, in remote areas where distances amongst the DERs are considerably long, it is impractical and costly to distribute dynamic sharing signals, which are characterized by their high bandwidth. To overcome these limitations, the use of decentralized control techniques has been proposed for microgrids.

In a decentralized approach, the control decisions, e.g., power optimization for meeting

load demands or maximizing power export to the main grid based on the market prices, are made by the LDRCs [17]. Moreover, LLCs are assumed to ensure safe and smooth operation of the loads that they control. In such systems, each unit must be able to operate independently without intercommunications. The main task of each LC in a decentralized control scheme is not to only maximize the revenue of its corresponding unit but to also improve the overall performance of the microgrid. Thus, the control system architecture must be able to include economic functions, environmental factors, and technical requirements [7].

The most widely adopted decentralized technique to ensure power sharing and coordinated voltage/frequency regulation is to droop the frequency and magnitude of the output voltage of each DER, versus the real and reactive powers that the DER delivers to the network [18]. Thus, the DER controllers typically make their adjustments based on the frequency and magnitude of the inverter terminal voltage. The frequency droop allows the DERs to share the total real power variations in a manner determined by their frequency droop characteristic; it essentially utilizes the system frequency as a communication link between the DER control systems. Similarly, a droop in the voltage amplitude, with respect to reactive power, can ensure reactive power sharing. This load sharing technique is based on the power flow theory in an AC system, which states that the flow of the real and reactive powers between two sources can be controlled by adjusting the power angle and the voltage magnitude of the systems, respectively. In the droop control scheme, the droop characteristics can mathematically be expressed as

$$\omega = \omega_0 - (D_P)P , \quad (1.1)$$

$$v = V_0 - (D_Q)Q , \quad (1.2)$$

where  $P$  and  $Q$  are real- and reactive-power outputs of the DER, respectively;  $\omega_0$  and  $V_0$  respectively signify the nominal power system frequency and nominal network voltage magnitude; and the constant parameters  $D_P$  and  $D_Q$  denote real- and reactive-power droop coefficients, respectively. Figs. 1.3(a) and (b) illustrate the typical  $P - \omega$  (real power versus frequency) and  $Q - V$  (reactive power versus voltage magnitude) droop characteristics, in which the subscripts “*min*” and “*max*” are employed to demonstrate the minimum and maximum permissible levels of a variable.

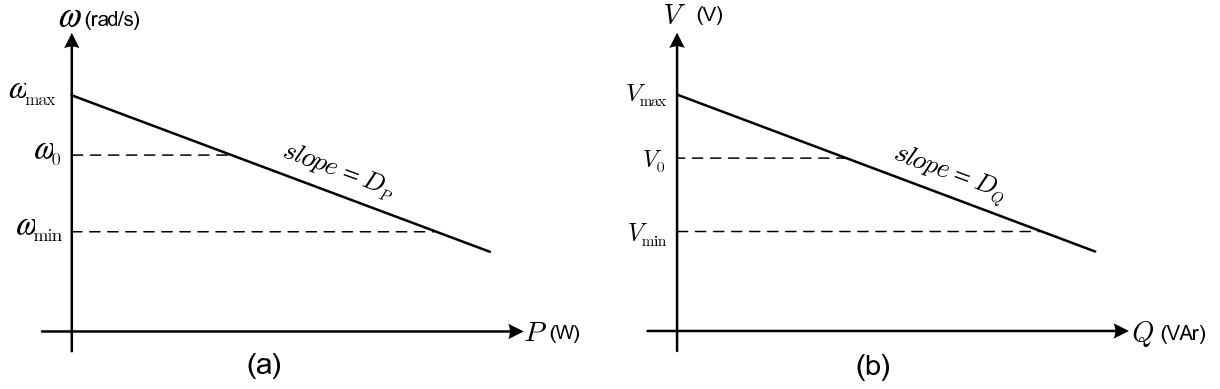


Figure 1.3: (a) Real power versus frequency ( $P$ - $\omega$ ) droop characteristic and (b) reactive power versus voltage ( $Q$ - $V$ ) droop characteristic.

### 1.3.2 Control of DERs

Control strategy of a DER within a microgrid is selected based on the required functions and network operational scenarios. Control of the DER is also determined by the nature of its interactions with the system and other DERs. Two main functions of the control of a DER are (i) real- and reactive-power control in the grid-connected mode of operation and (ii) microgrid voltage and frequency regulation in the islanded mode of operation. Table 1.1 provides a general categorization of the major control strategies for a DER and classifies the strategies into the grid-connected-mode (grid-following) and islanded-mode (grid-forming) controls [7]. Each category is further divided into noninteractive and interactive techniques. The objective of the following subsections is to briefly describe the aforementioned strategies.

#### 1) Grid-Connected-Mode Control

The grid-connected-mode control approach is employed when direct control of the magnitude and frequency of the DER terminal voltages is not required, e.g., due to the existence of a significantly large-capacity DER [19] or due to the connection to the main utility grid. In the grid-connected mode of operation, the voltage magnitude and frequency of the DER are dictated by the grid. Thus, the control task boils down to the regulation of the real and reactive powers that the DERs exchange with the host network.

If the real- and reactive-power outputs of a DER are controlled independent of other DERs/loads (nondispatchable DER), it is a noninteractive grid-connected-mode control strategy. However, if the real and reactive powers of a DER are determined as input



Table 1.1: Classification of Control Strategies for DERs

Control Type	Grid-Connected-Mode Control	Islanded-Mode Control
Noninteractive techniques	Constant-power delivery	Voltage and frequency control
Interactive techniques	Dispatchable-power delivery with real- and reactive-power support	Load sharing (droop control)

commands to the DER controllers (dispatchable DER), the strategy is called an interactive grid-connected-mode control strategy. The setpoints of dispatchable DER controllers are specified based on a power-dispatch method or real-/reactive-power compensation of loads.

As mentioned in Section 1.1, EC-DERs are interfaced with the network through power-electronic converters. The interface converters provide another layer of conversion and/or control, and offer fast dynamic responses for EC-DERs. They also provide the flexibility required for the plug-and-play functionality of the microgrid, since the controls of EC-DERs need to ensure that the EC-DERs can be added to the system without additional modification to the existing equipment [1], [6]. The control schemes of EC-DERs are different from those employed in traditional rotating-machine-based DERs, which can significantly affect the performance of the electric networks. Thus, this study mainly focuses on the control of EC-DERs. In the grid-connected mode of operation, real and reactive powers of an EC-DER can be controlled based on two distinct methods; these are discussed next.

**a) Voltage-Mode Control:** The first approach for the control of a grid-connected EC-DER, which is commonly referred to as “*voltage-mode control*” [20], has been illustrated in Fig. 1.4 in which the power source (modeled by a time-varying DC voltage source) is interfaced with the grid through a Voltage-Sourced Converter (VSC) and a three-phase inductor,  $L_s$ ;  $P_s$  and  $Q_s$  are respectively real- and reactive-power outputs of the EC-DER, and the superscript “\*” is used for reference values. In the voltage-mode control strategy, real- and reactive-power outputs of the DER are controlled, respectively, by the phase angle and magnitude of the VSC AC-side terminal voltage  $v_{tabc}$ , relative to those of the DER terminal voltage  $v_{sabc}$ . If the magnitude and phase angle of the VSC terminal voltage are close to those of the DER terminal voltage (resistance of  $L_s$  is not significant), the real and reactive powers are almost decoupled, and two independent compensators can be employed for their control. The voltage phase angle  $\varphi(t)$  is determined by a

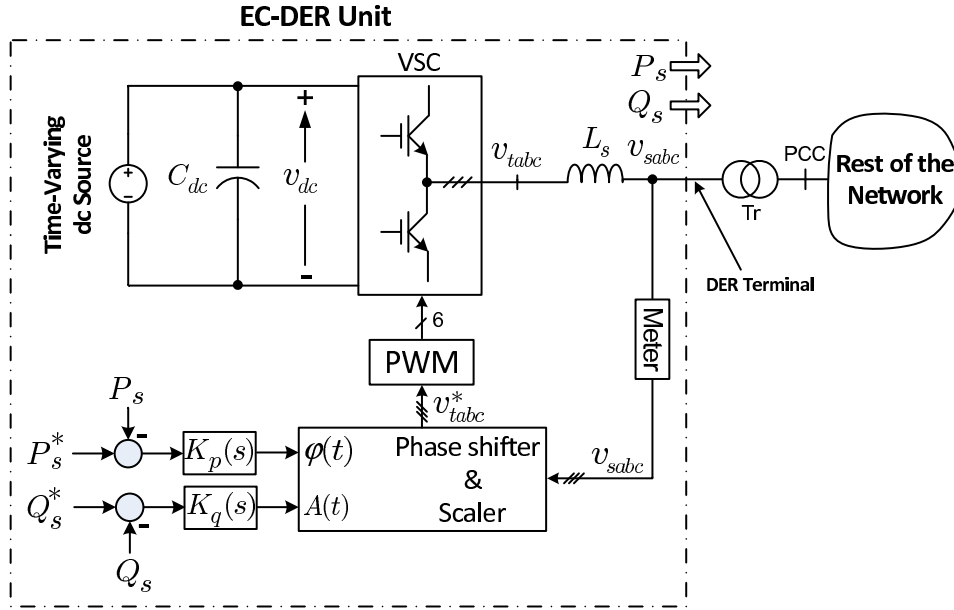


Figure 1.4: Voltage-mode control of the real- and reactive-power outputs of a grid-connected EC-DER.

control loop that processes the error between  $P_s$  and its respective setpoint, while the voltage magnitude  $A(t)$  is similarly specified by the reactive-power control loop. Thus, the voltage-mode control has the merit of being simple and having a low number of control loops. However, since there is no control loop dedicated to the VSC output current, the VSC is not protected against overcurrent conditions [20].

**b) Current-Mode Control:** The second approach to control the real- and reactive-power outputs of an EC-DER in the grid-connected mode of operation is known as the “*current-mode control*”. In this method, the VSC AC-side current (i.e.,  $i_{tabc}$ ) is first controlled by a dedicated control scheme, through the VSC terminal voltage. Then, both real and reactive powers are controlled by the phase angle and the magnitude of the VSC line current, with respect to the DER terminal voltage. Due to the current regulation scheme, the VSC is protected against overload conditions. Other advantages of the current-mode control include robustness against variations in parameters of the VSC and AC system, superior dynamic performance, and higher control precision. To that end, current-mode control is a popular technique in utility applications. Fig. 1.5 illustrates the current-control mode of a grid-connected EC-DER, which is detailed in [20] and [21].

In the control strategies of Figs. 1.4 and 1.5, the real- and reactive-power outputs of

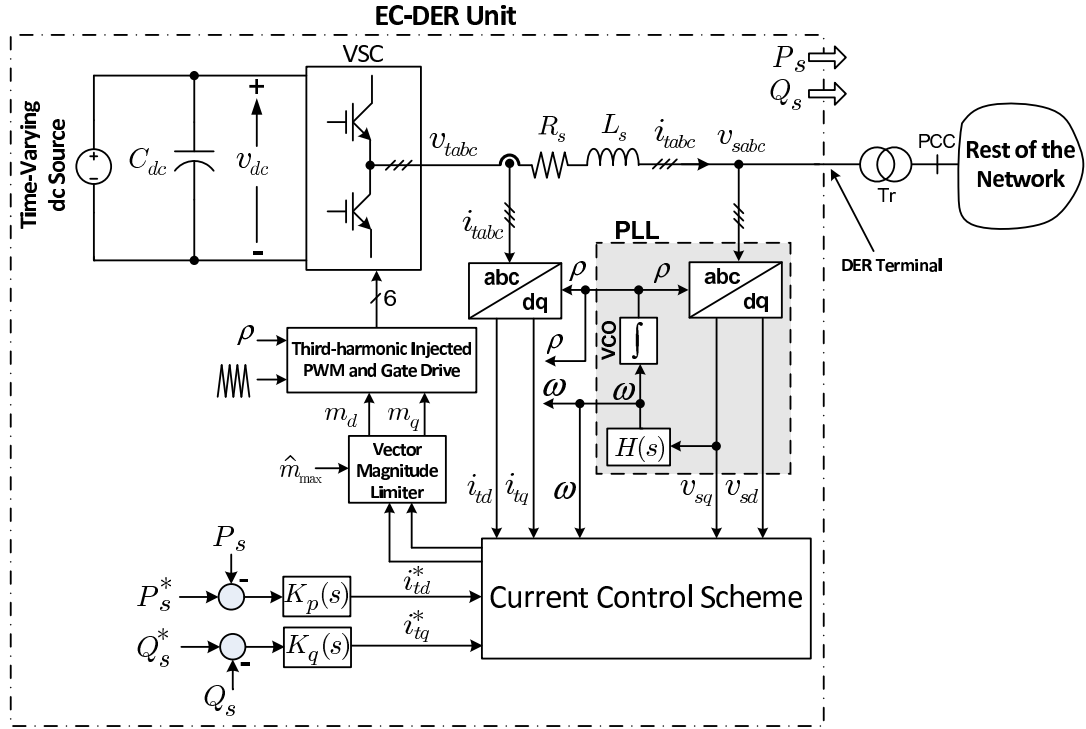


Figure 1.5: Current-mode control of the real- and reactive-power outputs of a grid-connected EC-DER.

the grid-connected DER can be externally controlled through the adjustment of  $P_s^*$  and  $Q_s^*$ , e.g., by the MCC. These types of DERs are called dispatchable DERs. By contrast, the output power of a nondispatchable DER is normally controlled based on the optimal operating condition of its input power source. For example, to maximize the output power of a nondispatchable DER, a control strategy based on Maximum Power Point Tracking (MPPT) is normally used to extract the maximum possible power from the input power source under all possible conditions [22].

Fig. 1.6 illustrates a simplified schematic diagram of a nondispatchable DER (e.g., a PV system) in which the DER input source has been modeled by a DC voltage source whose voltage,  $v_{dc}$ , is related to the output current of the input source,  $i_{ext}$ , through a  $v-i$  characteristic [22]. As Fig. 1.6 illustrates, the kernel of the control system is the real- and reactive-power control scheme (of Fig. 1.5) by which  $P_s$  and  $Q_s$  can be controlled independently. In the system of Fig. 1.6, however, the setpoint for the real power,  $P_s^*$ , is determined by a feedback control mechanism that regulates  $v_{dc}$  at its corresponding setpoint,  $V_{dc}^*$ . The reactive power  $Q_s$  can be controlled independently by the setpoint  $Q_s^*$ . In many applications,  $Q_s^*$  is set at zero, for a unity power-factor operation.  $Q_s^*$  can also

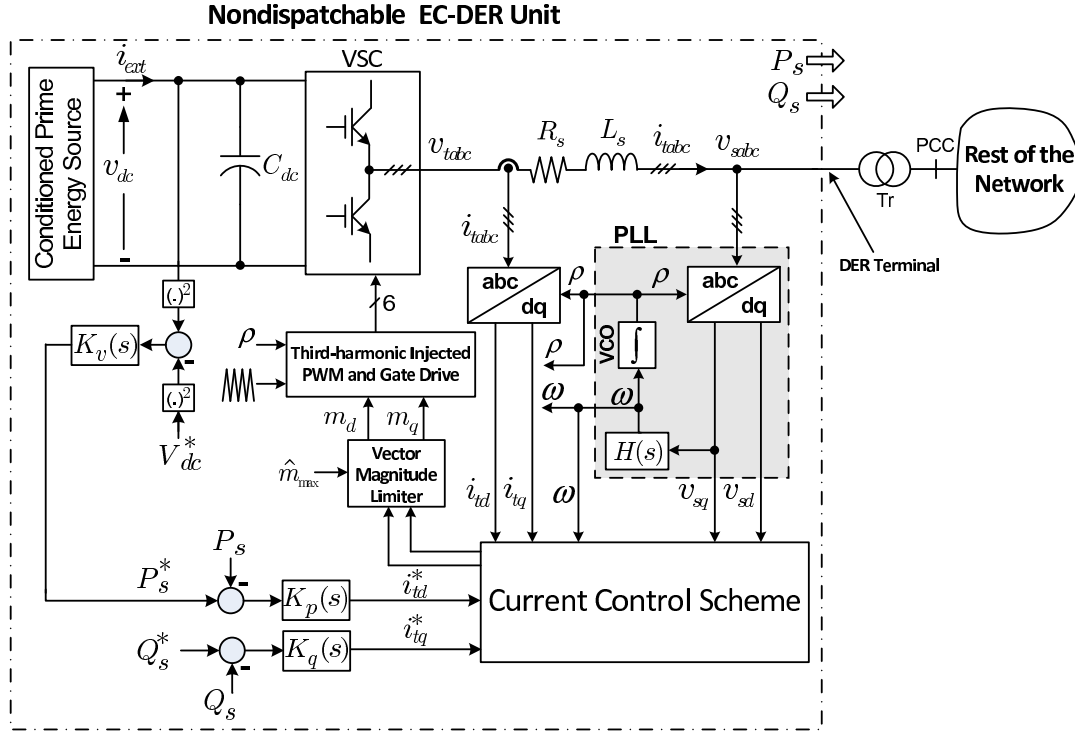


Figure 1.6: Current-mode control of the real- and reactive-power outputs of a nondispatchable grid-connected EC-DER.

be determined by a closed-loop mechanism whose function is to regulate the magnitude of the DER terminal voltage, where the DER unit is interfaced with the host grid [20].

## 2) Islanded-Mode Control

Islanded-mode control strategies are employed in the absence of the host utility grid. Islanding of a microgrid can take place either by unplanned events (e.g., network faults) or by planned actions (e.g., maintenance requirements). In the islanded mode of operation, the impact of loads switching incidents on the control is highly pronounced due to the absence of a connection to the main grid. Thus, the control strategies of EC-DERs must ensure the frequency and voltage control of the islanded microgrid to protect the microgrid against real- and/or reactive-power oscillations. Further, the control must be able to manage the real and reactive power sharing of DERs.

If a DER attempts to supply the balance of reactive and real power while it is respectively regulating the voltage magnitude and the frequency of the islanded microgrid, it has employed a noninteractive islanded-mode control strategy. However, in a multi-unit microgrid where two or more DERs share the load demand, an interactive control strat-

egy should be employed to ensure load sharing through changing voltage and frequency of the DERs [7]. The islanded-mode control can be exercised centrally, as discussed in Section 1.3.1–1. Centralized approaches, however, require remarkable data transfer capacities and reliable communication links [14], [19]. As such, they may be suitable for small-scale microgrids in which the DERs are close together. For DERs that are scattered over a large geographical span, the decentralized control schemes of Section 1.3.1–2 are preferable since they do not need data communications [16]. This thesis mainly focuses on the decentralized control schemes for the islanded mode of operation.

## 1.4 Protection of Microgrids

Traditionally, distribution networks have been designed to operate radially, that is, the power flows from the upper voltage levels down to the customers connected to radial feeders. This simple configuration has enabled straightforward protection strategies for typical distribution systems. Thus, the conventional distribution networks are protected by such simple protective devices as fuses, reclosers, and overcurrent relays [23], [24]. The practice of operating microgrids, however, disturbs the traditional protection strategies which are based on the assumption of a radial network structure featuring large fault currents and unidirectional power flows. The protection scheme of a microgrid must ensure safe operation of the microgrid in both modes of operation. Therefore, the protection issues associated with each mode of operation should separately be addressed by the protection algorithm. In the following subsections, the traditional protection of typical distribution systems will first be reviewed, then the challenges associated with the microgrid protection are briefly introduced.

### 1.4.1 Traditional Protection Coordination

As mentioned in the previous section, overcurrent protective devices, most commonly fuses, reclosers, and inverse-time overcurrent relays, are employed for the protection of traditional distribution networks. In a feeder, fuses must be coordinated with the recloser installed at the beginning or middle of the feeder. The coordination means that a fuse must operate only if a permanent fault impacts the feeder (fuse-saving scheme). For a temporary fault, however, the recloser must rapidly open (fast mode) to isolate the feeder and give the fault a chance to self-clear. If the fuse fails to operate for a permanent fault, the recloser will back it up by operating in its slow mode. The feeder relay will operate

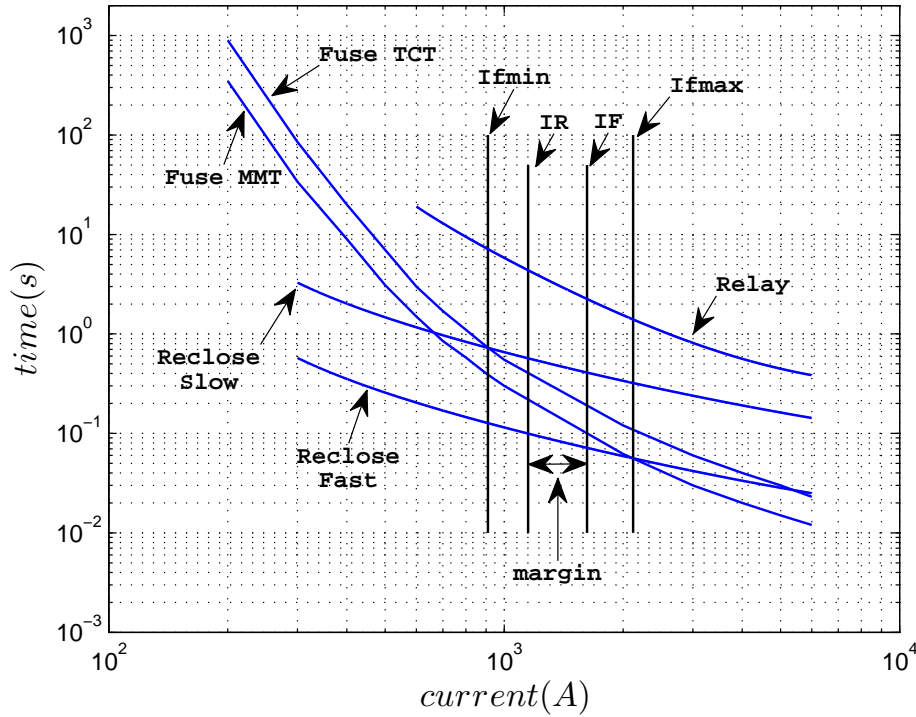


Figure 1.7: Typical characteristic curves, their coordination, and the margin remaining after the addition of a DER.

lastly only if both the recloser and the fuse fail [25]-[27].

Fig. 1.7 illustrates the basics of the conventional coordination practice for the relay, recloser, and fuses in a typical distribution network. The figure illustrates that the devices are coordinated in such a way that, for all fault currents between  $I_{fmin}$  (minimum fault current of the feeder) and  $I_{fmax}$  (maximum fault current of the feeder), the fast characteristic curve of the recloser lies below the fuse Minimum Melting Time (MMT) curve, whereas the slow characteristic curve of the recloser lies above the fuse Total Clearing Time (TCT) curve (descriptions of these curves are provided in Appendix B). Hence, the recloser opens before the fuse starts to melt and gives temporary faults a chance to self-clear. However, for a permanent fault, the fuse will operate before the recloser opens in the slow mode. Fig. 1.7 also indicates that the relay provides an overall backup protection since its characteristic curve lies above all the other curves (the relay characteristic curves are also described in Appendix B). Hence, to maintain the coordination, one has to ensure that (i) the fault current passing through the devices remains between  $I_{fmin}$  and  $I_{fmax}$ ; and (ii) the fault currents of all protective devices are

fairly equal. As Fig. 1.7 shows, if the difference between the fuse fault current ( $I_F$ ) and the recloser fault current ( $I_R$ ) is more than a margin, the protection coordination is lost.

### 1.4.2 Grid-Connected-Mode Protection

In the grid-connected mode, fault currents are fairly large due to the contribution of the host grid and, thus, the employment of conventional overcurrent relays is possible. However, due to the existence of DERs, the radial structure of the networks is compromised, and protection coordination may be affected, or entirely lost in some cases [2], [3], [28]. Addition of a DER to a radial feeder anywhere downstream of the feeder recloser may (i) change the minimum and maximum fault current of the feeder, (ii) decrease the fault current of an upstream protective device as compared to that of downstream devices, and (iii) result in a bidirectional power flow. Thus, depending on the DER type, DER location and DER size, several issues may arise in the grid-connected mode of operation.

The main protection issues associated with the introduction of DERs to a distribution network include “*blinding of protection*”, “*false/sympathetic tripping*”, “*recloser-fuse miscoordination*”, “*fuse-fuse miscoordination*”, and “*failed auto-reclosing*” [3], [28]-[30]. They are briefly described next.

- **blinding of protection:** refers to a situation in which a DER(s) is connected somewhere between the fault location and the feeding substation. Due to the contribution of the DER(s), the fault current measured by the feeder relay, which is located at the beginning of the feeder, decreases as compared to the situation that no DER is connected to the network. This may result in delayed operation of the relay or even undetected faults.
- **false/sympathetic tripping:** refers to a scenario in which a fault takes place outside the feeder that embeds a DER(s), e.g., a fault at the neighboring feeder. In such a case, the DER(s) contributes to the fault via its feeder, and the fault current flows upwards on the feeder. Thus, the nondirectional relay of the healthy feeder may falsely detect a fault and isolate its feeder, which is undesirable.
- **recloser-fuse and fuse-fuse miscoordination:** the introduction of a DER to a feeder, whether upstream or downstream of the lateral connection points, changes the minimum and maximum fault currents of the feeder and, therefore, compromises the coordination between the protective devices of the laterals. It is remembered

that traditional coordination strategies (described in Section 1.4.1) are exercised for a fault current range, and cannot guarantee the protection coordination for the currents beyond the defined range. This issue is also referred to as the “*fuse nuisance blowing*” in some references.

- **failed auto-reclosing:** may occur when the DER(s) remains connected to the feeder during the dead time of the autoreclosing sequences. In this case, the DER(s) usually tends to drift away from the synchronism with respect to the grid and, hence, the reclosure would couple two asynchronously operating systems after the reclosure. This may cause serious damage to the generators as well as the neighboring networks. Moreover, the DER maintains the voltage in the network and the arc at the fault point during the dead time of the reclosing mechanism. This, in turn, causes the fault to seem permanent and, thus, the reclosing fails.

### 1.4.3 Islanded-Mode Protection

As discussed in Sections 1.2.2 and 1.3.2, power-electronic converters should be protected against overcurrent conditions, as their switches have limited current ratings. This, in turn, results in the limited fault current capability of EC-DERs. Therefore, fault currents are relatively small in the islanded mode of operation, as compared to those experienced in the grid-connected mode of operation. Moreover, depending on the ratio of the power generated by rotating-machine-based DERs to the power generated by EC-DERs, the fault current magnitude can vary over a fairly wide range in an islanded microgrid. Consequently, the conventional overcurrent protection schemes are no longer adequate for the islanded mode of operation [4]. In addition, undervoltage protection functions may fail to detect all types of faults, as a fault might include a significant resistance. Therefore, there is a need to have a fresh look into the fundamentals of relaying to come up with a protection scheme capable of responding appropriately to different types of faults within an islanded microgrid.

## 1.5 Thesis Contributions

The main contributions of the thesis can be listed as follows:

- The thesis proposes an enhanced control strategy that improves the performance of an EC-DER under network faults and transient disturbances, in a multi-unit mi-



crogrid setting. The proposed control strategy does not require the detection of the mode of operation and switching between different controllers (for grid-connected and islanded modes), and it enables the adopted EC-DERs to ride through network faults, irrespective of whether they take place within the host microgrid or impact the upstream grid. Moreover, the proposed control ensures an acceptable power quality for the duration of the faults, which is an important feature for protection against certain classes of faults (e.g., high-impedance faults), as well as for sensitive loads. The controllers also incorporate synchronization algorithms for ensuring safe reconnection of the islanded microgrid to the utility grid when the grid fault is cleared. Further, the thesis proposes a supplementary control loop that improves the microgrid post-fault recovery; a modified phase-locked loop is also presented to provide the frequency information under severely unbalanced conditions.

- The thesis further proposes an effective strategy for the coordination of protective devices in typical radial distribution networks with DERs. Moreover, the steps taken to characterize the impact of the future addition of DERs on the protection coordination, for host and neighboring feeders, are presented in the thesis. Expanding on this idea, the thesis proposes a protection strategy based on microprocessor-based relays for low-voltage microgrids. The structure of a new relay enabling the proposed protection strategy is also presented. One of the salient features of the developed protection scheme is that it does not require communications or adaptive protective devices. In addition, it is to a large extent independent of the fault current magnitude, the microgrid operational mode, and the type and size of the DERs, subject to the modified relay setting for the grid-connected mode of operation.
- Finally, the thesis proposes a communication-assisted protection strategy implementable by commercially available microprocessor-based relays, for protection of inverter-based medium-voltage microgrids. Even though the developed protection strategy benefits from communications, it offers a backup protection strategy to manage communication network failures. Similarly, the proposed protection strategy is independent of the fault current levels; type, size, and location of the DERs; and the operational mode of the microgrid. The thesis further looks into the control and protection of an existing distribution network, which is supposed to operate as a microgrid. In particular, the thesis studies a Canadian distribution network to (i) identify the conditions under which the network can operate as a microgrid,

and (ii) present the control and protection strategies that enable islanded mode of operation; the optimal solution can then be selected by the local distribution company based on the system requirements/limits.

## 1.6 Thesis Outline and Related Literature Review

This thesis has been organized in seven chapters as follows:

In the first chapter, an introduction to the research topic along with its importance to the area of Power System Engineering is presented. Research objectives and the contribution of the thesis are also outlined in Chapter 1. Chapter 2 of the thesis focuses on modeling and control of EC-DERs; in particular, the control of the magnitude and frequency of the DER terminal voltage in both operational modes of a microgrid is presented. The performance of the control strategy is then enhanced under system imbalances and network faults such that the quality of power and the post-fault recovery of the microgrid are improved.

Almost all publications in the area of microgrids have assumed sound network conditions and concentrated on voltage and frequency regulation strategies [31]-[34], dynamic analysis and control design [12], [16], [35]-[38], power quality [39]-[42], and supervisory control and optimal operation [15], [43]-[46]. However, compared to the conventional rotating-machine-based DERs, EC-DERs respond very differently to network faults. As mentioned in Section 1.4.3, an EC-DER employs intricate power semiconductor switches of limited current handling capabilities and, as such, must be equipped with additional control loops that limit its current output to protect its semiconductor switches. On the other hand, the existence of the internal control loops renders the response of the EC-DER to a fault very much dependent on the type of fault, winding configuration of the interconnection transformer, degree of the voltage drop, pre-fault operating point of the EC-DER, and operating mode of the host microgrid. Therefore, it is important to study and characterize the response of EC-DERs to network faults, and to devise control strategies that enable them to ride through faults, preserve power quality, and maintain stability of the host microgrid. Such studies have thus far dealt with EC-DER behaviors in the context of (grid-connected) distributed generation, and not microgrids [47]-[50]; these references have only investigated the analysis and design of the controllers in the grid-connected mode of operation where a fault impacts the grid.

To the best of our knowledge, reference [51] is the only publication that has demon-

strated sample microgrid responses under faulted network conditions. The scenarios presented in [51] deal with those faults that strike the upstream grid when the microgrid is in the grid-connected mode, but do not consider the faults in the islanded mode. In fact, the objective of the study reported in [51] is not to present an optimal control strategy for microgrids or EC-DERs, but is to identify future areas of research. The potential issues identified in [51], as well as the need to enrich the technical literature, in terms of the modeling of EC-DERs for protection and control studies of microgrids, have motivated the study reported in Chapter 2 of the thesis.

In Chapter 3 of the thesis, a simple and effective protection strategy is proposed that provides coordination amongst protective devices of a radial distribution system embedding DERs. The proposed strategy aims to address the issues of blinding of protection, false tripping, recloser-fuse and fuse-fuse miscoordination, and failed auto-reclosing. The impact of future additions of DERs on the coordination is also investigated, and the requirements for preservation of the coordination are identified in Chapter 3.

The impact of DERs on the system short-circuit current has been investigated in [2]. The authors recommend that the margin required for preserving the protection coordination be checked whenever a new DER is added to the network. The possibility of maintaining the coordination in radial distribution systems with DERs, if there is enough margin between relay characteristic curves, has been demonstrated in [3]; however, the authors have not formulated the problem. According to [3], the relay parameters have to be reset to revised relay curves in case the coordination is lost although no method has been presented for the revision. Reference [52] proposes the use of adaptive microprocessor-based reclosers to resolve the fuse-recloser coordination problem in a typical one-feeder test system embedding a DER; however, the other aforementioned issues have not been considered, and also recloser settings must be changed after the first reclosure. In references [53] and [54], the idea is to employ Fault Current Limiters (FCLs) for limiting fault currents to such low levels that the coordination issue does not manifest itself. Although consistent with the general sense that EC-DERs do not compromise the protection coordination, at least as drastically as their rotating machine-based counterparts, the studies reported in [53] and [54] have not formulated or characterized the problem, nor have they considered the effectiveness of the scheme for transient regimes.

Chapters 4 and 5 of this thesis concentrate on the protection of Low-Voltage (LV) and Medium-Voltage (MV) microgrids, respectively. The goal of these chapters is to detect and isolate the faults that impact the host microgrid, in both modes of operation,

in a selective (coordinated) manner. Further, the structure of new microprocessor-based relays enabling the proposed protection strategies are presented. Chapter 6 of the thesis deals with an existing distribution network and studies different control scenarios that enable the network to operate as a microgrid. Practical protection strategies that could be effective for the established microgrid (considering the system constraints) are also discussed in Chapter 6.

The protection scheme of a microgrid must ensure its safe operation in both operational modes. In the grid-connected mode of operation, fault currents are large due to the contribution of the host grid. This allows the employment of the conventional overcurrent relays despite the fact that the protection coordination may be compromised or even entirely lost, due to the existence of DERs [3], [52], [55]-[58]; thus, the existing relay settings should carefully be revised while DERs are in place. In the islanded mode of operation, however, fault currents may be significantly smaller than those experienced in the grid-connected mode due to the limited current contribution of EC-DERs. Consequently, the conventional overcurrent protection is ineffective for the islanded mode of operation [4], [59]-[68].

In reference [55], an adaptive strategy has been proposed for protecting distribution systems with high penetration of DERs. The strategy proposed in [55] is based on communications amongst the equipment, does not accommodate the islanded mode of operation, and is applicable only if the penetration of DERs is high. References [56]-[58] present communication-based protection strategies for grid-connected microgrids based on the assumption of large fault currents (due to the host grid) and coordinated employment of OverCurrent Relays (OCRs) to isolate the faults within the microgrid; if a fault impacts the utility grid, the microgrid is disconnected from the upstream network and operated in the islanded mode, whereas if a fault takes place within the islanded microgrid, all embedded DERs are dropped after a prespecified delay. Although an option, especially for those microgrids that do not embed sensitive loads, the protection strategies proposed in [56]-[58] do not offer a method for fault detection in the islanded mode of operation, nor do they allow operation of the microgrid in the islanded mode if a fault occurs within the islanded microgrid.

Reference [59] has proposed an admittance relay for protection of microgrids in both modes of operation. However, it does not present a reliable method to measure the exact value of the admittance for different fault scenarios; the issue especially manifests itself when the distribution lines are short. Reference [4] proposes the post-fault switching of

the operational mode of a microgrid, to the islanded mode, and protecting the islanded microgrid based on current sequence components. However, the proposed method does not enable single-phase tripping and also fails to ensure full protection against three-phase faults. The employment of differential relays for protecting microgrids has been suggested in some papers [60]-[62]. Expanding on the ideas presented in [60] and [61], reference [62] proposes a protection scheme using communication-assisted digital relays for protection of microgrids with customer-owned DERs. However, the proposed strategy, which relies on differential currents, is expected to be costly, and assumes technical features that are absent in the state-of-the-art equipment.

Another approach proposed for protection of microgrids is the use of voltage measurements [63]-[65]; in particular, reference [65] presents a voltage-based protection method in a rotating frame, which seems suitable for islanded microgrids. However, the proposed method does not consider the grid-connected mode of operation, single-phase tripping, and high-impedance faults. In reference [66], a fault detection method has been presented for microgrids with a high penetration of EC-DERs. The method, however, does not consider the grid-connected mode of operation. Moreover, no study results have been presented to validate the proposed strategy. References [67] and [68] propose the integration of energy storage devices with a high short-circuit capacity (e.g., a flywheel energy storage unit) into the microgrid. The proposed approach makes it possible to rely on the (modified) traditional overcurrent protection, but needs adaptive protective devices. Moreover, the cost associated with a dedicated energy storage device with a boosted short-circuit capacity is disadvantageous.

Finally, the thesis is summarized and concluded in Chapter 7. Chapter-wise summary of the thesis, the conclusions of the conducted research, and the future areas of research are also included in this chapter.

## 1.7 Summary and Conclusion

A brief introduction to the concept of the microgrid and its importance for future power systems were provided in this chapter. Challenges associated with microgrids and the motivations behind the conducted research were also discussed. Further, the research objectives, contribution and outline of the thesis, and literature survey pertinent to thesis contributions are presented in the chapter. Mathematical modeling and control of EC-DERs are discussed in the following chapter.

# Chapter 2

## Control of EC-DERs

### 2.1 Introduction

As discussed in Chapter 1, control of a microgrid requires fast and reliable regulation of the magnitude and frequency of the DER terminal voltage. This task, however, is more challenging under network faults and severe unbalanced conditions. In this chapter, a control strategy is proposed for EC-DERs to improve the performance of the host microgrid under network faults and transient disturbances. The chapter first reviews the mathematical modeling and control design of three-phase EC-DERs. The basic control strategy is then modified for a multi-unit microgrid under system imbalances, network faults, load switching, and transient incidents. Modeling and control of single-phase EC-DERs are also discussed in this chapter, and a generic model for single-phase EC-DERs is presented.

The proposed control strategy takes advantage of a Phase-Locked Loop (PLL) and thus avoids the use of external frequency synthesizer. The PLL, however, has been modified for unbalanced conditions. The proposed control strategy does not require controller mode switchings and enables the EC-DERs to ride through network faults, irrespective of whether they take place within the host microgrid or impact the upstream grid. Moreover, the proposed control ensures an acceptable power quality for the duration of the faults, which is an important feature for protection against certain classes of faults, as well as for sensitive loads. Further, this chapter proposes a supplementary control loop that improves the microgrid post-fault recovery; the controllers also enable safe reconnection of the microgrid to the host grid. The effectiveness of the proposed control strategy is demonstrated through a comprehensive set of simulation studies, conducted in

the PSCAD/EMTDC software environment. PSCAD (Power System Computer-Aided Design) is an electromagnetic power transient software that is widely used to carry out simulation and/or visualization of the simulation in the electric power system [69].

## 2.2 Network Faults and Their Implications on the Control of EC-DETs

Network faults can be broadly classified under “*symmetrical*” and “*asymmetrical*” faults [70]. Symmetrical faults are those that equally affect all three phases; thus, the three-phase voltages experience the same condition in terms of their amplitudes (no phase shift is experienced), and the system remains balanced. Symmetrical faults are quite rare and constitute about 5% of network faults [26]. Three-phase faults are the members of this class. By contrast, an asymmetrical or unbalanced fault is one that does not equally affect all the three phases. Therefore, the three-phase voltages exhibit different voltage sags and, usually, phase shifts also develop between them. Single-phase-to-ground, double-phase-to-ground, and phase-to-phase faults are the members of this class.

References [71] and [72] provide a detailed description of grid faults with an emphasis on asymmetrical faults. In reference [72], the impact of transformer winding configuration on asymmetrical faults has been investigated, and it is shown that the interconnection transformers may influence the way that the network voltage appears at the DER terminals. As discussed in [72], all asymmetrical faults create both uneven voltage magnitudes and phase angle jumps at the DER terminals, when a  $\Delta$ /GY (Delta/Grounded-Wye) transformer is used as an interface connection between the DER and the network. An important characteristic of an asymmetrical fault is the appearance of a negative-sequence voltage component at the DER terminals. This results in double frequency oscillations and/or harmonic distortion in the DER voltages, currents, and control parameters; it also compromises reactive power regulation [73], [74]. These oscillations can, thus, lead to negative influences on the control of the VSCs, e.g., producing a non-sinusoidal current reference. Further, the network power quality degrades and even power system protection may be affected [48], [50].

Another major issue arises when a fault or transient incident impacts a multi-unit microgrid. In this situation, the EC-DETs cannot quickly retrieve their steady-state operating points, subsequent to the clearance of a temporary/permanent fault. This can particularly affect the microgrid in the islanded mode of operation, as will be further

discussed in Section 2.5.3. Considering the above discussion, the influence of the network faults on the control of EC-DETs must be investigated. The main objective of this chapter is to propose a control strategy for three-phase EC-DETs when running on network faults or transient disturbances, such that the aforementioned issues are resolved. The control scheme employed for single-phase EC-DETs is also briefly discussed in Section 2.6; however, the control of conventional rotating-machine-based DETs is not presented in this chapter, as it is beyond the purpose of this study.

## 2.3 Structure of the EC-DEt

Fig. 2.1 illustrates a schematic diagram of the three-phase EC-DEt considered in this study. The EC-DEt consists of (i) a DC voltage source, which represents a conditioned prime energy source augmented with an energy storage device, connected in parallel with the VSC DC-side terminals and DC-link capacitor  $C_{dc}$ ; (ii) a current-controlled VSC; (iii) a three-phase low-pass LC filter; and (iv) the interface switch  $SW$  which ensures that the EC-DEt unit can be connected to the rest of the microgrid only if its terminal voltage  $v_{sbac}$  is in phase with the network voltage  $v_{gabc}$  (this process is referred to as the “*local DEt synchronization*” and will be explained in Section 2.5.4). The circuit components  $L_s$  and  $C_s$  respectively denote the inductance and capacitance of the LC filter, and  $R_s$  represents the ohmic loss of  $L_s$  and also embeds the effect of the on-state resistance of the VSC switches. The EC-DEt exchanges with the rest of the microgrid (including the interconnection transformer Tr) the real- and reactive-power components  $P_s$  and  $Q_s$ , by adjusting the phase angle and magnitude of the voltage  $v_{sbac}$ .

## 2.4 Basic Control Strategy for EC-DEt

This section reviews the mathematical model and control strategy that are proposed in [20] and [33] for a three-phase EC-DEt. The section also presents modifications that are required to protect the VSC against overcurrents and to enable operation of the EC-DEt in a multi-unit microgrid.

### 2.4.1 Current-Control Scheme of the VSC

The function of the current-control scheme is to regulate  $i_{tabc}$ , that is, the VSC AC-side current, by means of the Pulse-Width Modulation (PWM) switching strategy. As Fig.



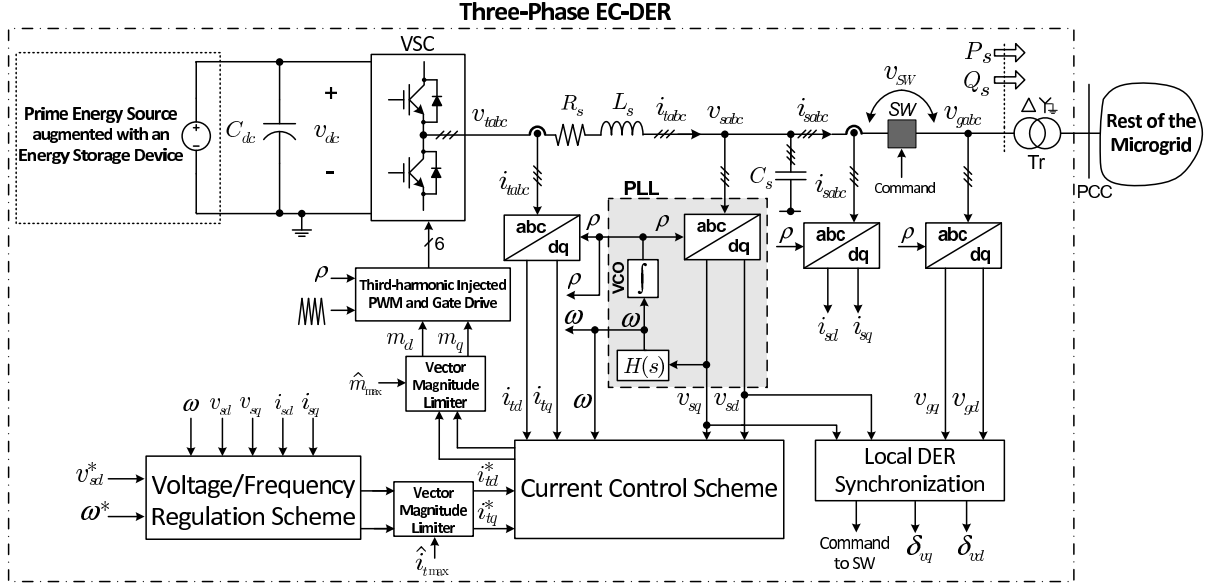


Figure 2.1: Schematic diagram of the three-phase EC-DER and its control architecture.

2.1 indicates, the control is performed in a  $dq$  reference frame whose  $d$ -axis makes angle  $\rho$  against the horizontal axis of the stationary frame [20]. The angle  $\rho$  is determined by a PLL which also calculates  $\omega$ , i.e., the frequency of the EC-DER terminal voltage  $v_{sabc}$ .

Dynamics of the  $dq$ -frame components of  $i_{tabc}$  are governed by [33]

$$L_s \frac{di_{td}}{dt} = -R_s i_{td} + L_s \omega i_{tq} + m_d \left( \frac{v_{dc}}{2} \right) - v_{sd}, \quad (2.1)$$

$$L_s \frac{di_{tq}}{dt} = -R_s i_{tq} - L_s \omega i_{td} + m_q \left( \frac{v_{dc}}{2} \right) - v_{sq}, \quad (2.2)$$

where  $m_d$  and  $m_q$  respectively denote the  $d$ - and  $q$ -axis components of the three-phase PWM modulating signal  $m_{abc}(t)$ . The variable  $\omega$  is related to the angle  $\rho$  as

$$\omega = \frac{d\rho}{dt}. \quad (2.3)$$

Fig. 2.2 illustrates a block diagram of the current-control scheme, indicating that  $i_{td}$  and  $i_{tq}$  are first compared to their respective setpoints,  $i_{td}^*$  and  $i_{tq}^*$ , and the errors signals are processed by two corresponding Proportional-Integral (PI) compensators. The compensator outputs are then augmented with feed-forward and decoupling signals<sup>1</sup> (to

<sup>1</sup>The signals are calculated based on Equations (2.1) and (2.2).

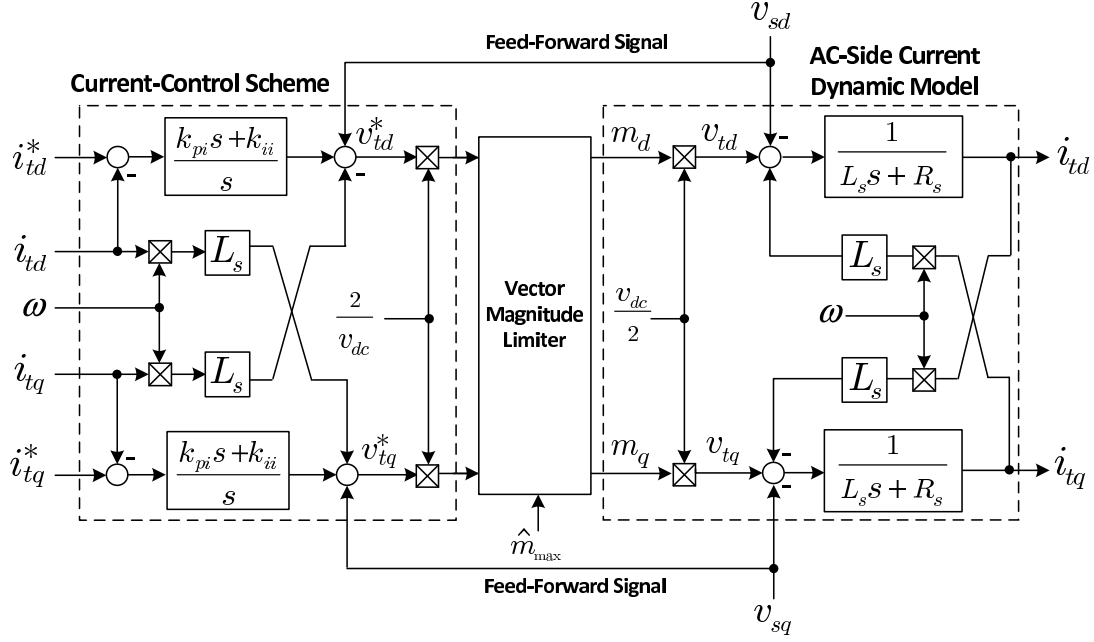


Figure 2.2: Block diagram of the current-control scheme of the three-phase EC-DER.

mitigate the impact of load voltage variations on the regulation of  $i_{td}$  and  $i_{tq}$ ), and the resulting signals are normalized to the VSC gain  $v_{dc}/2$  and produce  $m_d$  and  $m_q$  for the PWM gating pulse generator. Finally, using the angle  $\rho$ , the PWM gating pulse generator transforms  $m_d$  and  $m_q$  to  $m_{abc}(t)$ , compares each component of  $m_{abc}(t)$  to a high-frequency carrier signal, and determines the switching instants for each leg of the converter.

To operate the VSC in its linear modulation region,  $m_d$  and  $m_q$  are limited by a block that ensures  $\sqrt{m_d^2 + m_q^2} \leq \hat{m}_{max}$ , where  $\hat{m}_{max}$  is the maximum permissible magnitude of  $m_{abc}(t)$ ; it is unity for the conventional PWM strategy, and 1.15 for PWM with third-order harmonic injection [20]. The module, labeled in Figs. 2.1 and 2.2 as the “vector magnitude limiter”, however, does not change the ratios  $m_d/\sqrt{m_d^2 + m_q^2}$  and  $m_q/\sqrt{m_d^2 + m_q^2}$  (i.e., it does not change the phase angle of  $m_{abc}(t)$ ).

If the PI compensator gains are chosen as

$$k_{pi} = \frac{L_s}{\tau_i}, \quad (2.4)$$

and

$$k_{ii} = \frac{R_s}{\tau_i}, \quad (2.5)$$

then the closed-loop current-control scheme becomes equivalent to two decoupled first-order systems described by

$$\frac{I_{td}(s)}{I_{td}^*(s)} = \frac{1}{\tau_i s + 1}, \quad (2.6)$$

$$\frac{I_{tq}(s)}{I_{tq}^*(s)} = \frac{1}{\tau_i s + 1}, \quad (2.7)$$

in which the design parameter  $\tau_i$  turns out to be the time-constant of the closed-loop step responses. As Fig. 2.1 shows,  $i_{td}^*$  and  $i_{tq}^*$  are limited by a corresponding vector magnitude limiter to ensure that  $\sqrt{(i_{td}^*)^2 + (i_{tq}^*)^2} \leq \hat{i}_{tmax}$ , where  $\hat{i}_{tmax}$  is the maximum permissible magnitude of the VSC AC-side current and is, typically, larger than the VSC rated current magnitude by about 20 to 50 percent. The process ensures that the VSC is protected against fault incidents and overload conditions. It is again noted that the vector magnitude limiter does not change the ratios  $i_{td}^*/\sqrt{(i_{td}^*)^2 + (i_{tq}^*)^2}$  and  $i_{tq}^*/\sqrt{(i_{td}^*)^2 + (i_{tq}^*)^2}$  (i.e., does not change the phase angle of  $i_{tabc}^*(t)$ ).

## 2.4.2 Voltage Magnitude Regulation Scheme

The objective of the voltage magnitude regulation scheme is to regulate  $\hat{v}_s$ , that is, the magnitude of  $v_{sabc}$  ( $\hat{v}_s = \sqrt{v_{sd}^2 + v_{sq}^2}$ ). As will be discussed in Section 2.4.4, the voltage component  $v_{sq}$  is controlled in a scheme that is referred to as the “*frequency regulation scheme*”. It will also be discussed that the steady-state value of  $v_{sq}$  is zero. Therefore, the regulation of  $\hat{v}_s$  boils effectively down to the regulation of  $v_{sd}$  at the magnitude setpoint  $v_{sd}^*$  [33]. In a single-unit microgrid,  $v_{sd}^*$  can be assigned a value equivalent to the nominal magnitude of the network voltage. In a multi-unit system, however,  $v_{sd}^*$  is commonly obtained from the droop characteristic

$$v_{sd}^* = D_Q(Q^* - Q) + V_0, \quad (2.8)$$

where  $Q^*$  denotes the setpoint for the reactive-power output of the EC-DER in the grid-connected mode of operation, and  $V_0$  signifies the nominal network voltage magnitude;  $Q$  is the reactive-power output of the EC-DER, and the constant parameter  $D_Q$  is the droop coefficient. It should be noted that any exchange of reactive power between the EC-DER and the network requires a difference between the magnitudes of the DER terminal and

network voltages. Therefore, based on (2.8),  $Q$  tracks  $Q^*$  with some steady-state error, unless  $Q^*$  is set to zero. The steady-state error can be avoided if  $v_{sd}^*$  includes the integral of the signal  $Q^* - Q$  [31]; however, this option has not been exercised in this thesis.

Dynamics of  $v_{sd}$  and  $v_{sq}$  are governed by [33]

$$C_s \frac{dv_{sd}}{dt} = C_s \omega v_{sq} + i_{td} - i_{sd}, \quad (2.9)$$

$$C_s \frac{dv_{sq}}{dt} = -C_s \omega v_{sd} + i_{tq} - i_{sq}, \quad (2.10)$$

which suggest that the DER terminal voltage (i.e.,  $v_{sd}$  and  $v_{sq}$ ) can be controlled by the VSC AC-side current (i.e.,  $i_{td}$  and  $i_{tq}$ ). Equations (2.9) and (2.10) also indicates that the DER output current components, that is,  $i_{sd}$  and  $i_{sq}$ , are the responses of the rest of the microgrid to  $v_{sd}$ ,  $v_{sq}$ , and  $\rho$ . In general, dynamics of  $i_{sd}$  and  $i_{sq}$  are coupled, nonlinear, time varying, and of a high order. Thus, the control of  $v_{sd}$  and  $v_{sq}$  is not a straightforward task, from the controller tuning and stability viewpoints. Hence, measures of  $i_{sd}$  and  $i_{sq}$  should also be included in the control process, as feed-forward signals.

The regulation of  $v_{sd}$  and  $v_{sq}$  at their respective setpoints is achieved through the scheme of Fig. 2.3, illustrating that the error signals  $v_{sd}^* - v_{sd}$  and  $v_{sq}^* - v_{sq}$  are processed by two corresponding PI compensators and produce the current setpoints  $i_{td}^*$  and  $i_{tq}^*$ . Fig. 2.3(b) also shows that measures of  $i_{sd}$  and  $i_{sq}$  are added as feed-forward signals to the outputs of the two compensators; the objective is to weaken the dynamic linkage between the EC-DEr and the rest of the microgrid. Fig. 2.3 further shows that the coupling between  $v_{sd}$  and  $v_{sq}$  is compensated for, through the inclusion of proper feed-forward signals. The outcome is that the closed-loop control system is split, approximately, to two decoupled single-input-single-output control loops, as shown in Figs. 2.4(a) and (b); the compensator design for the loops of Fig. 2.4 is quite straightforward.

### 2.4.3 Phase-Locked Loop (PLL)

As indicated in Section 2.4.1, the angle  $\rho$  is used for the *abc-to-dq* frame transformations and also for the *dq-to-abc* frame transformation. The angle is calculated by means of a PLL whose schematic diagram is shown in Fig. 2.5. As indicated in the figure, the PLL transform  $v_{sabc}$  to  $v_{sdq}$  and adjusts the rotational speed of the *dq*-frame, that is,  $\omega$ , in such a way that  $v_{sq}$  is forced to zero in the steady state [75]. Fig. 2.5 also shows that the

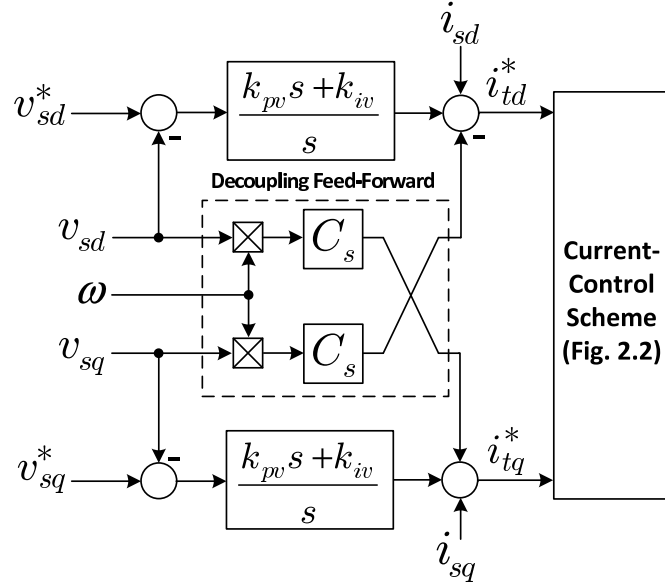


Figure 2.3: Block diagram of the voltage magnitude regulation scheme of the three-phase EC-DER.

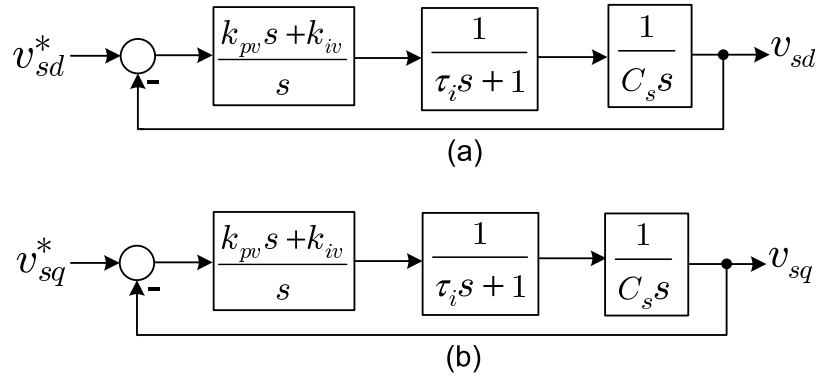


Figure 2.4: Block diagrams of the equivalent decoupled loops for regulation of  $v_{sd}$  and  $v_{sq}$ .

PLL processes  $v_{sq}$  through a filter,  $H(s)$ , and determines  $\omega$ . The control of  $\omega$  then, based on (2.3), results in determination of  $\rho^1$ . The process requires  $H(s)$  to have at least one pole at the origin of the complex frequency plane ( $s=0$ ), and is described by the equation

$$\Omega(s) = H(s)V_{sq}(s), \quad (2.11)$$

<sup>1</sup>Assuming  $v_{sa} = \hat{v}_s \cos(\omega_0 t + \theta_0)$ , the end result is that  $\rho = \omega_0 t + \theta_0$  and  $v_{sd} = \hat{v}_s$ .

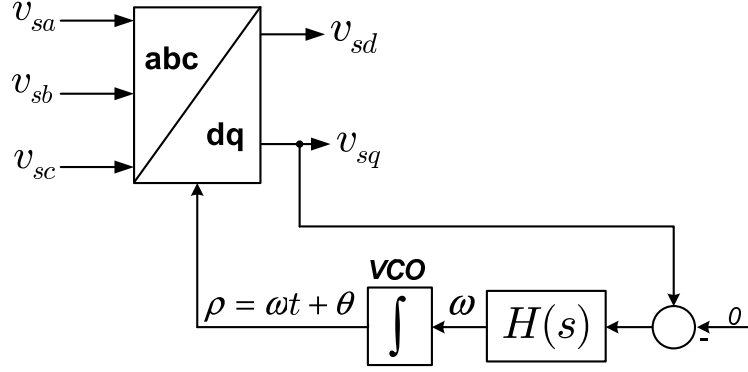


Figure 2.5: Schematic diagram of the PLL.

in which  $\Omega(s)$  and  $V_{sq}(s)$  denote Laplace transforms of  $\omega$  and  $v_{sq}$ , respectively. It should be pointed out that in the block diagram of Fig. 2.5, the integrator of (2.3) is realized by means of a Voltage-Controlled Oscillator (VCO). The VCO can be regarded as a resettable integrator whose output,  $\rho$ , is reset to zero whenever it reaches  $2\pi$ .

#### 2.4.4 Frequency Regulation Scheme

The objective of the frequency regulation scheme is to regulate  $\omega$ , that is, the frequency of  $v_{sabc}$ , at the setpoint  $\omega^*$ . In a single-unit microgrid,  $\omega^*$  can be assigned a constant value corresponding to the network nominal frequency, e.g., 377 rad/s for a 60-Hz power system. However, in a multi-unit microgrid,  $\omega^*$  is determined by the droop characteristic

$$\omega^* = D_P(P^* - P) + \omega_0, \quad (2.12)$$

for which  $P^*$  denotes the setpoint for the real-power output of the EC-DER in the grid-connected mode of operation, and  $\omega_0$  signifies the nominal power system frequency;  $P$  is the real-power output of the EC-DER, and the constant parameter  $D_P$  is the droop coefficient.

In the islanded mode of operation,  $\omega$  can be regulated by  $v_{sq}$ , based on (2.11) and through the control of  $v_{sq}^*$ . This is achieved by the control loop of Fig. 2.6, in which the error between  $\omega$  and  $\omega^*$  is processed by a compensator,  $K_\omega(s)$ , and  $v_{sq}^*$  is constructed for the  $q$ -axis magnitude regulation loop (see Figs. 2.3 and 2.4(b)). As mentioned earlier,  $H(s)$  includes an integrator. Hence, to ensure a zero steady-state error,  $K_\omega(s)$  is sufficient to be a pure gain, i.e.,

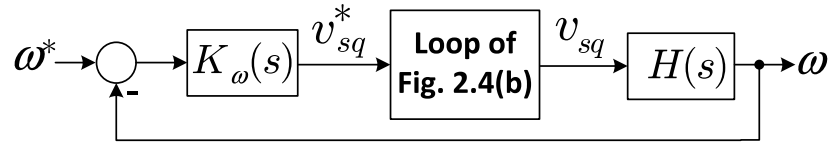


Figure 2.6: Block diagram of the frequency regulation loop.

$$K_{\omega}(s) = k_{\omega} . \quad (2.13)$$

## 2.5 Enhanced Control Strategy for EC-DETs

The following subsections outline the shortcomings of the basic control strategy of Section 2.4, and proposes modifications to overcome the issues and ensure proper operation of the EC-DEr under network faults and severe voltage imbalances. Moreover, a complementary control mechanism will be proposed that significantly improves the post-fault recovery of the EC-DEr and its host microgrid. The controllers also incorporate synchronization algorithms for safe reconnection of the islanded microgrid to the host grid.

### 2.5.1 Modifications to the Voltage Magnitude Regulation Scheme

The magnitude regulation scheme of Fig. 2.3 performs satisfactorily if the network voltage is fairly balanced. However, under an unbalanced voltage condition, e.g., due to an asymmetrical network fault, the  $dq$ -frame components of the voltage and current are distorted by double-frequency ripple components, as will be further discussed in Section 2.5.2. The distortions, in turn, deteriorate the quality of the corresponding three-phase waveforms. Hence, the magnitude regulation scheme of Fig. 2.3 is modified in this section to that shown in Fig. 2.7. In the modified scheme, the signals  $i_{sd}$ ,  $i_{sq}$ ,  $v_{sd}$ , and  $v_{sq}$  are passed through corresponding notch filters that eliminate the double-frequency ripple components. The resonant frequency of the notch filters is placed at two times the nominal microgrid frequency, e.g., 120 Hz for a 60-Hz power system. In addition, the PI compensators (see Fig. 2.3) are replaced by more elaborate linear compensators,  $K_v(s)$ . The compensator must include a factor that exhibits a significant gain drop at the second harmonic of the network (nominal) frequency, in addition to an integral term; thus,  $K_v(s)$  has a general form as the following equation

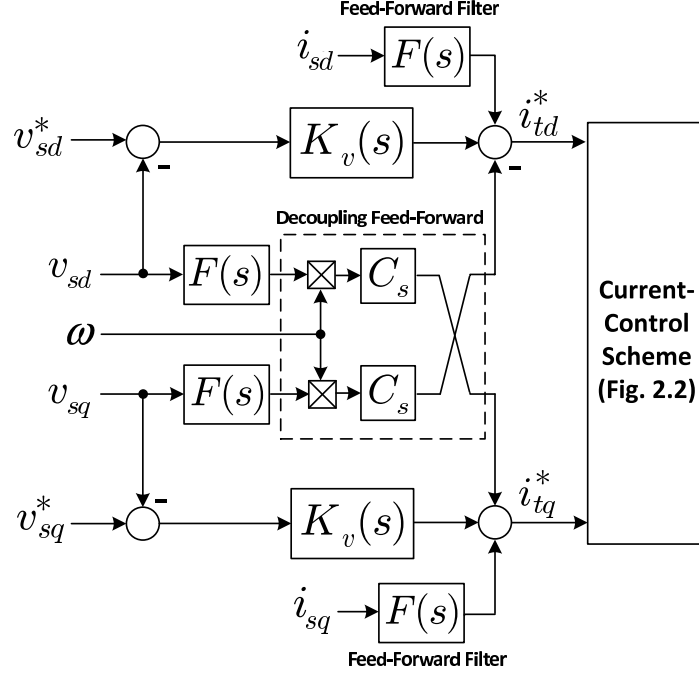


Figure 2.7: Block diagram of the enhanced voltage magnitude regulation scheme for the three-phase EC-DER.

$$K_v(s) = \frac{s^2 + 2\frac{b}{a}\omega_t s + \omega_t^2}{s^2 + 2\frac{1}{a}\omega_t s + \omega_t^2} \cdot \frac{L(s)}{s} , \quad (2.14)$$

In (2.14),  $\omega_t$  is the tuned frequency; other factors of  $K_v(s)$  (i.e.,  $a$ ,  $b$ , and  $L(s)$ ) must be determined based on the desired bandwidth and stability margins for the  $d$ - and  $q$ -axis voltage regulation loops (replace the PI compensators with  $K_v(s)$  in Figs. 2.4(a) and (b)). In this study,  $K_v(s)$  has been designed with the use of bode diagrams.

## 2.5.2 Modifications to the Phased-Locked Loop

As discussed in Section 2.5.1, under an unbalanced voltage condition,  $v_{sq}$  possesses a double-frequency pulsating component, which, if not filtered, distorts  $\rho$  and  $\omega$ ; the distortions of  $\rho$  and  $\omega$ , in turn, entail distortions in the AC voltages and currents of the EC-DER. Under faulty conditions, instantaneous quantities of unbalanced voltages can be represented as

$$v_{sabc} = v_{sabc}^p + v_{sabc}^n + v_{sabc}^0 , \quad (2.15)$$



where subscripts “ $p$ ”, “ $n$ ”, and “ $0$ ” respectively denote positive-, negative-, and zero-sequence components. Since zero-sequence components of unbalanced voltage sags do not exist in three-wire systems, nor can they propagate to the secondary side of delta (or ungrounded star) transformer configurations in four-wire systems, only positive- and negative-sequence components are considered in this study. Even for unbalanced systems with zero-sequence voltages, four-leg inverter topologies can eliminate zero-sequence currents through an appropriate control scheme. Therefore, the matrix form of (2.15) can be expressed as

$$\begin{bmatrix} v_{sa} \\ v_{sb} \\ v_{sc} \end{bmatrix} = V_{sp} \begin{bmatrix} \cos(\omega t + \theta_p) \\ \cos(\omega t + \theta_p - \frac{2\pi}{3}) \\ \cos(\omega t + \theta_p + \frac{2\pi}{3}) \end{bmatrix} + V_{sn} \begin{bmatrix} \cos(\omega t + \theta_n) \\ \cos(\omega t + \theta_n + \frac{2\pi}{3}) \\ \cos(\omega t + \theta_n - \frac{2\pi}{3}) \end{bmatrix}, \quad (2.16)$$

where  $V_{sp}$  and  $V_{sn}$  are the voltage magnitude of the positive- and negative-sequence voltages, respectively;  $\theta_p$  and  $\theta_n$  respectively signify the phase angle of the positive- and negative-sequence voltages. The space-vector equivalent of (2.16) is represented as

$$\vec{v}_s = V_{sp} e^{j(\omega t + \theta_p)} + V_{sn} e^{-j(\omega t + \theta_n)}, \quad (2.17)$$

where the space phasor is defined by the generic equation  $\vec{f}(t) = (2/3)(f_a(t)e^{j0} + f_b(t)e^{j2\pi/3} + f_c(t)e^{j4\pi/3})$  in which  $f_a(t)$ ,  $f_b(t)$ , and  $f_c(t)$  constitute a three-phase signals or (current/voltage) waveforms. The PLL transforms  $\vec{v}_s$  to  $v_{sdq}$  based on the following equation [20]

$$v_{sdq} = v_{sd} + jv_{sq} = \vec{v}_s e^{-j\rho}, \quad (2.18)$$

By forcing  $v_{sq}$  to zero, the PLL actually attempts to adjust  $\rho$  in order to ensure that  $\rho = \omega t + \theta_p$  (assuming that the amplitude of the positive-sequence components are higher than the negative-sequence ones in normal conditions). Thus, equation (2.18) can be rewritten as

$$v_{sd} + jv_{sq} = V_{sp} + V_{sn} e^{-j(2\omega t + \theta_n + \theta_p)} \quad (2.19)$$

Equation (2.19) is split into

$$v_{sd} = V_{sp} + \cos(2\omega t + \theta_n + \theta_p), \quad (2.20)$$

$$v_{sq} = \sin(2\omega t + \theta_n + \theta_p) , \quad (2.21)$$

The recent equations show that  $d$ - and  $q$ -axis components of the EC-DER terminal voltage under faulty conditions include double-frequency harmonics in addition to their DC components. Thus, transfer function of the PLL, i.e.,  $H(s)$ , cannot be selected as a simple PI compensator. To filter the pulsating components of  $v_{sq}$ , the filter  $H(s)$  must also have the property of exhibiting a low gain at the second harmonic of the power system (nominal) frequency, that is

$$H(s) = \frac{s^2 + 2\frac{b}{a}\omega_t s + \omega_t^2}{s^2 + 2\frac{1}{a}\omega_t s + \omega_t^2} \cdot \frac{T(s)}{s} , \quad (2.22)$$

where  $\omega_t$  is the tuned frequency; parameters  $a$  and  $b$  and the transfer function  $T(s)$  are specified in such a way to fulfill the requirement of the control loop shown in Fig. 2.5.

### 2.5.3 Proposed Phase-Angle Restoration Scheme

One major issue in a multi-unit microgrid is that, subsequent to a temporary fault, the EC-DERs do not quickly reclaim their pre-disturbance operating conditions. This is also the case when the host microgrid undergoes a major transient disturbance, e.g., when it slides from the islanded mode of operation to the grid-connected mode of operation, or vice versa. The reason is that major transient incidents often significantly disturb the magnitude and frequency of the terminal voltages of the EC-DERs (and to a lesser extent those of rotating-machine-based DERs), and the frequency excursions result in phase shifts in the DER terminal voltages. By contrast, the frequency setpoints of the EC-DERs do not deviate much from their pre-disturbance steady-state values as the droop coefficients are relatively small. The terminal voltage phase shifts can, in turn, remarkably disturb the real- and reactive-power outputs of the EC-DERs, and may even lead to system instabilities. As expected, this effect is pronounced more in the islanded mode of operation.

To mitigate the aforementioned effect, it is proposed that the output of the compensator  $K_\omega(s)$  (see Fig. 2.6) be augmented with an auxiliary signal,  $u_\rho$ , which is obtained from a mechanism that is illustrated in Fig. 2.8 and referred to as the “*phase-angle restoration scheme*”. The function of the phase-angle restoration scheme is to expedite the post-disturbance recovery of the phase angle of the terminal voltage of the host EC-DER. As Fig. 2.8 shows, a compensator,  $K_\rho(s)$ , processes the error  $e_\rho = \rho^* - \rho$  and

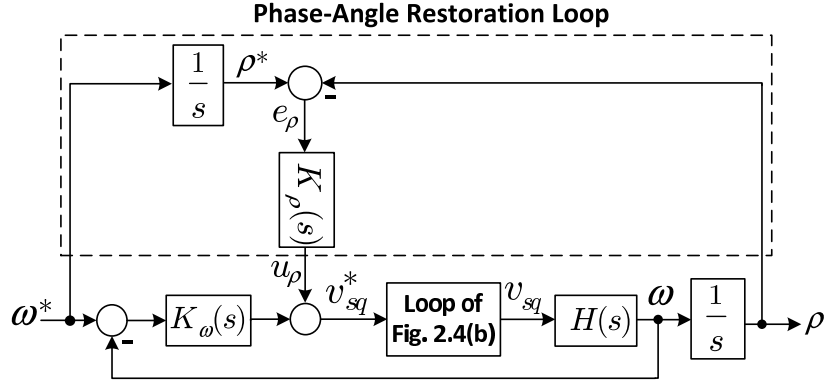


Figure 2.8: Block diagram of the frequency regulation loop, augmented with the proposed phase-angle restoration loop.

generates the signal  $u_\rho$  which augments the setpoint  $v_{sq}^*$ ; the setpoint  $\rho^*$  is, in turn, calculated from the frequency setpoint, based on  $\rho^* = \int_0^t \omega^* d\tau$ . Since the process inherently involves signal integration,  $K_\rho(s)$  can be a pure gain:

$$K_\rho(s) = k_\rho. \quad (2.23)$$

In the absence of the proposed phase-angle restoration loop, even though  $\omega$  quickly settles once a transient disturbance subsides, the phase angle  $\rho$  takes a relatively long time to revert to its pre-disturbance value relative to the other DETs, due to the integral relationship between  $\omega$  and  $\rho$ . The phase-angle drift, which has developed due to the deviation of  $\omega$  from  $\omega^*$  during the transient period, results in remarkable output power shocks. However, the phase-angle restoration loop attempts to regulate  $\rho$  at its reference command  $\rho^*$ , through fine-tuning of  $v_{sq}^*$ . It is remembered that  $\omega^*$  (and thus  $\rho^*$ ) is adjusted through the droop mechanism and does not drift much during a transient incident, since the droop coefficients are typically small.

#### 2.5.4 Network-Wide and Local Synchronization Processes

A network-wide synchronization process is necessary prior to reconnecting an islanded microgrid to the upstream grid. The process ensures that the voltage phasors corresponding to the microgrid-side voltage ( $v_{Mabc}$ ) and the grid-side voltage ( $v_{Gabc}$ ) at the MMS are cophasal and of equal magnitudes, such that the instantaneous voltage across the MMS,  $v_{MMS}$ , is reasonably small for an adequately large time [76]. This objective is fulfilled by controlling the terminal voltage frequency and magnitude setpoints of the DETs

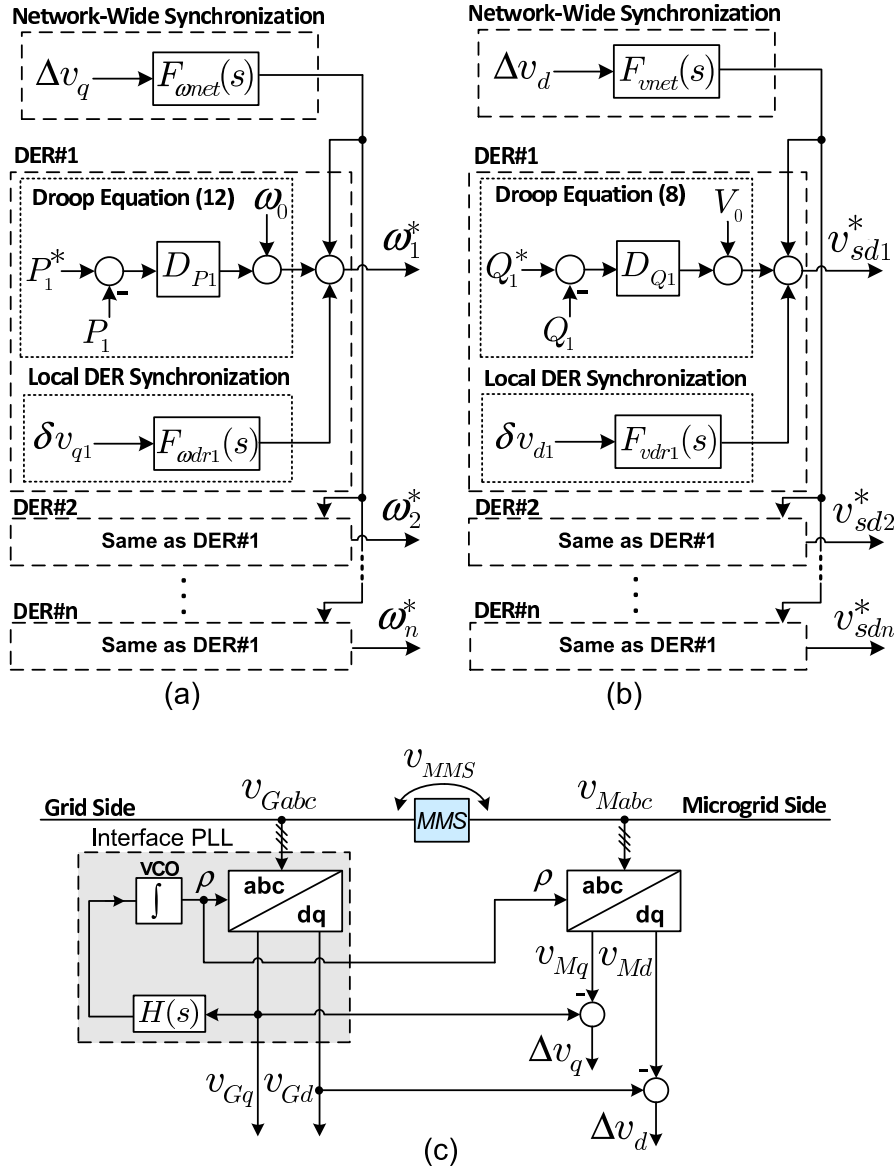


Figure 2.9: Block diagram of the scheme for network-wide and local synchronization processes: calculation of the (a) frequency setpoint, (b) voltage magnitude setpoint, and (c)  $d$ - and  $q$ -axis components of the voltage across the MMS.

through two corresponding filters,  $F_{\omega net}(s)$  and  $F_{v net}(s)$ , as illustrated in Figs. 2.9(a) and (b) (note the boxes labeled as “network-wide synchronization”). Fig. 2.9(c) shows that the inputs to the filters,  $\Delta v_d$  and  $\Delta v_q$ , are generated by a PLL, labeled as the “interface PLL”, that processes the grid-side voltage  $v_{Gabc}$  and the microgrid-side voltage  $v_{Mabc}$  (see also Fig. 2.11). Thus,  $\Delta v_d$  is proportional to the difference between the magnitudes of  $v_{Mabc}$  and  $v_{Gabc}$ , whereas  $\Delta v_q$  provides a measure of the phase difference between the two voltages. Hence,  $v_{Mabc}$  is forced to slowly track  $v_{Gabc}$ , in magnitude, phase angle, and fre-

quency, until both  $\Delta v_d$  and  $\Delta v_q$  become smaller, in absolute values, than corresponding thresholds [76]. It is noted that the signals  $\Delta v_d$  and  $\Delta v_q$  are communicated to the DERs by the microgrid supervisory intelligence.

Once the synchronization process is complete and the MMS closed, the microgrid supervisory intelligence sends a signal (not shown in the diagrams) to the DERs, to inhibit the process and preclude interference with the normal operation of the microgrid. The filters  $F_{\omega_{net}}(s)$  and  $F_{v_{net}}(s)$  can be of the PI type with small gains, to ensure that the magnitude and frequency of the DER terminal voltages vary gradually. This, in turn, avoids real- and reactive-power oscillations between the DERs during the synchronization process.

In addition to the network-wide synchronization mechanism described, each DER is also equipped with a local synchronization scheme. The local synchronization is achieved by aligning the voltage phasors corresponding to the voltages at the two sides of the interface switch that connects the DER to the microgrid (for example, switch SW in the EC-DER of Fig. 2.1). This task can be accomplished by augmenting the DER frequency and voltage magnitude setpoints with two corresponding corrective signals, as shown in Figs. 2.9(a) and (b) (note the boxes labeled as “*local DER synchronization*”). The corrective signals are obtained from two corresponding filters,  $F_{\omega_{dr}}(s)$  and  $F_{v_{dr}}(s)$ , which respectively process the signals  $\delta v_d$  and  $\delta v_q$ ; these two signals are the  $d$ - and  $q$ -axis components of the voltage across the interface switch, in the local  $dq$  frame of the host DER (see Fig. 2.1). Once the local synchronization process is complete, the interface switch is closed and the two corrective signals are inhibited, so that they do not interfere with the normal operation of the DER.

## 2.6 Generic Model of Single-Phase EC-DEs

The single-phase EC-DEs are modeled in this thesis based on the configuration of Fig. 2.10, in which the prime energy source is modeled by a dependent current source. The source current is determined by dividing a positive value, which can also be time-varying, by the DC voltage across the current source. The positive value represents the real power generated by a wind turbine or photovoltaic (PV) array, and is thus set based on assumed environmental conditions and/or the operation strategy (for example, the existence or absence of stall or pitch controls, maximum power-point tracking, etc.). As such, the

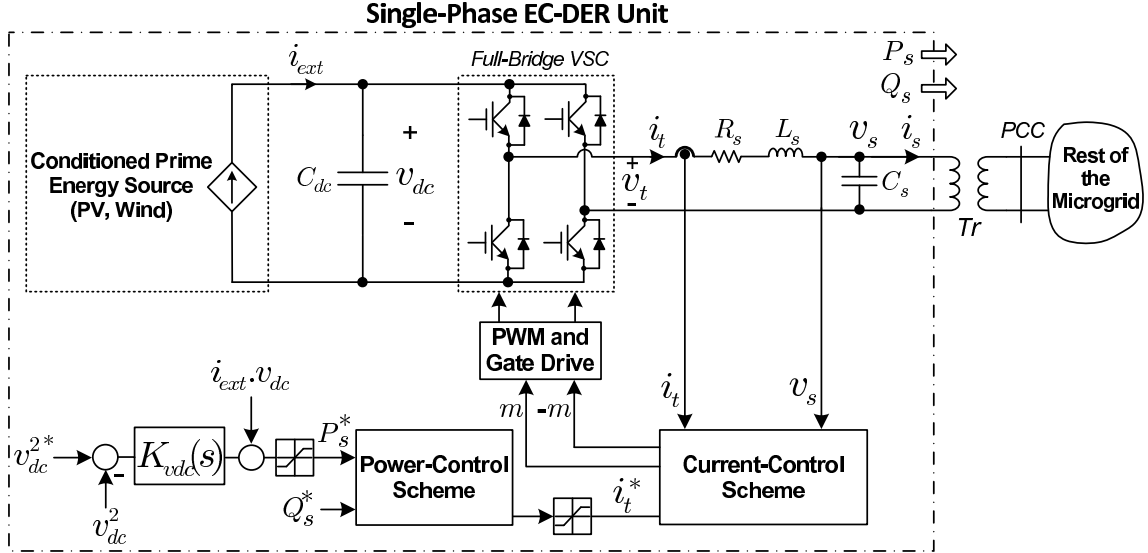


Figure 2.10: Generic model of single-phase EC-DERs.

current representing the prime energy source output is computed as

$$i_{ext} = P_{ext}/v_{dc}, \quad (2.24)$$

where, as mentioned above, the exogenous input  $P_{ext}$  can be assigned a positive waveform that corresponds to the power generated by a wind turbine or PV array, under the assumed environmental conditions.

A current-controlled full-bridge single-phase VSC regulates the voltage across the current source and, therefore, delivers to the network a real power that equals the assumed positive value,  $P_{ext}$ . In other words, the power output  $P$  tracks the waveform  $P_{ext}$  since the DC-link voltage  $v_{dc}$  is regulated by the VSC. The VSC can also regulate the reactive-power that is delivered to the network. In this study, however, the reactive-power output is set to zero, for unity power-factor operation. The aforementioned configuration and control strategy can emulate the behavior of small wind and PV energy systems that are employed in low- and/or medium-voltage distribution networks.

## 2.7 Test Microgrid and Study Cases

To assess the effectiveness of the proposed control strategy, a low-voltage microgrid has been modeled in the PSCAD/EMTDC software environment. Several study cases have been simulated to highlight the microgrid performance in the islanded and grid-connected

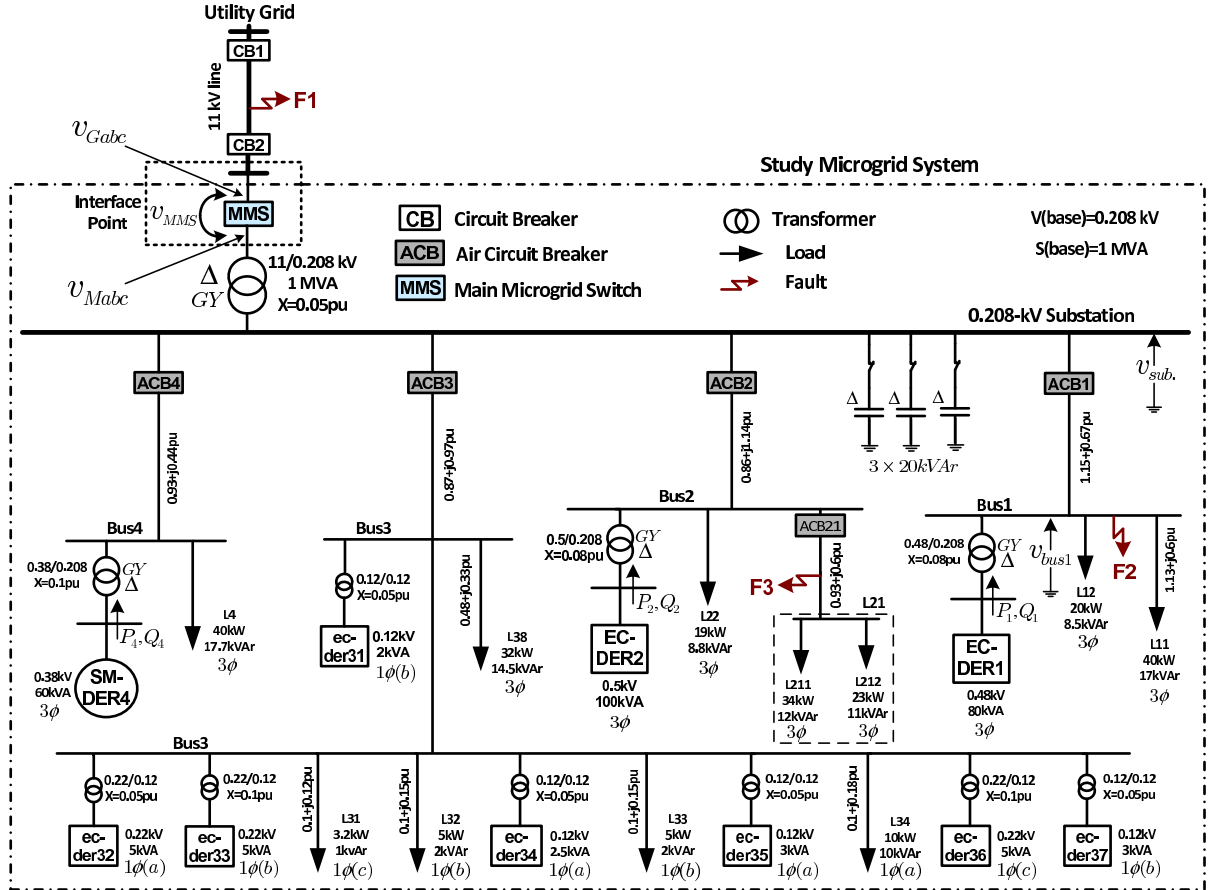


Figure 2.11: Single-line schematic diagram of the study low-voltage microgrid.

modes of operation. The cases are chosen such that they demonstrate both the steady-state and dynamic responses of the microgrid, under faults, transient incidents, and operating mode switching events. In the graphs to follow, currents are expressed in A, voltages in V, real powers in kW, and reactive powers in kVAr. Hereafter, the control strategy of Section 2.4 and the control strategy proposed in Section 2.5 are referred to as the “*basic control*” and “*enhanced control*”, respectively.

Fig. 2.11 shows a single-line diagram of the study microgrid. The microgrid is a 208-V, four-feeder, distribution network, which is interfaced with the host utility grid through a  $\Delta$ /GY substation transformer and a 11-kV line. The substation is equipped with three banks of three-phase shunt capacitors, each with a capacity of 20 kVAr, which can be switched on and off, automatically or by the system operator. The utility grid is equivalent to a 11-kV bus with a short-circuit capacity of 80 MVA. The configuration and line parameters of the network are taken from the benchmark system presented in [77] and [78]; some modifications have been made to allow for the operation of the microgrid

in the islanded mode, in the context of the North American power system.

As Fig. 2.11 shows, a combination of three-phase and single-phase loads are supplied by the four feeders. The microgrid includes two three-phase EC-DERs, i.e., EC-DER1 and EC-DER2, connected to Bus1 and Bus2, respectively, one synchronous-machine-based DER, i.e., SM-DER4, connected to Bus4, and seven single-phase EC-DERs, i.e., ec-der31 through ec-der37, which are all connected to Bus3. The three-phase DERs are interfaced with the microgrid through corresponding  $\Delta$ /GY interconnection transformers, whereas the single-phase EC-DERs utilize single-phase interconnection transformers.

The two three-phase EC-DERs are droop-controlled, as discussed in Section 2.4, and represent battery energy storage systems, or represent generators that are augmented with energy storage, such as fuel-cells augmented with supercapacitors; as such, they can act as both power sources and sinks. However, SM-DER4 can only source power; it, for example, represents a biomass-fueled generator. The DER parameters and controller compensators are given in Appendix A.

The single-phase EC-DERs are also modeled based on the discussion of Section 2.6. To enable simulation of the cases within manageable CPU times, the VSCs of the EC-DERs are replaced in the PSCAD models with their averaged-value equivalents [79]. Therefore, switching ripples are absent from the variables. This has allowed us to remove the filters from the model, with the assumptions of large switching frequency and filter bandwidths (which is quite achievable).

### 2.7.1 Grid-Connected Mode of Operation

**1) Response to Transient Disturbances:** This case demonstrates the effectiveness of the enhanced control strategy when the microgrid is subjected to a transient disturbance in the grid-connected mode of operation. Thus, at  $t = 2.0$ s, a temporary and bolted phase-to-ground (AG) fault strikes the 11-kV line at point F1, while the MMS is closed; the fault lasts for 5.5, 60-Hz cycles.

Figs. 2.12(a) and 2.13(a) represent the system response under the basic control strategy. As Fig. 2.12(a) shows, the voltage waveform of Bus1 becomes severely distorted for duration of the fault. Moreover, as Fig. 2.13(a) indicates, subsequent to the fault clearance, the real-power outputs of the three-phase EC-DERs do not revert to their respective pre-disturbance values (the current and reactive-power waveforms exhibit similar qualities, but are not shown due to space limitations). Figs. 2.12(b) and 2.13(b) represent the system response to the same fault, but when the enhanced control is employed for the



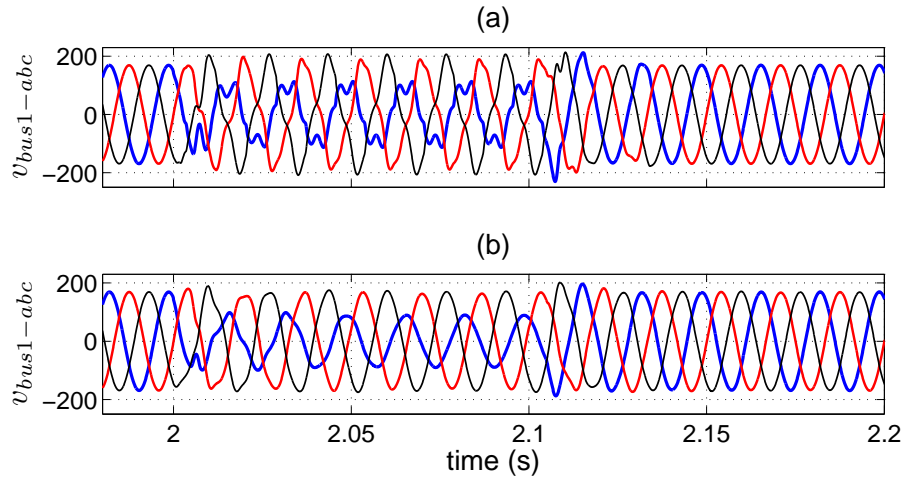


Figure 2.12: Waveforms of Bus1 voltage under a transient grid fault at point F1; (a) basic control and (b) enhanced control.

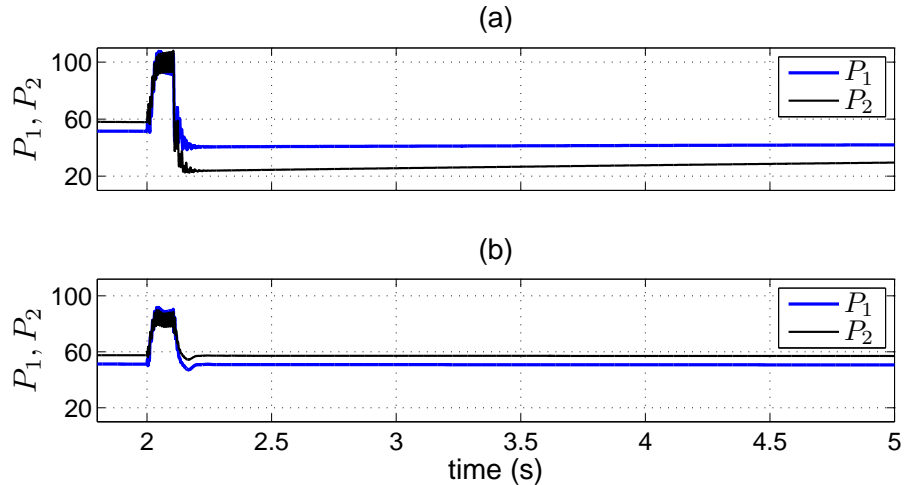


Figure 2.13: Real-power output waveforms of the three-phase EC-DERs under a transient grid fault at point F1; (a) basic control and (b) enhanced control.

EC-DERs. It is observed that, under the enhanced control the bus voltage is considerably less distorted, and the three-phase EC-DERs rapidly reclaim their pre-disturbance real-power outputs.

Fig. 2.14 shows the current response of EC-DER1 to a temporary fault at point F1 under the enhanced control strategy. Fig. 2.14(a) indicates the converter output current whereas Fig. 2.14(b) depicts the output current of the EC-DER. It is evident from the figure that the converter output current is kept balanced under the enhanced control,

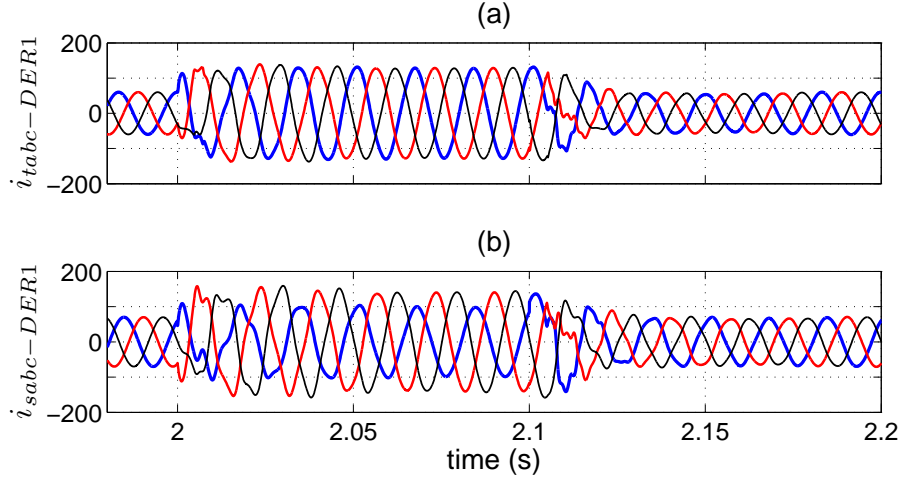


Figure 2.14: Waveforms of the (a) converter output current and (b) DER output current under a transient grid fault at point F1 (EC-DER1).

through the elimination of the double-frequency pulsating components. However, the output current of the EC-DER is still unbalanced as it is imposed by the network load.

**2) Response to Temporary Faults:** In this case, a temporary and bolted double-phase-to-ground (BCG) fault impacts the microgrid at point F1, Fig. 2.11. The fault lasts for longer than 5.5 cycles and, therefore, is isolated by triple-pole operation of the circuit breakers CB1 and CB2, in about 6 cycles from its inception; consequently, the microgrid gets islanded at  $t = 2.1$  s. The circuit breakers exercise triple-pole auto-reclosing to give the fault a chance to self-clear. Thus, the auto-reclosing process attempts to reconnect the microgrid to the utility grid, in about 24 to 30 cycles after the circuit breakers open, e.g., at  $t = 2.5$  s. In this case, since the fault is cleared before the first reclosure, the reclosing is successful.

Fig. 2.15 illustrates the real-power outputs of the two three-phase EC-DERs under the basic control (Fig. 2.15(a)) and enhanced control (Fig. 2.15(b)). It is observed that, under the enhanced control strategy, the power outputs of the EC-DERs are quickly retrieved. Fig. 2.16 illustrates the waveform of the magnitude of Bus1 voltage, under the basic control (Fig. 2.16(a)) and enhanced control (Fig. 2.16(b)). A comparison between Figs. 2.16(a) and (b) reveals that the bus voltage magnitude is to a large extent insensitive to the reclosing incidents under the enhanced control. The reason is that the phase-angle restoration loops of the three-phase EC-DERs prevent their respective voltage phase angles from drifting during the reclosing dead time and, thus, mitigate the

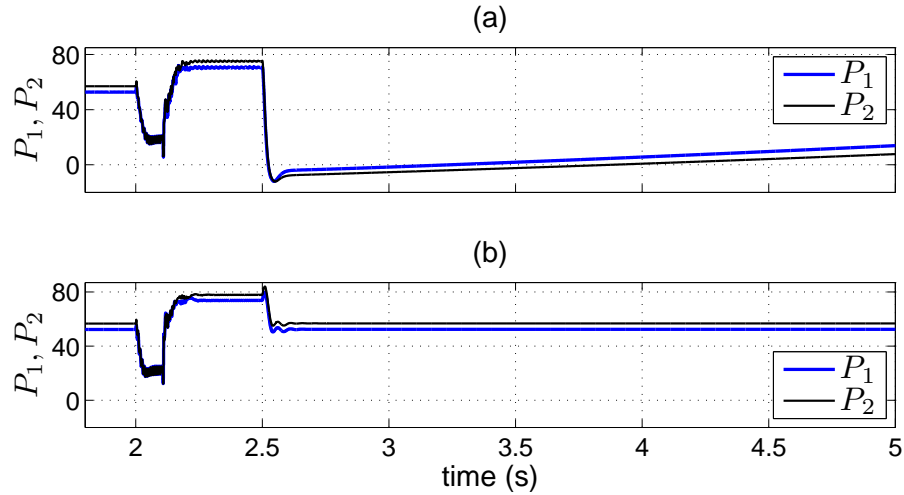


Figure 2.15: Real-power output waveforms of the three-phase EC-DERs during and subsequent to successful reclosure of the 11-kV line at  $t=2.5$  s; (a) basic control and (b) enhanced control.

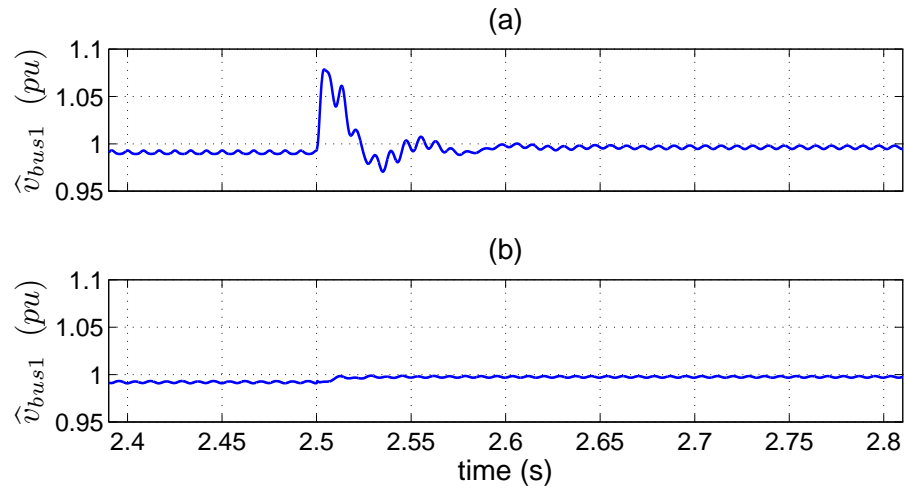


Figure 2.16: Waveforms of the magnitude of Bus1 voltage in response to successful reclosure of the 11-kV line at  $t=2.5$  s; (a) basic control and (b) enhanced control.

impact of out-of-phase reclosing. This is also evident from the waveforms of the voltage drop across MMS during the reclosing dead time, as shown in Fig. 2.17(a) (basic control) and Fig. 2.17(b) (enhanced control).

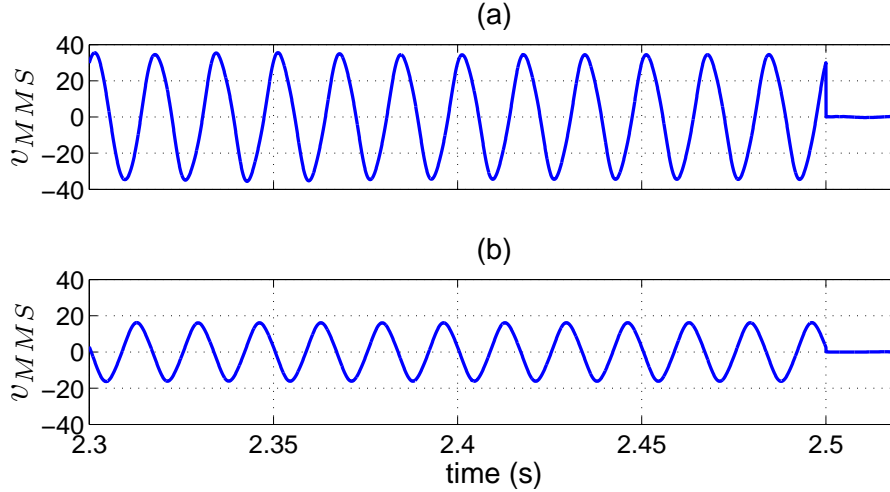


Figure 2.17: Waveforms of the voltage drop across MMS during the dead time of the reclosing process; (a) basic control and (b) enhanced control.

## 2.7.2 Islanded Mode of Operation

**1) Response to Transient Disturbances:** This case assumes that a temporary and bolted phase-to-ground (AG) fault impacts point F2 of the islanded microgrid and lasts for 5.5 cycles. Fig. 2.18 illustrates the power output waveforms of the two three-phase EC-DERs, under the basic control, (Fig. 2.18(a)) and enhanced control (Fig. 2.18(b)). It is observed that, under the enhanced control the two EC-DERs quickly reclaim their pre-disturbance shares of power, due to the phase-angle restoration loop of the EC-DERs. To demonstrate the impact of the phase-angle restoration loops, waveforms of the phase-angle error for the three-phase EC-DERs have been plotted in Fig. 2.19, under the basic control (Fig. 2.19(a)) and enhanced control (Fig. 2.19(b)). It is observed that, under the enhanced control the phase-angle errors remain fairly small, and rapidly decay to zero subsequent to the fault clearance. However, in the absence of the phase-angle restoration loop (basic control), the phase angle takes a relatively long time to revert to its pre-disturbance value due to the integral relationship between the frequency and phase angle. It should be pointed out that the value of the phase angle error and the phase-angle restoration time in the basic control strategy highly depends on the type, location, and severity of the fault. Fig. 2.20 illustrates the voltage waveform of Bus1 under the basic control (Fig. 2.20(a)) and enhanced control (Fig. 2.20(b)). The figures confirm that the voltage distortion is remarkably lower under the enhanced control, as compared to that under the basic control.

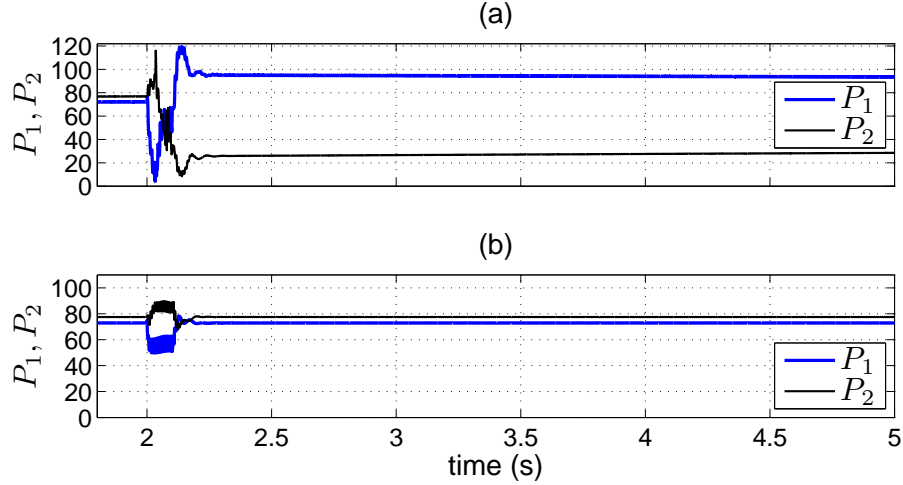


Figure 2.18: Real-power output waveforms of the three-phase EC-DERs under a temporary fault at point F2 of the islanded microgrid; (a) basic control and (b) enhanced control.

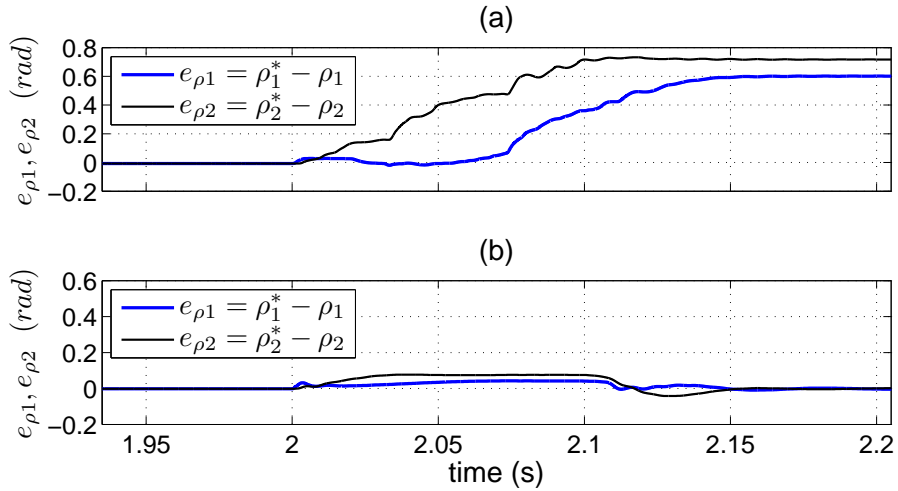


Figure 2.19: Waveforms of the phase-angle error for the three-phase EC-DERs under a temporary fault at point F2 of the islanded microgrid; (a) basic control and (b) enhanced control.

**2) Response to Permanent Faults:** In this case, it is assumed that a permanent double-phase-to-ground (BCG) fault impacts point F3 of the microgrid, Fig. 2.11, while the microgrid is islanded. Consequently, the relay that controls the circuit breaker ACB21 detects the fault in about 6 cycles and disconnects phases b and c of the load L21. Fig. 2.21 indicates the real-power output waveforms of the three-phase EC-DERs, under the basic control (Fig. 2.21(a)) and enhanced control (Fig. 2.21(b)). It is observed

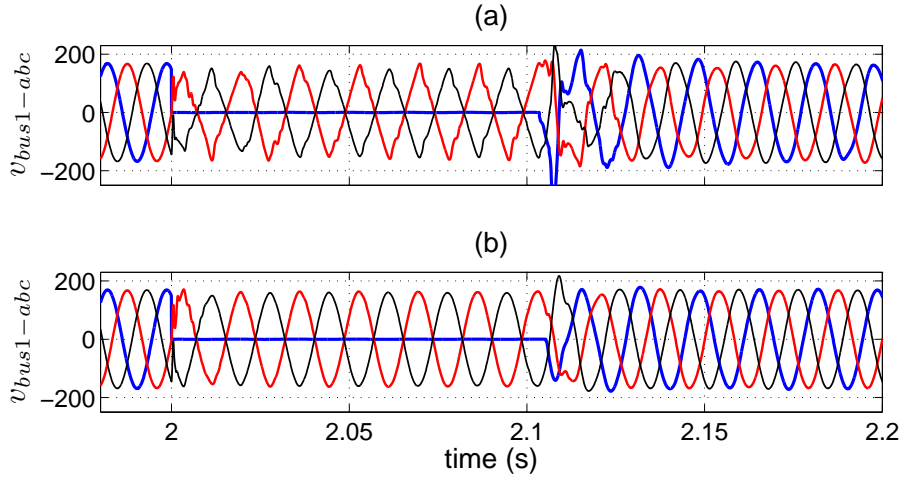


Figure 2.20: Waveforms of Bus1 voltage under a temporary fault at point F2 of the islanded microgrid; (a) basic control and (b) enhanced control.

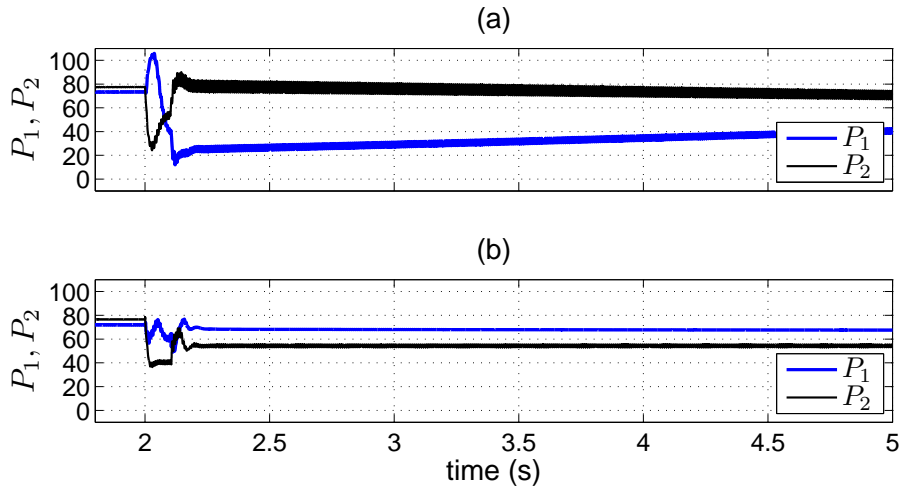


Figure 2.21: Real-power output waveforms of the three-phase EC-DERs under a permanent fault at point F3 of the islanded microgrid; (a) basic control and (b) enhanced control.

that, under the basic control the output powers are superimposed by significant ripple components and also take a long time to settle. By contrast, under the enhanced control the output powers are smooth and rapidly settle at their respective steady-state values.

Fig. 2.22 illustrates the waveforms of the substation bus voltage,  $v_{sub.}$ , during and subsequent to the fault, under the basic control (Fig. 2.22(a)) and enhanced control (Fig. 2.22(b)). It is observed that the voltage is remarkably distorted under the basic control strategy, even after the fault is isolated. The reason is that the action of the

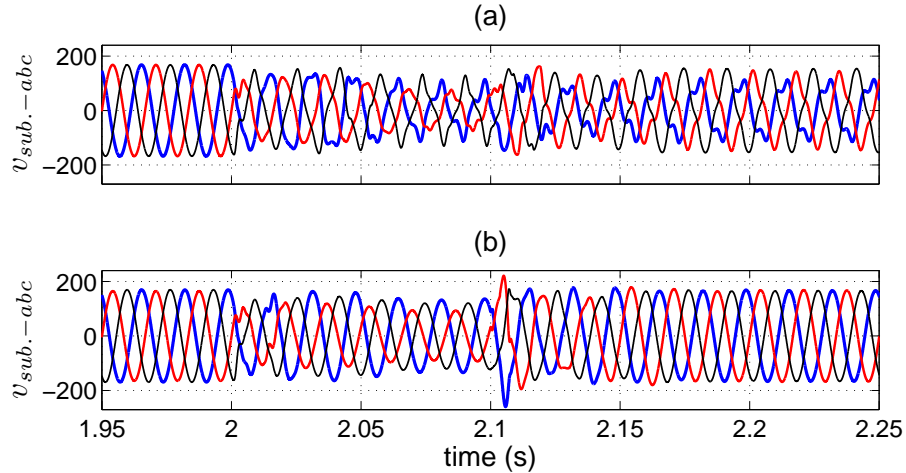


Figure 2.22: Waveforms of the substation bus voltage under a permanent fault at point F3 of the islanded microgrid; (a) basic control and (b) enhanced control.

circuit breaker ACB21 leaves the EC-DERs with an even more unbalanced network and, therefore, the shortcomings of the basic control strategy manifest themselves. It can be verified that, under the enhanced control the voltage harmonic distortion remains limited to the permissible value specified in [80].

### 2.7.3 Response to Operation Mode Switching Incidents

**1) Switching from the Grid-Connected Mode to the Islanded Mode:** Let us assume that a permanent and bolted phase-to-ground (AG) fault strikes point F1 of the 11-kV line, at  $t = 2.0$ s. In this case, the reclosing is unsuccessful due to the permanent nature of the fault, and the microgrid will be subjected to the same fault, again, at  $t = 2.5$ s and  $t = 3.0$ s. Thereafter, the circuit breakers CB1 and CB2 remain open. Fig. 2.23 illustrates the power output waveforms of the three-phase EC-DERs, under the basic control (Fig. 2.23(a)) and enhanced control (Fig. 2.23(b)). The figure indicates that, under the enhanced control the power outputs of the three-phase EC-DERs settle quickly. However, under the basic control strategy, the output powers exhibit level shifts, subsequent to each reclosing incident, and also take a relatively long time to settle at their steady-state values after the fault is permanently isolated.

**2) Switching from the Islanded Mode to the Grid-Connected Mode:** The objective of this study case is to demonstrate the effectiveness of the synchronization algorithm of Section 2.5.4. Fig. 2.24 illustrates the waveform of  $v_{MMS}$ , that is, the

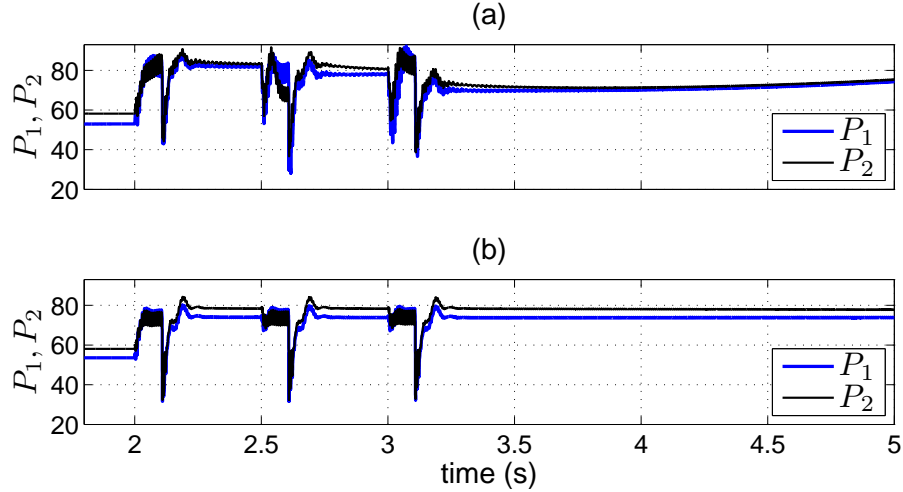


Figure 2.23: Real-power output waveforms of the three-phase EC-DERs under a permanent grid fault at point F1 and successive reclosing; (a) basic control and (b) enhanced control.

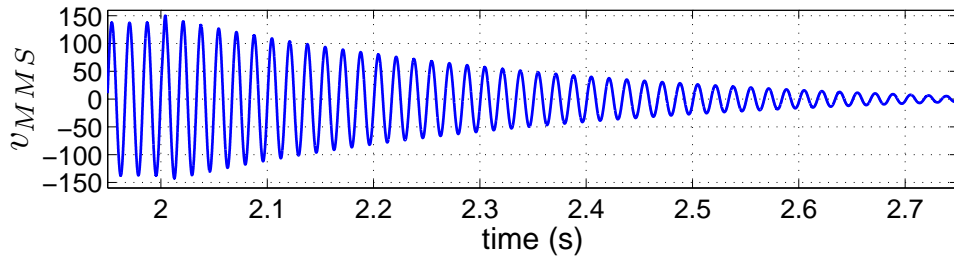


Figure 2.24: Waveform of the voltage across MMS (phase a) during the synchronization process.

voltage across MMS (phase a), during the synchronization process which is assumed to have started at  $t = 2.0$ s. The figure indicates that the synchronization scheme is successful in forcing the microgrid-side voltage of MMS to track its grid-side voltage. Figs. 2.25(a) and (b) illustrate the waveform of the real- and reactive-power outputs of the three-phase DERs, respectively. It is observed that the power outputs rise during the synchronization process to ramp up both the microgrid voltage and frequency (which have dropped slightly below their nominal values, due to the droop characteristics).



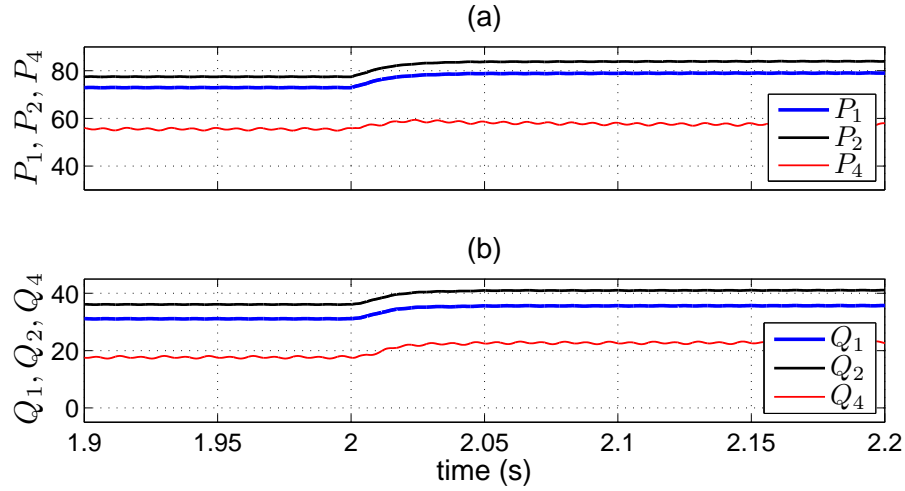


Figure 2.25: Real- and reactive-power output waveforms of the three-phase DERs during the synchronization process.

## 2.8 Summary and Conclusion

In this chapter, an enhanced control strategy was proposed for EC-DERs. It was demonstrated that the proposed control improves the performance of the host microgrid under network imbalances and transient disturbances. More specifically, it was shown that under the proposed control, the host microgrid can ride through network faults, irrespective of whether they take place within the microgrid jurisdiction or strike the upstream grid, and quickly reclaim its pre-fault operating condition. It was further shown that the proposed control enables the microgrid to retain its power quality for the duration of the faults, in both modes of operation, which is a desirable property for detection of certain classes of faults, as well as for sensitive loads. In the following chapter, protection of distribution networks embedding DERs is dealt with.

# Chapter 3

## Protection of a Typical Distribution Network Embedding DERs

### 3.1 Introduction

The protection issues associated with the introduction of DERs to distribution networks were discussed in Chapter 1. It was shown that DERs can compromise the protection coordination amongst the protective devices. Therefore, it is required to retrieve the protection coordination in the presence of DERs, if possible. This chapter presents the steps taken to characterize the impact of DERs on the protection coordination, for host and neighboring feeders, in a typical distribution network. In other words, the chapter looks into the characterization of protection coordination, in radial distribution systems embedding DERs, to determine whether or not the coordination is lost subsequent to the addition of a (new) DER; it is also investigated how the coordination can be resumed if the DER addition has compromised it.

For the cases that the protection coordination is lost, this chapter proposes a simple and effective protection strategy that accommodates the effects of DERs in radial distribution networks. The proposed strategy benefits from microprocessor-based reclosers and directional elements for feeder relays, and addresses the issues of blinding of protection, false tripping, recloser-fuse and fuse-fuse miscoordination, and failed auto-reclosing. In addition, the proposed coordination strategy can be employed for the protection of microgrids in the grid-connected mode of operation, as will be further discussed in Chapter 4. The effectiveness of the proposed algorithm is demonstrated by digital time-domain simulation case studies conducted on a model of an example distribution network, in the

PSCAD/EMTDC software environment.

## 3.2 Impact of DERs on Traditional Coordination and the Proposed Solution

Traditional coordination practice of protective devices has been discussed in Section 1.4.1 of the thesis. It is explained that protective devices are coordinated in such a way that an equal fault current is assumed for all of them; this, however, may not be true in the presence of DERs. As mentioned in Section 1.4.2, addition of a DER to a feeder, anywhere downstream of the relay and the recloser, changes  $I_{fmax}$  and  $I_{fmin}$  and also increases the fuse current as compared to the recloser current [3]. The immediate consequence is that the coordination will be lost if the fault current exceeds  $I_{fmax}$ , due to the existence of DERs. The other consequence is that, since as shown in Fig. 1.7 the recloser current  $I_R$  becomes less than the fuse current  $I_F$ , the fuse may melt before the recloser opens in its fast mode of operation [52]. To accommodate the impact of distributed generation in the protection coordination, and to overcome the issues mentioned in Section 1.4.2, the following algorithm is proposed in this chapter.

1. The impact of the DER to be added on the recloser-fuse coordination of the host feeder or a neighboring feeder is investigated. This is possible based on the approach introduced in Section 3.3.4. If the coordination remains intact in spite of the addition of a DER, the algorithm is to be followed from Step 6. Otherwise, the algorithm is exercised from Step 2.
2. The fault current extremes  $I_{fmin}$  and  $I_{fmax}$  are calculated for the feeder under study; the former extreme is calculated with no DER considered, whereas the latter one is calculated for the configuration where all DERs are in place. Such a choice of  $I_{fmin}$  and  $I_{fmax}$  ensures preservation of the coordination, even if the DERs are disconnected from the network, for example due to an anti-islanding exercise.
3. The characteristic curves of the devices are coordinated based on the conventional method explained in Section 1.4.1, which requires the values  $I_{fmin}$  and  $I_{fmax}$ .
4. Since in the presence of DERs the recloser fault current  $I_R$  is smaller than the fuse fault current  $I_F$ , the recloser fast characteristic curve, obtained in Step 3, is revised.

This requires that the lowest value of  $I_R/I_F$  (less than unity) be calculated, e.g. using an appropriate phase-sequence equivalent circuit, for the worst-case scenario.

5. The recloser fast characteristic curve is shifted down through its multiplication by the minimum value of  $I_R/I_F$ . The revised fast characteristic curve is programmed in the recloser. Thus, the proposed methodology assumes that the recloser is of the microprocessor-based type and therefore programmable.
6. The impact of the DER on the fuse-fuse coordination of the neighboring feeders is studied to confirm that the coordination is preserved. The study methodology and a simple solution for the case where coordination is lost will be introduced in Section 3.3.4, which is based on the slight increase in impedance of the DER interconnection transformer. It should be emphasized that the fuse-fuse coordination loss is unlikely to happen in the host feeder. This is due to our assumption that the DERs get disconnected after the first operation of the recloser and, thus, the coordination fulfilled as explained above retains its validity.

The algorithm proposed above assumes that a directional relay is employed at the beginning of the feeders that embed DERs, in order to guarantee that false tripping is avoided. Moreover, to avoid out-of-phase autoreclosing, it is assumed that the DERs will be dropped out once the feeder recloser opens the circuit [3], [52]; this is ensured by a transfer-trip mechanism and/or the anti-islanding schemes incorporated in the individual DERs, as also identified by the IEEE Std. 1547 [76]. Fig. 3.1 provides a graphical illustration of the proposed algorithm.

### 3.3 Design Example

To illustrate its effectiveness, the proposed methodology is applied to, and discussed in the context of, an example distribution network which, hereinafter, is referred to as the “*test system*” in this chapter.

#### 3.3.1 Distribution Network Structure

Fig. 3.2 illustrates a single-line schematic diagram of the test system, which consists of a 13.8-kV two-feeder distribution subsystem that supplies the loads L1 through L4 via two feeders, i.e., Feeder 1 and Feeder 2. The subsystem is radially connected to the main

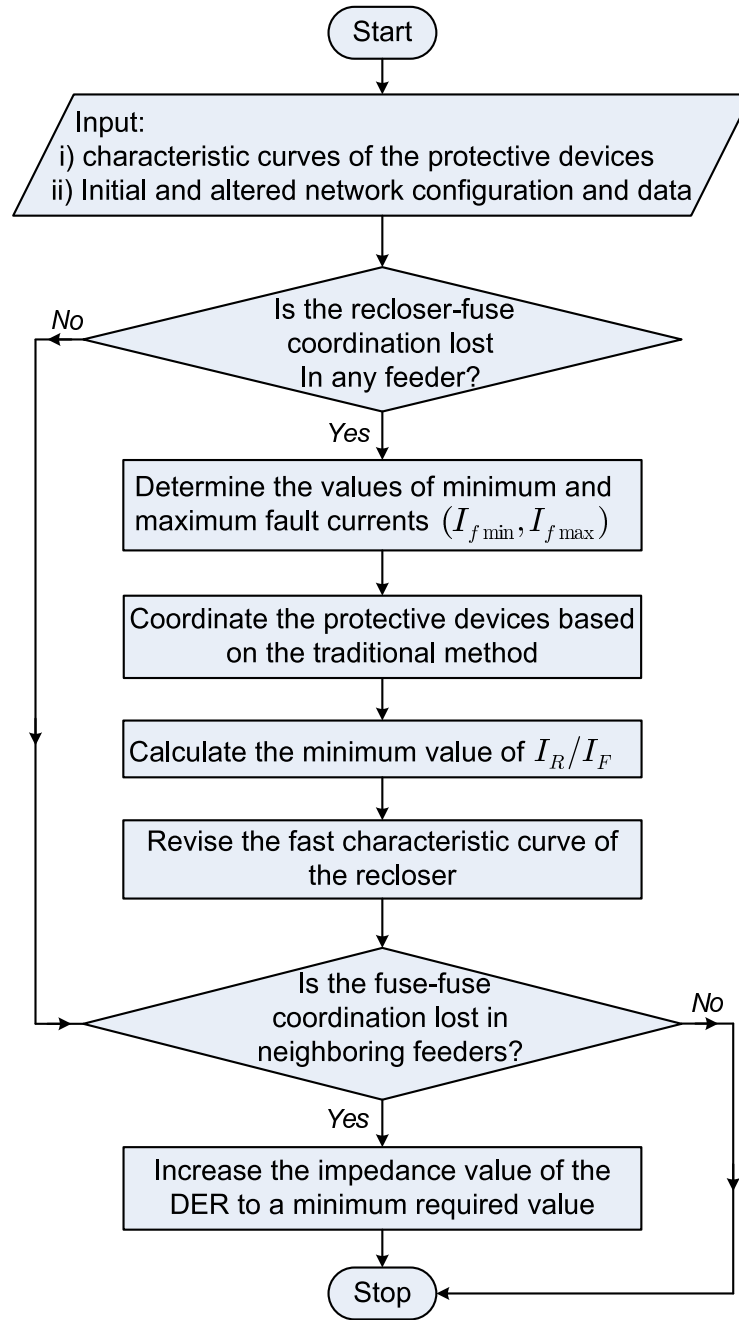


Figure 3.1: Flowchart of the proposed coordination method.

grid through a transformer and a 69-kV line. The grid is represented by a 69-kV bus of 1000-MVA short-circuit capacity. The loads consist of linear RL branches of different power factors. The basic system configuration and parameters are extracted from the benchmark system of the IEEE Std. 399 [81].

The test system described above also includes two DERs, DER1 and DER2, of the

corresponding capacities of 5.4 MVA and 3.8 MVA, interfaced with Feeder 1 and Feeder 2, respectively. The DERs are considered to be based on the synchronous machines, since electronically interfaced DERs have limited fault current capability and, thus, they may not reveal the protection coordination issues.

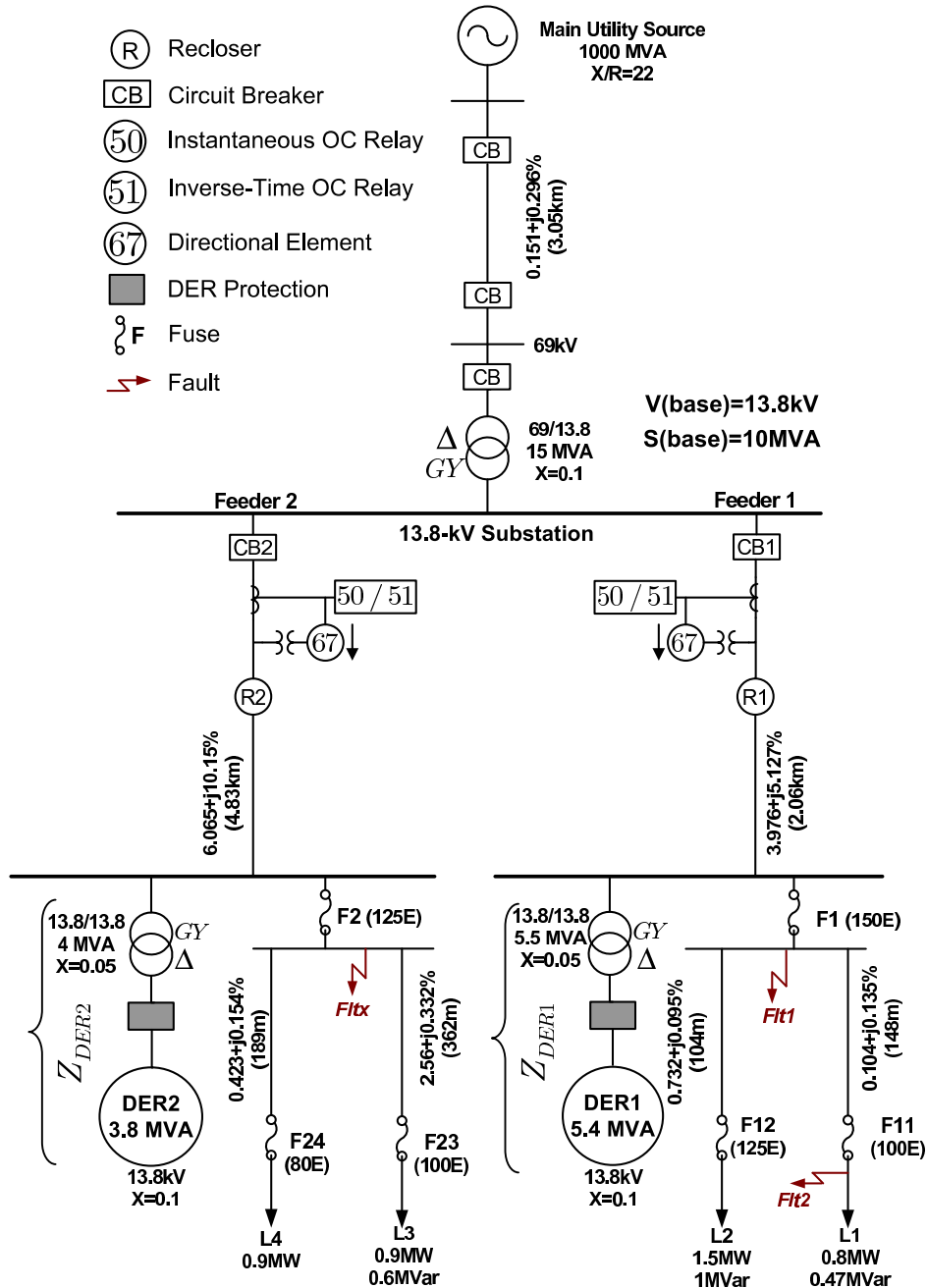


Figure 3.2: Single-line schematic diagram of the studied test system.

### 3.3.2 Coordination of Protection

Let us first assume that DER2 has not yet been connected to the system and, as such, the protective devices are coordinated for the configuration in which only DER1 exists on Feeder 1. We also assume that DER1 can disrupt the initial coordination of Feeder1, achieved through the traditional practice (Section 1.4.1). Thus, the worst-case scenario that can affect the protection coordination is considered, and then the coordination strategy of Section 3.2 is employed to reclaim the coordination for Feeder 1. To consider the worst condition, we assume the capacity of DER1 to be 200% of the maximum feeder load; any larger capacity is considered unrealistic [52]. We further assume that the impedance of DER1 is 0.1 pu, as the worst condition [23]. Moreover, the leakage reactance of the corresponding interface transformer is assumed to be conservatively low, i.e., 5% [52], to further contribute to the worst-case condition. The foregoing scenario corresponds to the maximum contribution of DER1 to the fault current (for our test system) and results in the largest disparity between the fault currents passing through the fuses and the recloser. If the coordination can be fulfilled for this scenario, it can be achieved for any other condition.

The first step of the coordination process is a fault analysis based on Step 2 of the proposed algorithm (see Section 3.2), in order to determine  $I_{fmin}$  and  $I_{fmax}$ . For the test system of Fig. 3.2, it can be shown that the maximum fault current corresponds to a fault taking place at the fuse end of Feeder 1, i.e., location  $Flt1$ , when DER1 is in place, whereas the fault current is minimum when the fault takes place at the end of the load feeder, location  $Flt2$ , in the absence of DER1; such a calculation is made separately for phase and ground faults, since different settings are usually employed for phase and ground relays. Table 3.1 reports the fault analysis results for single- and three-phase faults impacting Feeder 1, obtained through simulation of the test system. The table also includes the value of  $I_R/I_F$ , for each fault scenario. The fault analysis can also be conducted based on appropriate phase-sequence equivalent circuits, such as the one shown in Fig. 3.3 which corresponds to the three-phase fault worst case; a similar equivalent circuit can also be constructed for a single-phase fault. It can be observed that the value of  $I_R/I_F$  based on the equivalent circuit of Fig. 3.3 closely agrees with the minimum value of  $I_R/I_F$  in Table 3.1. Based on Fig. 3.3, the value of  $I_R/I_F$  is

$$\frac{I_R}{I_F} = \frac{Z_{DER1}}{Z_{th} + Z_{DER1}} = 0.65, \quad (3.1)$$

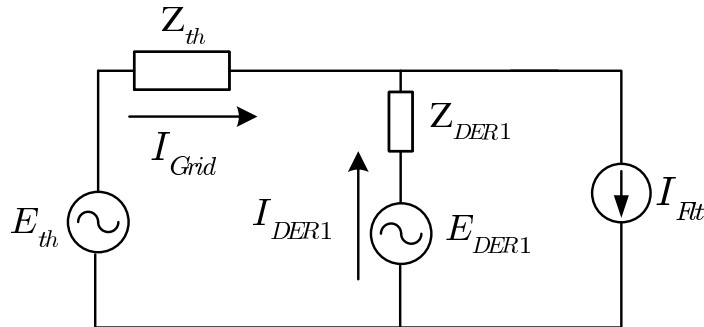
Table 3.1: Fault Calculation Results for the Test System

Fault Location	Fault Type	No DER		with DER1		$I_R/I_F$ with DER1
		$I_F(A)$	$I_R(A)$	$I_F(A)$	$I_R(A)$	
<i>Flt1</i>	ABC	3219	3219	4661	3011	0.646
	A-G	1814	1814	2196	1548	0.705
<i>Flt2</i>	ABC	3052	3052	4231	2733	0.646
	A-G	1737	1737	1901	1334.5	0.702

where  $Z_{DER1}$  is the aggregate of the impedance of DER1 and the impedance of the transformer that connects DER1 to the network;  $E_{th}$  and  $Z_{th}$  are respectively the network Thevenin voltage and impedance, viewed from the DER1 point of interconnection.

After selection of appropriate characteristic curves based on Step 3 of the proposed methodology, Section 3.2, the original recloser fast characteristic curve is multiplied by the minimum value of  $I_R/I_F$ , and the new curve is stored in the program of the recloser. The revised characteristic curve is effective even after the first opening of the recloser when DER1 gets disconnected. The rationale is that any fault current that might develop after the first action of the recloser will certainly be between  $I_{fmin}$  and  $I_{fmax}$ , and, therefore, the coordination made in Steps 2 through 5, Section 3.2, is still applicable; it is remembered that  $I_{fmax}$  has been calculated with the contribution of DER1 considered, whereas  $I_{fmin}$  is obtained in the absence of DER1 (see Step 2 of Section 3.2).

Figs. 3.4 and 3.5 illustrate the original and revised characteristic curves employed for the phase and ground units. It should be noted that the recloser must be coordinated with the fastest fuse of the feeder (100E in this example). In this study, the characteristics curves of the fuse and recloser are constructed based on the analytical equations given in Appendix B.

Figure 3.3: Equivalent circuit for  $(I_R/I_F)$  calculation.



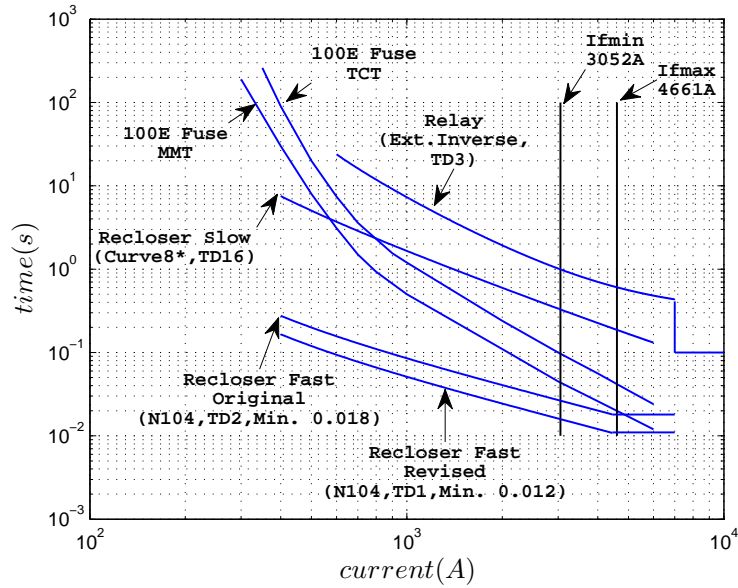


Figure 3.4: Coordination of protective devices of Feeder 1 for phase unit.

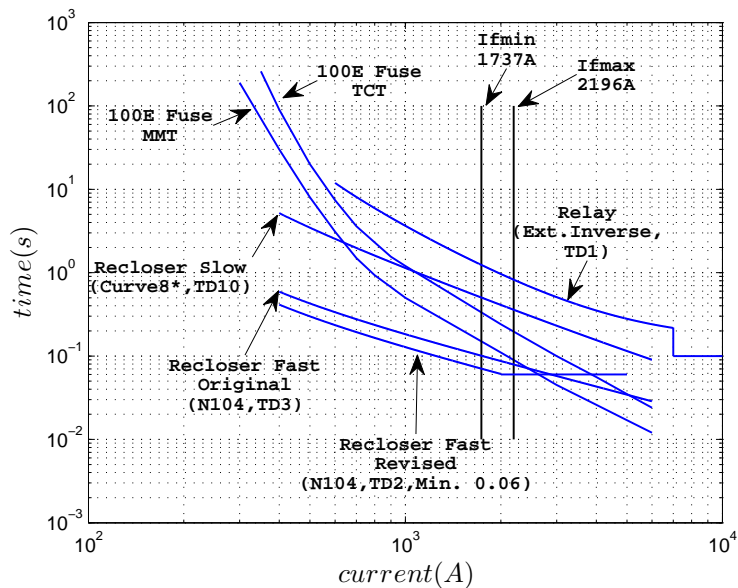


Figure 3.5: Coordination of protective devices of Feeder 1 for ground unit.

### 3.3.3 The Use of Directional Elements

As pointed out in Section 3.2, the proposed algorithm requires a directional element on each feeder that embeds DERs, to preclude false tripping when a fault impacts a neighboring feeder. In such a scenario, the directional element of the feeder under study

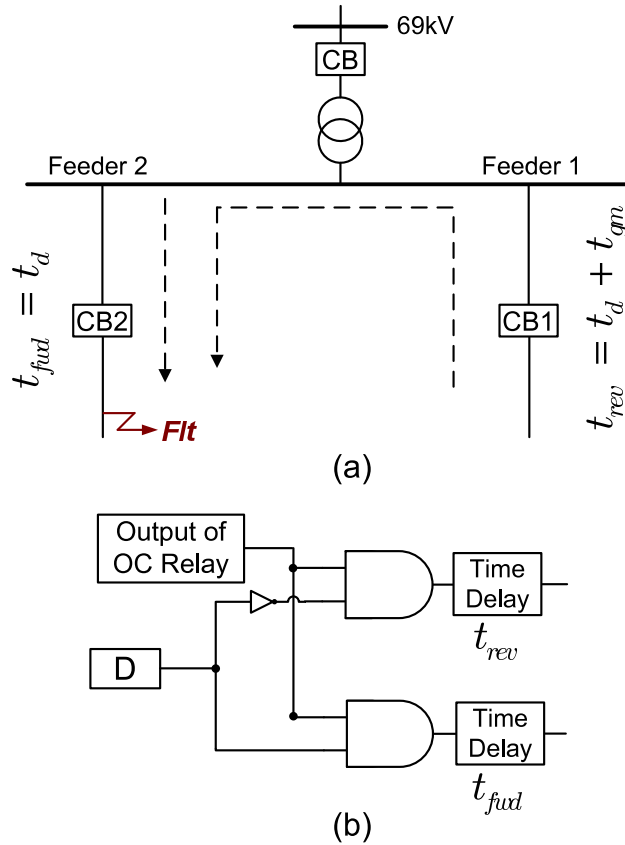


Figure 3.6: Diagrams showing (a) forward and reverse definite times for relays, and (b) logics of implementation.

rapidly block its own circuit breaker, for a pre-specified period of time, to allow the protective devices of the faulty feeder to isolate the fault on their own. The blockage, however, does not continue any longer than the duration of the relay reverse definite time; afterwards, the circuit breaker is commanded to open, as a back-up protection. This concept is illustrated in Fig. 3.6 (a) where  $t_d$  and  $t_d + t_{gm}$  denote the relay forward and reverse definite times, respectively, with  $D$  denoting the output of the directional element. It is noted that the reverse definite time is larger than its forward counterpart by a suitable grading margin,  $t_{gm}$ . Fig. 3.6 (b) shows digital implementation of the proposed protection coordination.

One potential issue that may arise due to the inclusion of directional elements is that of protection loss in case a fault directly impacts the substation. To circumvent this issue, all circuit breakers are commanded to open once their directional elements simultaneously detect a reverse fault. For the test system of Fig. 3.2, this function is realized by the logic circuit illustrated in Fig. 3.7, where  $D_1$  and  $D_2$  signify the outputs of the directional

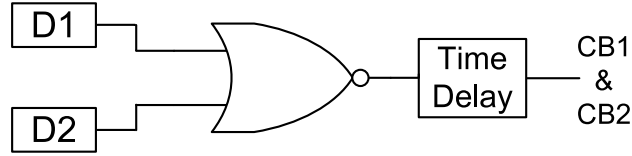


Figure 3.7: Symbolic logic circuit for substation protection.

elements for Feeder 1 and Feeder 2, respectively (modeling of a directional element and its characteristics is introduced in more detail in Appendix B). Nevertheless, one may prefer to design a separate bus protection scheme in a distribution network embedding DERs, if higher reliability is required.

### 3.3.4 Impact of a new DER on the Protection Coordination

Thus far, we have ignored the impact of DER2 on the protection coordination. It is thus imperative to revisit the design, in order to ensure that the coordination is preserved if DER2 also comes on line. We start this by investigating the impact of DER2 on its own feeder protection, and then its impact on the coordination of Feeder 1 will be studied.

**1) Impact on the recloser-fuse coordination of the host feeder (Feeder 2):** To investigate the impact of DER2 on Feeder 2, the worst condition in which a three-phase fault takes place downstream of DER2 is considered. Considering the presence of DER1, a Thevenin equivalent circuit is derived for the network seen from the point of DER2 connection. The result will look something similar to the equivalent circuit of Fig. 3.3, in which subscript “1” is replaced by “2”. The equivalent circuit is used for calculation of  $I_F$  and  $I_R$  which are substituted in (B.1) and (B.2), Appendix B, to determine the minimum melting time of fuse  $F2$ , i.e.  $MMT_{F2}$ , and the operating time of recloser  $R2$ , i.e.  $t_{R2}$ . The coordination is preserved if the recloser operates faster than the fuse, that is,  $t_{R2} \leq MMT_{F2}$  ( $t_{R2} - MMT_{F2} \leq 0$ ).

Fig. 3.8 illustrates the grading time  $t_{R2} - MMT_{F2}$  as a function of (the inverse of)  $Z_{DER2}$  (see Fig. 3.2), for different network Thevenin impedances. The figure shows that, for a given network Thevenin impedance, the recloser-fuse coordination is preserved if  $Z_{DER2}$  is larger than a minimum value. In our example, this value is 3.71 pu for the network Thevenin impedance of 0.2 pu. Also, for a given  $Z_{DER2}$ , the coordination is preserved if the network Thevenin impedance is larger than a threshold.

As will be discussed in Section 3.3.4–3, the fuse-fuse coordination of a feeder cannot

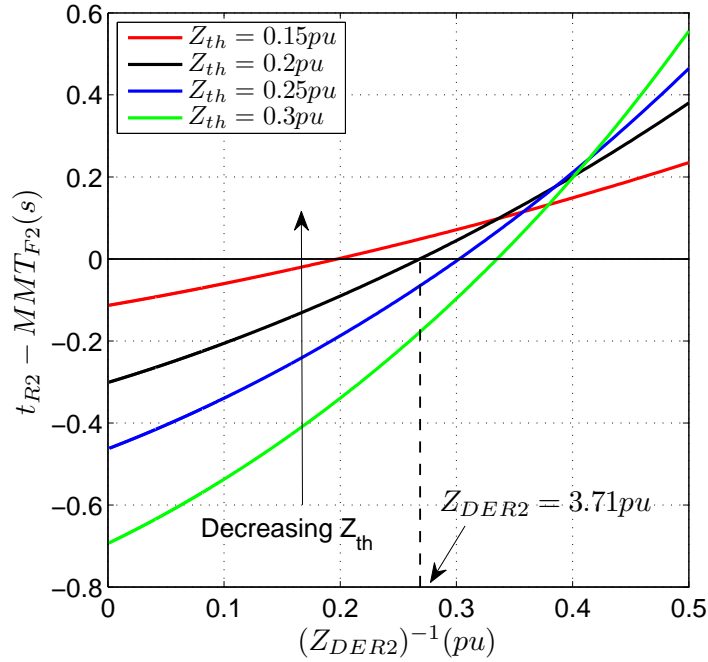


Figure 3.8: Curves characterizing the recloser-fuse grading time as a function of (the inverse of)  $Z_{DER2}$ .

be compromised by DERs on that feeder, and therefore is not dealt with in this thesis.

## 2) Impact on the recloser-fuse coordination of a neighboring feeder (Feeder1):

An investigation similar to the one introduced in the previous subsection can be conducted to identify the impact of DER2 on the coordination between recloser  $R1$  and fuse  $F1$ , of Feeder 1. The results indicate that the threshold value of  $Z_{DER2}$  that causes miscoordination between  $R1$  and  $F1$  is considerably smaller than that caused miscoordination in Feeder 2. In our test system, this value is 0.395 pu for the network Thevenin impedance of 0.2 pu. Thus, it is expected in general that any impedance of a DER (i.e.,  $Z_{DER}$ ) that does not disrupt the recloser-fuse coordination of its host feeder, will not compromise that coordination of the neighboring feeders embedding DERs if the proposed algorithm is used for the protection coordination of the feeders. However, the impedance of a DER may be so low that the recloser-fuse coordination of the host feeder is lost. This may also result in disruption of the recloser-fuse coordination in a neighboring feeder. If this is the case, the coordination algorithm of Section 3.2 must be executed for the neighboring feeder, as well as the host feeder.

### 3) Impact on the fuse-fuse coordination of a neighboring feeder (Feeder 1):

As pointed out in Section 1.4.2, DERs may compromise fuse-fuse coordinations. Based on the design procedure of Section 3.2, DERs cannot disrupt the coordinations between the fuses of their host feeder, since the recloser is supposed to operate first for any fault impacting the host feeder and, then, the DERs get dropped out. However, DERs may affect the fuse-fuse coordination of neighboring feeders. For example, if a three-phase fault impacts branch  $L2$ , recloser  $R1$  operates first, and DER1 will be disconnected. Therefore, DER1 cannot affect the coordination between  $F1$  and  $F12$ ; however, DER2 is still on line and can disrupt that coordination. This is better shown by Fig. 3.9 where the coordination grading time between  $F1$  and  $F12$ , i.e.  $TCT_{F12} - MMT_{F1}$ , is plotted as a function of (the inverse of)  $Z_{DER2}$ , for a three-phase fault (worst condition) that has taken place at branch  $L2$ . Thus, the fuse-fuse coordination is maintained if the minimum melting time of  $F1$  is less than the total clearing time of  $F12$ , that is,  $TCT_{F12} - MMT_{F1} \leq 0$ . As Fig. 3.9 indicates, this happens if and only if  $Z_{DER2}$  is larger than 0.088 pu. It is seen again if  $Z_{DER2}$  can keep coordination between recloser and the fuse, it will certainly ensure the fuse-fuse coordination for the studied system.

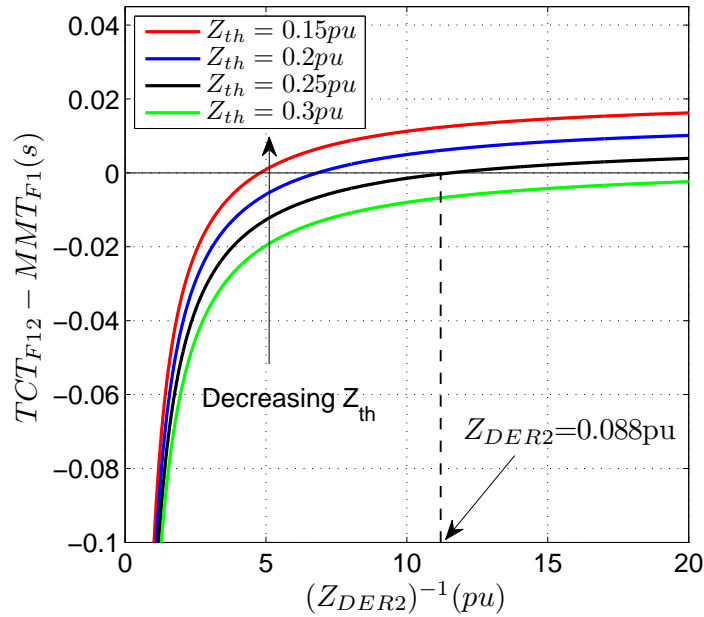


Figure 3.9: Curves characterizing the fuse-fuse grading time as a function of (the inverse of)  $Z_{DER2}$ .

### 3.3.5 Retrieval of protection Coordination after System Alterations

Let us consider the worst-case scenario in which the capacity of DER2 is two times the host feeder load, and its impedance is 0.1 pu. For our test system, it turns out that this condition results in disruption of the recloser-fuse coordination of both feeders (see Sections 3.3.4–1 and 3.3.4–2), but it does not affect the fuse-fuse coordination of Feeder 1 (see Section 3.3.4–3). Consequently, we need to repeat the algorithm proposed in Section 3.2 for both feeders, with both DER1 and DER2 considered, to retrieve the coordination. Had the fuse-fuse coordination of Feeder 1 been also lost, we would have needed to increase  $Z_{DER2}$  as the last step of the coordination practice.

Figs. 3.10 and 3.11 illustrate the original and the revised characteristic curves, respectively, for the phase and ground relays. The curves are for the devices of Feeder 2; the settings of the protective devices of Feeder 1 are produced in a similar fashion, but are not shown here due to space limitations.

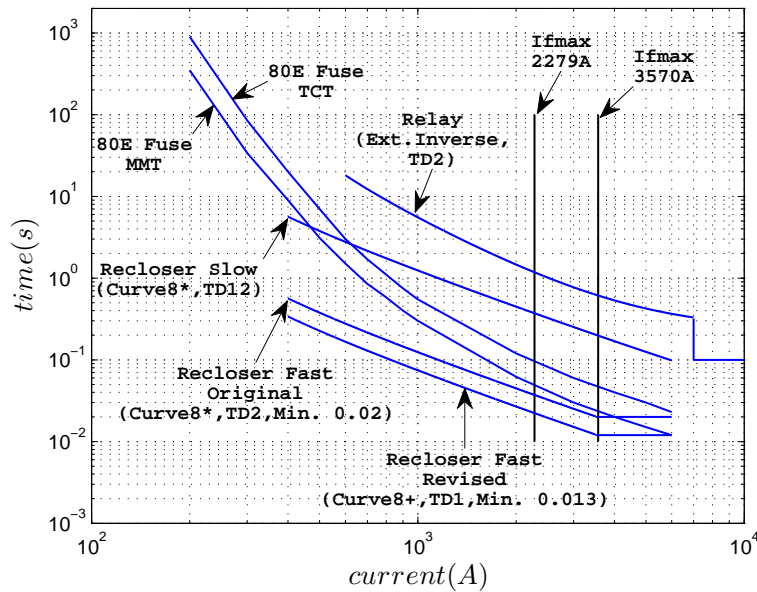


Figure 3.10: Coordination of protective devices of Feeder 2 for phase unit.

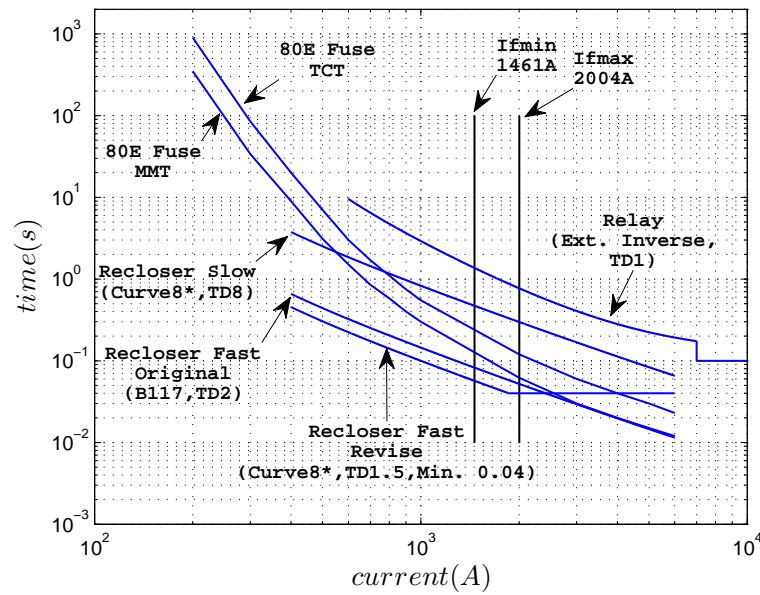


Figure 3.11: Coordination of protective devices of Feeder 2 for ground unit.

### 3.4 Simulation Results

To verify the effectiveness of the proposed coordination algorithm, the test system of Fig. 3.5 has been modeled and simulated by PSCAD/EMTDC software. To that end, the same characteristic curves used for the analytical studies of protective devices have also been utilized for simulation of the relays, reclosers, and fuses (see Appendix B). This section reports the simulation results corresponding to the worst-case fault scenario, i.e., the three-phase fault. The results for other types of fault are similar and thus not included, due to the limited space.

Let us first assume that DER2 is not connected to the system, the devices of Feeder 2 are coordinated according to the traditional method<sup>1</sup>, and a permanent three-phase fault impacts location “*Fltx*” on Feeder 2, at  $t = 0.5$ s. Fig. 3.12 illustrates the current waveforms of recloser *R1* and fuse *F2*. It can be observed that the recloser operates twice in the fast mode and, then, the fuse interrupts the fault current. The tripping times of the recloser and fuse are depicted in Fig. 3.13. It should be noted that the typical operating sequence of a recloser is fast-fast-slow-slow, with a time delay between each two consecutive actions [3], [52]. Fig. 3.12 shows that the fault causes the current

<sup>1</sup>Based on the proposed methodology of Section 3.3.4, DER1 does not disrupt protection coordination of its neighboring feeder (Feeder 2).

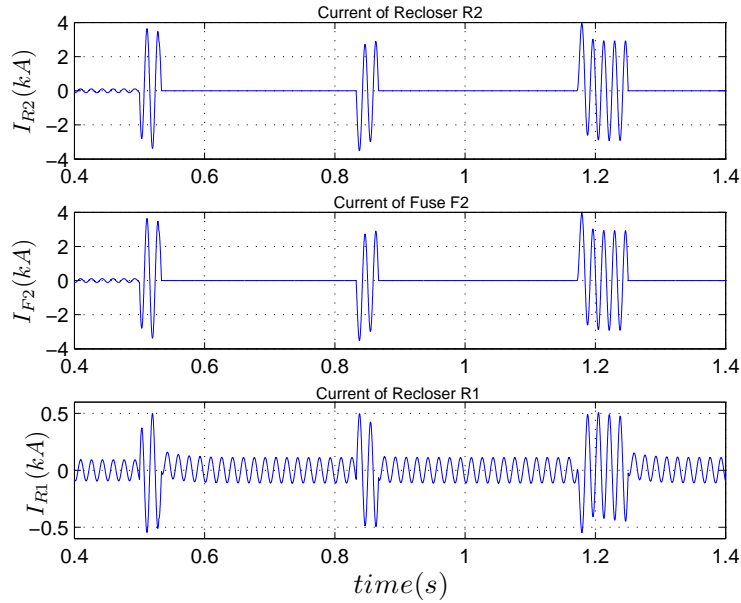


Figure 3.12: Coordination of devices when DER2 is not in place.

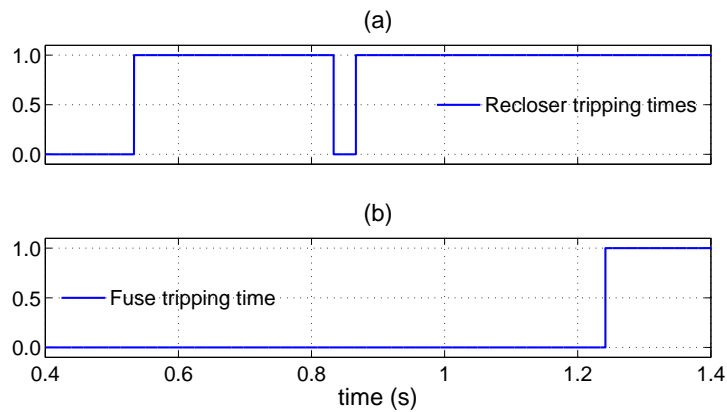


Figure 3.13: Tripping times of the recloser and fuse when DER2 is not in place.

of Feeder 1 to increase, but does not result in the operation of Recloser 1; this is due to the blockage exercised by the directional element of the relay of Feeder 1.

Fig. 3.14 shows the simulation results for the case where DER2 is also present, while the devices are coordinated in the same way as that for the previous case. It is observed that, the same three-phase fault results in the loss of coordination for this case, that is, fuse F2 operates before recloser R2. This is due to the fact that DER2 contribute to the fault and, thus, the fault current of recloser decreases as compared to the situation that DER2 is not connected to the system. This leads to the non-operation operation of



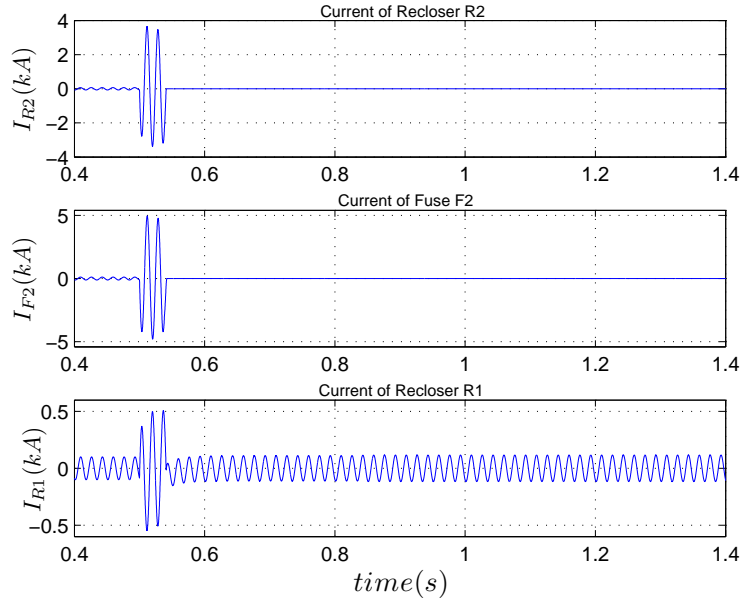


Figure 3.14: Coordination loss when DER2 is added to the test system.

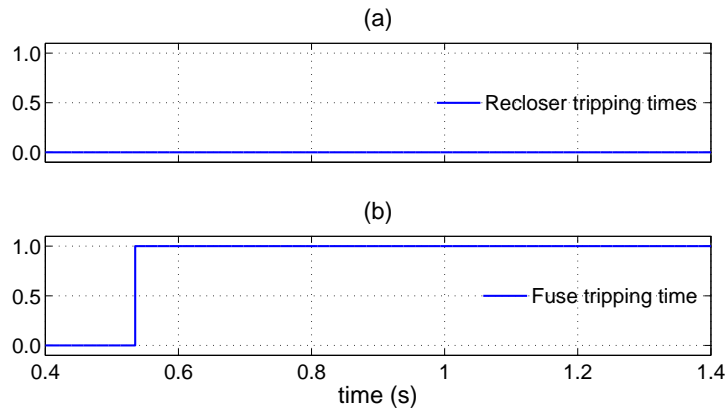


Figure 3.15: Tripping times of the recloser and fuse when DER2 is in place.

recloser R2, as shown in Fig. 3.15.

Fig. 3.16 demonstrates the protection response for the case where DER2 is in place and the coordination has been revised according to the strategy of Section 3.3.5. Thus, the proper sequence of operation has been restored for the protective devices, and recloser R2 operates before fuse F2 is damaged. In this scenario, once the recloser opens for the first time, DER2 will be disconnected subject to a brief delay and, consequently, the fault current stops flowing in both the recloser and the fuse. Therefore, the recloser and the fuse will be subjected to the same current as in the scenario without DER2, once the

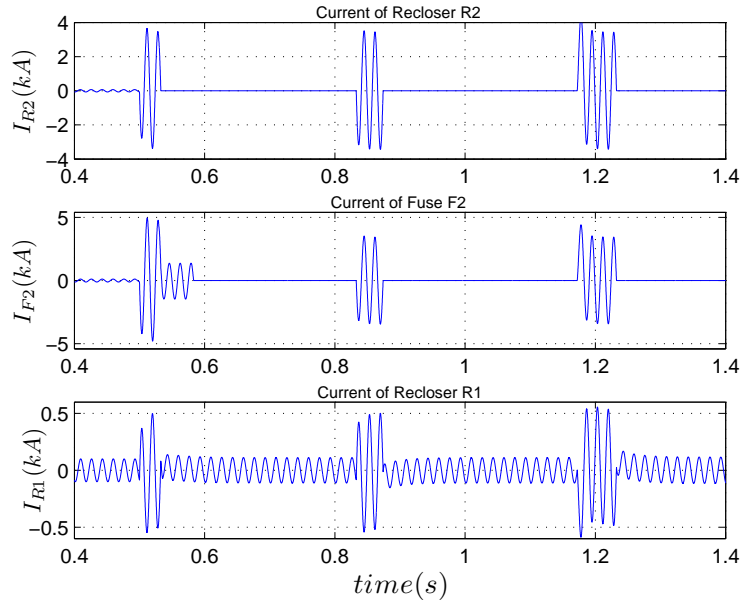


Figure 3.16: Retrieval of coordination after the addition of DER2.

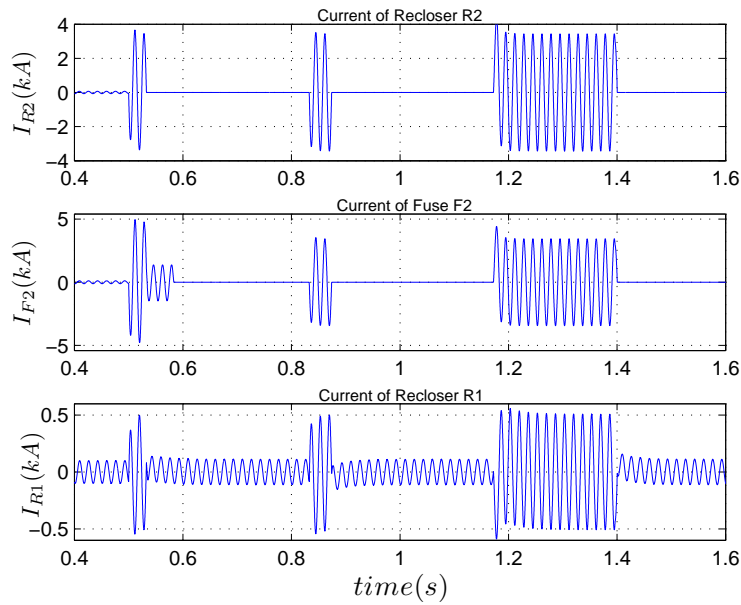


Figure 3.17: Operation of the recloser in the slow mode when the fuse fails to operate.

recloser makes the circuit. Nonetheless, the coordination remains effective. If the fuse fails to operate, the recloser takes action in the slow mode of operation and breaks the fault current, as shown in Fig. 3.17.

## 3.5 Summary and Conclusion

This chapter investigated the impact of distributed generation on the protection coordination of radial distribution networks. First, a simple and effective protection strategy was proposed that provides coordination between protective devices of a radial distribution system embedding DERs. The proposed strategy benefits from microprocessor-based reclosers and directional elements for feeder relays, and addresses the main issues associated with the existence of DERs in distribution networks. Moreover, the proposed strategy does not require communications or adaptive protective devices. Then, the impact of future additions of DERs on the coordination was investigated, and the requirements for preservation of the coordination were identified. It was further discussed in this chapter that the proposed algorithm could be applied for the worst-case scenario, to reclaim the coordination in case the requirements are not to be met. The simulation results for a test system indicated the effectiveness of the method. In the next chapter, protection of low-voltage/residential microgrids will be discussed.

# Chapter 4

## Protection of Low-Voltage Microgrids

### 4.1 Introduction

As discussed in Chapter 1, microgrids have been proposed as a way of integrating large numbers of renewable energy resources with distribution systems. The microgrid concept, however, challenges the operating principals of distribution networks. In particular, one problem with microgrid implementation is designing a proper protection scheme. It has been shown that traditional protection schemes does not successfully work for microgrids and, thus, it is required to have a fresh look into the fundamentals of network protection such that the safe operation of the microgrids is ensured.

One of the major issues associated with microgrid protection is to devise an appropriate protection strategy that is effective in the grid-connected as well as islanded mode of operation. This chapter proposes a protection strategy for low-voltage microgrids. Further, the structure of a new relay enabling the proposed protection strategy is presented. One of the prominent feature of the developed protection scheme is that it does not require communications or adaptive protective devices. Moreover, it is to a large extent independent of the fault current magnitude and the mode of operation. Transient time-domain simulation studies are conducted to demonstrate the effectiveness of the proposed protection strategy and its enabling relay, using PSCAD/EMTDC software package.

## 4.2 Characteristics of Low-Voltage Distribution Networks and Assumptions Made

The following subsections introduce some important characteristics of a Low-Voltage (LV) distribution network, as they pertain to the operation and protection of a microgrid. The characteristics will be considered in Sections 4.3 and 4.4, for the development of the proposed protection strategy.

### 4.2.1 Structure

An LV microgrid is based on a designated area of a secondary distribution network which is supplied by a step-down transformer. By assumption, the designated area embeds sufficient amount of generation and is thus able to operate in isolation from the rest of the network. The rating of the step-down transformer, which connects the primary (MV) network to the secondary (LV) network, is typically from a few hundred kVA to several MVA [77], [78]; hence, the peak power demand of an LV microgrid is assumed to be limited to a maximum of several MVA. It is further assumed that microgrid loads are supplied by a number of radial Secondary Mains (SMs), which may be branched by one or more laterals, and that the presence of single-phase loads and/or DERs makes the LV microgrid an inherently unbalanced network.

### 4.2.2 Conventional Protection

In general, simple overcurrent devices, most commonly in the form of fuses, are employed in secondary distribution networks to protect equipment and ensure safety. Secondary network conductors are typically protected by the so-called limiters. A limiter is a high-capacity fuse that is installed on each phase conductor of the SMs at each junction point. The step-down transformer is protected by a network protector, which is an LV air circuit breaker with a tripping/closing mechanism controlled by a self-contained relay. In addition, the network protector has fuses that provide backup protection for the step-down transformer [86]. Since the fault should rapidly be isolated by the limiters, before the network protector operates, the time-current characteristics of the limiters must be coordinated with those of the network protector [86], [87]. This practice ensures that the smallest possible area of the secondary network is de-energized in response to a fault incident. The secondary side of the step-down transformer may not necessarily be protected

by dedicated equipment, as the SMs are commonly equipped with corresponding dedicated network fuses [78]. Hereafter, due to its more common usage, the term “*network fuse*” or “*fuse*” is used instead of limiter.

### 4.2.3 Grounding Practices

An LV microgrid is subject to the same safety requirements and standards as those set for a conventional secondary distribution network. In a microgrid, a fault incident may result in a substantial ground voltage, even if the DERs operate at low voltages [88]. Moreover, the neutral grounding practice in a microgrid can affect protection. Therefore, the grounding strategies of the equipment in an LV microgrid must be adopted judiciously.

Typically, a  $\Delta$ /GY winding configuration is used for the step-down transformer. Thus, either of the two grounding strategies TT and TN [88] can be adopted, since the ground will be available at the LV side of the step-down transformer, even if the microgrid is islanded. However, compared to the TT method, fault currents are higher in the TN approach, due to the low-impedance return path (neutral or protective earth conductor) that exists in the TN method. The reason is that, in the TN approach only a small fraction of the fault current is diverted to the ground, but the rest flows through the neutral path. This characteristic enables the use of ground-fault relays in the TN approach, for the neutral conductor of an SM. For the reason mentioned above, the popularity of TN method [68], and the system safety requirements, the TN-C-S [89] grounding configuration of Fig. 4.1 is assumed in this study. The LV network grounding techniques and their corresponding terminology can be found in [88] and [89].

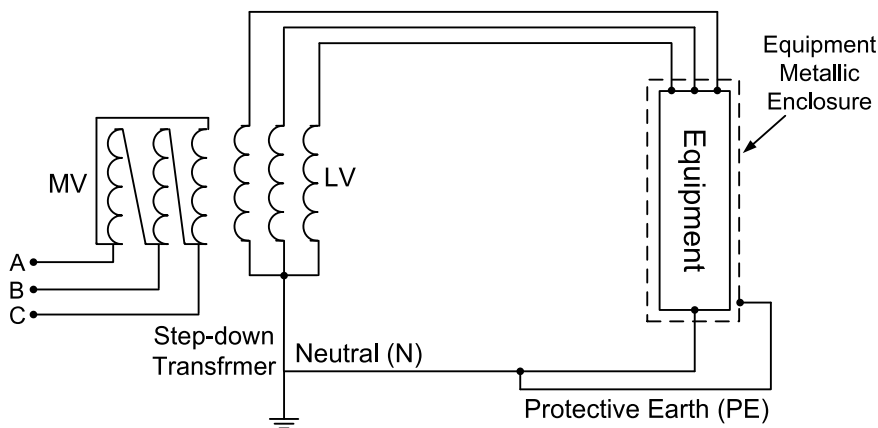


Figure 4.1: The TN-C-S grounding configuration in an LV network.

#### 4.2.4 DER Interface Mechanisms

The DERs of an LV microgrid can be of the single-phase or three-phase type, based on rotating machines or interfaced through power-electronic converters of the VSC types. A single-phase DER is connected between a phase conductor and the neutral conductor, typically through a single-phase isolation transformer. Thus, the TN-C-S grounding strategy ensures that the DER can contribute to a phase-to-ground fault current, through the low-impedance path of the fault current loop. The TN-C-S grounding configuration can also be adopted for a three-phase DER for which a  $\Delta$ /GY interconnection transformer is employed.

#### 4.2.5 DER Control Strategies

In this chapter, the droop-based voltage/frequency regulation strategy of Section 2.5 has been employed for the EC-DERs. The conventional rotating-machine-based DERs are also droop-controlled, that is, the excitation and governor systems of the machine are also included in their model. The control scheme of each DER embeds a respective synchronization mechanism for safe reconnection of the islanded microgrid to the utility grid. To ensure that traditional basic protection functions, more specifically the directional function, can also be employed here, the built-in controls of DERs are designed in such a way that the DERs behave similarly to the conventional synchronous machines, in the sense that they more or less maintain the balance of their terminal voltages when an asymmetrical fault strikes the network; in an EC-DER, of course, the magnitude of the terminal voltage drops to limit the fault current contribution (see Sections 2.4 and 2.5).

### 4.3 Proposed Protection for the Islanded Mode of Operation

#### 4.3.1 Household Consumer Protection

Traditionally, household consumers are protected by small fuses or miniature circuit breakers. Commonly, the devices are of 6-A, 16-A, and 32-A current ratings, for a 208-V network [90], and there is no need to replace them. The reason is that the fault current contributed by the DERs is expected to be sufficiently large to force the fuses to act in about 5 cycles from the fault inception, even in the islanded mode of operation [90], [91].

Table 4.1: Currents Required for Safe Operation of Household Fuses in 5 Cycles (83ms) from the Fault Inception

Fuse Type	Fuse Rate (A)	Required Current (A)
BS Fuse (BS88, Enclosed)	6	28
	16	110
	32	250
IEC/Euro Fuse (gF Curve, Cylindrical)	6	37
	16	80
	32	260
ANSI Fuse (NS-HRCII/Canadian)	6	22
	16	120
	32	250

For example, let us consider a 208-V microgrid in which EC-DERs supply 200kVA. Thus, the DERs solely contribute an aggregate fault current of 555A, which is adequate to blow the household consumer fuses in 5 cycles from the fault instant. Table 4.1 reports the fault current magnitudes required to break three common types of household consumer fuses, in 5 cycles from the fault inception, i.e., 83ms for a 60-Hz power system. It is observed that the desired operating time (5 cycles) is compatible with the operating times provided by common international standards.

### 4.3.2 Network Protection

As discussed in Section 4.2.2, secondary distribution networks are generally protected by network protectors and fuses, such that they are coordinated for the grid-connected mode of operation. However, due to inadequate fault currents, the coordination may be compromised in the islanded mode of operation, i.e, small fault currents can result in a slow operation of network overcurrent devices. On the other hand, unlike household consumer fuses, fast operation cannot be guaranteed for larger fuses and protective devices once the microgrid gets islanded. For example, a 100-A BS88 fuse requires 1150A to operate in 5 cycles after the fault inception, which is not in the range of the currents of Table 4.1. Consequently, faults within the microgrids need to be cleared with techniques that do not necessarily rely on high fault currents.

Considering the above discussion, this chapter proposes that some of the network protective devices of the LV microgrid be replaced by circuit breakers that are governed by



a suitable relaying scheme; replacement of all protective devices by circuit-breakers/relays is costly and time-consuming. Thus, it is proposed to replace by a relay the network protector that is located at the microgrid interface point, i.e., where the microgrid is interfaced with the utility grid. Moreover, the chapter proposes to replace by relays the fuses that are located at the beginning of the SMs, but to maintain all other network fuses; the remaining fuses and the added relays shall be coordinated for the grid-connected mode of operation; this is discussed in Section 4.4. As mentioned, each circuit breaker is controlled by a corresponding microprocessor-based relay which, hereafter, is referred to as the “*Microgrid Protection Relay*” (MPR). The relay that is installed at the microgrid interface point, is referred to as the “*Interface Microgrid Protection Relay*” (IMPR). The introduction of those relays provides an acceptable system reliability for the host LV microgrid; however, if the same number of isolation points as those possible in the grid-connected mode were required, more fuses should be replaced by circuit-breakers/relays. Section 4.3.5 deals with such a scenario.

It is further proposed in this chapter that the circuit breakers installed at the beginning of the SMs have the single-phase tripping capability, to only isolate the smallest possible part of the network. By contrast, the circuit breaker located at the microgrid interface point is intended for three-phase tripping. Additionally, it is assumed that each DER is dropped out if the network frequency and/or voltage are not within their permissible ranges, for a prespecified period of time. This is ensured by the corresponding anti-islanding mechanism which intervenes and disconnects a DER, e.g., through over-/under-voltage and/or over-/under-frequency relays, as required by IEEE Std. 1547 [76].

### 4.3.3 Fault Detection

**1) Solid Faults:** Solid faults are those that do not have a significant fault impedance<sup>1</sup>. A solid fault within an islanded microgrid results in a network-wide voltage drop, which can be utilized for fault detection. In addition, an instantaneous overcurrent relay, which is set based on the thermal properties of the conductors, can provide a preliminary redundant protection for solid faults, despite the fact that the fault current may not be large in the islanded mode of operation.

**2) Medium-Impedance Faults:** For a medium-impedance fault, neither the voltage drop nor the fault current may be large. Consequently, the protection scheme may not be

---

<sup>1</sup>In some papers, solid faults are also referred to as the “*bolted faults*”.

able to distinguish a faulty condition from a network overload condition. Therefore, this chapter proposes an additional fault detection strategy that serves as a main redundant mechanism should the protection functions mentioned in Section 4.3.3–1 fail to operate. It is proposed to extract the zero- and negative-sequence components of the currents, and to utilize them as a redundant fault detection mechanism. Thus, if the sequence components exceed their respective thresholds for a certain time period, an algorithm issues a trip command. To circumvent false detection due to network voltage and/or current imbalance, the trip thresholds should be selected judiciously. As discussed in Section 4.2.5, it is assumed that appropriate voltage regulation strategies are employed by the DERs such that the network voltage imbalance is maintained down to the standard limits (i.e., less than 2%) [92]; in this study, a 1.5% voltage imbalance and a 25% load imbalance have been assumed. The trip thresholds employed in this chapter are specified in Appendix C.

**3) High-Impedance Faults:** A reliable protection scheme must also be able to detect High-Impedance Faults (HIFs), which may have current magnitudes similar to those of normal loads and therefore not cause any noticeable voltage drop. Even ground-fault relays may not be able to detect HIFs, especially in systems with multiple grounded points where the earth return current can take various paths. Almost all of the methods proposed for HIF detection rely on extracting HIF current waveform characteristics, such as the energy level [93], high frequency components [94], and harmonic content [95]. This chapter adopts the method proposed in [93] for the HIF detection module that is incorporated in the MPRs.

#### 4.3.4 Protection Coordination

**1) Grading:** In an islanded microgrid, the voltage drop caused by a fault appears more or less across the entire network, due to the limited geographical span. Therefore, it is almost impossible to coordinate protective devices based on the voltage profile. To ensure coordination, this chapter proposes the use of a directional element, in conjunction with fault detection modules. The combination of a fault detection module and a directional element, with proper definite time delays for forward and reverse faults, can offer an acceptable protection coordination.

Since no damaging large fault current is expected to exist in the islanded mode of operation, a definite-time grading technique, starting at the load side of an SM and end-

ing at the generation side of the SM (microgrid interface point), can ensure a suitable coordination. In other words, a longer fault clearance time at the generation side of the grading path is unlikely to damage the microgrid equipment. Thus, inverse-time overcurrent devices are not necessary for the islanded microgrid; however, the traditional inverse-time overcurrent relays are also employed for the grid-connected mode of operation, as will be discussed in Section 4.4. The upper limits for the definite time delays at the generation side of the grading paths are determined based on constraints such as the sensitivity of the critical loads to voltage disturbances, the duration over which an EC-DER can contribute to the fault current, and the stability of the conventional rotating-machine-based generators.

The proposed grading method requires incorporation of directional elements in each MPR, to preclude false tripping when a fault impacts a neighboring SM. The grading technique is similar to what is explained in Section 3.3.3 of the thesis, that is, the directional elements of a sound SM rapidly blocks its respective circuit breaker(s), for a prespecified period of time, once it detects a fault in a neighboring SM (reverse direction); this is to allow the protective devices of the faulty SM to isolate the fault first. The blockage, however, does not continue for any longer than the duration of the relay reverse definite time; afterwards, the circuit breaker(s) of the sound SM is commanded to open, as a backup protection. This concept is illustrated by Fig. 4.2 in which  $t_f$  and  $t_f + t_m$  respectively denote the forward and reverse definite time delays of the relays. It is remembered that the circuit breaker installed at the microgrid interface point is open in the islanded mode of operation.

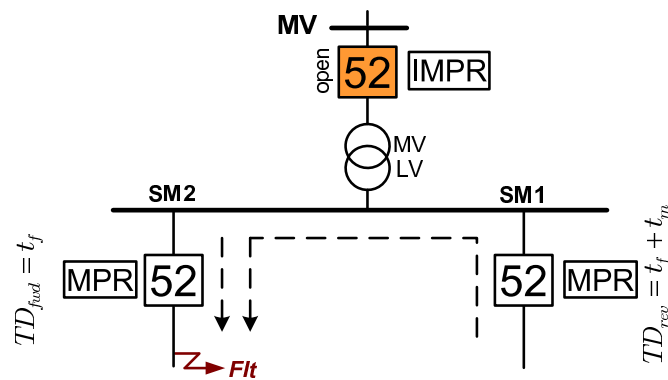


Figure 4.2: Diagram showing the coordination of MPRs in the islanded mode of operation.

**2) Directional Element:** The directional characteristic function is modeled in this chapter by a comparator whose inputs are derived from the voltage and current of the SM (see Appendix B). A fault is identified as a forward fault, that is,  $D = 1$ , if

$$-\frac{\pi}{2} + \theta \leq \varphi \leq \frac{\pi}{2} + \theta, \quad (4.1)$$

where  $D$  denotes the output of the directional element,  $\varphi$  is the phase difference between the voltage and current of the SM, and  $\theta$  conceptually emulates the angle of the effective impedance of the SM, which also includes the impedance of the current transformer. It is noted that six directional elements must be used to cover all types of faults. Additionally,  $\varphi$  should have a minimum discrepancy from either of the two bounds specified by (4.1), before the directional decision is endorsed. This requirement avoids erroneous decisions if either the voltage or the current is so small that its angle is unreliable. Moreover, since the voltage magnitude is very small for close-in faults, a cross or self polarization technique is employed to extract the voltage of the SM, in order to overcome operation failure for close-in faults [96]. To deal with close-in faults, it is also possible to use memory polarization technique for extracting the voltage of the SM, as discussed in [97]. In the cross polarization technique, voltages of the healthy phases are used to find the angle of the faulty voltage, whereas a memory voltage (recorded by the relay) is employed in the memory polarization method to obtain the angle of the faulty voltage.

**3) Negative-Sequence Directional Element:** The abovementioned direction detection strategy may need some additional provisions if a fault does not involve all three phases and the fault current magnitude approaches that of the load. For example, for phase-to-phase faults, the directional element described above may fail to detect the correct direction. Thus, in addition to the three directional elements of each SM (one for each phase), a negative-sequence directional element is also employed. The negative-sequence directional element is based on the same algorithm as the one described for a regular directional element, except that the algorithm output is logically inverted, compared to the positive-sequence directional element.

**4) Secondary Mains without DER:** If an SM does not include any DERs, or it includes an insignificant amount of generation, the directional decision is not reliable, since the power drawn by the loads in such SMs is considerably larger than the power generated by the DERs. Thus, the directional element may erroneously declare a forward

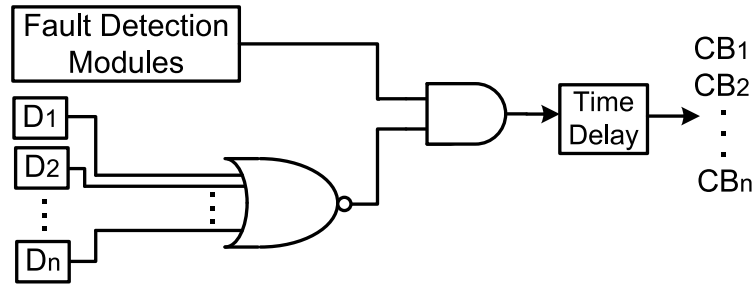


Figure 4.3: Symbolic logic circuit for substation bus protection.

direction and disconnect the SM for a fault that is in a neighboring SM. In order to overcome this issue, this chapter proposes to supplement the aforementioned directional decision-making strategy with a current-magnitude comparison technique. Thus, the directional decision for a forward fault is endorsed if the current magnitude of the host SM is larger than its full-load current magnitude. The reason for this condition is that, in a healthy SM the current magnitude drops remarkably in the phase(s) that corresponds to the affected phase(s) of a neighboring faulty SM.

**5) Substation Bus Protection:** One potential issue that may arise due to the inclusion of directional elements is that the protection may be lost if a fault directly impacts the substation. To circumvent this condition, all circuit breakers of the SMs that embed a DER must be commanded to open after a time delay, once their directional elements simultaneously detect a reverse fault. For an LV microgrid with  $n$  SMs that all of which have DER(s), this function is realized by the logic circuit illustrated in Fig. 4.3;  $D_1$  through  $D_n$  denote the outputs of the directional elements for SM#1 through SM# $n$ , respectively.

### 4.3.5 Protection Scheme Extension

As explained in Section 4.3.2, the employment of an MPR at the beginning of each SM ensures sufficient reliability for the host LV microgrid. However, one may prefer to extend the protection scheme and utilize multiple MPRs along the radial SMs, to enhance the system reliability. In case a radial SM contains more than one MPR, it is necessary to coordinate them through a suitable grading method. Fig. 4.4 shows the basics of the definite-time grading method, for an example LV microgrid with two SMs that employs more than one (four, in this example) MPR in each radial SM.

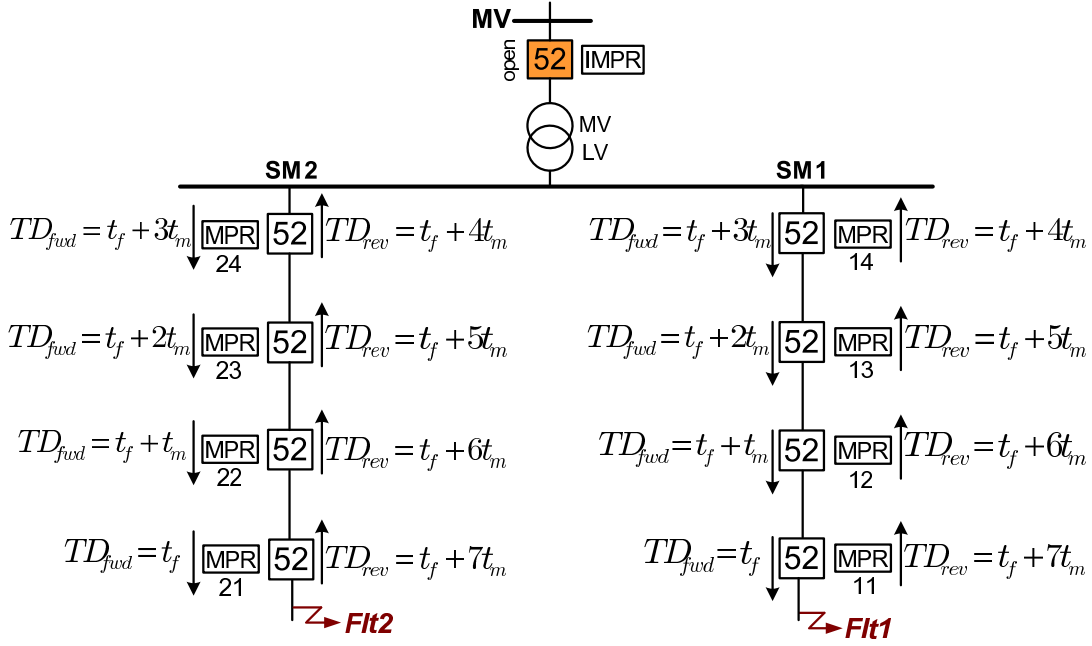


Figure 4.4: Extending the protection scheme for SMs including four MPRs.

Each MPR in Fig. 4.4 has its own forward and reverse time delays and is intended to protect a protection zone; the time delays used for forward and reverse operations of the MPRs are also indicated on the figure. Fig. 4.4 shows that for a forward fault at location  $Flt1$ , MPR11 operates first with a delay of  $t_f$ . This time delay is chosen in such a way that it allows the lateral protection to clear the fault if it is within the household/lateral installations. Therefore,  $t_f$  should be selected based on the practice that is accepted for the system under study [25], [98]. If MPR11 fails to operate, MPRs 12, 13, and 14, in sequence, are expected to clear the fault through their delayed operations. The same grading strategy is employed to coordinate the MPRs for the reverse path, e.g., for a fault at location  $Flt2$ . The same coordination grading scheme can also be employed for a microgrid with several (more than two) SMs.

Assuming that (i) the maximum time required for the fault detection, i.e.,  $t_f$ , is about 15 (60-Hz) cycles, (ii) the time considered for the margin, i.e.,  $t_m$ , is about 15 cycles, and (iii) the time needed by a circuit breaker to open is about 5 cycles, it takes less than three seconds for MPR11 to clear a fault at location  $Flt2$  in the reverse direction, if all MPRs fail to operate (which is a fairly rare scenario). If this operating time is not acceptable, e.g., in view of the system safety, the microgrid can be divided into smaller islanded systems, as suggested in [66].

## 4.4 Proposed Protection for the Grid-Connected Mode of Operation

As mentioned earlier, the conventional overcurrent protection can still be employed for the protection of a microgrid in the grid-connected mode of operation. The conventional coordination practice amongst the overcurrent protective devices was also explained in Section 1.4.1. Fig. 4.5 illustrates an example of the conventional protection coordination for two fuses, a main relay, and a backup relay for a typical distribution network. The figure indicates that the devices are coordinated for a fault current range, i.e.,  $(I_{fmin}, I_{fmax})$ , such that the MMT and TCT curves of the fuses lie below the characteristic curves of the relays, to ensure that the fuses will operate before the relays intervene [25]. In addition, a coordination must also be made between the fuses (the characteristic curves of the protective devices are described in Appendix B). If the fuses fail to operate for a fault, the main relay will back them up by operating according to its inverse-time characteristic. The backup relay will operate only if the main relay and the fuses fail to act. It should be pointed out that the (main and backup) relays are normally employed at the MV side of the substation transformer (utility grid side), and not within the LV network (microgrid side).

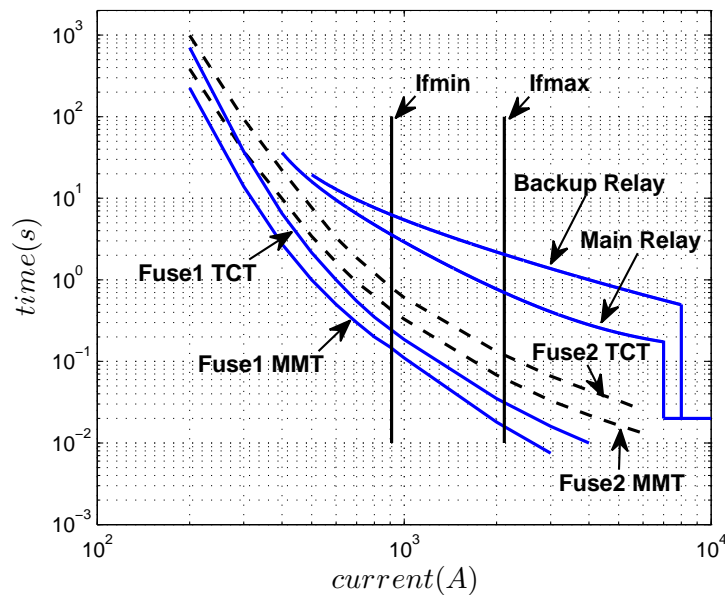


Figure 4.5: Traditional coordination of fuses and relays in a typical distribution network.

As it is evident from Fig. 4.5, one has to ensure that the fault current passing through the devices has a value between  $I_{fmin}$  and  $I_{fmax}$ , in order to maintain the coordination. However, the addition of a DER to an SM, anywhere downstream of the relay, affects  $I_{fmax}$  and  $I_{fmin}$  and also causes the fuse current to exceed the current seen by the relay (see Section 1.4.2). Chapter 3 proposed an effective solution to accommodate the impact of DERs on the coordination of protective devices (including reclosers), in a conventional distribution network. The method proposed in Chapter 3 utilizes microprocessor-based relays, but does not require communications or adaptive protective devices. Therefore, it is also adopted in this chapter as the coordination method for the fuses and MPRs in the grid-connected mode of operation. It is noted that, due to their limited fault current contributions, EC-DERs cannot significantly affect the protection coordination. In addition, it is assumed in this chapter that the secondary distribution network does not include any recloser [86], [87]. Thus, coordination of protective devices for the grid-connected mode of operation of an LV microgrid whose DERs are predominantly of the electronically coupled types is more straightforward than the general example analyzed in Chapter 3.

#### 4.4.1 External Faults

For a fault taking place outside of the microgrid jurisdiction, a low fault current may be contributed by the (grid-connected) microgrid, which does not guarantee the operation of the overcurrent protection scheme of the relay that is located at the microgrid interface point, i.e., IMPR. To address this shortcoming, the IMPR must also employ the islanded-mode protection strategy of Section 4.3, despite the fact that it always operates in the grid-connected mode. The only difference is that definite-time grading of the IMPR starts at the microgrid interface point and ends at the load side of the SMs; Fig. 4.6 illustrates the process for two adjacent SMs with their respective MPRs.

#### 4.4.2 Neutral Voltage Displacement (NVD) Protection

Another issue concerning the IMPR may arise when the microgrid operates in the islanded mode of operation. Although the neutral grounding of the LV microgrid is preserved due to the LV-side star winding configuration of the step-down transformer, the MV side of the step-down transformer, which is still energized, becomes ungrounded in the islanded mode of operation. Therefore, overvoltages may be experienced if a ground fault impacts



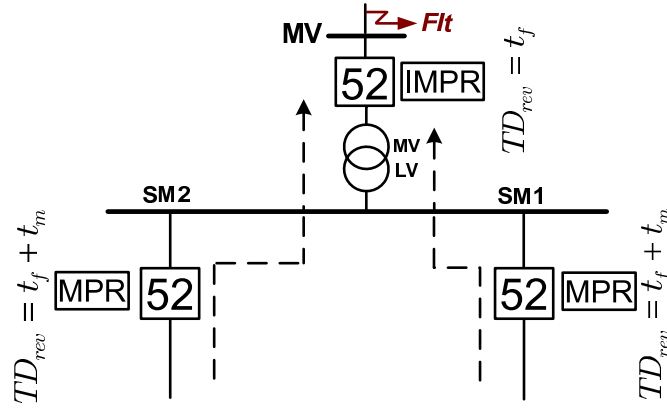


Figure 4.6: Coordination of the IMPR and MPRs for an external (grid) fault.

the ungrounded MV side of the step-down transformer (area “A” in Fig. 4.8), in the islanded mode of operation. To address this issue and to detect such faults, this study proposes the use of a Neutral Voltage Displacement (NVD) protection function in the IMPR [99].

## 4.5 Proposed Microgrid Protection Relay (MPR)

The protection strategy proposed in Sections 4.3 and 4.4 can be implemented through a microprocessor-based relay. The present-day digital relays typically offer standard over-current, overvoltage/undervoltage, and overfrequency/underfrequency protection functions. In addition, they are self metering, have oscillographic event reporters and communication links, and offer logic programming capabilities [100], [101].

Fig. 4.7 illustrates a simplified block diagram of the proposed MPR, showing the functional modules and key elements of the relay and that the MPR consists of three distinct phase modules which independently protect the corresponding phases of the host SM. This ensures a continuous supply for the single-phase loads that are connected to sound phase(s), and thus enhances the security of supply. Fig. 4.7 also indicates that an additional module, the three-phase protection module, is employed to provide a redundant protection based on zero-/negative-sequence components. The three-phase module works only through three-phase tripping, as Fig. 4.7 shows. Further, an interface module is included in the IMPR to enable reconnection of the islanded microgrid to the utility grid. In addition, a module has also been dedicated to negative-sequence directional function. Finally, a tripping module determines the type of the trip signal

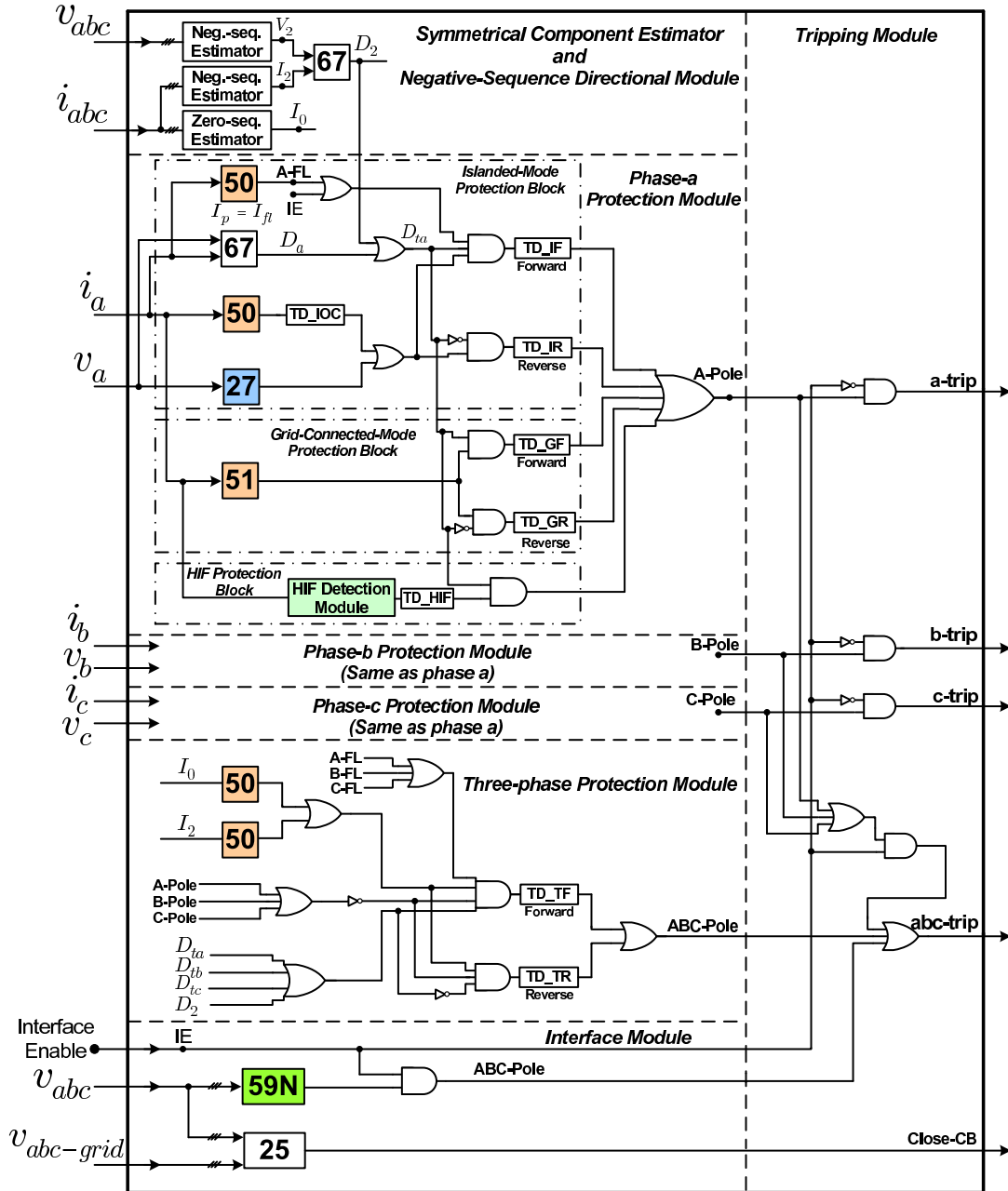


Figure 4.7: Simplified schematic diagram of the proposed MPR (or IMPR).

that will be sent out by an MPR or the IMPR.

Fig. 4.7 further shows that three different blocks, namely, the islanded-mode protection block, the grid-connected-mode protection block, and the HIF protection block, are included in a phase module. The islanded-mode protection block is implemented based on the discussions of Sections 4.3.3 and 4.3.4, whereas the materials presented in Section 4.4 are the base for the implementation of the grid-connected-mode protection

block. It must be noted that the forward and reverse time delays are generally different in the islanded mode of operation, compared to the grid-connected mode of operation. It is pointed out that HIF detection algorithm, which provides protection against HIFs, is fairly slow compared to other modules [93]. This, however, does not pose a serious problem since HIF currents are very small.

The three-phase protection module in the MPR of Fig. 4.7 operates with a prespecified delay should the phase protection modules fail to clear the fault (see Section 4.3.3–2). In addition, an NVD protection elements is employed to help the IMPR detect faults at the MV side of the step-down transformer. A synchronism-check relay is also used in the IMPR, to ensure safe reconnection of the (islanded) microgrid to the utility grid. The device and/or protection function numbers used in this study have been specified in Appendix C.

#### 4.5.1 Special Case

Typically, settings of the inverse-time overcurrent relays are determined in a manner to provide coordination for a fairly wide range of the short-circuit capacity of the utility grid. This is performed through the proper selection of  $I_{fmin}$  and  $I_{fmax}$  (see Chapter 3). However, if the utility grid is so weak that the fault current magnitudes are comparable in both modes of operation, the grid-connected-mode protection block of Fig. 4.7 is not necessarily required, and one can deactivate it through assigning fairly large values to time delays TD\_GF and TD\_GR. Otherwise, it will operate with a delay and may interfere with the islanded-mode protection block, which is now responsible for protection of the microgrid in both modes of operation. It is remembered that an instantaneous overcurrent relay (with a prespecified time delay, TD\_IOC) is also utilized in the islanded-mode protection block, as shown in Fig. 4.7.

## 4.6 Simulation Results

To demonstrate the effectiveness of the proposed protection scheme and the MPRs/IMPR, a realistic LV microgrid system has been simulated in the PSCAD/EMTDC software environment. The structure of the simulated micogrid which, hereinafter, is referred to as “*study microgrid*”, is almost the same as the study system of Chapter 2 and is briefly described next; then, study cases are presented.

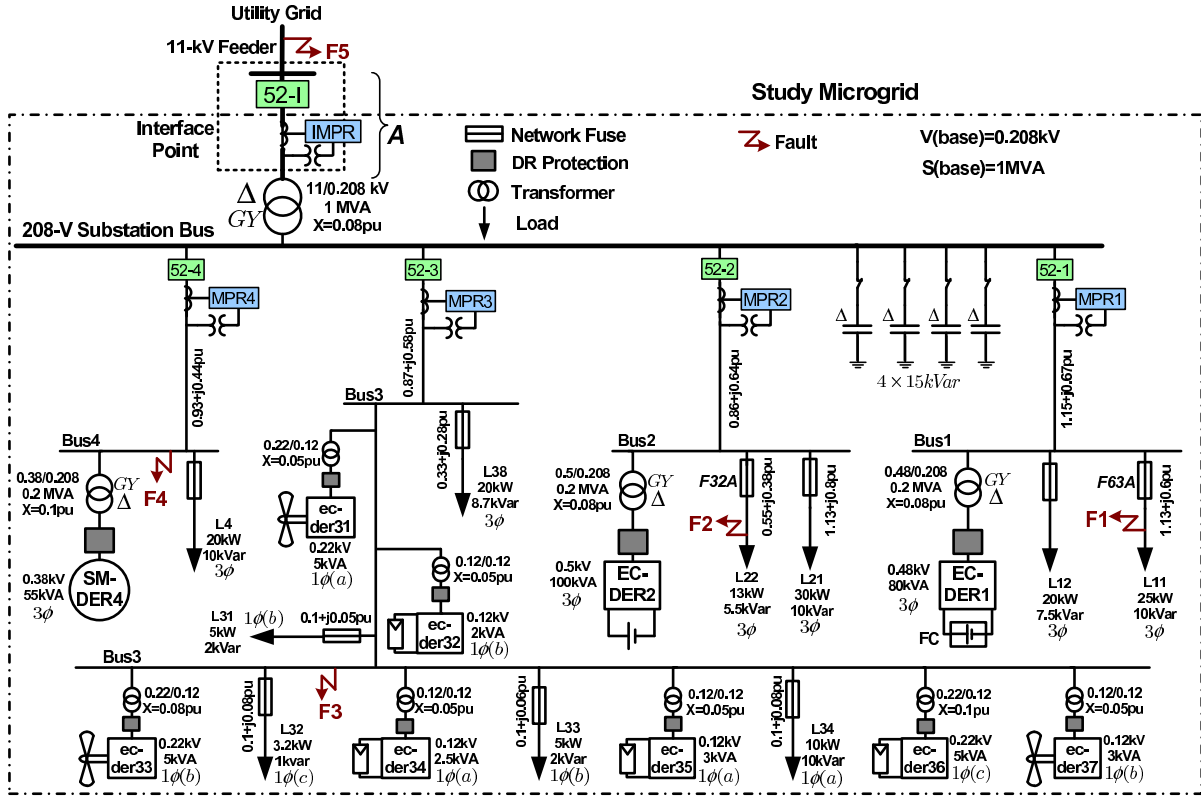


Figure 4.8: Single-line diagram of the study LV microgrid.

#### 4.6.1 Study Microgrid

Fig. 4.8 shows a single-line diagram of the study microgrid, of which basic configuration and majority of parameters are taken from the benchmark system presented in [77] and [78]. As Fig. 4.8 shows, the backbone of the study microgrid is a 208-V, four-SM, distribution subsystem, which is connected to the main utility grid through a  $\Delta$ /GY step-down transformer and an 11-kV radial feeder. The distribution substation is equipped with four banks of three-phase shunt capacitors, each with the capacity of 15 kVA. The grid is represented by an 11-kV bus with a short-circuit capacity of 80 MVA. A combination of different three-phase and single-phase loads is energized through the four radial SMs. The system also includes two three-phase EC-DERs, a conventional three-phase synchronous-machine-based DER, and seven single-phase EC-DERs. The units EC-DER1, EC-DER2, and ec-der31 through ec-der37 utilize VSCs as their interface media, whereas SM-DER4 is directly interfaced with the network. The three-phase DERs are connected to the network through respective  $\Delta$ /GY interconnection transformers, and the single-phase DERs utilize single-phase interconnection transformers. The EC-

DERs are of the wind, photovoltaic, battery, and fuel cell types, as indicated in Fig. 4.8. To protect the microgrid, five MPRs, four at the beginning of the SMs and one at the interface point, have been used. Fuses and traditional relaying functions are modeled in this chapter based on the analytical equations presented in Appendix B.

## 4.6.2 Study Cases

### 1) Islanded Mode of Operation

System studies have been performed, with the MPR settings and time delays calculated based on the strategy proposed in Sections 4.3 and 4.4; the time delays used in this study are specified in Appendix C. Let us assume that a fault impacts the microgrid while it is isolated from the main grid. Tables 4.2 and 4.3 report the primary and backup relay operating times for different fault scenarios in the islanded mode of operation. A large number of simulation tests have been conducted considering several fault scenarios; however, due to space limitation, only a limited number of study cases have been reported in this thesis. In the reported results, it has been tried to cover different types of faults, different locations, and different fault resistances. Table 4.2 shows the simulation results for solid faults while the results of Table 4.3 corresponds to high-impedance faults.

Since in the islanded mode of operation a fault results in an insufficient fault current, the network fuses take a relatively long time to operate. Therefore, the faults are cleared by the MPRs. For solid faults, the voltage drop across the microgrid is significant and the undervoltage protection can detect and isolate the faults. However, for high-impedance faults, only three-phase protection modules (3-Ph) or HIF detection modules (HIF) operate, as no voltage dip is detected by the undervoltage protection function. The HIF detection module ensures protection against HIFs even if zero-/negative-sequence current components are smaller than the threshold values required for detection. As Table 4.3 indicates, HIF detection algorithm is fairly slow compared to other modules. HIFs are modeled in this chapter based on the method presented in [62].

To demonstrate the effectiveness of the proposed method and MPR for the fault scenarios in which the fault currents are very small, SM4 was disconnected from the substation, and therefore the synchronous-machine-based DER (SM-DER4) was sent out of service, assuming that, for example, a fault had impacted the SM. Then, similar fault studies were conducted, and the results were found to be very similar to those of the previous cases in which SM-DER4 was connected to the microgrid. However, only a

selected number of scenarios have been reported in Tables 4.2 and 4.3.

## 2) Grid-Connected Mode of Operation

Several cases have also been simulated for the grid-connected mode of operation but, due to space limitations, the results of only a limited number of them have been reported in Tables 4.4 and 4.5. Tables 4.4 and 4.5 show the primary and backup relay operating times for different internal and external faults, at various locations, while the microgrid operates in conjunction with the main grid. Similar to the islanded mode of operation, it is observed that if the MPR which is responsible for the primary protection fails to operate, other MPRs provide suitable backup protection.

## 4.7 Summary and Conclusion

This chapter proposed a protection strategy and an enabling relay for protection of low-voltage microgrids in the islanded mode as well as grid-connected mode of operation. The proposed protection strategy can be implemented through programmable microprocessor-based relays, and can address protection issues of a microgrid in both modes of operation. The proposed strategy does not require communication links or adaptive protective devices. More important, its effectiveness is to a large extent independent of the fault current levels, the mode of operation, and the type and size of distributed energy resource units, subject to the modified relay setting for the grid-connected mode of operation. Further, the proposed protection strategy enables single-phase tripping to increase security of supply. Several study cases were presented based on digital time-domain simulation of a model microgrid, to demonstrate the effectiveness of the proposed protection scheme and the enabling relay. Protection of large medium-voltage microgrid will be discussed in the following chapter.

Table 4.2: Operating Times of Primary and Backup Protection for Selected Solid Fault Scenarios in the Islanded Mode of Operation

Fault Type	Fault Loc.	Solid Faults					
		Primary Protection			Backup Protection		
		Oper. Relay	Prot. Type	Oper. Time (s)	Oper. Relay	Prot. Type	Oper. Time (s)
<b>SM4 is connected (SM-DER4 is in service)</b>							
AG	F1	MPR1	27	0.085	MPR2	27	0.485
					MPR3	27	0.489
					MPR4	27	0.483
	F2	MPR2	27	0.087	MPR1	27	0.483
					MPR3	27	0.491
					MPR4	27	0.483
	F3	MPR3	27	0.084	MPR1	27	0.483
					MPR2	27	0.484
					MPR4	27	0.477
BCG	F2	MPR2	27	0.086	MPR1	27	0.483
					MPR3	27	0.487
					MPR4	27	0.483
	F4	MPR4	27	0.088	MPR1	27	0.485
					MPR2	27	0.485
					MPR3	27	0.486
BC	F1	MPR1	27	0.084	MPR2	27	0.481
					MPR3	27	0.485
					MPR4	27	0.481
	F3	MPR3	27	0.082	MPR1	27	0.482
					MPR2	27	0.480
					MPR4	27	0.479
ABC	F1	MPR1	27	0.084	MPR2	27	0.483
					MPR3	27	0.484
					MPR4	27	0.483
	F4	MPR4	27	0.080	MPR1	27	0.477
					MPR2	27	0.478
					MPR3	27	0.480
<b>SM4 is not connected (SM-DER4 is out of service)</b>							
AG	F2	MPR2	27	0.086	MPR1	27	0.483
					MPR3	27	0.491
	F3	MPR3	27	0.083	MPR1	27	0.483
					MPR2	27	0.489
BCG	F1	MPR1	27	0.085	MPR2	27	0.482
					MPR3	27	0.497
	F2	MPR2	27	0.086	MPR1	27	0.485
					MPR3	27	0.494

Table 4.3: Operating Times of Primary and Backup Protection for Selected High-Impedance Fault Scenarios in the Islanded Mode of Operation

Fault Type	Fault Loc.	High-Impedance Faults ( $\approx 30$ kW)					
		Primary Protection			Backup Protection		
		Oper. Relay	Prot. Type	Oper. Time (s)	Oper. Relay	Prot. Type	Oper. Time (s)
<b>SM4 is connected (SM-DER4 is in service)</b>							
AG	F1	MPR1	3-Ph	0.285	MPR2	3-Ph	0.685
					MPR3	3-Ph	0.688
					MPR4	3-Ph	0.684
	F2	MPR2	3-Ph	0.287	MPR1	3-Ph	0.685
					MPR3	3-Ph	0.685
					MPR4	3-Ph	0.685
	F3	MPR3	3-Ph	0.283	MPR1	3-Ph	0.685
					MPR2	3-Ph	0.684
					MPR4	3-Ph	0.684
BCG	F2	MPR2	3-Ph	0.286	MPR1	3-Ph	0.686
					MPR3	3-Ph	0.688
					MPR4	3-Ph	0.683
	F4	MPR4	3-Ph	0.286	MPR1	3-Ph	0.688
					MPR2	3-Ph	0.688
					MPR3	3-Ph	0.689
BC	F1	MPR1	3-Ph	0.283	MPR2	3-Ph	0.686
					MPR3	HIF	$\approx 4.0$
					MPR4	3-Ph	0.682
	F3	MPR3	3-Ph	0.282	MPR1	3-Ph	0.686
					MPR2	3-Ph	0.686
					MPR4	3-Ph	0.682
ABC	F1	MPR1	HIF	$\approx 3.5$	MPR2	HIF	$\approx 4.0$
					MPR3	HIF	$\approx 4.0$
					MPR4	HIF	$\approx 4.0$
	F4	MPR4	HIF	$\approx 3.5$	MPR1	HIF	$\approx 4.0$
					MPR2	HIF	$\approx 4.0$
					MPR3	HIF	$\approx 4.0$
<b>SM4 is not connected (SM-DER4 is out of service)</b>							
AG	F2	MPR2	3-Ph	0.284	MPR1	3-Ph	0.679
					MPR3	3-Ph	0.688
	F3	MPR3	3-Ph	0.284	MPR1	3-Ph	0.682
					MPR2	3-Ph	0.687
BCG	F1	MPR1	3-Ph	0.288	MPR2	3-Ph	0.691
					MPR3	HIF	$\approx 4.0$
	F2	MPR2	3-Ph	0.285	MPR1	3-Ph	0.686
					MPR3	HIF	$\approx 4.0$



Table 4.4: Operating Times of Primary and Backup Protection for Selected Solid Fault Scenarios in the Grid-Connected Mode of Operation

Fault Type	Fault Loc.	Solid Faults					
		Primary Protection			Backup Protection		
		Oper. Relay	Prot. Type	Oper. Time (s)	Oper. Relay	Prot. Type	Oper. Time (s)
<b>Internal Faults</b>							
AG	F1	F63A	O/C	0.054	MPR1	51	0.211
					IMPR	51	0.569
					MPR2	3-Ph	0.685
					MPR3	3-Ph	0.685
					MPR4	3-Ph	0.684
	F2	F32A	O/C	0.031	MPR2	51	0.199
					IMPR	51	0.554
					MPR1	3-Ph	0.685
					MPR3	3-Ph	0.685
					MPR4	3-Ph	0.685
BCG	F1	F63A	O/C	0.042	MPR1	51	0.194
					IMPR	51	0.557
					MPR2	3-Ph	0.792
					MPR3	3-Ph	0.790
					MPR4	3-Ph	0.686
	F3	MPR3	51	0.188	IMPR	51	0.540
					MPR1	3-Ph	0.767
					MPR2	3-Ph	0.769
					MPR4	3-Ph	0.761
					BC	F3	MPR3
MPR1	3-Ph	0.772					
MPR2	3-Ph	0.775					
MPR4	3-Ph	0.771					
ABC	F4	MPR4	51	0.184	IMPR	51	0.530
					MPR1	3-Ph	0.685
					MPR2	3-Ph	0.685
					MPR3	3-Ph	0.688
<b>External Faults</b>							
ABC	F5	IMPR	27	0.079	MPR1	27	0.483
					MPR2	27	0.483
					MPR3	27	0.486
					MPR4	27	0.483
AG	F5	IMPR	27	0.081	MPR1	27	0.485
					MPR2	27	0.485
					MPR3	27	0.488
					MPR4	27	0.485

Table 4.5: Operating Times of Primary and Backup Protection for Selected High-Impedance Fault Scenarios in the Grid-Connected Mode of Operation

Fault Type	Fault Loc.	High-Impedance Faults ( $\approx 30$ kW)					
		Primary Protection			Backup Protection		
		Oper. Relay	Prot. Type	Oper. Time (s)	Oper. Relay	Prot. Type	Oper. Time (s)
<b>Internal Faults</b>							
AG	F1	MPR1	3-Ph	0.286	IMPR	3-Ph	0.615
					MPR2	3-Ph	0.688
					MPR3	3-Ph	0.691
					MPR4	3-Ph	0.685
BCG	F2	MPR2	3-Ph	0.288	IMPR	3-Ph	0.619
					MPR1	3-Ph	0.689
					MPR3	3-Ph	0.693
					MPR4	3-Ph	0.685
BCG	F1	MPR1	3-Ph	0.283	IMPR	3-Ph	0.623
					MPR2	3-Ph	0.689
					MPR3	3-Ph	0.791
					MPR4	3-Ph	0.689
BCG	F3	MPR3	3-Ph	0.283	IMPR	3-Ph	0.619
					MPR1	HIF	$\approx 4.0$
					MPR2	HIF	$\approx 4.0$
					MPR4	HIF	$\approx 4.0$
BC	F3	MPR3	3-Ph	0.285	IMPR	3-Ph	0.611
					MPR1	HIF	$\approx 4.0$
					MPR2	HIF	$\approx 4.0$
					MPR4	3-Ph	0.682
ABC	F4	MPR4	HIF	$\approx 3.5$	IMPR	HIF	$\approx 4.0$
					MPR1	HIF	$\approx 4.0$
					MPR2	HIF	$\approx 4.0$
					MPR3	HIF	$\approx 4.0$
<b>External Faults</b>							
ABC	F5	IMPR	HIF	$\approx 3.5$	MPR1	HIF	$\approx 4.0$
					MPR2	HIF	$\approx 4.0$
					MPR3	HIF	$\approx 4.0$
					MPR4	HIF	$\approx 4.0$
AG	F5	IMPR	3-Ph	0.276	MPR1	3-Ph	0.678
					MPR2	3-Ph	0.679
					MPR3	3-Ph	0.778
					MPR4	3-Ph	0.768

# Chapter 5

## Protection of Medium-Voltage Microgrids

### 5.1 Introduction

The protection strategy proposed in Chapter 4, for LV microgrids, does not require communications or adaptive settings; however, since it relies on the definite-time grading technique for coordination of relays, it may take a relatively long time to isolate a fault within a large medium-voltage (MV) microgrid (especially in the islanded mode of operation). Therefore, a faster protection strategy should be devised for large MV microgrids, where fast fault clearance is desired. On the other hand, with the advent of the “*Smart Grid*” concept, the future power system is envisioned to heavily rely on communications and massive computing power. Thus, a communication-based protection scheme would be a possible option for the protection of large MV microgrids, where a more rapid and faithful protection scheme is required.

This chapter proposes a communication-assisted protection strategy implementable by commercially available microprocessor-based relays for protection of MV microgrids. Even though the developed protection strategy benefits from communications, it offers a backup protection strategy to manage communication network failures; this ensures that the network is always protected. The strategy is effective in both modes of operation, and does not require to detect the mode of operation and switch between different protection schemes (for the grid-connected and islanded modes). The structure of the relay proposed in Chapter 4 is also modified in this chapter; the modified relay enables the designer to implement the proposed protection strategy. Comprehensive simulation studies are

carried out to verify the effectiveness of the proposed protection strategy under different fault scenarios, in the PSCAD/EMTDC environment.

## 5.2 Typical Medium-Voltage Distribution Networks

Traditionally, distribution networks have been designed to operate radially, that is, the energy flows down from the upper voltage levels to the loads connected to radial feeders. Even though some networks may have loop-closing feeders, the loops are kept open by normally-open switches which are closed only when other parts of the loops are opened, e.g., when a fault impacts the network; thus, the radial configuration of the network is always preserved [62].

Fig. 5.1 shows the schematic diagram of a typical MV distribution network which is supplied by a step-down substation transformer. As Fig. 5.1 indicates, the loads are supplied by a number of radial (overhead or underground) lines. Fig. 5.1 also shows that simple overcurrent devices are employed to protect the equipment and to ensure safety. Thus, protection is commonly offered by fuses, sectionalizers, and reclosers for overhead lines, and circuit breakers for underground lines. As explained in Chapter 1, these devices are coordinated in such a way that the smallest possible part of the network is de-energized subsequent to a fault incident [25].

## 5.3 Medium-Voltage Microgrids

Fig. 5.2 shows the schematic diagram of a hypothetical microgrid which is based on the distribution network of Fig. 5.1. As Fig. 5.2 indicates, the microgrid embeds a great deal of EC-DERs, along with the traditional rotating-machine-based generators. This is due to the fact that the control of EC-DERs is more flexible, as compared to their rotating-machine-based counterparts; in addition, EC-DERs play an important role in obtaining a cleaner environment, as they are generally based on renewable energy systems. Fig. 5.2 shows that the LV side of the substation transformer is defined for the microgrid as the “*interface bus*”, where the microgrid is interfaced with the host power system.

The DERs offset the power that the microgrid imports from the grid in the grid-connected mode of operation; they, however, supply the total microgrid load power if the microgrid is isolated from the grid at the interface bus (i.e., in the islanded mode of operation). It is assumed in this chapter that a signal-processing entity, referred hereafter

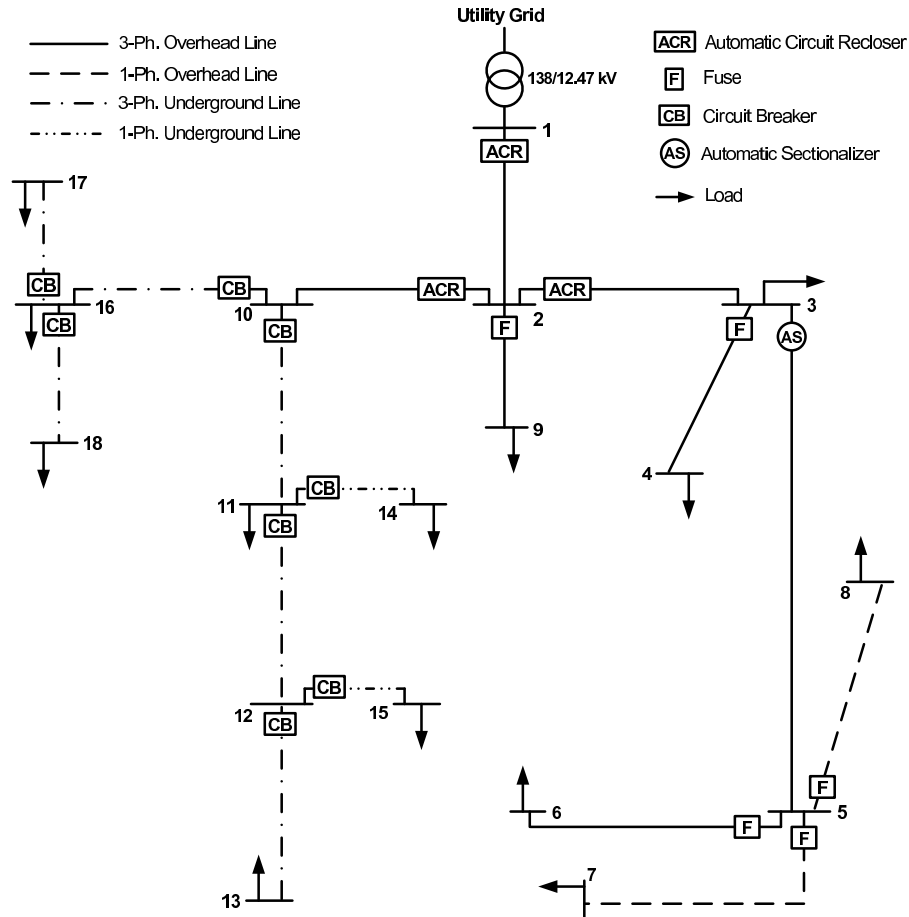


Figure 5.1: Single-line diagram of a typical medium-voltage distribution network and its conventional protection devices.

to as the “*Microgrid Protection Commander*” (MPC), coordinates the communication-assisted activities of the microgrid protection. In Fig. 5.2, the MPC is shown to be at the interface bus. However, it can be located anywhere within the microgrid from the physical location viewpoint.

## 5.4 Structure of the Relay Enabling the Proposed Protection Strategy

In this chapter, a communication-assisted protection strategy is proposed for MV microgrids. The proposed protection strategy employs microprocessor-based relays to detect faults and to isolate them in a selective (coordinated) manner. The proposed protection strategy is, thus, enabled by a proposed relay which is referred to as the microgrid pro-

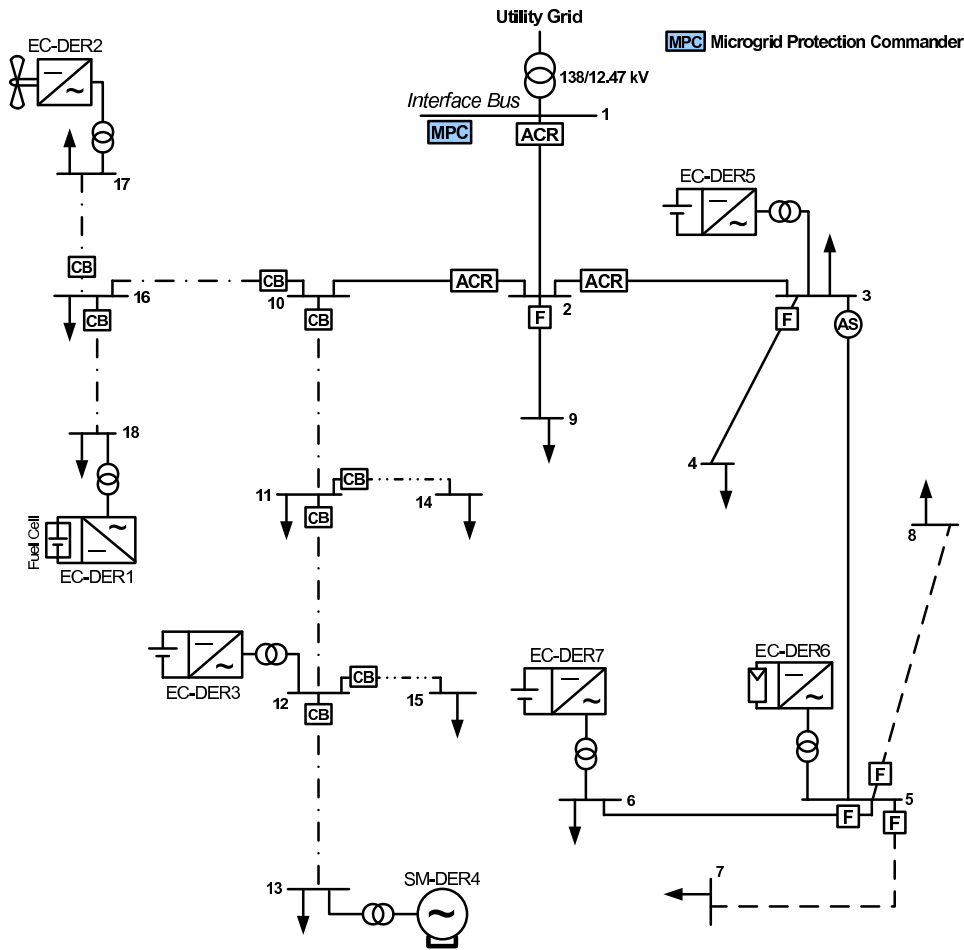


Figure 5.2: The network of Fig. 5.1 that is equipped with DERs and can be operated as an MV microgrid.

tection relay or MPR. The objective of this section is to introduce the structure and key features of the MPR. If an MPR has the capability to communicate with other devices, it is referred to as a “*Communication-Assisted Microgrid Protection Relay*” (CMPR). Hence, the only difference between an MPR and a CMPR is that the former does not use communications.

As discussed in Chapter 4, different protection functions are required to design an appropriate protection scheme for microgrids. The aforementioned protection functions can be embedded in commercially available microprocessor-based relays. Fig. 5.3 illustrates the schematic diagram and functional modules of the proposed MPR/CMPR, which are the revised versions of the relay proposed in Chapter 4. As Fig. 5.3 shows, five modules exist in an MPR/CMPR: “*the directional module*”, “*the islanded-mode protection module*”, “*the grid-connected-mode protection module*”, “*the interface module*”,

and “the tripping module”. The directional module determines the direction of the fault and also calculates the ratio  $F$  (to be defined in Section 5.4.1), based on the method presented in Sections 5.4.1 and 5.4.2. The output of the directional module is used by the islanded-mode protection module and the grid-connected-mode protection module; these two modules are to protect the microgrid in the islanded and grid-connected modes of operation, respectively, for the backup protection strategy of Section 5.5.2. The interface module consists of neutral voltage displacement (NVD) and synchronism-check functions. The synchronism-check relay is used to ensure safe reconnection of the islanded *small microgrid* (to be defined in Section 5.5.1) to the rest of the network or to the main utility grid; the function of NVD relay was explained in Section 4.4.2. Finally, the tripping module decides whether or not a trip signal should be issued. More details about the proposed relay will be discussed in Section 5.5.

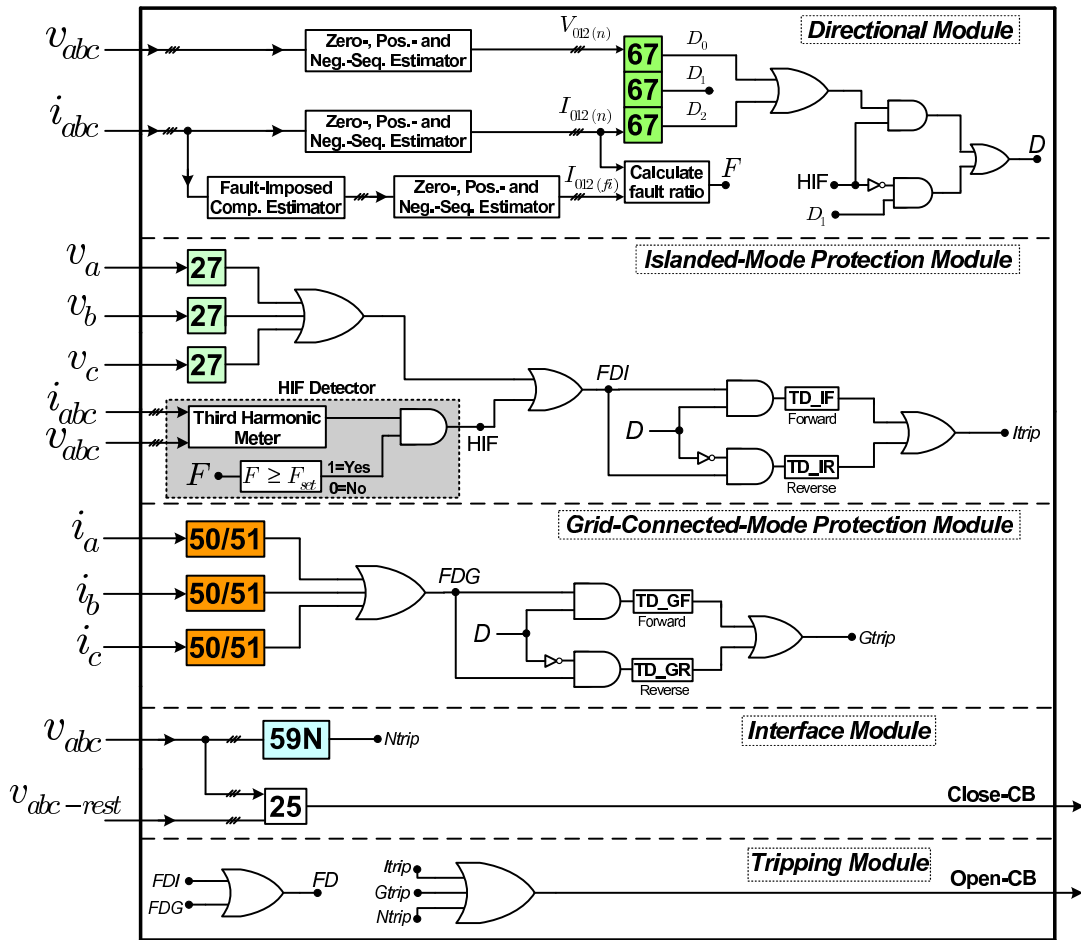


Figure 5.3: Simplified schematic diagram of an MPR/CMPR.

### 5.4.1 Strategy for High-Impedance Fault Detection

High-impedance faults (HIFs) are difficult to detect by conventional techniques. Although various methods have been proposed in the past to address the issue [93]- [95], there exists no comprehensive solution thus far. This chapter presents a technique for the detection of HIFs that basically relies on the measurement of current sequence components. The advantage of the proposed technique is that it can be readily incorporated into digital relays. However, due to the inherent unbalanced nature of distribution networks, sequence components also exist under normal operating conditions that may give rise to mal-operation of sequence-component-based protection schemes. The issue gets even more complicated when the fault currents are not sufficiently larger than the nominal load currents, e.g., for HIFs or even for faults in the islanded mode of operation. To circumvent the issue, this chapter proposes the use of fault-imposed current components [103].

Fault-imposed components of electrical variables are the ones that appear when a fault impacts the network. They possess signatures of the fault and are independent of the normal-running form of the variables. Based on the superposition theorem, a current or voltage variable can be considered to consist of two components: (1) a normal-running component, and (2) a fault-imposed component. The fault-imposed component can be calculated using superimposed networks [103], [104]. Assuming that  $i_n(t)$  is the current of the normal system (normal-running current),  $i_f(t)$  is the current of the faulted system (fault current), and  $i_{fi}(t)$  is the current of the superimposed network (fault-imposed current), one can write:

$$i_f(t) = i_n(t) + i_{fi}(t) , \quad (5.1)$$

or

$$i_{fi}(t) = i_f(t) - i_n(t) . \quad (5.2)$$

As (5.2) indicates, the fault-imposed current can be calculated by subtracting the normal-running (pre-fault) current from the fault (post-fault) current. Thus, the fault-imposed component does not exist under normal condition but appears if a fault takes place within the network. The scheme used for calculating the fault-imposed component is known as the Delta Filter [105]. The basic Delta Filter subtracts the delayed version of an input signal from the input signal itself, where the delay is an integer multiple of the



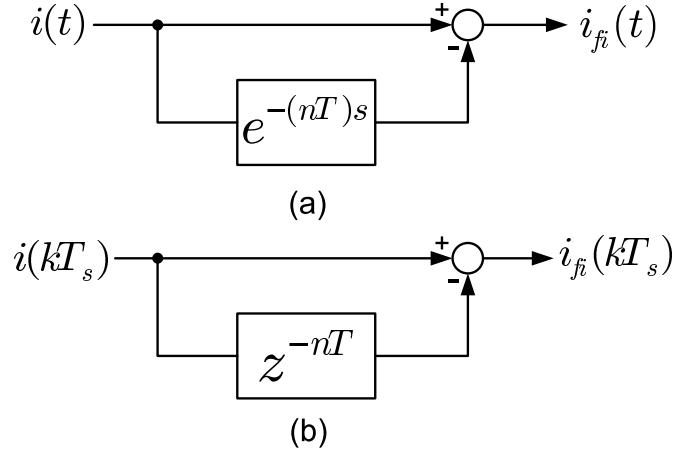


Figure 5.4: Concept of a Delta-Filter for a time-varying waveform: (a) continuous-time form, and (b) discrete-time form.

signal period; Fig. 5.4(a) illustrates the process for a continuous-time implementation. Thus, the fault-imposed component of the signal  $i$  can be calculated as

$$i_{fi}(t) = i(t) - i(t - nT), \quad (5.3)$$

where  $T$  is the signal period, and  $n$  is an integer ( $n=6$  in this study). In a microprocessor-based relay, the normal-running and fault current components are obtained by periodic sampling of the current waveform. Hence, the discrete-form of the Delta Filter, Fig. 5.4(b), is used; the discrete form of (5.3) is

$$i_{fi}(kT_s) = i(kT_s) - i(kT_s - nT), \quad (5.4)$$

in which  $T_s$  is the sampling period that should be sufficiently smaller than the signal period  $T$ ;  $k$  is the sampling step ( $k=0, 1, 2, \dots$ ).

Now, let us consider a three-phase current whose phase components are  $i_a(t)$ ,  $i_b(t)$ , and  $i_c(t)$ . Then, the instantaneous symmetrical components of  $i_{abc}$  are calculated by [106].

$$\begin{bmatrix} i_0(t) \\ i_1(t) \\ i_2(t) \end{bmatrix} = \frac{1}{\sqrt{3}} \begin{bmatrix} 1 & 1 & 1 \\ 1 & q^{-2} & q^{-1} \\ 1 & q^{-1} & q^{-2} \end{bmatrix} \begin{bmatrix} i_a(t) \\ i_b(t) \\ i_c(t) \end{bmatrix}, \quad (5.5)$$

where  $q^{-1}$  is a time-domain delay operator that causes a delay equal to  $T/3$ , i.e.,  $q^{-1}x(t) = x(t - T/3)$ ;  $i_0(t)$ ,  $i_1(t)$ , and  $i_2(t)$  are instantaneous zero-, positive-, and negative-sequence

components, respectively. The current  $i_{abc}(t)$  can be the normal-running current, the fault current, or the fault-imposed current. Thus, (5.5) provides three corresponding sets of sequence components which can be used to define a ratio, [107], [108], that is hereafter called the “*system imbalance ratio*”. This ratio, denoted by  $R$ , shows the change in the zero- and negative-sequence components relative to the positive-sequence component and is defined as

$$R = \frac{|i_0(t)| + |i_2(t)|}{|i_1(t)|}, \quad (5.6)$$

where  $|i_0(t)|$ ,  $|i_1(t)|$ , and  $|i_2(t)|$  are the rms values of the zero-, positive-, and negative-sequence components, respectively. Let  $R_n$ ,  $R_f$ , and  $R_{fi}$  be the values of  $R$  when  $i_{abc}(t)$  is respectively the normal-running current, the fault current, and the fault-imposed current. Then, it is noted that the ratio  $R_n$  is not zero since distribution networks are inherently unbalanced; the system imbalance, however, is not very large under normal conditions, and it is typically less than 20% [92], [109], [110]. When a solid fault strikes the system,  $R_n$  changes significantly (to the value of  $R_f$ ). Therefore,  $R_f$  is an effective means for detecting solid faults. On the other hand, the zero- and negative-sequence components corresponding to a HIF are not necessarily larger than their counterparts under a normal-running condition and, therefore, one cannot ignore the system imbalance when detecting HIFs. To address the issue, this chapter proposes the use of the fault-imposed component for fault detection, i.e., instead of  $R_f$  the ratio  $R_{fi}$  is used to detect faults. To further desensitize the protection algorithm, this chapter also proposes a new ratio, the “*fault ratio*”, for detecting HIFs; the fault ratio is defined as

$$F = \frac{R_{fi}}{R_n}. \quad (5.7)$$

As compared to  $R$ , which represents the change in the zero- and negative-sequence components with respect to the positive-sequence component, the ratio  $F$  indicates the change in the sequence components, from the normal-running condition to the fault condition. Therefore,  $F$  is less sensitive to network imbalance and can be effectively used for fault detection. If  $F$  is larger than a threshold,  $F_{set}$ , for a prespecified period of time, the presence of a fault is established, and an action is taken based on the proposed coordination strategy of Section 5.5; in this study, the threshold  $F_{set}$  has been assumed to be 1.2. One problem associated with the proposed fault detection scheme is that it may fail to operate for high-impedance three-phase-to-ground faults. This, however, is

not very problematic since: (i) a very small percentage of the network faults (less than 0.1%, if not zero) are of high-impedance three-phase-to-ground type, and (ii) the current level for this type of fault is in the range of load current, and is unlikely to damage the system equipment in a short time. However, to prevent safety risks to the public, further studies should be conducted to resolve this issue.

Another issue concerning the HIF detection strategy arises when a single-phasing incident takes place, during which one phase of a three-phase circuit is missing or de-energized. Thus, the proposed strategy may not be able to distinguish a single-phasing event from a HIF. To address the issue, the HIF detection strategy is augmented with a “*third harmonic meter*” block, as shown in Fig. 5.3. The block monitors the changes in the magnitude and phase angle of the feeder third harmonic current, as these changes follow a unique pattern for HIFs [95]. It should be noted that the third-harmonic meter is not able to detect all HIFs solely [93] and, thus, the use of the proposed HIF detection strategy along with this block is necessary.

### 5.4.2 Directional Decision Making

The proposed communication-assisted protection strategy requires directional elements which are simulated based on the method presented in Chapter 4. When a HIF impacts the network, the directional elements may fail to indicate the correct location of the fault. To deal with the issue, this chapter proposes the employment of zero-sequence directional elements; the strategy is similar to the one exercised in directional groundfault relays to protect isolated-neutral or impedance-grounded networks, where the fault current may be small [103], [111]. Moreover, a negative-sequence directional element is used to ensure protection against faults with small current magnitudes that do not include all three phases, e.g., phase-to-phase faults [97]. As shown in Fig. 5.3, different combinations of zero-, negative-, and positive-sequence directional signals are used in the proposed strategy to constitute the main directional signal,  $D$ , according to the fault type [96].

## 5.5 Proposed Protection Strategy

This section describes the proposed communication-assisted protection strategy, enabled by the relay of Section 5.4. The proposed protection strategy offers the main and backup protections.

### 5.5.1 Main Protection

Based on the proposed protection strategy, a microgrid is divided into a desired number of subnetworks so that each can be isolated from the rest of the microgrid through the commands delivered to one or more CMPRs. This requires that some protective devices of the original distribution network be replaced by CMPRs, each protecting a corresponding subnetwork. The division of the microgrid into the subnetworks is performed based on the system requirements, constraints, and configuration; however, the proposed protection strategy would be even more effective if a generation-demand balance existed within the subnetworks so that they could be operated as islands. If that is the case, some protective devices within each subnetwork could also be replaced by MPRs to provide higher reliability and isolate the faults within each subnetwork. Otherwise, the subnetworks must be dropped out when they get islanded, due to a fault either within themselves or in their neighboring subnetworks. Therefore, the use of MPRs is optional; the number of the MPRs that are employed in each subnetwork is determined based on the required reliability. Hereafter, a subnetwork is referred to as a “*small microgrid*”, even if it cannot be operated autonomously.

The proposed strategy assumes that each CMPR (which is responsible for protecting a corresponding small microgrid) sends two signals to the MPC: (1) the “*fault detection signal*” (FD) which indicates whether or not the CMPR has detected a fault within its jurisdiction, and (2) the “*fault direction signal*” (D) which indicates the direction of the fault from the CMPR perspective; the derivations of FD and D were explained in Sections 5.4.1 and 5.4.2, respectively. The MPC receives the signals FD and D from all CMPRs and determines, through a suitable logic mechanism, the *small microgrid* in which a fault has occurred. The logic algorithm is similar to the “*directional comparison*” protection method and will be explained in more detail in Section 5.6.

Once the occurrence of a fault is established (by the use of FD signals), the MPC waits for a short prespecified time to receive new directional signals and determine the faulty small microgrid. Then, appropriate trip signals are sent to the circuit breakers associated with the CMPRs, to open and isolate the impacted small microgrid. The trip signals are sent after a time delay (greater than 0.1s, but less than 0.15s [25], [98]) in order to give a chance to the downstream protective devices to operate first (especially, in the grid-connected mode of operation where the fault currents are fairly large). Hence, the proposed protection strategy is applicable irrespective of the mode of operation. Due to the limited geographical spans of a small microgrid, the aforementioned definite-time

margin can satisfy coordination of the CMPRs with the downstream devices, for the main protection. However, to make sure that each CMPR gives enough chance to its downstream protective devices to operate, one may choose different time delays for the CMPRs, in the program that is loaded into the MPC.

If a circuit breaker fails, a breaker failure trip signal is sent to the neighboring circuit breakers such that the smallest possible area of the microgrid is isolated. The breaker failure trip signal is sent after a time delay (greater than 0.3s, but less than 0.4s) if any of the fault detection signals is still active; the time delays are selected based on common practices [25]. The backup protection mode is enabled after about 0.4s from the fault incident and, thus, gives a chance to the first two aforementioned trip signals to be sent. Therefore, if the communication link fails and the CMPRs do not receive any signal for some time, all CMPRs will be automatically switched to the backup protection mode. The backup protection does not require communications, but, compared to the main protection, may take a relatively long time to operate (the backup protection strategy is explained in Section 5.5.2). Fig. 5.5 provides a flowchart of the proposed communication-assisted protection algorithm.

Once an impacted small microgrid is disconnected from the rest of the microgrid, one of the two following actions can be exercised if the fault persists: (i) the entire small microgrid is dropped out after a prespecified time delay, or (ii) the fault is isolated by the MPRs embedded in the small microgrid, and the small microgrid is operated autonomously (see Section 5.6). The MPRs must be coordinated with the existing conventional protective devices based on the backup protection strategy of Section 5.5.2. It should be pointed out that the strategy (ii) above is applicable if there is a generation-load match in the affected small microgrid. This strategy enhances the continuity of service, albeit at the higher cost. If the fault is temporary and cleared after the isolation of the small microgrid from the rest of the microgrid, the islanded small microgrid can be synchronized to the rest of the network through the built-in synchronization schemes of its DERs (see Chapter 2).

It should be pointed out that the proposed protection strategy can be augmented with the automatic reclosing. To do so, once the MPC detects a fault within a small microgrid, it should immediately send trip signals to the corresponding CMPR(s) to isolate the faulty small microgrid instantaneously. At the same time, trip signals are also sent to the DERs embedded in the impacted small microgrid, to disconnect them. Therefore, when the CMPR recloses the circuit, after the reclosing dead time, no DER is connected

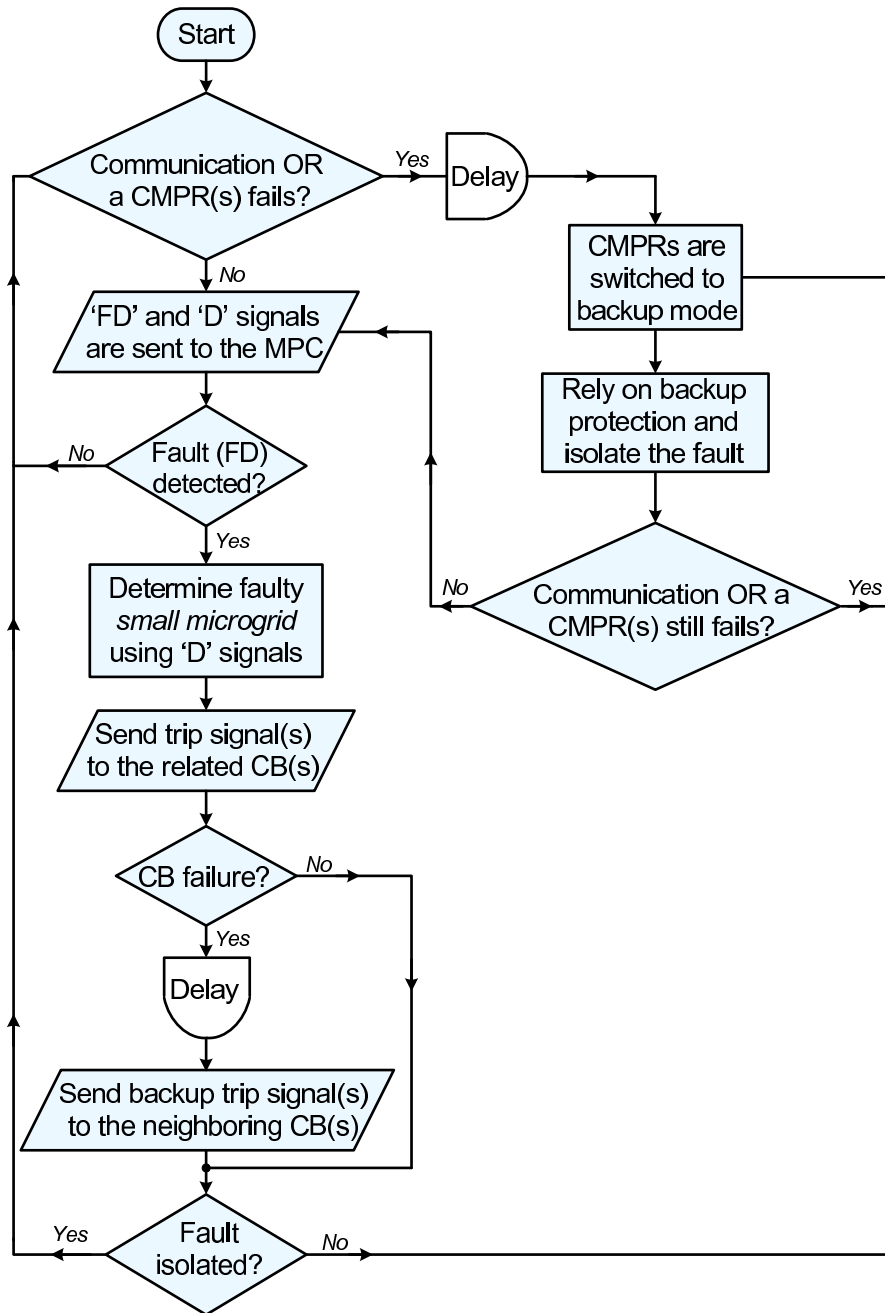


Figure 5.5: Flowchart of the proposed protection scheme.

to the small microgrid and the autoreclosing succeeds, if the fault is temporary. After two reclosures, if the fault does still exist (permanent fault), the protection algorithm is exercised according to the flowchart of Fig. 5.5. It is noted that the disconnection of DERs in the grid-connected mode of operation is not problematic, as the host grid can provide the additional power. In the islanded mode of operation, however, there is no

connection to the grid, and one cannot ensure successful autoreclosing. One scenario that could be envisioned is to disable reclosing mechanism of the CMPRs once the microgrid gets islanded. This can be done by sending a disabling signal to the CMPRs, based on the status of the interface circuit breaker, that is, the circuit breaker that connects the microgrid to the main grid.

**Communication Medium:** To implement the proposed protection strategy, one can utilize the communication capabilities of the smart grid. For example, if the smart grid technologies have already been developed, the corresponding communication channel can be used for the proposed protection strategy. With the advancements in wireless communications, standardized technologies are offered for wide area, metropolitan area, local area, and personal area networks. Compared to wired communications, wireless communications has several advantages including low installation cost, rapid deployment, remote location coverage, and high mobility [112]. For distances under 30 kilometers, wireless signal transmissions take less than 1ms (including the processing time), which is acceptable for most distribution network applications [62], as well as for the proposed protection strategy. For distances larger than 30 kilometers, however, a phasor measurement unit (PMU) may be required to synchronize the measured signals.

One possible communication option<sup>1</sup> for the proposed protection strategy is IEEE 802.11 based Wireless Local Area Network (WLAN) protocol, augmented with long-range wireless Ethernet Bridge. IEEE 802.11 based WLAN provides robust, high speed point-to-point and point-to-multipoint communications [113]. With the use of long-range Ethernet Bridge, the WLAN technology provides a long coverage in excess of 80 kilometers (for example, see reference [114]). The commercially available wireless Ethernet Bridge, besides having a link to another Bridge, can also operate as an access point for up to 32 additional remote Bridges. Further, current technologies based on IEEE 802.11a can provide data rates up to 54 Mbps. The proposed option is a fairly economical choice, and can be extended in case of the future development of the distribution network. Fig. 5.6 illustrates a simplified schematic diagram of the proposed communication medium for an example microgrid. As Fig. 5.6 shows, the proposed communication medium has the capability to be developed for the future upgrades.

---

<sup>1</sup>One other option could be long-range radio modem that benefits from serial communications. The only issue with radio modems is that they are based on point-to-point communications, which is translated into a slightly higher cost compared to the WLAN technology.

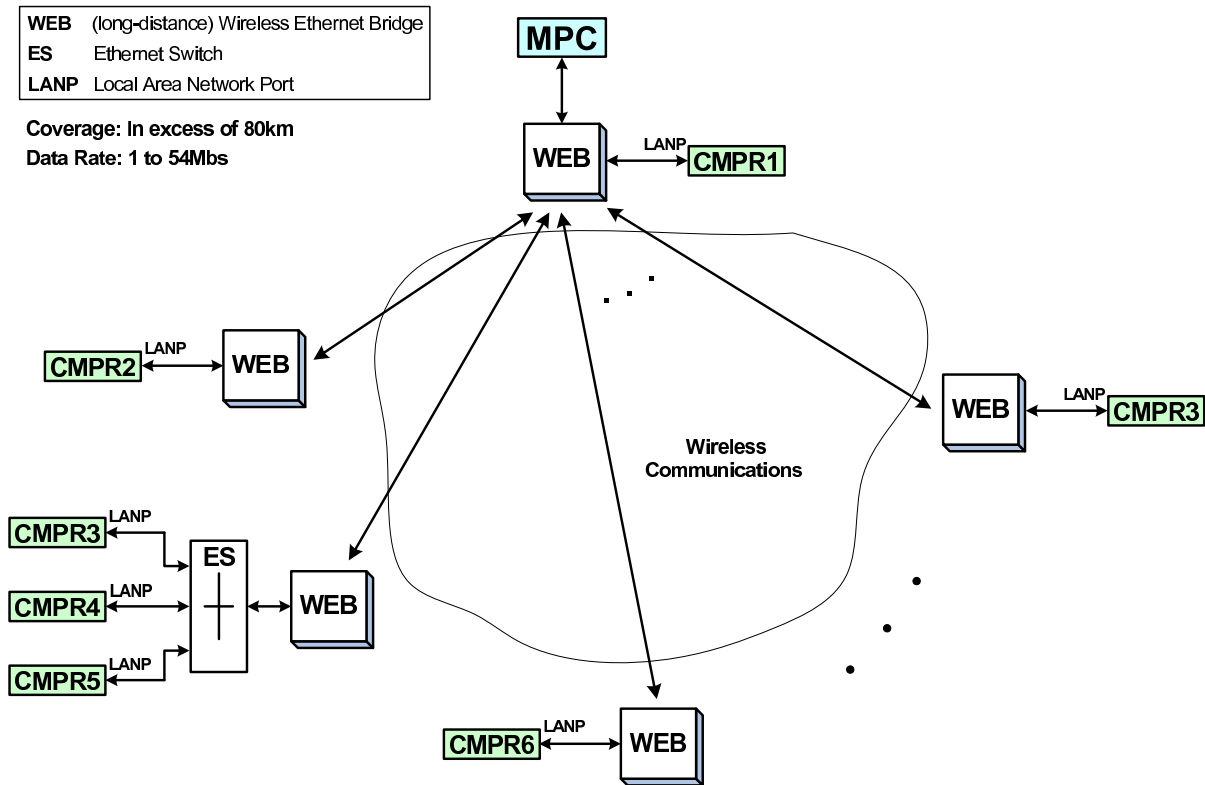


Figure 5.6: Schematic Diagram of the WLAN communication protocol, augmented with wireless Ethernet Bridges, for the proposed protection strategy implemented in an example microgrid.

### 5.5.2 Backup Protection

The backup protection strategy is based on the methods presented in Chapter 4, and does not require communications or adaptive relay settings. The MPRs always execute the backup protection algorithm; however, the CMPRs switch to the backup protection mode only if the communication fails, as explained in Section 5.5.1.

For the backup protection, all the relays are coordinated for the islanded and grid-connected modes of operation; this is achieved through the appropriate selection of time delays and protection function settings. The details of the grading strategy for the backup protection strategy can be found in Chapter 4. Based on the method of Sections 4.3 and 4.4, the forward and reverse time delays of an CMPR/MPR are generally different in the islanded mode of operation (TD<sub>IF</sub> and TD<sub>IR</sub> in Fig. 5.3), compared to the grid-connected mode of operation (TD<sub>GF</sub> and TD<sub>GR</sub> in Fig. 5.3).



## 5.6 Design Example

To illustrate its effectiveness, the proposed protection strategy is applied to and discussed in the context of the microgrid of Fig. 5.2. The microgrid of Fig. 5.2 is based on a realistic North American system that is introduced in [24] and [62]; the detailed network data are given in [24]. The network is an 18-bus distribution network which supplies loads with an aggregate capacity of 3 MVA, through a 10-MVA substation transformer. The load of buses are reported in Appendix D.

Fig. 5.7 shows a more detailed diagram of the microgrid. It is noted that the microgrid embeds six EC-DERs and one synchronous-machine-based DER (SM-DER). Further, the microgrid is interfaced with the host grid through the circuit breaker CB1, installed downstream of the interface bus; by opening this circuit breaker, the microgrid gets islanded. The EC-DERs are of the wind, photovoltaic, battery, and fuel cell types, and can deliver a maximum aggregate power of 2600 kW; the type and power rating of each EC-DER have been indicated in Fig. 5.7. A maximum power of 400 kW can also be delivered by SM-DER4. Each DER is interfaced with the network through a corresponding  $\Delta$ /GY interconnection transformer. Hereafter, the microgrid of Fig. 5.7 is referred to as the “*study microgrid*”, in this chapter.

A droop-based voltage/frequency regulation strategy has been assumed for the SM-DER and EC-DERs, such that the microgrid can operate in both modes of operation without controller mode switching. The control strategy of each DER also incorporates a synchronization algorithm to ensure safe reconnection of the islanded microgrid to the upstream grid (see Chapter 2). Moreover, to ensure that traditional basic protection functions (in particular the directional function) can also be employed here, the controls of EC-DERs make them behave similar to the conventional synchronous machines, in the sense that they more or less maintain the balance of their terminal voltages when an asymmetrical fault strikes the network. More details on the controls of DERs can be found in Chapter 2.

As Fig. 5.7 indicates, the study microgrid has been divided into four “*small microgrids*” and an “*interface region*”, by relays CMPR1 through CMPR6. The boundaries of the small microgrids have been determined in such a way that there is an approximate generation-load balance in each small microgrid. Relay CMPR1, which is also named as the “*interface relay*”, is responsible for moving the study microgrid from the grid-connected mode of operation to the islanded mode of operation, if a fault impacts the interface bus or the utility grid. Relay CMPR2 is employed to prevent disconnection of

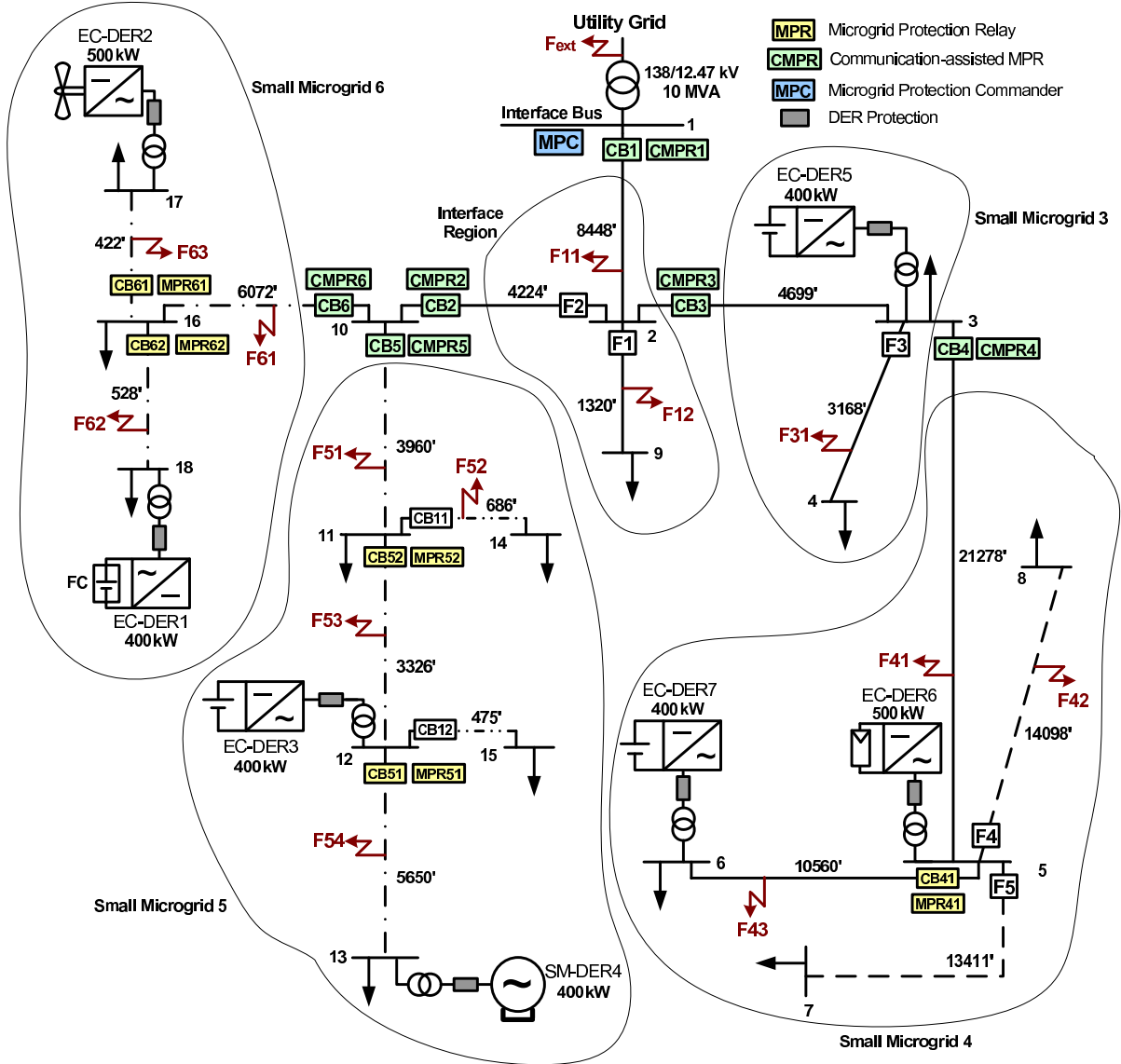


Figure 5.7: Single-line diagram of the study microgrid with the embedded MPRs and CMPRs.

Small Microgrids 5 and 6 if a fault takes place in the interface region; it also provides backup protection for CMPRs 5 and 6. However, CMPR2 can be omitted if there are not such reliability concerns. All relays enable reconnection of the islanded small microgrids to the rest of the microgrid, once the fault is cleared.

As discussed in Section 5.5.1, each CMPR sends two signals, the fault detection signal and the fault direction signal, to the MPC. The protection algorithm analyzes the data provided by all the received signals and determines the location of the fault. Then, after a prespecified time delay, the trip signal(s) will be sent to the corresponding circuit

Table 5.1: Logics for Detecting and Isolating a Fault within the Study Microgrid

Fault Loc.	Oper. Mode	D <sub>1</sub>	D <sub>2</sub>	D <sub>3</sub>	D <sub>4</sub>	D <sub>5</sub>	D <sub>6</sub>	FD <sub>t</sub>	Main CBs	Backup CBs
IR <sup>1</sup>	GC <sup>2</sup>	1	0	0	0	0	0	1	CB1	Grid CB(s)
	Isld <sup>3</sup>	N/A	0	0	0	0	0	1	CB2 CB3	CB5 & CB6 CB4
SMG3 <sup>4</sup>	GC	1	0	1	0	0	0	1	CB3	CB2 (& CB1)
	Isld	N/A	0	1	0	0	0	1	CB4	N/A
SMG4	GC	1	0	1	1	0	0	1	CB4	CB3
	Isd	N/A	0	1	1	0	0	1		
SMG5	GC	1	1	0	0	1	0	1	CB5	CB2 & CB6
	Isld	N/A	1	0	0	1	0	1		
SMG6	GC	1	1	0	0	0	1	1	CB6	CB2 & CB5
	Isld	N/A	1	0	0	0	1	1		
UG <sup>5</sup>	GC	0	0	0	0	0	0	1	CB1	CB2 & CB3
	Isld	N/A	N/A	N/A	N/A	N/A	N/A	N/A		

1. IR: Interface Region

2. GC: Grid-Connected mode

3. Isld: Islanded mode

4. SMG: Small MicroGrid

5. UG: Utility Grid

breaker(s) to isolate the impacted part of the network. Table 5.1 reports the logics that are used to detect and isolate faults within the study microgrid.  $D_i$  denotes the output of the directional element of the  $i$ th CMPR, and  $FD_t$  is the logical *OR* combination of all fault detection signals sent by the CMPRs. The table also indicates the main and backup circuit breakers, for the case of a circuit breaker failure. It should be pointed out that a fault is considered to be a forward fault if  $FD=1$  and  $D=1$ . For the islanded mode of operation, relay CMPR1 does not take part in the protection task as its corresponding circuit breaker is open for that mode of operation. Fig. 5.7 further shows that a number of MPRs have been employed for each small microgrid to provide protection in case that the small microgrid gets islanded; thus, the strategy (ii) of Section 5.5.1 has been adopted to deal with permanent faults.

Fig. 5.8 illustrates the definite-time grading of the MPRs/CMPRs for the backup protection strategy, where  $t_f + pt_m$  and  $t_f + (p + q)t_m$  respectively denote the relay forward and reverse definite time delays ( $p$  and  $q$  are positive integers). It is noted that the reverse definite time delay is larger than its forward counterpart, by a suitable grading margin,  $qt_m$ . Such a grading strategy can also ensure the coordination of MPRs within a small microgrid, even if it is isolated from the rest of the network through the operation of the circuit breakers commanded by the CMPRs. As also evident from

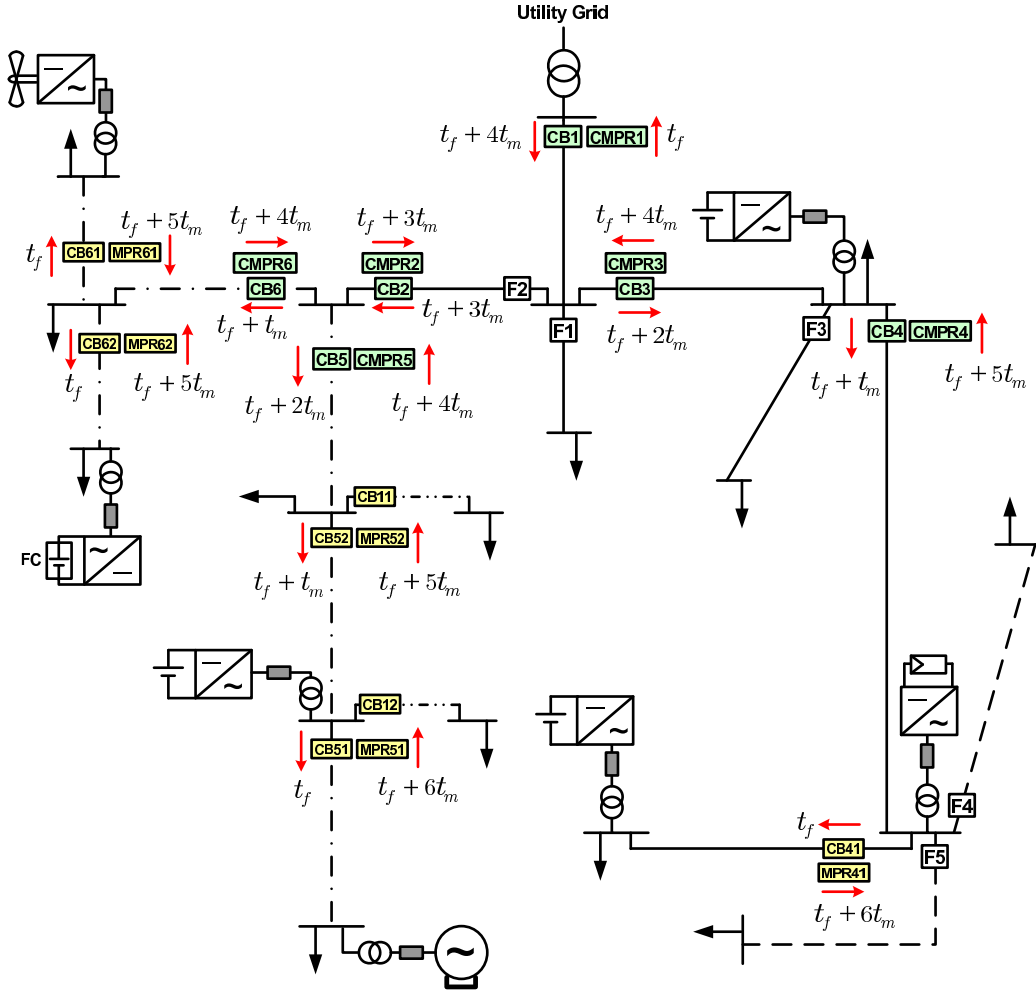


Figure 5.8: Grading scheme of the study microgrid relays for the backup protection strategy.

Fig. 5.8, due to the aforementioned definite-time grading strategy, the backup protection takes a longer time to isolate a fault, compared to the communication-assisted strategy. For example, assuming that: (i) the maximum time required for the fault detection (i.e.,  $t_f$ ) is about 7 (60-Hz) cycles, (ii) the time delay considered for the margin (i.e.,  $t_m$ ) is about 20 cycles, and (iii) the time needed by a circuit breaker to open is about 5 cycles, MPR41 takes about 2.5s to isolate a fault in the reverse direction, which is a fairly long time. The operation times of the other relays, especially in their reverse directions, are more or less the same; however, these delays are acceptable for the backup protection. Coordination of the CMPRs/MPRs with the existing protective devices of the original distribution network (mostly inverse-time overcurrent devices), for the backup protection, is performed based on the methods presented in Chapters 3 and 4.

## 5.7 Study Cases and Simulation Results

To evaluate the effectiveness of the proposed protection strategy and its CMPRs/MPRs, a detailed model of the study microgrid has been constructed in the PSCAD/EMTDC software environment, and study cases are simulated. For the simulations, the CMPR/MPR settings and time delays have been calculated based on the discussion of Sections 5.5.1, 5.5.2, and 5.6. Fuses and traditional relaying functions are modeled based on the analytical equations presented in Appendix B. The simulations include faults at various locations of the study microgrid; the fault types include single phase-to-ground faults, double phase-to-ground faults, phase-to-phase faults, three-phase-to-ground faults, and high-impedance faults (HIFs).

HIFs are modeled in this study based on the method presented in [62]. Most researchers use a  $40\text{-}\Omega$  resistance, as the maximum reasonable resistance, between a fallen conductor and the ground; this value is also assumed by many utilities [115]. In this chapter, however, a  $100\text{-}\Omega$  resistance has been assumed for HIFs, to simulate a more severe condition. Further, circuit breaker and communication link failures have been simulated to test the efficacy of the backup protection strategy.

### 5.7.1 Islanded Mode of Operation

Let us assume that a fault impacts the study microgrid in the islanded mode of operation. Tables 5.2 and 5.3 report the main and backup relay operating times for a selected number of fault scenarios. In the presented simulation results, we have tried to be as judicious as possible in covering different types of faults, different locations, and different fault resistances. For example, Table 5.2 shows the simulation results for solid faults while the results of Table 5.3 corresponds to HIFs. Since in the islanded mode of operation a fault results in a small fault current, the network fuses take a relatively long time to isolate the fault. Therefore, the faults are first isolated by the CMPRs, through the communication-assisted strategy. Even if the communication network fails to operate, the CMPRs/MPRs will operate based on the backup protection strategy.

For solid faults, the voltage drop across the microgrid is significant, and the undervoltage protection function can detect the faults. However, for HIFs, only the sequence-component-based protection function (fault ratio in the islanded-mode protection module of Fig. 5.3) operates, as no voltage dip is detected by the undervoltage relays.

### 5.7.2 Grid-Connected Mode of Operation

Several cases have also been simulated for the grid-connected mode of operation but, due to space limitations, the results of only a limited number of them have been reported in Tables 5.4 and 5.5. The tables indicate the main and backup relay operating times for different internal and external faults, at various locations. It is observed that if a CMPR/MPR responsible for the main protection fails to operate, other CMPRs/MPRs provide suitable backup protection. Again, coordination is performed in such a way that the smallest part of the faulted microgrid is de-energized in response to a fault incident.

As discussed in Section 5.5.1, the communication-assisted protection strategy sends the trip signals after a prespecified time delay from the fault inception, to give a chance to temporary faults to self clear or to first allow downstream protective devices to isolate the fault. For example, it can be observed from Tables 5.2 and 5.3 that for a phase-to-ground (AG) fault at location F54, relay MPR51 operates and isolates the fault before CMPR5 intervenes through the communication-assisted strategy. It can also be seen in Table 5.4 that for an AG fault at location F12, Fuse  $F1$  breaks the fault current before CMPR1, CMPR2, and CMPR3 operate. Therefore, for some fault scenarios, the existing protective devices of the distribution network may operate before the communication-assisted (main) protection strategy, in order to isolate the smallest possible area of the faulted microgrid.

## 5.8 Summary and Conclusion

In this chapter, a communication-assisted protection strategy was proposed for protection of inverter-based medium-voltage microgrids. Also, a backup protection strategy was proposed to handle communication network failures. The communication-assisted and backup protection algorithms can be embedded into programmable microprocessor-based relays with directional elements and are effective in both modes of operation. The effectiveness of the proposed scheme, which does not require adaptive protective devices, is to a large extent independent of the fault current levels, the mode of operation, and the type and size of the microgrid DERs. Several study cases were presented based on time-domain simulation of a sample MV microgrid, to demonstrate the effectiveness of the proposed protection strategy and its enabling relay. The following chapter looks into the operation of an existing distribution network as a microgrid.

Table 5.2: Operating Times of Main and Backup Protections for Selected Solid Fault Scenarios in the Islanded Mode of Operation

Fault Type	Fault Loc.	Solid Faults					
		Communication-Assisted Protection				Backup Protection	
		Main		CB Failure		Oper. Relay	Oper. Time(s)
		Oper. Relay	Oper. Time(s)	Oper. Relay	Oper. Time(s)		
AG	F11	CMPR2	0.123	CMPR4	0.473	CMPR2	1.483
		CMPR3	0.123	CMPR5	0.473	CMPR3	1.816
				CMPR6	0.473	CMPR4	2.158
						CMPR5	1.817
						CMPR6	1.817
AG	F31	CMPR3	0.125	CMPR2	0.475	CMPR3	1.152
		CMPR4	0.125			CMPR2	1.487
						CMPR4	2.158
						MPR41	2.484
AG	F41	CMPR4	0.125	CMPR3	0.475	CMPR4	0.819
						CMPR3	1.154
						MPR41	2.487
AG	F54	CMPR5	0.126	CMPR2	0.476	MPR51	0.084
				CMPR6	0.476	MPR52	0.419
						CMPR5	1.159
AG	F61	CMPR6	0.122	CMPR2	0.472	CMPR6	0.818
				CMPR5	0.472	CMPR2	1.503
						CMPR5	1.821
						MPR61	2.153
						MPR62	2.153
BCG	F62	CMPR6	0.122	CMPR2	0.472	MPR62	0.083
				CMPR5	0.472	CMPR6	0.819
BCG	F42	CMPR4	0.124	CMPR3	0.474	MPR61	2.155
						CMPR4	0.822
						CMPR3	1.152
BCG	F42					MPR41	2.487
BC	F51	CMPR5	0.122	CMPR2	0.472	CMPR5	1.162
				CMPR6	0.472	CMPR2	1.503
						CMPR6	1.820
						MPR52	2.157
ABC	F12	CMPR2	0.123	CMPR4	0.473	CMPR2	1.483
		CMPR3	0.123	CMPR5	0.473	CMPR3	1.817
				CMPR6	0.473	CMPR4	2.151
						CMPR5	1.817
						CMPR6	1.817

Table 5.3: Operating Times of Main and Backup Protections for Selected High-Impedance Fault Scenarios in the Islanded Mode of Operation

Fault Type	Fault Loc.	High-Impedance Faults (100 $\Omega$ )					
		Communication-Assisted Protection				Backup Protection	
		Main		CB Failure			
		Oper. Relay	Oper. Time(s)	Oper. Relay	Oper. Time(s)	Oper. Relay	Oper. Time(s)
AG	F11	CMPR2	0.129	CMPR4	0.479	CMPR2	1.496
		CMPR3	0.129	CMPR5	0.479	CMPR3	1.833
				CMPR6	0.479	CMPR4	2.189
						CMPR5	1.830
						CMPR6	1.830
	F31	CMPR3	0.128	CMPR2	0.478	CMPR3	1.171
		CMPR4	0.128			CMPR2	1.495
						CMPR4	2.172
						MPR41	2.499
	F41	CMPR4	0.136	CMPR3	0.486	CMPR4	0.847
						CMPR3	1.203
						MPR41	2.491
	F54	CMPR5	0.131	CMPR2	0.481	MPR51	0.096
				CMPR6	0.481	MPR52	0.431
						CMPR5	1.217
	F61	CMPR6	0.125	CMPR2	0.475	CMPR6	0.833
				CMPR5	0.475	CMPR2	1.516
						CMPR5	1.834
						MPR61	2.176
					MPR62	2.176	
BCG	F62	CMPR6	0.125	CMPR2	0.475	MPR62	0.097
				CMPR5	0.475	CMPR6	0.838
						MPR61	2.184
	F42	CMPR4	0.127	CMPR3	0.477	CMPR4	0.850
				CMPR3	1.171		
				MPR41	2.511		
BC	F51	CMPR5	0.125	CMPR2	0.475	CMPR5	1.200
				CMPR6	0.475	CMPR2	1.515
						CMPR6	1.831
						MPR52	2.199
ABC	F12	N/A					



Table 5.4: Operating Times of Main and Backup Protections for Selected Solid Fault Scenarios in the Grid-Connected Mode of Operation

Fault Type	Fault Loc.	Solid Faults					
		Communication-Assisted Protection				Backup Protection	
		Main		CB Failure		Oper. Relay	Oper. Time(s)
		Oper. Relay	Oper. Time(s)	Oper. Relay	Oper. Time(s)		
AG	F12	CMPR1	0.122	CMPR4	0.472	<i>F1</i>	0.038
		CMPR2	0.122	CMPR5	0.472	CMPR1	1.818
		CMPR3	0.122	CMPR6	0.472	CMPR2	1.486
	F43	CMPR4	0.129	CMPR3	0.479	MPR41	0.058
						CMPR4	0.821
F52	CMPR5	0.121	CMPR2	0.471	CB11	0.046	
			CMPR6	0.471	CMPR5	1.154	
					MPR52	2.153	
F63	CMPR6	0.122	CMPR2	0.472	MPR61	0.081	
			CMPR5	0.472	CMPR6	0.828	
					MPR62	2.152	
$F_{ext}$	CMPR1	0.122	CMPR2	0.472	CMPR1	0.503	
			CMPR3	0.472	CMPR2	1.487	
					CMPR3	1.818	
BCG	F61	CMPR6	0.121	CMPR2	0.471	CMPR6	0.824
				CMPR5	0.471	CMPR2	1.485
						CMPR5	1.817
						MPR61	2.150
					MPR62	2.150	
F53	CMPR5	0.122	CMPR2	0.472	MPR52	0.425	
			CMPR6	0.472	CMPR5	1.155	
					MPR51	2.486	
BC	F41	CMPR4	0.128	CMPR3	0.478	CMPR4	0.824
						CMPR3	1.155
						MPR41	2.484
F51	CMPR5	0.125		CMPR2	0.475	CMPR5	1.158
						CMPR6	1.487
							1.817
							2.157
ABC	F31	CMPR3	0.127	CMPR1	0.477	<i>F3</i>	0.042
		CMPR4	0.127	CMPR2	0.477	CMPR3	1.151
						CMPR4	2.151
						MPR41	2.483

Table 5.5: Operating Times of Main and Backup Protections for Selected High-Impedance Fault Scenarios in the Grid-Connected Mode of Operation

Fault Type	Fault Loc.	High-Impedance Faults (100 $\Omega$ )					
		Communication-Assisted Protection				Backup Protection	
		Main		CB Failure			
		Oper. Relay	Oper. Time(s)	Oper. Relay	Oper. Time(s)	Oper. Relay	Oper. Time(s)
AG	F12	CMPR1	0.128	CMPR4	0.478	CMPR1	1.831
		CMPR2	0.128	CMPR5	0.478	CMPR2	1.492
		CMPR3	0.128	CMPR6	0.478	CMPR3	1.835
	F43	CMPR4	0.137	CMPR3	0.487	MPR41	0.097
						CMPR4	0.848
	F52	CMPR5	0.122	CMPR2	0.472	CMPR5	1.190
				CMPR6	0.472	CMPR2	1.502
						CMPR6	1.840
	F63	CMPR6	0.122	CMPR2	0.472	MPR61	0.106
				CMPR5	0.472	CMPR6	0.852
						MPR62	2.164
	F <sub>ext</sub>	CMPR1	0.134	CMPR2	0.484	CMPR1	0.509
				CMPR3	0.484	CMPR2	1.493
						CMPR3	1.824
	BCG	F61	CMPR6	0.123	CMPR2	0.473	CMPR6
CMPR5					0.473	CMPR2	1.503
						CMPR5	1.832
						MPR61	2.159
						MPR62	2.159
F53		CMPR5	0.123	CMPR2	0.473	MPR52	0.436
			CMPR6	0.473	CMPR5	1.159	
					MPR51	2.495	
BC	F41	CMPR4	0.130	CMPR3	0.480	CMPR4	0.838
						CMPR3	1.162
						MPR41	2.508
	F51	CMPR5	0.127	CMPR2	0.477	CMPR5	1.164
			CMPR6	0.477	CMPR2	1.507	
					CMPR6	1.842	
					MPR52	2.167	
ABC	F31	N/A					

# Chapter 6

## Operation of an Existing Distribution Network as a Microgrid

### 6.1 Introduction

With the increasing attention to the concept of microgrid, it has become important to identify the requirements that enable an existing electric distribution network to operate as a microgrid. In this chapter, a Canadian utility distribution network embedding DERs is studied with the first objective of determining the conditions under which the network can operate as a microgrid in both the grid-connected and islanded modes. The likelihood of operation of the distribution network in isolation from the utility grid is investigated, and (minimal) required changes for the control of the islanded network are discussed. Two of the possible options, i.e., (i) the addition of a conventional dispatchable DER to the distribution network and (ii) the addition of an integrated energy storage device to the existing network, are investigated, and the control scenarios that could enable the network to operate in the islanded mode are presented; the optimal solution can then be selected based on the system limitations/constraints. Moreover, the possibilities and requirements for the reconnection of the islanded system to the main utility grid when the grid fault is cleared are studied.

The second objective of the chapter is to devise practical and appropriate protection strategies that are effective in the grid-connected as well as the islanded mode of operation. The protection strategies aim to provide the microgrid with acceptable reliability against various types of faults, at different locations and during different operational conditions; the best option is, however, chosen based on the system requirements and

constraints. The effectiveness of the proposed control and protection strategies is demonstrated through a comprehensive set of simulation studies on a detailed model of a realistic distribution network, in the PSCAD/EMTDC software environment.

## 6.2 Study System

As mentioned in Section 6.1, a realistic distribution network is studied in this chapter to identify the changes required for the microgrid operation of an existing network. In other words, control and protection scenarios presented in this chapter are discussed and explained in the context of a “*study system*”, which is introduced in this section; this, however, does not compromise the generality of the presented methodologies and discussions. Fig. 6.1 shows a simplified single-line schematic diagram of a Canadian radial distribution network that is used to investigate typical microgrid operational scenarios. The radial network is connected to the utility grid through a 115/27.6-kV transmission substation, and includes a capacitor bank on its main feeder in addition to a circuit breaker with an automatic reclosing mechanism. The network has single- and three-phase loads and a variety of transformers at different voltage levels; the transformers are distributed along the main feeder (with a total length of 40km) and the laterals. The main feeder autorecloser is set to operate in the fast and slow modes [52], in a coordinated way. It is assumed that a DER unit is installed 15km away from the main circuit breaker. This DER is interfaced with the grid at the Point of Common Coupling (PCC) through a  $\Delta$ /GY transformer, as indicated in Fig. 6.1. The distribution feeders are modeled by  $\Pi$  sections along with all of its loading details.

## 6.3 Microgrid Formation due to Islanding

As discussed in Chapter 1, a microgrid is a portion of a distribution network that possesses enough generation (one or more DERs) such that it can continue to operate even if it is disconnected from the upstream utility grid. In the context of the study system of Fig. 6.1, the 27.6-kV distribution system, including the loads and the DER, constitutes a microgrid. Fig. 6.1 also illustrates the electrical boundary where the isolation and reconnection with the grid can take place. The microgrid can be isolated from the main grid by the operation of a circuit breaker that is located at the medium-voltage side of the substation transformer. In this chapter, this circuit breaker is referred to as the

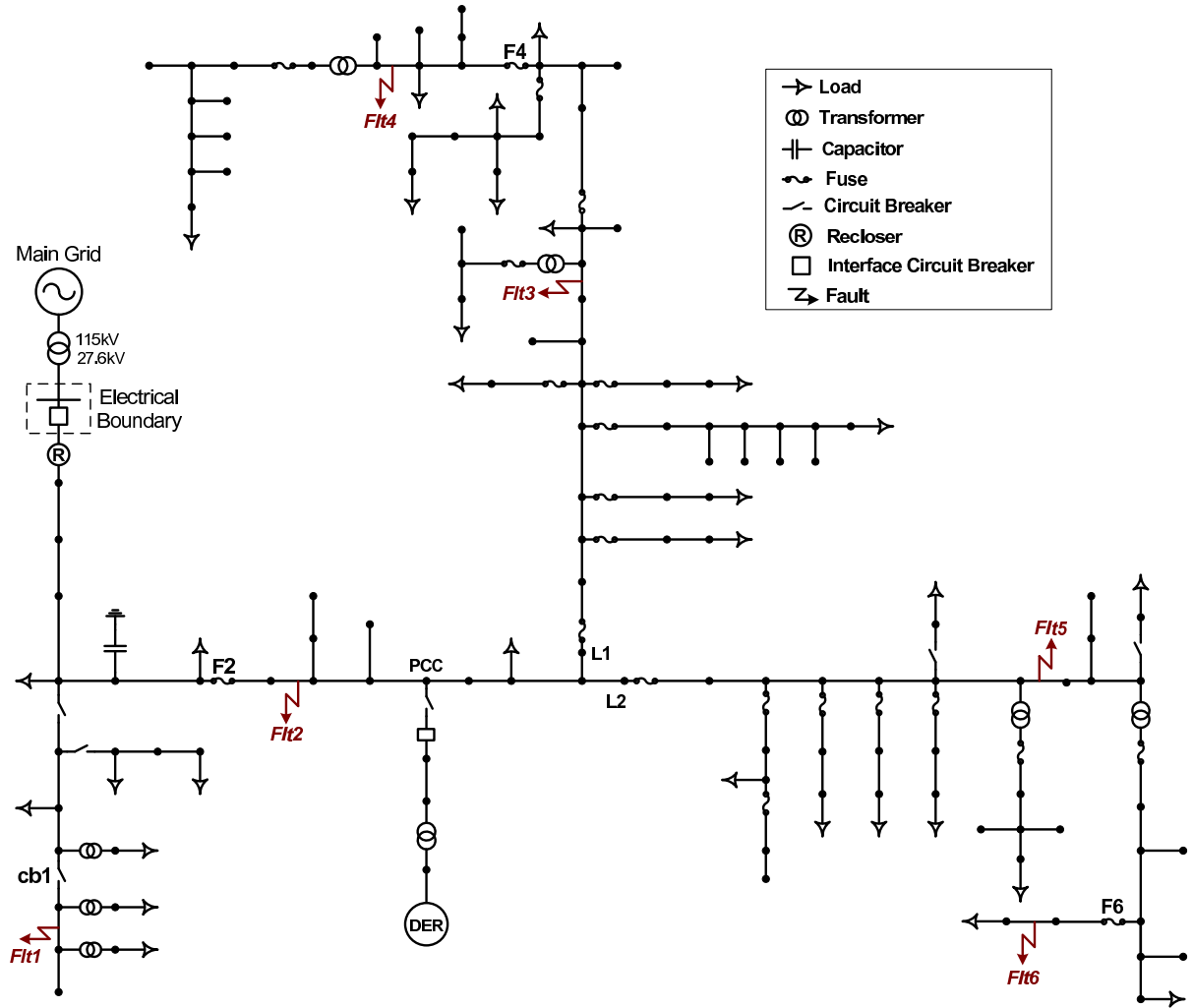


Figure 6.1: Single-line schematic diagram of the study system.

“interface circuit breaker”.

The islanding process can be caused due to either preplanned or unplanned switching incidents. In case of a preplanned islanding, the operating condition of the microgrid can wisely be scheduled such that the islanding process leads to minimum transients, and a fairly seamless transition between the modes of operation is achieved. However, an unplanned islanding can occur due to a fault or some other unexpected switching incidents; thus, the operating condition of the microgrid prior to an unplanned islanding could widely vary, e.g., the DER(s) can share loads in various manners and the microgrid may be delivering or importing power to/from the main grid. Further, the disturbance can be caused by any type of fault that could even be followed up with single or multiple reclosure actions. Thus, the transients that are experienced by a microgrid, subsequent to

an unplanned islanding process, is dependent on several factors such as (i) pre-islanding operating conditions, (ii) type, location, and severity of the fault, (iii) fault clearing time, (iv) post-fault switching actions, and (v) type of the DER(s) employed in the microgrid [51]. In this chapter, which is mainly focused on the unplanned islanding, it is investigated how some of these factors can affect the microgrid performance in different control scenarios.

Once the microgrid is islanded, it should be able to continue safe operation till the fault is cleared and the microgrid can reconnect to the utility grid. Therefore, a synchronization process is also necessary prior to reconnecting an islanded microgrid to the upstream grid. The voltage phasors at the microgrid and utility sides of the interface circuit breaker must be aligned, and their magnitude must be made equal, to ensure that the voltage across the circuit breaker is reasonably small; the reconnection can proceed if the voltage has had a sufficiently small magnitude, for an adequately large time [76]. For example, for a microgrid with DERs in the range of 1.5 to 10MW, reconnection is acceptable if voltage error is below 3%, frequency error is below 0.1Hz, and phase-angle error is below  $10^\circ$  [76]. Adhering to these limits ensures that the reconnection of the microgrid to the main utility grid be achieved with minimal transients in the overall system.

## 6.4 Operation as a Microgrid: Control

### 6.4.1 Scenario 1: Conventional DER(s)

The first possible scenario is to connect a conventional rotating-machine-based DER to the distribution network at the PCC. For the system of Fig. 6.1, the maximum load is 3.5 MVA, and it is assumed that a 5-MVA synchronous generator is connected to the network at the PCC. For this scenario, the DER is modeled as a single-mass synchronous machine with two rotor windings on each axis [116]; the excitation and governor systems are also included in the machine model. The electrical parameters of the machine, represented in a rotating dq frame, are reported in Appendix E. Considering the fault rate and repair time in a North-American distribution system [117]-[120], the use of a synchronous-machine-based DER is an economical solution for making a temporary island. For the period of time that the fault is being taken care of, this solution can effectively work and make the system to operate in the islanded mode. The use of conventional DERs has such advantages as simple, well-known, and inexpensive control system; and independence of the environmental conditions.

**Requirements for the Islanded Mode of Operation:** In the grid-connected mode of operation, the DERs are controlled in a constant-power mode meaning that they deliver a pre-specified constant active/reactive power to the distribution network. As such, the host grid offsets the provided power by the DERs, i.e., the utility grid absorbs/injects power from/to the distribution network. In the islanded mode of operation, however, the entire microgrid should only be energized by the DER(s). Therefore, the DER must at least meet the two following requirements: (i) the DER must be dispatchable such that it can follow and fulfil the load demand. Therefore, as also mentioned in the previous section, the machine is equipped with the excitation and governor systems such that it can adjust its output power once the microgrid gets islanded. The voltage and frequency setpoints of the excitation and governor systems are determined based on the well-known droop strategy; the technique is similar to what is done in large power-generation plants and does not require any communications. (ii) the DER must have enough capacity to satisfy the maximum demand of the islanded microgrid; otherwise, a load-shading scheme<sup>1</sup> must also be utilized for the islanded network. It is worth mentioning that a rotating-machine-based DER may employ a steam turbine, a gas turbine, a hydro turbine, or an internal combustion engine, depending on the available resources (biomass, natural gas, water, diesel fuel, etc.).

Despite the advantages of the conventional rotating-machine-based DERs, they cause serious issues in the electric power system among them high noises, fuel storage requirements, engine maintenance, and greenhouse gas emission. Moreover, due to the relatively slow dynamic response of the conventional DERs, the system response to fault incidents and transient disturbances is significantly affected, which may not be acceptable for some local distribution networks. Considering the abovementioned drawbacks, the use of renewable energy systems in electric power networks has attracted a considerable attention, as will be discussed in the following section.

### 6.4.2 Scenario 2: Electronically Coupled DER(s)

Recently, due to the environmental concerns and depletion of fossil fuel reserves, the deployment of renewable energy systems has rapidly increased. Renewable energy resources are clean, safe, and sustainable; and require less maintenance than traditional generators. Amongst the renewable energy resources, wind power is an environmentally attractive form, from an overall fuel consumption perspective. Currently, wind power is

---

<sup>1</sup>Load-shading algorithms are not discussed in the thesis, as they are beyond the scope of this study.

accounted for 2% (5265MW) of the total electricity generation in Canada [121], with an annual growth rate averaging 40% over the next 15 years. Therefore, the wind power generation is a technology with a vast potential for the future power system. For Scenario 2 of this study, it is assumed that three 2.3-MW Doubly-Fed Induction Generator-based (DFIG-based) wind-power units are installed at the PCC; thus, the whole wind farm is capable of generating 6.9MW under nominal environmental condition (12-14m/s wind speed in this case [122]).

### 1) Control of the EC-DER (Wind-Power Units)

Although wind power technology has a vast potential, the intermittent nature of the wind power generation represents the most technical and economical challenge that one must overcome before wind power can effectively proliferate into the electric networks. Fig. 6.2 illustrates a schematic diagram of a DFIG wind-power unit whose main components are a wind turbine, a gearbox, a DFIG, a back-to-back AC/DC/AC converter, and an interface transformer. The DFIG wind-power unit is interfaced with the distribution network through its VSC and a  $\Delta$ /GY 2.3/27.6-kV interface transformer,  $T_r$ . The parameters of the simulated DFIG and wind turbine are reported in Appendix E. As the figure shows, the DFIG stator is directly connected to the LV side of  $T_r$ , whereas the rotor circuit is interfaced with  $T_r$  via the AC/DC/AC converter. Fig. 6.2 also shows that a three-phase capacitor  $C_f$  is connected to the low-voltage side of  $T_r$ , primarily, to suppress switching voltage harmonics. In addition,  $C_f$  supplies a relatively small reactive power to the network. The real- and reactive-power components that the DFIG wind-power unit delivers to the distribution network are denoted by  $P$  and  $Q$ , respectively.

As shown in Fig. 6.2, the AC/DC/AC converter is composed of two two-level voltage-sourced converters (i.e., the Rotor-Side Converter (RSC) and the Grid-Side Converter (GSC)), whose DC sides are connected in parallel to the DC-link capacitor,  $C_{dc}$ . The control of the DFIG wind-power unit of Fig. 6.2 consists of two main tasks. The first task is the machine torque control by means of the RSC, under the assumption that the DC-bus voltage is regulated by the GSC. The function of the torque control scheme is to regulate the DFIG torque through the vectorial control of RSC such that the power output is maximized. The power is maximized if the DFIG torque,  $T_e$ , is controlled based on the following law [20]

$$T_e = T_e^* = k_{opt} \cdot \omega_r^2, \quad (6.1)$$



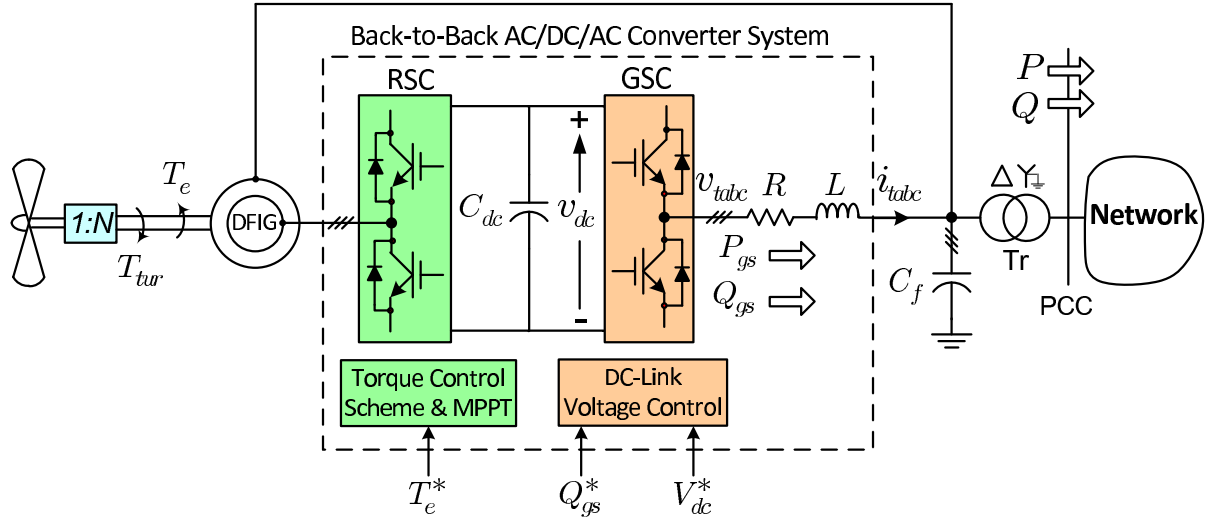


Figure 6.2: Schematic diagram of a DFIG wind-power unit.

where  $T_e^*$  is the reference value for the machine torque,  $\omega_r$  denotes the DFIG shaft speed, and  $k_{opt}$  is a proportionality constant.

The second control task of the DFIG wind-power unit is the DC-link voltage/reactive-power regulation by means of the GSC. In the wind-power unit of Fig. 6.2, the DC-link voltage is maintained in its reference value,  $V_{dc}^*$ , through the control of real-power component of the GSC, i.e.,  $P_{gs}$  (see also Fig. 1.6). The reactive-power component  $Q_{gs}$  is also controlled by the GSC to regulate the PCC voltage level. The two control tasks (i.e., the torque control and the DC-link voltage control) are independent of each other and thus treated separately. The details of the wind-power unit control schemes, which are performed in a  $dq$  reference frame, can be found in reference [20].

**Requirements for the Islanded Mode of Operation:** To operate the network of Fig. 6.1 as an islanded microgrid, a fine balance must be obtained between the wind-power generation and the total network power demand. This, however, is very difficult, if not impossible, to achieve due to the time-varying nature of the wind energy. Therefore, the islanded network must also embed a dispatchable (and adequately fast) DER to compensate for the mismatch between the wind and load powers.

A dispatchable DER may again be realized through rotating-machine-based DERs. However, conventional rotating machines are rather slow for compensation of fast power fluctuations (due to wind speed fluctuations). Therefore, the wind farm may need to

be augmented by faster dispatchable DERs such as fuel cells and/or Battery Energy Storage Systems (BESSs). While fuel cells are still facing technical challenges, batteries represent a relatively well-established and proven technology which is gaining even further momentum due to the transportation industry initiatives. Moreover, BESSs do not require any fuel storage; they can be recharged and thus offer more operational flexibility. Furthermore, integrating a BESS with a wind farm can smooth out the intermittent power from the wind farm [11]. In this chapter, a BESS is assumed to be the dispatchable DER of the microgrid for Scenario 2, but it is understood that the absence of a rotating-machine-based dispatchable DER may translate into a fairly large BESS.

The BESS is assumed to consist of a bank of lead-acid batteries; As Fig. 6.3 shows, the BESS is interfaced with the microgrid by means of a three-phase VSC and its three-phase low-pass LC filter; the whole dispatchable DER is connected to the network at a point of common coupling close to the electrical boundary (PCC1), through an interconnection transformer (see Fig. 6.3). The reason why this location has been selected for the connection of the BESS to the network is to facilitate the synchronization process (the synchronization algorithm will be discussed later in the text). However, if there are communication facilities available, the point where the wind farm is interfaced with the network (PCC) is the best option for the BESS interface point.

The VSC of the BESS is employed to control the rate of charge/discharge of the BESS. Since the average wind speed in the region under study is about 7.6m/s [123], a 3-MVA VSC would be a good choice considering smooth wind speed changes around the average value for most of the time. Moreover, with regard to the average repair/replacement time in a typical distribution system [119], the BESS size is considered to be 10MWh. Such a BESS can be build by taking the individual lead-acid batteries in series and parallel to get the desired voltage and energy ratings. For example, to realize the 10-MWh BESS with a DC voltage of 1.5kV (chosen to facilitate the VSC design), we need to connect 702 lead-acid batteries of 2.135V in series to get the desired voltage, and connect ten of these series strings in parallel to obtain the desired energy rating, which results in a total number of 7020 batteries [11].

## 2) Control of the BESS

A multimode control strategy can be adopted for a DFIG wind-power unit augmented with an energy storage device, to enable operation in the islanded mode as well as the grid-connected mode [124]. This control strategy, however, is suitable for small off-grid

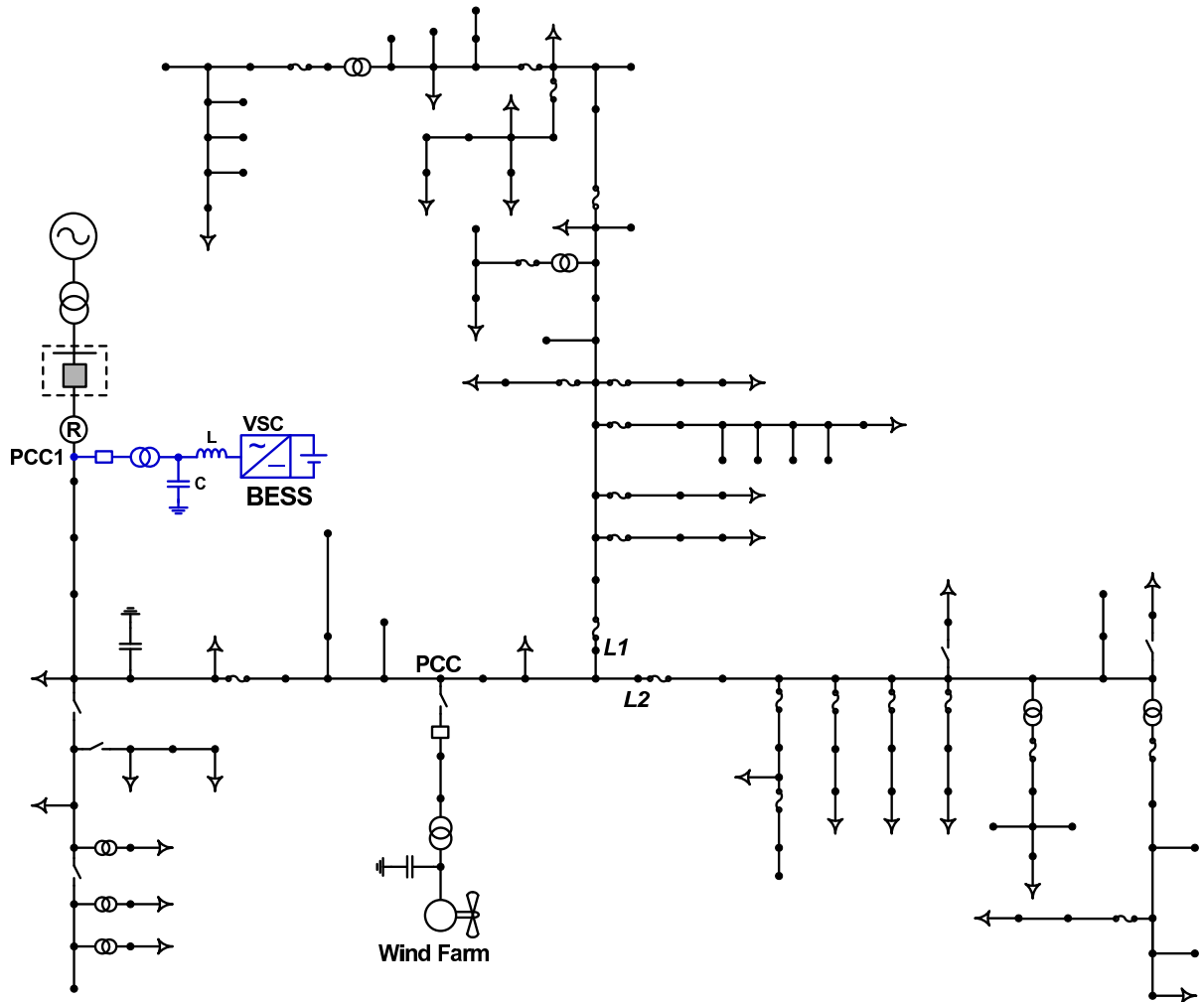


Figure 6.3: Single-line schematic diagram of the study system with the wind farm and the BESS.

communities that would only have one or two wind turbines. For larger wind farms, such as the one under study, the multimode control scheme is not a practical option as one should be dealing with scattered battery banks. Thus, this chapter proposes a voltage and frequency regulation strategy for the BESS and its VSC. In the islanded mode of operation, it is the BESS that regulates the microgrid voltage magnitude and frequency. The VSC of the BESS is pulse-width-modulated and controlled based on the control strategy discussed in Chapter 2, which also ensures protection of the VSC against overload conditions and network faults. The control strategy does not require controller mode switching and enables the BESS and its VSC to ride through network faults and transient disturbances. The controllers also incorporate synchronization algorithms for

ensuring safe reconnection of the islanded microgrid to the utility grid once the grid fault is cleared.

To enable the operation in the islanded mode, the voltage magnitude and frequency setpoints of the VSC control scheme are calculated based on an improved droop strategy, as shown in Fig. 6.4. In the scheme of Fig. 6.4,  $P_{BESS}^*$  and  $Q_{BESS}^*$  respectively denote the setpoints for the real- and reactive-power outputs of the BESS in the grid-connected mode of operation;  $\omega_0$  and  $V_0$  are the nominal values of the power system frequency and network voltage magnitude, respectively;  $P_{BESS}$  and  $Q_{BESS}$  respectively signify the real- and reactive-power outputs of the BESS;  $D_P$  and  $D_Q$  are the so-called droop coefficients;  $\omega^*$  and  $v_{sd}^*$  denote the reference values for the frequency and voltage magnitude of the BESS terminal voltage, respectively. As can be observed in Fig. 6.4, the voltage magnitude and frequency setpoints are also augmented with two corresponding signals that enable synchronization of the microgrid to the host grid, during transitions from the islanded mode of operation to the grid-connected mode of operation (note the boxes labeled as “*network synchronization*”). The corrective signals are obtained from two corresponding filters,  $F_\omega$  and  $F_v$ , which respectively process the signals  $\Delta v_q$  and  $\Delta v_d$ , that is, the  $d$ - and  $q$ -axis components of the voltage across the interface circuit breaker (see Chapter 2). It is noted that, due to the droop control strategy, the network voltage magnitude and frequency in the islanded mode of operation are slightly different from their respective nominal values.

### 3) Pitch-Angle Control

When the wind speed is higher than the nominal value (12-14m/s), the wind turbine blades are pitched in order to limit the rotor speed and the power extracted from the wind (turbine). For wind speeds lower than the rated value, the optimal pitch angle is approximately zero [125]. Therefore, the power generated by the DFIG retains its maximum value, which is expressed as

$$P = k_{opt} \cdot \omega_r^3, \quad (6.2)$$

however, the pitch angle increases steadily as the wind speed exceeds its nominal value. It should be pointed out that the pitch angle can only change at a finite rate due to the size of the rotor blades of modern wind turbines. In this study, the maximum rate of pitch angle change is set to  $6^\circ/\text{s}$  [122]. A simplified version of the pitch-angle control scheme

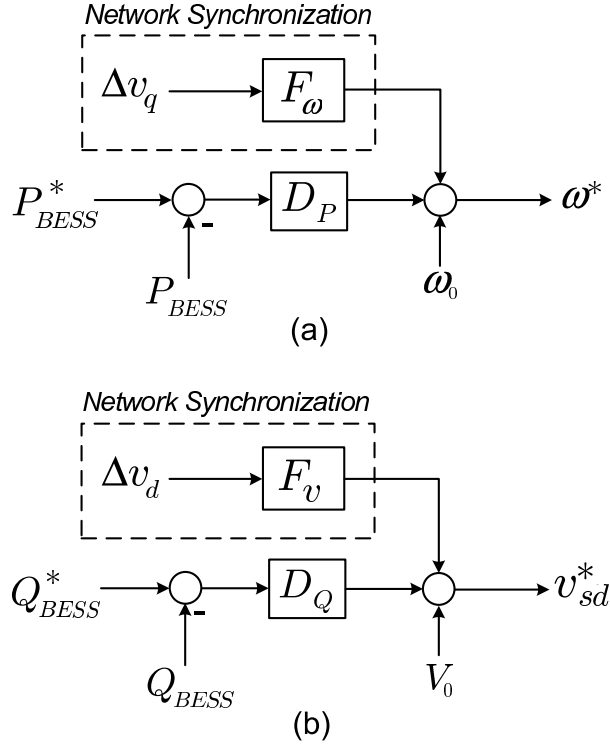


Figure 6.4: Droop-based power management strategy; (a) real power compensator with synchronization function and (b) reactive power compensator with synchronization function.

is depicted in Fig. 6.5(a) in which  $K_p$  is the proportional gain coefficient of the speed controller;  $\omega_r$  signifies the rotor angular speed; and  $\beta$  is the blade pitch angle. Similar to previous chapters, the superscript “\*” is utilized for reference values. As can be observed in the figure, a proportional controller is employed for the speed control as (i) a slight overspeeding of the rotor over its nominal value can be allowed and (ii) the system is never in steady state due to the time-varying nature of the wind speed and, thus, the advantage of an integral part, i.e., zero steady state error, is not applicable [125].

In order to regulate the BESS charging power in the islanded mode of operation, the built-in pitch-angle controls of the wind-power units (see Fig. 6.5(a)) are augmented with an additional pitch-angle control whose block diagram is shown in Fig. 6.5(b). In the islanded mode of operation, if the wind speed is high while the network load is small, the additional pitch-angle controller increases the pitch angle to prevent the battery from getting overcharged. In the control scheme of Fig. 6.5(b), the variable  $\beta_S^*$  is the pitch-angle reference which supplements the built-in pitch-angle references of each constituent wind-power unit, and  $v_W$  is some sort of the average wind speed for the wind farm;  $\beta_{ref}$

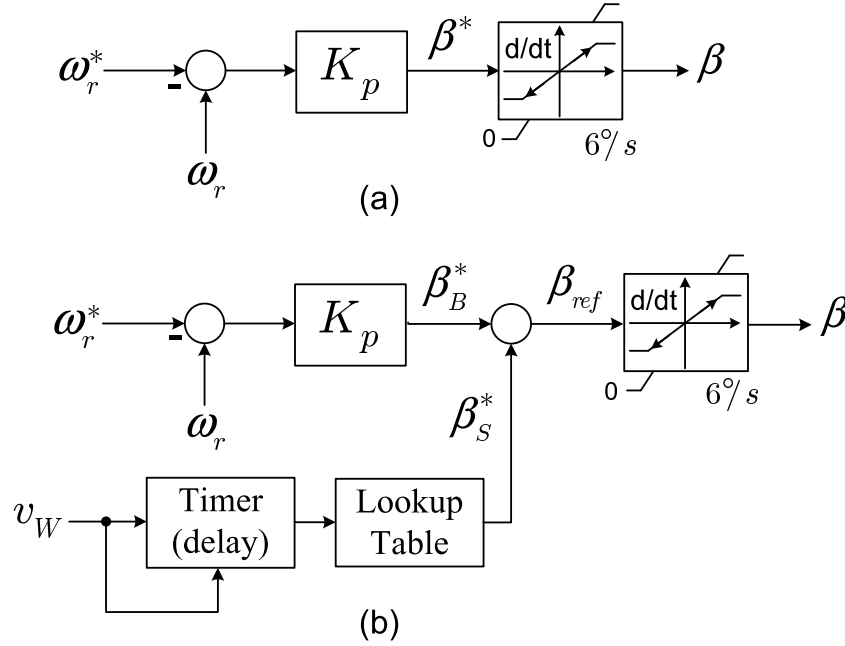


Figure 6.5: (a) Conventional pitch-angle control scheme and (b) proposed pitch-angle control scheme, for the wind-power units.

is the final pitch-angle setpoint. As Fig. 6.5(b) indicates,  $\beta_S^*$  is generated based on  $v_W$ , i.e., if  $v_W$  is high for a specified period of time, the pitch-angle reference is increased to limit the output real power of the wind farm. It is noted that the “high speed” is defined based on the maximum load of the network in the islanded mode of operation as well as environmental conditions. The value of delay is also adapted based on the averaged wind speed. Moreover, the lookup table and time are set based on the operator experiences or experimental results in the area. With the use of the additional controller, one can make the control react faster to rapid changes of the wind speed.

## 6.5 Operation as a Microgrid: Protection

Since a microgrid has two modes of operation, an effective protection scheme is required to protect the microgrid in both modes of operation, considering the fact that one must deal with different protection issues in each mode of operation. This section describes the requirements and possible solutions for the protection of an existing (medium-voltage) distribution network that is to operate as a microgrid.

### 6.5.1 Grid-Connected Mode of Operation

As discussed in Chapter 1, several protection issues may arise in the grid-connected mode of operation, depending on the DER type, size, and location. One of the main issues associated with the addition of DERs to the distribution network is recloser-fuse miscoordination. Reference [126] has proposed a method to find the threshold value of the DER capacity, beyond which the recloser-fuse coordination is lost. The simulations show satisfactory results; however, the capacity of the DER is not a design option in many practical cases. In [127], a classification technique is presented to search for the best DER location where minimum recloser-fuse miscoordination occurs for different fault scenarios. Although an option, the location of the DER may also be forced to the designer in many cases. Therefore, it is necessary to come up with a technique that can retrieve the recloser-fuse coordination while DERs are in place. In this chapter, the coordination method proposed in Chapter 3 is adopted to coordinate the recloser and fuses in the presence of the DERs such that the recloser always operates first, once a fault impacts the network. To do so, the main feeder recloser should be replaced with a commercially available microprocessor-based recloser. Then, the settings of the recloser are carefully selected to accommodate the impacts of DERs (see Section 3.2).

It should be pointed out that the proposed coordination algorithm is employed to coordinate the recloser with the lowest-rating fuse of the main feeder so that higher-rating fuses (upstream fuses) are automatically coordinated with the recloser. Therefore, when a fault strikes the network, the recloser operates first (according to its fast-mode characteristic curve) and gives a chance to temporary faults to self clear. In case the fault is permanent, the fuses and the recloser (in its slow mode of operation) provide backup protection, respectively. Once the recloser of the feeder operates in response to a fault incident, two scenarios can be considered to protect the distribution system when the recloser recloses the circuit for the first time, and the fault does still exist. In what follows, these scenarios are described:

**1) Scenario 1:** The first scenario is to disconnect the DER(s) as soon as the recloser operates for the first time. This requires to establish some sort of communications between the recloser and the DER(s) such that the disconnection of the DER(s) can be performed by a transfer-trip mechanism. Applying this scenario can ensure the coordination of the protective devices after the first reclosure of the recloser, as there would be

no DER connected to the network to interrupt the coordination. Moreover, the issues associated with the reconnection of two asynchronous systems, once the recloser recloses the circuit, are resolved. However, the disadvantage is that the DER(s) get dropped out for any transient incident or temporary fault, and the required power for the distribution network should be provided by the utility grid during this period. In addition, establishing a communication channel between the recloser and the DER(s) is translated in the more expenses.

**2) Scenario 2:** The second scenario is to keep the DER(s) connected to the network, even during the dead time of the reclosing mechanism. Adopting this strategy may, however, compromise the coordination amongst the fuses once the recloser recloses the circuit. To prevent fuse-fuse miscoordination in this situation, two options can be envisioned: (i) to replace all downstream fuses of the DER(s) with such high-rating fuses that are coordinated under the new condition, i.e., with the existence of the DER(s); this option, however, is both costly and time-consuming. (ii) to employ a fault current limiter(s) (FCL) in series with the DER(s) in order to limit DER fault currents to such low levels that the coordination issues do not manifest themselves [53], [54], [128].

In general, an FCL is a series device that is considered to be hidden to the network (zero/low impedance) in normal operation, but takes fast action to limit the instantaneous magnitude of the short-circuit current to a preset value. The task is performed by inserting a high impedance of predesigned value into the network [54]. Since FCLs limit the fault current contribution of DERs, they can either prevent miscoordination between the recloser and fuses or facilitate the process of recloser-fuse coordination that was described in Section 6.5.1. However, to incorporate the transient regime of the FCLs [128], the coordination algorithm of Chapter 3 is still employed in this study to ensure the coordination between the recloser and the fuses. It is noted that the dead time of the reclosing mechanism is assumed to be less than 0.5s (30 cycles) and, thus, no significant asynchronization is generated [51]. Further, the asynchronization can be reduced through the adoption of the control strategy of Section 6.4.2–2 (see also Chapter 2).

## 6.5.2 Islanded Mode of Operation

As explained in the previous chapters, fault currents are typically small in the islanded mode of operation. Consequently, the conventional overcurrent protection is not adequate for this mode. For an existing distribution network, three protection scenarios can be



envisioned for the islanded mode of operation considering the likelihood of the microgrid formation [117]- [120]. These scenarios are as the following:

**1) Scenario 1:** The first scenario is to preserve the existing protection scheme. Thus, when a fault impacts the islanded microgrid, the protections of the DER(s) must detect the fault and disconnect the DER(s), after an appropriate time delay. This means that once a fault takes place within the islanded microgrid, the entire microgrid is shut down. Therefore, any fault results in a service disruption in the whole microgrid and, thus, the reliability of the system is easily compromised. Moreover, if the protections of the DER(s) fail to operate for any reason, there will not be any remote backup protection which can result in serious damage to the equipment. Nonetheless, considering the likelihood of the fault occurrence for the period of time that the system is islanded [119], this simple scheme may suffice, particularly for those microgrids that do not embed critical/sensitive loads. However, this scenario is not studied in the chapter due to the well-known responses and consequences.

**2) Scenario 2:** The second scenario is to replace some of the protective devices of the microgrid with overcurrent relays. The overcurrent relays should, thus, be equipped with two distinct setting groups, one for the islanded mode of operation and the other for the grid-connected mode of operation. The settings for the grid-connected mode of operation are determined based on the method presented in Section 6.5.1. However, in the islanded mode of operation, a traditional protection coordination method (see Section 1.4.1) can be employed to coordinate overcurrent relays; the only point that should be taken into account is that one may need to use directional element(s) to prevent false tripping, in case there are more than one DER in the microgrid; this was explained in Chapters 3 and 4. It should also be pointed out that the appropriate setting group is selected based on the status of the interface circuit breaker. Therefore, the setting group of the relay should change by an operator or through a communication-based method, once the status of the interface circuit breaker changes. An anti-islanding mechanism can also be employed along with overcurrent relays to switch the “grid-connected setting group” to the “islanded setting group”.

**3) Scenario 3:** The third and last scenario is to devise a more sophisticated microprocessor-based relay that embeds different protection functions and can fully protect the

microgrid in both operational modes, with no need to protection mode switching. Such a relay, which was proposed in Chapter 4, can also ensure protection against all types of faults including high-impedance faults, and is thus expected to enhance the system reliability. Therefore, it is necessary to replace some of the network protective devices by the circuit breakers governed by such microprocessor-based relays. Hypothetically, replacement of all protective devices with microprocessor-based relays is possible. However, one should replace the existing protective devices by microprocessor-based relays based on the system requirements and constraints/limits.

For the study system of this chapter, a modified version of the relay proposed in Chapter 4 can be employed. Fig. 6.6 illustrates the schematic diagram of the Microgrid Protection Relay (MPR) that is employed in this chapter. The figure shows that the proposed MPR consists of five modules: (i) the “*directional module*” which is responsible to determine the fault direction. (ii) the “*islanded module*” which is supposed to provide protection in the islanded mode of operation. As can be observed in Fig. 6.6, under-voltage elements are employed in the islanded module as the fault currents are relatively small in the islanded mode of operation. A current-magnitude supervision is also employed in the module to prevent mal-operation of the MPR for the laterals with no DERs. (iii) the “*grid-connected module*” which is responsible for the protection of the network in the grid-connected mode of operation. The settings of the inverse-time overcurrent elements of this module are specified based on the method of Section 6.5.1. The HIF detection element is also supposed to detect high-impedance faults using the sequence components and signal energy levels (see Chapters 4 and 5). (iv) the “*interface module*” is only enabled for the relay installed at the electrical boundary; the module includes NVD and synchronism-check functions. (v) the “*tripping module*” finally decides whether or not a trip signal should be issued.

Since the voltage drop caused by a fault appears more or less across the entire microgrid, directional modules may be required to obtain protection coordination. The forward and reverse time delays are set by proper selection of TD\_IF, TD\_GF, TD\_IR, and TD\_GR such that the coordination is achieved for both forward and reverse faults; the details of the coordination technique can be found in Chapter 4. As will be discussed in Section 6.6.2, it is not required to use directional modules for the MPRs installed within the study system of this chapter.

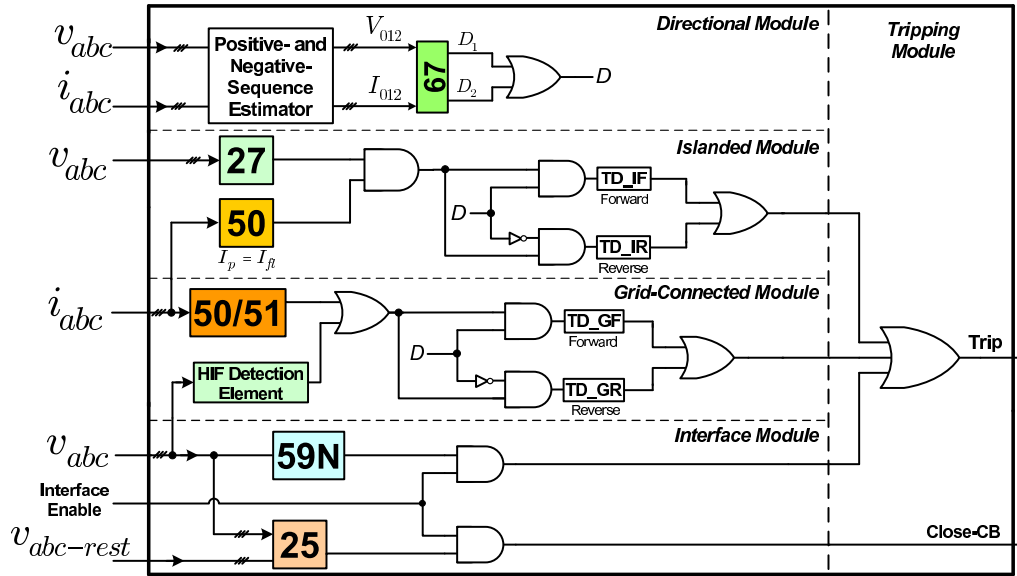


Figure 6.6: Simplified schematic diagram of the MPR employed in this chapter.

## 6.6 Simulation Results

Comprehensive simulation studies are conducted on a detailed switched model of the study system in the PSCAD/EMTDC software, to evaluate the performance of the system under different control and/or protection scenarios in the grid-connected mode of operation, islanded mode of operation, and during sliding between operational modes. The results are compared to help the local distribution company choose its best option. Case studies are chosen to illustrate both the steady-state response to the changes in the system operating point, and the dynamic response when the system undergoes a transient.

For the wind farm, a lumped model is used to represent the aggregate effect of the three wind-power units. The lumped model, which is interfaced with the network through a  $\Delta$ /GY 2.3/27.6-kV transformer, is developed using the method presented in [124]. The wind farm can deliver a rated power of 6.9MVA at the rated wind speed of 12m/s; the parameters of the simulated DFIG and wind turbine are reported in Appendix E. The fuses and traditional relaying functions are modeled based on the analytical equations presented in Appendix B. For all cases, average wind speeds subject to step changes are employed as test signals.

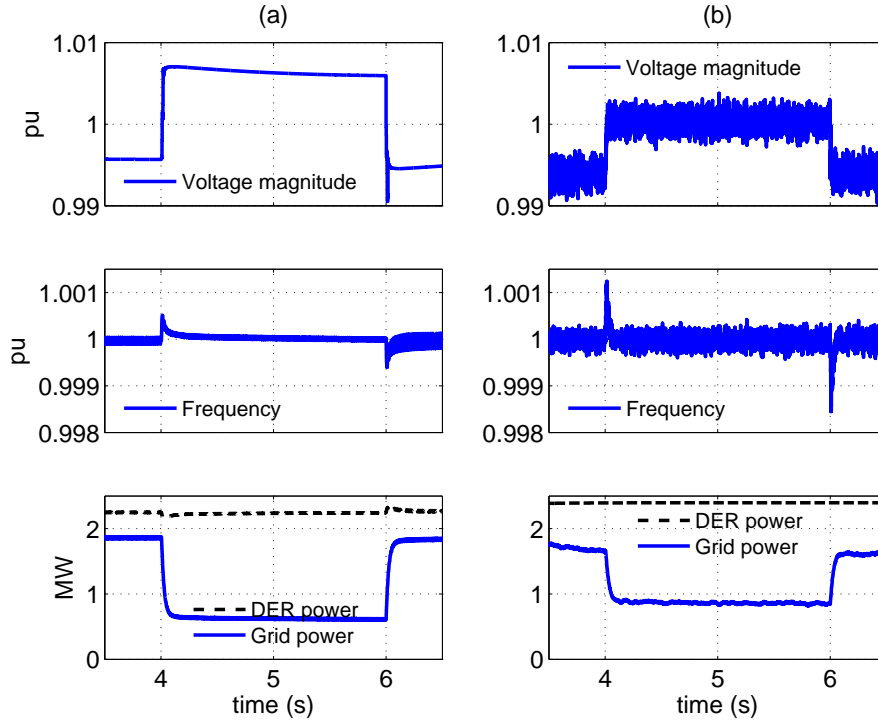


Figure 6.7: Case 1: operation in the grid-connected mode; (a) with synchronous DER and (b) with EC-DER.

### 6.6.1 Control Schemes

**Case 1–Operation in the Grid-Connected Mode:** In this section, the performances of the two control scenarios presented in Section 6.4.1 (synchronous DER) and Section 6.4.2 (EC-DER) are compared in the grid-connected mode of operation, where the output power of the DER is set at a prespecified value. Thus, any change in the power demand is offset by the main grid. Assume that the Lateral L1, Fig. 6.1, is disconnected at  $t=4.0$  s, through the operation of its circuit breaker (to be described in Section 6.6.2), and is switched on again at  $t=6.0$ s. Fig. 6.7 shows the impact of such a switching incident on the PCC voltage, network frequency, and the real-power outputs of the DER and grid.

It is observed in Fig. 6.7 that the voltage and frequency are within their standard limits for both scenarios. However, for the scenario in which an EC-DER is employed, the voltage experiences fewer fluctuations, as the BESS adjusts its reactive-power output (not shown in the figure), through the control of the  $q$ -axis component of its converter current, to stabilize the PCC voltage. Fig. 6.7 also indicates that, based on the adopted strategy, the required power is fully provided by the grid. However, the BESS can be controlled to rapidly adjust its real power in addition to the reactive power, if it is required.

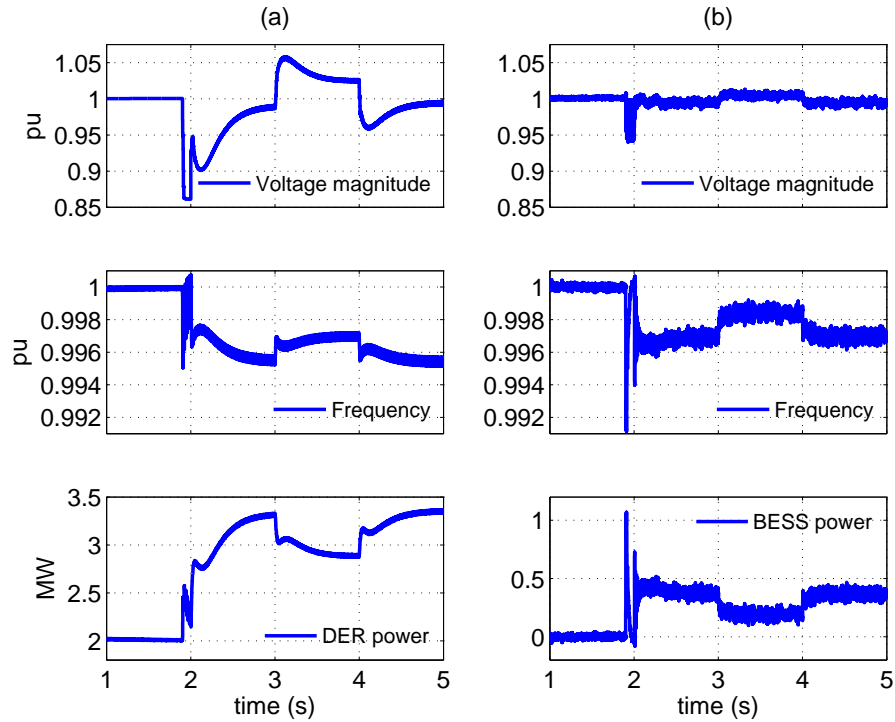


Figure 6.8: Case 2: operation in the islanded mode; (a) with synchronous DER and (b) with EC-DER.

**Case 2–Islanding and operation in the Islanded Mode:** The objective of this section is to compare the performance of the study microgrid under the two aforementioned control scenarios, subsequent to an unplanned islanding. Let us assume that the network gets islanded at  $t=2.0\text{s}$  (due to a fault), and Lateral L1 is switched off and on at  $t=3.0\text{s}$  and  $t=4.0\text{s}$ , respectively. Fig. 6.8 illustrates the system responses under the two scenarios. It is observed that the network voltage changes up to  $\pm 10\%$  of its nominal value in the scenario in which a synchronous DER is employed; this may not be acceptable by some local distribution companies. For the second scenario with the EC-DERs, however, voltage and frequency respectively set within the  $\pm 1\%$  and  $\pm 3\%$  of their corresponding nominal values. It is also observed in Fig. 6.8 that the responses of the EC-DER is faster than conventional DER, such that voltage and frequency of the second scenario are quickly settled on their final value after a disturbance or switching incident. Moreover, once the microgrid gets islanded, the synchronous machine controller must switch to the islanded-mode control while the VSC control strategy does not need any controller mode switching, as discussed in Chapter 2.

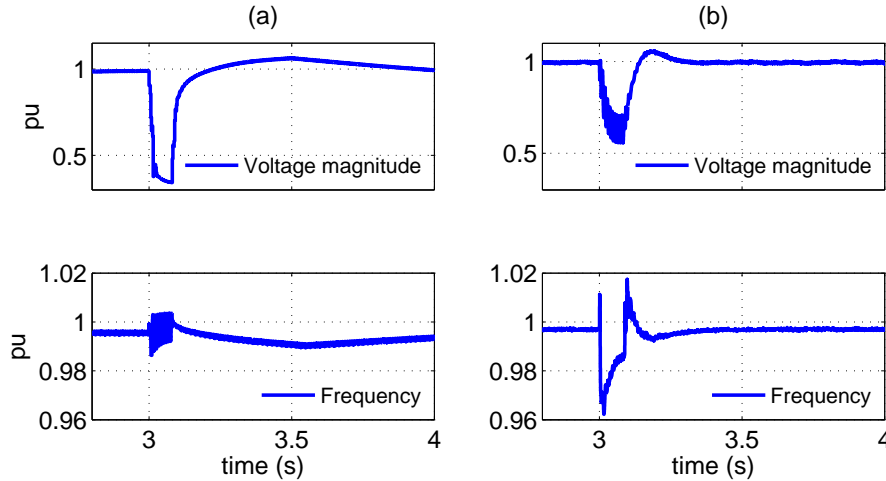


Figure 6.9: Case 3: system response to a temporary fault in the islanded mode; (a) with synchronous DER and (b) with EC-DER.

**Case 3–Islanded Operation under Faults and Transient Disturbances:** The performance of the islanded microgrid under faults and transient disturbances, which has not been investigated in most of the literatures, is discussed in this section. Let us assume that a temporary single-phase-to-ground (AG) fault strikes point *Flt5* of the study microgrid, Fig. 6.1, while it is islanded. Fig. 6.9 shows the system responses for an AG fault that starts at  $t=3.0$ s and lasts for 80ms. It is observed that both control scenarios are able to recover the pre-fault condition once the fault is self cleared. However, the post-fault recovery is faster for the second scenario, due to the adopted control strategy of the VSCs that enables fast post-fault recovery. Fig. 6.10 shows the response of the two systems when a permanent AG fault impacts point *Flt3* at  $t=3.0$ s; it is assumed that the fault is isolated by the protection system at  $t=3.1$ s, through the operation of a protective device that is installed at the beginning of L1. As Fig. 6.10 shows, the system become unstable for the scenario with the synchronous DER. The microgrid equipped with the EC-DER, however, can continue operation after the fault isolation, as the VSCs provide higher degree of speed and flexibility to control the microgrid.

**Case 4–Synchronization:** A synchronization process is required in order to reconnect an islanded microgrid to the host grid. For Scenario 1, where a synchronous DER is used, a communication channel/link should be established between the electrical boundary and the PCC to transfer the synchronization signals (see dash boxes in Fig. 6.4). For

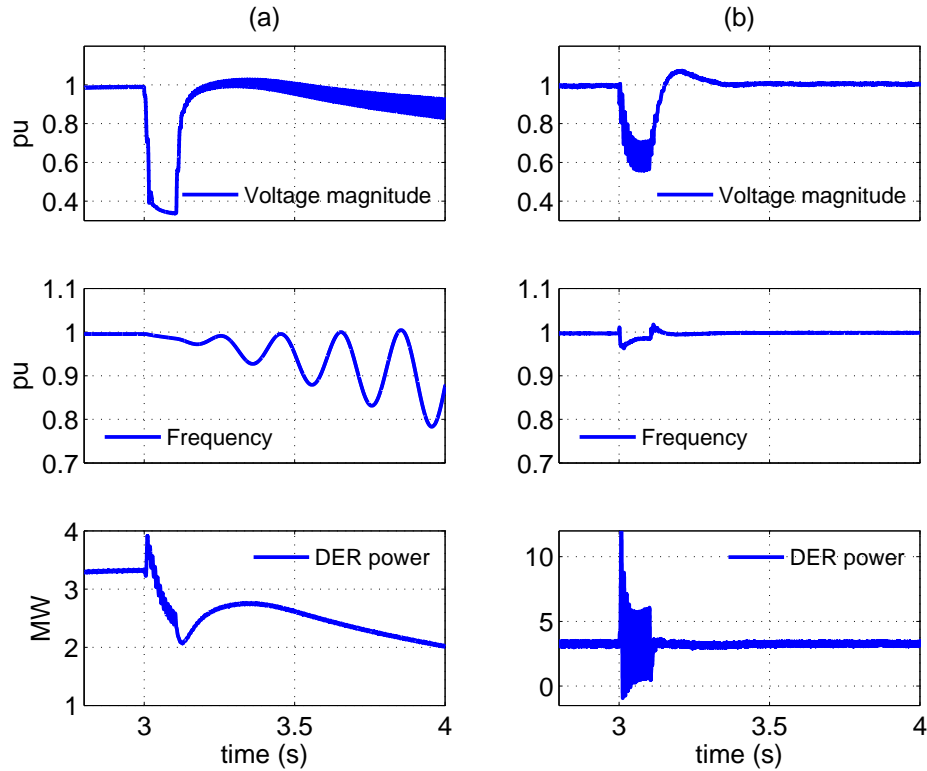


Figure 6.10: Case 3: system response to a permanent fault in the islanded mode; (a) with synchronous DER and (b) with EC-DER.

Scenario 2, however, the BESS is connected to the system at a place close to the electrical boundary (PCC1). Therefore, no communication is required, and the synchronization process can be performed locally. Fig. 6.11 shows the voltage across the interface circuit breaker during the synchronization process for the two control scenarios of Section 6.4; the synchronization process starts at  $t=2.5$ s. The real-power outputs of the units that are responsible for the synchronization are also shown in Fig. 6.11. It is observed that compared to the synchronous DER, the synchronization can be performed in a fairly short time when an EC-DER is employed in the microgrid. This is due to the fast response of the BESS control scheme. The faster response of the BESS control can also be observed in the real-power outputs of the units (see Fig. 6.11(b)).

**Case 5–Pitch Angle Control:** The objective of this section is to evaluate the performance of the microgrid equipped with EC-DERs in the islanded mode of operation, under the severe environmental changes and switching incidents. Let us assume that the

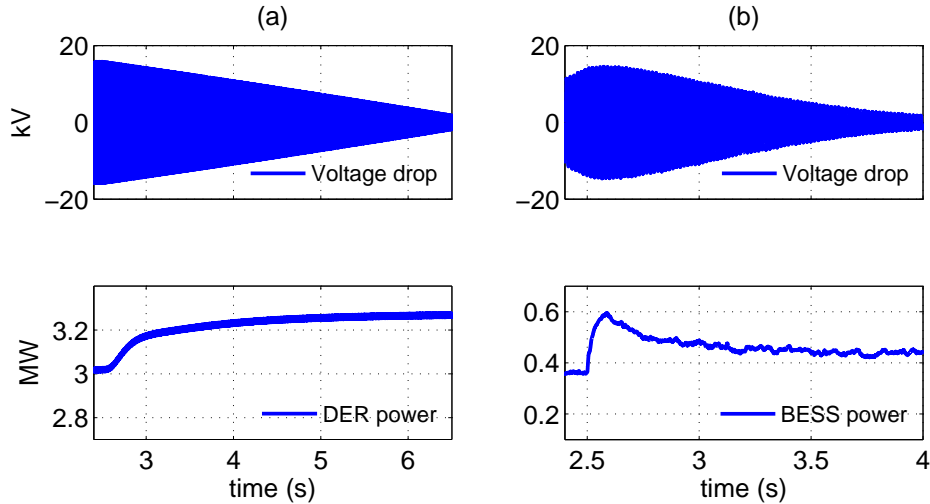


Figure 6.11: Case 4: synchronization process; (a) with synchronous DER and (b) with EC-DER.

study microgrid is initially in a steady state, in the grid-connected mode of operation, while the wind speed is 7.5m/s. At  $t=2.0$ s, the microgrid is isolated from the grid and, thereafter, the network is subjected to the following sequence of events: At  $t=2.5$ s, Lateral L2 is switched off through the intervention of its circuit breaker; at  $t=3.0$ s, the wind speed drops from 7.5m/s to 6.0m/s; at  $t=4.0$ s, Lateral L2 is switched on again; and at  $t=5.0$ s, the wind speed rises to 9.0m/s. Fig. 6.12 illustrates the system response to the aforementioned sequence of events.

As Fig. 6.12(a) indicates, the magnitude of the PCC voltage is within  $\pm 2\%$  of its nominal value despite the disturbances. Fig. 6.12(b) shows that the network frequency increases as the load power reduces and vice versa. Figs. 6.12(c) and (d) respectively show that the powers of the wind farm and BESS change according to the wind speed and load conditions.

Let us now assume that the microgrid gets islanded at  $t=2.0$ s, while the wind speed is 6.5m/s. At  $t=2.5$ s the wind speed rises to 12.5m/s; the maximum permissible value of the BESS power is assumed to be 1.0pu. Fig. 6.13 shows the system response to the disturbances. As Fig. 6.13(c) indicates,  $P_{BESS}$  is about 0.4pu prior to the wind speed change. However, it decreases as the wind farm power output rises. At  $t=2.7$ s,  $P_{BESS}$  exceeds 1.0pu (in absolute value) and, consequently, the control mechanism of Fig. 6.5(b) increases the pitch-angle reference command. Thus, as Fig. 6.13(d) shows, the pitch angle tracks the command, with a maximum rate of  $6^\circ/\text{s}$ , and settles at about



$10^\circ$  in the steady state in order to limit  $P_{BESS}$  to about 1.0pu (Fig. 6.13(c)). Figs. 6.13(a) and (b) show that the network voltage magnitude and frequency are regulated within 3.5% and 2.1% of their corresponding nominal values, respectively.

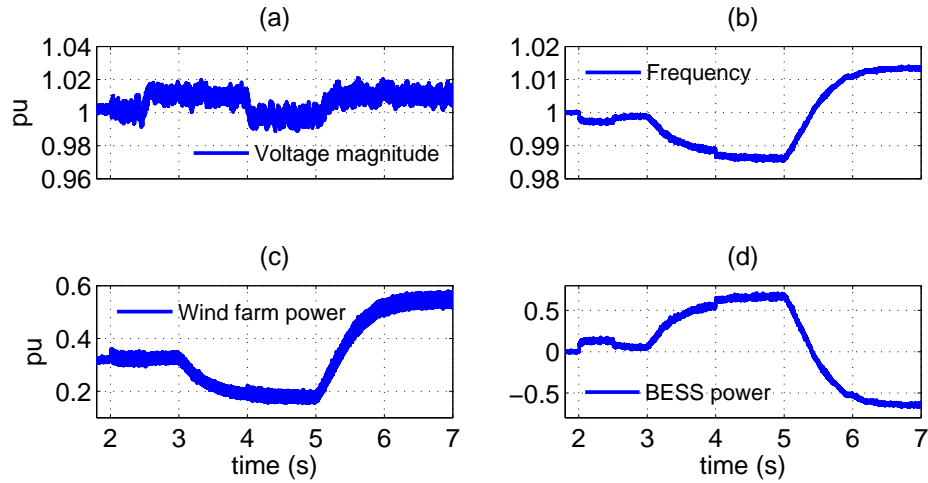


Figure 6.12: Case 5: system response under environmental changes in the islanded mode of operation (Scenario 2 of Section 6.4).

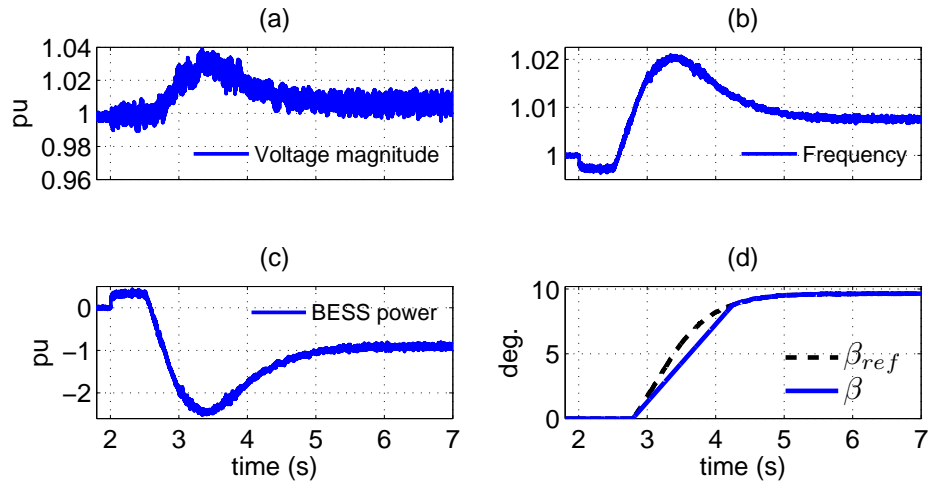


Figure 6.13: Case 5: system response when the pitch-angle control takes action in the islanded mode of operation (Scenario 2 of Section 6.4).

## 6.6.2 Protection Schemes

To demonstrate the effectiveness of the proposed protection schemes, several fault cases have been simulated in both the islanded and grid-connected modes of operation. However, due to space limitations, the results of only a limited number of cases are presented; the results of other cases are very similar and, thus, not reported in this thesis.

**Case 1–Grid-Connected Mode of Operation:** As mentioned in Section 6.5.1, the first step of the protection algorithm is to retrieve the recloser-fuse coordination in the grid-connected mode of operation, if it is lost. Therefore, the coordination algorithm of Fig. 3.1 is employed to coordinate the recloser with the lowest-rating fuse of the feeder in the presence of the DER(s); if the lowest-rating fuse is replaced by a relay, e.g., an MPR, the recloser should be coordinated with the corresponding MPR. Fig. 6.14 shows the characteristic curves of the recloser and the lowest-rating fuse (100-A fuse) of the study microgrid for the case that the synchronous DER is connected to the system. As can be observed in Fig. 6.14, the proposed coordination algorithm is separately exercised for the phase and ground units. It is remembered that recloser-fuse miscoordination is more likely to happen in the presence of the conventional DERs, as EC-DERs have limited fault current ratings. To simulate the worst-case transient condition for the recloser-fuse coordination, the impact of the FCL has not been considered in the calculation of the minimum and maximum fault currents, as discussed in Section 6.5.1–2. This also ensures that the recloser-fuse coordination can be achieved for both scenarios of Section 6.5.1; the calculation of the minimum and maximum fault currents ( $I_{fmin}$  and  $I_{fmax}$ ) is explained in Chapter 3. Fig. 6.14 shows that the recloser-fuse coordination is achieved for the grid-connected mode of operation such that the recloser always operates first for each fault incident.

Once the recloser operates in its fast mode, either of the two protection scenarios of Section 6.5.1 (i.e., the use of a transfer trip mechanism through a communication channel or the use of an FCL) can be adopted. The objective of the two options is to eliminate/limit the contribution of the DER(s) for a permanent fault so that the fuse-fuse coordination is preserved (see Chapter 3). However, the first option requires communications which may not be available or it may be costly; thus, the employment of the FCL is studied in this chapter. The FCL is assumed to be of the superconducting type [128], and its impedance value is determined in such a manner that the fuse-fuse coordination

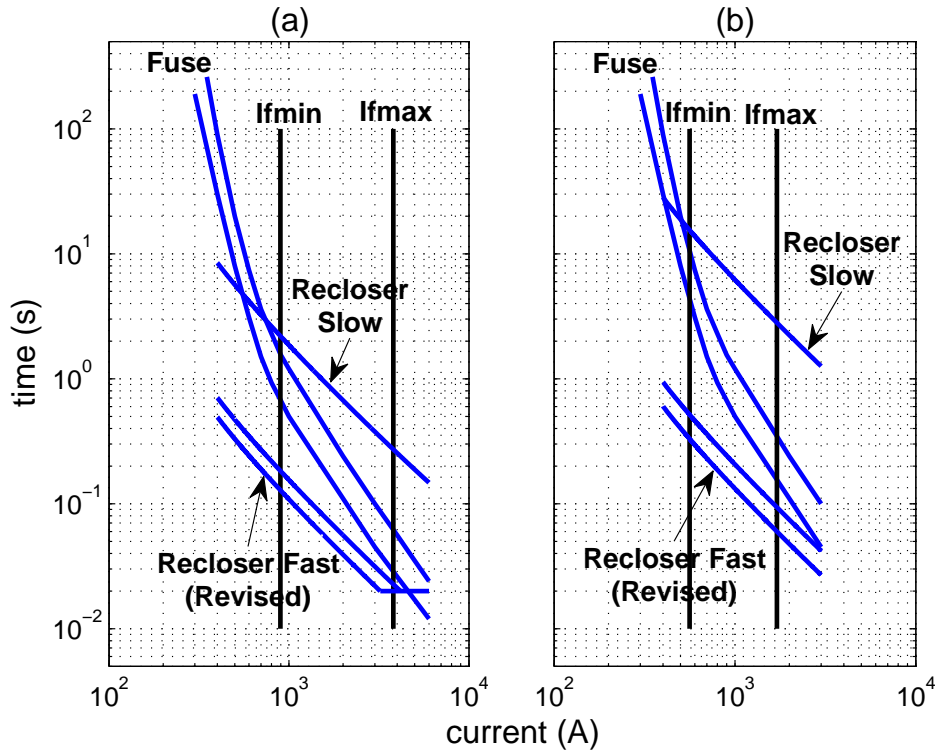


Figure 6.14: Coordination of the recloser and fuse of the study system in the grid-connected mode; (a) phase element and (b) ground element.

of the feeder is not compromised [54]. For the synchronous DER, a resistive FCL whose resistance is 5.8pu ensures fuse-fuse coordination; the resistance value, however, is less than 0.9pu for the wind-power units, due to the limited fault current of the VSCs.

**Case 2–Islanded Mode of Operation:** The next step is to ensure safe operation of the microgrid in the islanded mode of operation. To do so, the protection scenarios of Section 6.5.2–2 (the use of overcurrent relays with different setting groups) and Section 6.5.2–3 (the use of MPRs) are studied in this section. Therefore, some of the existing protective devices must be replaced by microprocessor-based relays. Although it is hypothetically possible to replace any number of protective devices with microprocessor-based relays and coordinate them together (see Section 4.3.5), the number of protective devices that are replaced depends on the system requirements and constraints. In this study, the two fuses at the beginning of Laterals L1 and L2 are replaced by microprocessor-based relays (overcurrent relays or MPRs); in addition, the recloser at the electrical boundary has been replaced by a microprocessor-based relay with reclosing capability (see Section

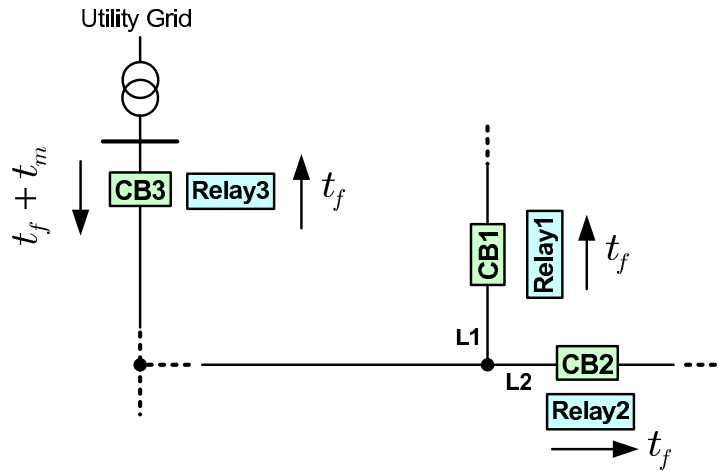


Figure 6.15: Diagram showing the coordination of digital relays within the study system.

6.6.2–1). It is noted that commercially available digital relays include standard over-current, under-/over-voltage and under-/over-frequency protection functions. They also offer communication and programming capabilities. Therefore, it is possible to model the inverse-time characteristic of the fuses/relays that are being replaced by digital relays.

Considering the location of the DER in the study system, there is no need to equip the downstream relays (Relays 1 and 2 in Fig. 6.15) with directional elements as the issue of “false tripping” does not occur for them [3]; however, to distinguish grid faults from the microgrid faults, a directional element should be employed for the interface relay (i.e., the relay located at the electrical boundary). It is worth mentioning that considering the likelihood of a fault within a distribution system and also the probability of operating a feeder in isolation from the grid, no automatic reclosing has been assumed in this chapter for the islanded mode of operation. The concept of protection coordination for the study system is illustrated by Fig. 6.15 in which  $t_f$  and  $t_f + t_m$  respectively denote the forward definite time delays of the microprocessor-based relays, and  $t_m$  is a grading margin (note that Relay 3 has the reclosing capability).

Tables 6.1 and 6.2 report operating times of the primary and backup protections for different fault cases in the grid-connected mode of operation (see Fig. 6.1 for fault locations), while either of the two protection scenarios (i.e., overcurrent relays and MPRs) have been adopted. The studies are also conducted for the cases where either a synchronous DER or an EC-DER is connected to the network. It is borne in mind that, depending on the microgrid operational mode, two different setting groups should be

employed for overcurrent relays, as discussed in Section 6.5.2. Switching from one setting group to the other one can be performed by an anti-islanding mechanism embedded in the digital relays and, thus, no communication link is required. Therefore, once the microgrid gets islanded, the anti-islanding signal is activated and the islanded setting group is enabled. It is also noted that the use of MPRS has the advantage of protecting the network against high-impedance faults.

Several cases have also been simulated for the islanded mode of operation but, due to space limitations, the results of only a selected number of them have been reported in Tables 6.3 and 6.4. Similar to the grid-connected mode of operation, it is observed that the coordination between the protective devices is obtained for any fault within the islanded microgrid, irrespective of the DER type.

## **6.7 Summary and Conclusion**

A realistic distribution network embedding a distributed energy resource was studied in this chapter to identify the conditions and scenarios under which the network can operate as a microgrid. Possible control scenarios that could enable autonomous operation of an existing distribution network were investigated in the chapter, and their advantages and disadvantages were discussed. A suitable control strategy was employed for the EC-DER such that the microgrid can ride through transient incidents, get synchronized with the host utility grid, and slide between two modes of operation. Practical protection strategies were also proposed to protect the study microgrid against different fault scenarios in both operational modes. The best control and protection options are selected based on the requirements and constraints of the local distribution companies. Several study cases were conducted based on digital time-domain simulation of the study system, to demonstrate the effective performance of the proposed control/protection strategies. The thesis is summarized and concluded in the next chapter.

Table 6.1: Operating Times of the Main and Backup Protection for Selected Fault Scenarios in the Grid-Connected Mode of Operation (with OCRs)

Fault Type	Fault Loc.	Overcurrent Relays (OCRs)			
		Main Protection		Backup Protection	
		Prot. Device	Opr. Time(s)	Prot. Device	Opr. Time(s)
<b>Rotating-Machine-Based DER</b>					
AG	<i>Flt1</i>	R	0.060	cb1	0.171
AG	<i>Flt4</i>	R	0.154	F4	0.417
AG	<i>Flt5</i>	R	0.096	OCR2	0.486
BCG	<i>Flt2</i>	R	0.092	F2	0.689
BC	<i>Flt3</i>	R	0.137	OCR1	0.509
ABC	<i>Flt6</i>	R	0.105	F6	0.311
<b>Electronically Coupled DER</b>					
AG	<i>Flt1</i>	R	0.053	cb1	0.174
AG	<i>Flt4</i>	R	0.141	F4	0.417
AG	<i>Flt5</i>	R	0.087	OCR2	0.486
BCG	<i>Flt2</i>	R	0.082	F2	0.690
BC	<i>Flt3</i>	R	0.104	OCR1	0.508
ABC	<i>Flt6</i>	R	0.090	F6	0.311

Table 6.2: Operating Times of the Main and Backup Protection for Selected Fault Scenarios in the Grid-Connected Mode of Operation (with MPRs)

Fault Type	Fault Loc.	Microgrid Protection Relays (MPRs)			
		Main Protection		Backup Protection	
		Prot. Device	Opr. Time(s)	Prot. Device	Opr. Time(s)
<b>Rotating-Machine-Based DER</b>					
AG	<i>Flt1</i>	R	0.060	cb1	0.171
AG	<i>Flt4</i>	R	0.154	F4	0.417
AG	<i>Flt5</i>	R	0.096	MPR2	0.461
BCG	<i>Flt2</i>	R	0.092	F2	0.689
BC	<i>Flt3</i>	R	0.137	MPR1	0.460
ABC	<i>Flt6</i>	R	0.105	F6	0.311
<b>Electronically Coupled DER</b>					
AG	<i>Flt1</i>	R	0.053	cb1	0.174
AG	<i>Flt4</i>	R	0.141	F4	0.417
AG	<i>Flt5</i>	R	0.087	MPR2	0.460
BCG	<i>Flt2</i>	R	0.082	F2	0.690
BC	<i>Flt3</i>	R	0.114	MPR1	0.460
ABC	<i>Flt6</i>	R	0.090	F6	0.311

Table 6.3: Operating Times of the Main and Backup Protection for Selected Fault Scenarios in the Islanded Mode of Operation (with OCRs)

Fault Type	Fault Loc.	Overcurrent Relays (OCRs)			
		Main Protection		Backup Protection	
		Prot. Device	Opr. Time(s)	Prot. Device	Opr. Time(s)
<b>Rotating-Machine-Based DER</b>					
AG	<i>Flt2</i>	DER	$\simeq 1$	N/A	N/A
AG	<i>Flt3</i>	OCR1	0.488	DER	$\simeq 1$
AG	<i>Flt6</i>	OCR2	0.487	DER	$\simeq 1$
BCG	<i>Flt5</i>	OCR2	0.485	DER	$\simeq 1$
BC	<i>Flt1</i>	DER	$\simeq 1$	N/A	N/A
ABC	<i>Flt4</i>	OCR1	0.495	DER	$\simeq 1$
<b>Electronically Coupled DER</b>					
AG	<i>Flt2</i>	DER&BESS	$\simeq 1$	N/A	N/A
AG	<i>Flt3</i>	OCR1	0.499	DER&BESS	$\simeq 1$
AG	<i>Flt6</i>	OCR2	0.511	DER&BESS	$\simeq 1$
BCG	<i>Flt5</i>	OCR2	0.499	DER&BESS	$\simeq 1$
BC	<i>Flt1</i>	DER&BESS	$\simeq 1$	N/A	N/A
ABC	<i>Flt4</i>	OCR1	0.528	DER&BESS	$\simeq 1$

Table 6.4: Operating Times of the Main and Backup Protection for Selected Fault Scenarios in the Islanded Mode of Operation (with MPRs)

Fault Type	Fault Loc.	Microgrid Protection Relays (MPRs)			
		Main Protection		Backup Protection	
		Prot. Device	Opr. Time(s)	Prot. Device	Opr. Time(s)
<b>Rotating-Machine-Based DER</b>					
AG	<i>Flt2</i>	DER	$\simeq 1$	N/A	N/A
AG	<i>Flt3</i>	MPR1	0.461	DER	$\simeq 1$
AG	<i>Flt6</i>	MPR2	0.460	DER	$\simeq 1$
BCG	<i>Flt5</i>	MPR2	0.460	DER	$\simeq 1$
BC	<i>Flt1</i>	DER	$\simeq 1$	N/A	N/A
ABC	<i>Flt4</i>	MPR1	0.460	DER	$\simeq 1$
<b>Electronically Coupled DER</b>					
AG	<i>Flt2</i>	DER&BESS	$\simeq 1$	N/A	N/A
AG	<i>Flt3</i>	MPR1	0.460	DER&BESS	$\simeq 1$
AG	<i>Flt6</i>	MPR2	0.460	DER&BESS	$\simeq 1$
BCG	<i>Flt5</i>	MPR2	0.460	DER&BESS	$\simeq 1$
BC	<i>Flt1</i>	DER&BESS	$\simeq 1$	N/A	N/A
ABC	<i>Flt4</i>	MPR1	0.464	DER&BESS	$\simeq 1$

# Chapter 7

## Summary, Conclusions, and Future Work

### 7.1 Summary

The economical and environmental merits of microgrids have motivated extensive researches and development efforts toward resolving the technical challenges of this new and fast-growing technology. The main objective of this research is to address some concerns related to the control and protection of microgrids. The issues studied in the thesis can generally be classified into two parts: (i) control of EC-DERs under network faults and transient disturbances, and (ii) protection of the microgrid against different fault scenarios in both modes of operation.

In Chapter 1 of this thesis, the research objectives and the contributions of the thesis are presented. Chapter 1 also includes an introduction to the microgrid systems and their advantages and challenges. Chapter 2 mainly focuses on the modeling and control of EC-DERs; in this chapter, a basic control strategy is first adopted and modified for multi-unit microgrids. Then, the chapter outlines the shortcomings of the basic control strategy, modifies it for operation under fault incidents and severe network voltage imbalances, and proposes a phase-angle restoration loop to improve the post-fault recovery of the EC-DER and the host microgrid. A synchronization algorithm is also proposed in Chapter 2 of the thesis.

Coordination of protective devices in radial distribution networks embedding DERs is discussed in Chapter 3. A simple and effective protection strategy is proposed in the chapter that provides coordination amongst protective devices of a typical distribution



system with DERs. Moreover, this chapter presents the steps taken to characterize the impact of future addition of DERs on the protection coordination, for host and neighboring feeders, in a typical distribution network.

Chapter 4 of the thesis investigates the issues associated with protection of microgrids and proposes a protection strategy for low-voltage/residential microgrids. The proposed protection strategy, which does not require communications or adaptive protective devices, can be implemented through programmable microprocessor-based relays; it also addresses protection issues of a microgrid in both modes of operation. In Chapter 5, a communication-assisted protection strategy is proposed for large medium-voltage microgrid, where a fast fault clearance is desired. A backup protection strategy is also offered in this chapter to manage communication network failures. The structure of new relays enabling the proposed protection strategies are also presented in Chapters 4 and 5.

Finally, Chapter 6 of the thesis studies an existing distribution network and presents different control scenarios that enable the network to operate as a microgrid. Practical protection strategies that are effective for the established microgrid (considering the system requirements/constraints) are also discussed in Chapter 6. The main goal of this chapter is to provide the reader with practical scenarios enabling a realistic distribution network to operate as a temporary island.

## 7.2 Conclusion

The conclusions of this thesis are as follows:

- Fast and reliable regulation of the magnitude and frequency of DER terminal voltages is an essential task in the control of microgrids. It was discussed that the terminal voltage of an EC-DER can seriously be affected by system imbalances, network faults, and transient incidents; the effect appears as an undesirable harmonic distortion in the DER terminal voltage. The thesis showed that, under unbalanced load conditions, an enhanced control strategy based on multiple control loops (i.e., an inner current loop and an outer voltage loop) can effectively regulate the terminal voltage magnitude and frequency; it can also mitigate the impacts of load dynamics, inherent intercoupling, and severe network imbalances on the system performance and preserve the quality of power. The thesis further explained that the rapid post-fault recovery of the microgrid can be achieved by augmenting the  $q$ -axis component of the terminal voltage through a supplementary

control loop.

- The thesis discussed that the integration of DERs into distribution networks can compromise the coordination amongst the protective devices of the network. The impacts of DERs on the protection coordination and the corresponding issues were addressed in the thesis. It was demonstrated that an effective coordination algorithm can retrieve the protection coordination in typical/radial distribution networks embedding DERs, if programmable digital reclosers are employed at the beginning of the network feeders. The proposed coordination scheme can address the issues associated with the grid-connected operation of a microgrid.
- It is essential to protect a microgrid in the islanded mode as well as the grid-connected mode of operation, against all types of faults. The major issue in the islanded mode of operation arises due to the limited fault current capability of EC-DERs. The thesis demonstrated that a protection strategy based on commercially available microprocessor-based relays can be devised to protect low-voltage/residential microgrids in both operational modes. The salient feature of the developed protection strategy is that it does not require communications or adaptive protective devices, and is independent of the fault current magnitude and the mode of operation. The structure of a new relay enabling the proposed protection strategy is also presented in the thesis.
- The proposed protection scheme for low-voltage microgrids can also be applied for a large medium-voltage microgrid; however, it may take a relatively long time to isolate a fault within medium-voltage microgrids, as it applies a definite-time grading strategy for protection coordination. Therefore, the thesis proposed a communication-assisted protection strategy for medium-voltage microgrids where faster fault isolation is required. The proposed protection scheme also offers a backup protection in case the communication network fails to operate. The proposed strategy aims to detect and isolate the faults within radial distribution networks that are operated as a microgrid, in a selective (coordinated) manner. It was demonstrated that the effectiveness of the proposed strategy, which benefits from directional elements and microprocessor-based relays, is to a large extent independent of the fault current levels, the mode of operation, as well as the type and size of DERs, subject to the modified relay settings for the grid-connected mode of operation.

## 7.3 Future Works

The following topics are suggested for a future work:

- An investigation into the type, transient regimes, and impedance calculation of fault current limiters (FCLs): One of the methods proposed to retrieve the coordination of overcurrent devices in distribution networks with DERs is the use FCLs (see Chapter 6). However, most of the researches have not formulated or characterized the problem of impedance calculation for FCLs, nor have they studied the transient regimes associated with FCLs; this could be a potential area for future research.
- Real-time simulation of the proposed protection/control methods with the use of Real-Time Digital Simulator (RTDS): The real-time simulation results are more reliable than those obtained by offline simulation; therefore, real-time simulation is preferably performed after offline simulation but before experimental investigation, as a sequential procedure for testing the system performance in such complex plants as electric power systems. The real-time simulation is, thus, the next step toward the realization of the proposed strategies.
- Designing a reliable protection strategy for microgrids with loop structure: As the penetration of DERs increases, distribution networks will experience looped operation to achieve higher reliability. This, in turn, results in looped configurations within the future microgrids. Therefore, it is required to devise appropriate protection schemes that enable safe operation of the looped microgrids in both operational modes.

# Appendix A

## Specifications of the EC-DERs of Chapter 2

### A.1 EC-DER Controllers

The following compensators and filters have been used for the two three-phase EC-DERs of Chapter 2.

$$k_{pi1}=24.0 [\Omega] , \quad k_{ii1}=28.8 [\Omega s^{-1}] ,$$

$$k_{pi2}=20.0 [\Omega] , \quad k_{ii2}=47.8 [\Omega s^{-1}] ,$$

$$K_{v1}(s) = K_{v2}(s) = \left( \frac{s + 553}{s + 1028} \right) \left( \frac{s^2 + 754^2}{s^2 + 1000s + 754^2} \right) [\Omega^{-1}] ,$$

$$K_{\omega 1}(s)=7.0 [V.s] , \quad K_{\omega 2}(s)=5.0 [V.s] ,$$

$$K_{\rho 1}(s)=500 [V/rad] , \quad K_{\rho 2}(s)=600 [V/rad] ,$$

$$H_1(s) = H_2(s) = \left( \frac{25000}{s + 1800} \right) \left( \frac{s + 200}{s} \right) \left( \frac{s^2 + 0.1s + 754^2}{s^2 + 500s + 754^2} \right) [(V.s)^{-1}] ,$$

$$F_1(s) = F_2(s) = \frac{s^2 + 754^2}{s^2 + 1000s + 754^2} ,$$

$$F_{\omega net1}(s) = F_{\omega net2}(s) = 0.002 \left( \frac{s + 1.4}{s} \right) [(rad/s)/V] ,$$

$$F_{vnet1}(s) = F_{vnet2}(s) = \frac{5s + 2.8}{s} .$$

Table A.1: Parameters of the Three-Phase EC-DERs

EC-DER1		EC-DER2	
Parameter	Value	Parameter	Value
$L_s$	2.4 mH	$L_s$	2 mH
$R_s$	2.88 m $\Omega$	$R_s$	4.78 m $\Omega$
$C_s$	250 $\mu$ F	$C_s$	500 $\mu$ F
$f_s$	4860 Hz	$f_s$	4860 Hz
$v_{dc}$	1100 V	$v_{dc}$	1200 V
$S_{rated}$	80 kVA	$S_{rated}$	100 kVA
$v_{rated}$	480 V $_{ll(rms)}$	$v_{rated}$	500 V $_{ll(rms)}$
$D_{P1}$	0.45 V/kVAr	$D_{P2}$	0.33 V/kVAr
$D_{Q1}$	0.1 rad/kW.s	$D_{Q2}$	0.075 rad/kW.s
$P_1^*$	50 kW	$P_2^*$	60 kW
$Q_1^*$	35 kVAr	$Q_2^*$	25 kVAr

## A.2 EC-DER Parameters

Parameters of the two three-phase EC-DERs that have been modeled in Chapter 2 are listed in Table A.1.

# Appendix B

## Modeling of Protective Devices

### B.1 Analytical Equations of Protective Devices

#### B.1.1 Fuse

A Fuse is typically characterized by two characteristic curves: Minimum Melting Time (MMT) curve and Total Clearing Time (TCT) curve. The MMT curve indicates the time period between an overcurrent inception and the instant when the fuse starts to melt, whereas the TCT curve specifies the total time elapsing from the beginning of an overcurrent to the circuit interruption. The fuse characteristic curves can be approximated by an exponential function whose argument is a polynomial of the natural logarithm of the fuse current [27], [82]:

$$t_f = \exp \left[ \sum_{n=0}^k a_n \ln^n(I_f) \right], \quad (\text{B.1})$$

in which  $k$  is the polynomial order,  $I_f$  is the current magnitude, and  $t_f$  is MMT or TCT; the coefficients  $a_n$  are determined through a curve-fitting exercise. In this study, a fifth-order polynomial function of the natural logarithm of the fuse current has been used to approximate the fuse characteristic curve (i.e.,  $k = 5$ ) the coefficients of which are given in Table B.1.

Table B.1: Coefficients of Fuse Characteristic Curves

Fuse and Curve Types	$a_0$	$a_1$	$a_2$	$a_3$	$a_4$	$a_5$
80E, MMT	2976.4	-5341.2	3836.2	-1376	246.4	-17.6
80E, TCT	-77.68	192.64	-156.9	58.6	-10.46	0.73
100E, MMT	-138.13	354.83	-306.54	122.4	-23.38	1.74
100E, TCT	568.41	-859.72	528.3	-164	25.58	-1.6
125E, MMT	-1849.8	3143.8	-2104.6	696.1	-114	7.4
125E, TCT	498.37	-659.1	348.22	-91.14	11.69	-0.58
150E, MMT	-214.59	203.02	-57.515	7.07	-2.69	0.31
150E, TCT	1453.8	-2110.3	1231.1	-359.9	52.61	-3.07

### B.1.2 Recloser and Relay

Relays and reclosers are characterized by inverse-time characteristic curves. Such curves are generally represented by the following equation [92]:

$$t_{op}(I) = TD \left[ \frac{A}{\left( \frac{I}{I_{pick-up}} \right)^p - 1} + B \right], \quad (\text{B.2})$$

where  $t_{op}$  is the device operating time,  $I$  is the device current,  $TD$  is the time dial setting,  $I_{pick-up}$  is the device current set-point, and  $A$ ,  $B$  and  $p$  are constant parameters [84], [92].

### B.1.3 Directional Characteristic

The directional characteristic function has been realized in this thesis through a comparator whose inputs  $S_1$  and  $S_2$  are derived from the feeder voltage and current, as follows [85]:

$$S_1 = |S_1| \angle \alpha_1 = \sigma V, \quad S_2 = |S_2| \angle \alpha_2 = \chi I, \quad (\text{B.3})$$

where  $V$  and  $I$  are phasors of the feeder voltage and current, respectively;  $\sigma$  is a real number, and  $\chi = |\chi| \angle \theta$  is a complex number (of impedance dimension) which, conceptually, emulates the aggregate impedance of the feeder and current transformer and, thus, converts the feeder current into a suitable voltage. The comparator identifies a fault as

a forward fault, i.e.  $D=1$ , if

$$-\frac{\pi}{2} \leq \alpha_1 - \alpha_2 \leq \frac{\pi}{2} \quad (\text{B.4})$$

or

$$-\frac{\pi}{2} + \theta \leq \varphi_l \leq \frac{\pi}{2} + \theta \quad (\text{B.5})$$

where  $\varphi_l = \varphi_v - \varphi_i$  is the phase difference between the voltage and the current of the feeder, and  $\theta$  conceptually emulates the angle of the effective impedance of the feeder, which also includes the impedance of the current transformer. Fig. B.1 illustrates the characteristic of the directional elements used in this study.

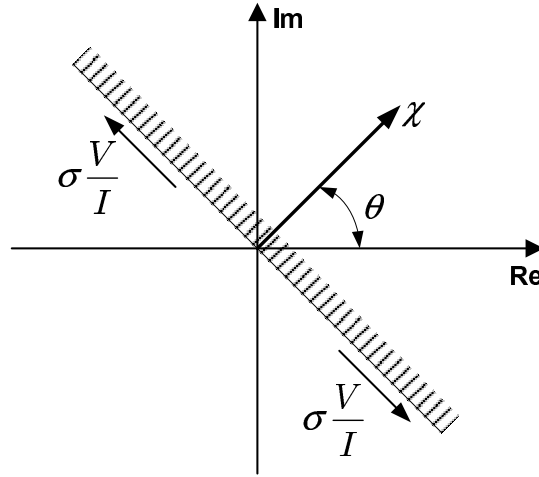


Figure B.1: Characteristic of the directional element (phase comparison).



# Appendix C

## Relay Settings and Device Numbers for Chapter 4

### C.1 Relay Settings

Tables C.1, C.2, C.3, and C.4 report the parameters of the MPRs and the IMPR that are employed in Chapter 4. The time delays of the MPRs and the IMPR (for the islanded and grid-connected modes of operation) are respectively shown in Table C.1 and C.2. Table C.3 reports the settings of the inverse-time overcurrent functions of the microgrid protection relays. Finally, the settings of the three-phase protection modules of the relays are indicated in Table C.4.

### C.2 Device/Function Numbers

Table C.5 shows the standard device/function numbers employed in this study. Each number with its corresponding function name is listed in the table. It is noted that the use of the word “*relay*” in the function names is intended to be generic, and does not necessarily imply a separate freestanding single function device. The numbers are extracted from IEEE Standard for Electrical Power System Device Function Numbers, Acronyms, and Contact Designations [102].

Table C.1: Time Delays for MPRs

Parameter	Value	Remark
TD_IF	50ms	Islanded block delay (forward)
TD_IR	433ms	Islanded block delay (reverse)
TD_GF	5ms	Grid-connected block delay (forward)
TD_GR	200ms	Grid-connected block delay (reverse)
TD_TF	250ms	Three-phase module delay (forward)
TD_TR	633ms	Three-phase module delay (reverse)
TD_IOC	500ms	Instantaneous overcurrent relay delay
TD_HIF	500ms	HIF module delay

Table C.2: Time Delays for the IMPR

Parameter	Value	Remark
TD_IF	433ms	Islanded Block Delay (Forward)
TD_IR	50ms	Islanded Block Delay (Reverse)
TD_GF	16.7ms	Grid-connected Block Delay (Forward)
TD_GR	50ms	Grid-connected Block Delay (Reverse)
TD_TF	566ms	Three-Phase Module Delay (Forward)
TD_TR	250ms	Three-Phase Module Delay (Reverse)
TD_IOC	500ms	Instantaneous Overcurrent Relay Delay
TD_HIF	500ms	HIF Module Delay

Table C.3: Inverse-Time Overcurrent Relay Parameters for MPRs and the IMPR

Parameter	Value	Remark
TD1	0.8	Time Dial Setting of MPR1
TD2	0.8	Time Dial Setting of MPR2
TD3	1.1	Time Dial Setting of MPR3
TD4	0.6	Time Dial Setting of MPR4
TDi	1.5	Time Dial Setting of the IMPR
$I_{pickup}$	5A	Pickup Current (all MPRs and the IMPR)
$A$	28.2	Characteristic Parameter (all MPRs and the IMPR)
$B$	0.1217	Characteristic Parameter (all MPRs and the IMPR)
$p$	2	Characteristic Parameter (all MPRs and the IMPR)

Table C.4: Three-Phase Protection Module Parameters for MPRs and the IMPR

Parameter	Value	Remark
LIR	25%	Load Imbalance Rate
VIR	1.5%	Voltage Imbalance Rate
$I_{p0}$	20A	Trip Level for Zero-Sequence Current
$I_{p2}$	25.5A	Trip Level for Negative-Sequence Current

Table C.5: Device/Function Numbers

Device Number	Device Function
2	Time Delay
21	Distance Relay
25	Synchronizing or Synchronism-Check Relay
27	Undervoltage Relay
32	Directional Power Relay
37	Undercurrent/Underpower Relay
46	Negative Sequence Current Relay
49	Thermal Relay
50	Instantaneous Overcurrent Relay
51	AC Inverse-Time Overcurrent Relay
51N	Inverse-time Ground-Fault Relay
52	AC Circuit Breaker
59	Overvoltage Relay
59N	Neutral Voltage Displacement Relay
60	Voltage/Current Balance Relay
64	Instantaneous Ground Fault Relays
67	AC Directional Element
67N	Directional Ground-Fault Alarm
79	Auto-Recloser
81	Frequency Relay
87	Differential Protective Relay

# Appendix D

## Load and Relay Parameters for Chapter 5

### D.1 Network Loads

Table D.1 reports the load of each bus of the study microgrid simulated in Chapter 5. The blank cells indicate unconnected phases. Other information about the network can be found in reference [24].

### D.2 Relay Signals

Table D.2 shows the definition of the signals and/or parameters that are employed in the proposed microprocessor-based relay of Chapter 5.

Table D.1: Bus Loads for the Distribution Network of Fig. 5.1.

Bus No.	Phase a		Phase b		Phase c	
	P (kW)	Q (kVAr)	P (kW)	Q (kVAr)	P (kW)	Q (kVAr)
3	117	73	121	65	90	98
4	97	33	86	35	91	36
6	46	15	77	23	64	19
7	100	65				
8			85	32		
9					275	123
11			100	36	79	57
13	75	34	75	34	75	34
14	111	53				
15					176	34
16	89	63	89	63	89	63
17			214	90		
18	210	99				

Table D.2: Relay Signals

Signal Name	Description
$D_0$	Zero-sequence directional signal
$D_1$	Positive-sequence directional signal
$D_2$	Negative-sequence directional signal
$D$	Fault direction signal
$F$	Fault ratio
$F_{set}$	Setting for the fault ratio
TD_GF	Forward time delay (grid-connected module)
TD_GR	Reverse time delay (grid-connected module)
TD_IF	Forward time delay (islanded module)
TD_IR	Reverse time delay (islanded module)
FDG	Fault detection by the grid-connected module
FDI	Fault detection by the islanded module
FD	Fault detection signal
Gtrip	Trip signal issued by grid-connected module
Itrip	Trip signal issued by islanded module
Ntrip	Trip signal issued by NVD relay

# Appendix E

## DER Parameters for Chapter 6

### E.1 Parameters of the DFIG and Wind Turbine

The parameters of the wind turbine and the DFIG studied in Chapter 6 have been reported in Tables E.1 and E.2, respectively.

### E.2 Parameters of the Synchronous Machine

Table E.3 reports the parameters of the synchronous DER that is simulated in Section 6.4.1, Chapter 6.

Table E.1: Parameters of the Wind Turbine.

Parameter	Value	Comments
$r$	89.35m	Turbine radius
$A$	25801m <sup>2</sup>	Rotor swept area
$k_{opt}$	0.495	Proportionality constant
$N$	220	Gearbox ratio
$H$	1.25s	Effective inertia constant
$\rho$	1.225kg/m <sup>3</sup>	Air density

Table E.2: Parameters of the DFIG Unit.

Parameter	Value	Comments
$S_n$	6.9MVA	Nominal power
$V_n$	2.3kV <sub>rms</sub>	Nominal voltage (line-to-line)
$f_n$	60Hz	Nominal frequency
$R_s$	0.0092pu	Stator resistance
$R_r$	0.007pu	Rotor resistance
$L_m$	4.13pu	Magnetizing inductance
$L_s$	4.43pu	Stator inductance
$L_r$	4.43pu	Rotor inductance
$\sigma_s$	0.0717	Stator leakage factor
$\sigma_r$	0.0717	Rotor leakage factor

Table E.3: Parameters of the Synchronous DER.

Parameter	Value	Comments
$S_n$	6.9MVA	Nominal power
$V_n$	2.3kV <sub>rms</sub>	Nominal voltage (line-to-line)
$f_n$	60Hz	Nominal frequency
$R_a$	0.006pu	Stator resistance
$X_{ls}$	0.2pu	Stator leakage inductance
$X_d$	2.16pu	$d$ -axis synchronous reactance
$X'_d$	0.47pu	$d$ -axis transient reactance
$X''_d$	0.22pu	$d$ -axis subtransient reactance
$X_q$	2.0pu	$q$ -axis synchronous reactance
$X'_q$	0.85pu	$q$ -axis transient reactance
$X''_q$	0.25pu	$q$ -axis subtransient reactance
$T'_{d0}$	3.5s	$d$ -axis transient open-circuit time constant
$T''_{d0}$	0.02s	$d$ -axis subtransient open-circuit time constant
$T'_{q0}$	0.54s	$q$ -axis transient open-circuit time constant
$T''_{q0}$	0.05s	$q$ -axis subtransient open-circuit time constant
$H$	2.9s	Inertia constant

# Bibliography

- [1] R. H. Lasseter, "Microgrids," in *Proc. IEEE Power Engineering Society Winter Meeting*, vol. 1, pp. 305-308, Jan. 2009.
- [2] N. Hadjsaid, J. F. Canard and F. Dumas, "Disperse generation impact on distribution network," *IEEE Computer Application in Power*, vol. 12, issue 2, pp. 22-28, Apr. 1999.
- [3] A. Girgis and S. M. Brahma, "Effect of distributed generation on protective device coordination in distribution system," in *Proc. Large Engineering Systems Conf. on Power Engineering*, pp. 115-119, Jul. 2001.
- [4] H. Nikkhajoei and R. Lasseter, "Microgrid protection," in *Proc. IEEE Power Engineering Soc. General Meeting*, pp. 1-6, Jun. 2007.
- [5] H. L. Wills and W. G. Scott, *Distributed Power Generation*, Marcell Dekker, New York, 2000.
- [6] N. Hatziargyriou, H. Asano, R. Iravani, and C. Marnay, "Microgrids," *IEEE Power and Energy Mag.*, vol. 5, no. 4, pp. 78-94, Jul./Aug., 2007.
- [7] F. Katiraei, R. Iravani, N. Hatziargyriou, and A. Dimeas, "Microgrids management," *IEEE Power and Energy Mag.*, vol. 6, no. 3, pp. 54-65, May-Jun. 2008.
- [8] Website of the Ministry of Energy (Government of Ontario), <http://www.energy.gov.on.ca/en/>
- [9] H. Nikkhajoei and R. H. Lasseter, "Distributed generation interface to the CERTS microgrid," *IEEE Trans. on Power Delivery*, vol. 24, no. 3, pp. 1598-1608, Jul. 2009.
- [10] F. Katiraei, M. R. Iravani, and P. W. Lehn, "Small-signal dynamic model of a microgrid including conventional and electronically interfaced distributed resources," *IJET Journal on Generation, Transmission & Distribution*, vol. 1, no. 3, pp. 369-378, May. 2007.



- [11] S. Teleke, M. E. Baran, A. Q. Huang, S. Bhattacharya, and L. Anderson, "Control strategies for battery energy storage for wind farm dispatching," *IEEE Trans. on Energy Conversion*, vol. 24, no. 3, pp. 725-732, Sep. 2009.
- [12] F. Katiraei and M. R. Iravani, "Power management strategies for a microgrid with multiple distributed generation units," *IEEE Trans. on Power Systems*, vol. 21, no. 4, pp. 1821-1831, November 2006.
- [13] B. Kroposki, R. Lasseter, T. Ise, S. Morozumi, S. Papathanassiou, and N. Hatziargyriou, "Making Microgrids Work," *IEEE Power and Energy Mag.*, vol. 6, no. 3, pp. 40-53, May-Jun. 2008.
- [14] A. G. Tsikalakis and N. D. Hatziargyriou, "Centralized control for optimizing microgrids operation," *IEEE Trans. on Energy Conversion*, vol. 23, no. 1, pp. 241-248, Mar. 2008.
- [15] A. L. Dimeas and N. D. Hatziargyriou, "Operation of a multiagent system for microgrid control," *IEEE Trans. on Power Systems*, vol. 20, no. 3, pp. 1447-1455, Aug. 2005.
- [16] Y. A. I. Mohamed and E. F. El-Saadany, "Adaptive decentralized droop controller to preserve power sharing stability of paralleled inverters in distributed generation microgrids," *IEEE Trans. on Power Electronics*, vol. 23, no. 6, pp. 2806-2816, 2008.
- [17] J. M. Guerrero, J. Matas, L. G. Vicuna, M. Castilla, and J. Miret, "Decentralized control for parallel operation of distributed generation inverters in microgrids using resistive output impedance," *IEEE Trans. on Industrial Electronics*, vol. 54, no. 2, pp. 994-1004, Apr. 2007.
- [18] M. C. Chandorkar, D. M. Divan and R. Adapa, "Control of parallel connected inverters in standalone ac supply systems," *IEEE Trans. on Industry Applications*, vol. 29, no. 1, pp. 136-143, Jan./Feb. 1993.
- [19] J. A. Peças Lopes and C. L. Moreira, "Defining control strategies for microgrids islanded operation," *IEEE Trans on Power Systems*, vol.21, no.2, pp.916-924, May 2006.
- [20] A. Yazdani and R. Iravani, *Voltage-Sourced Converters in Power Systems: Modeling, Control, and Applications*, Hoboken, NJ: IEEE/Wiley, 2010.

- [21] M. P. Kazmierkowski and L. Malesani, "Current-control techniques for three-phase voltage-source PWM converters: A survey," *IEEE Trans. on Industrial Electronics*, vol. 45, no. 5, pp. 691703, Oct. 1998.
- [22] A. Yazdani, A. R. Di Fazio, H. Ghoddami, M. Russo, M. Kazerani, J. Jatskevich, K. Strunz, S. Leva and J. A. Martinez, "Modeling guidelines and a benchmark for power system simulation studies of three-phase single-stage photovoltaic systems," *IEEE Trans. on Power Delivery*, vol. 26, no. 2, pp. 1247-1264, Apr. 2011.
- [23] P. P. Barker and R. W. de Mello, "Determining the impact of distributed generation on power systems: part I-radial distribution systems", in *Proc. IEEE Power Engineering Soc. Summer Meeting*, pp. 1645-1656, Jul. 2000.
- [24] Cooper Power Systems, *Electrical Distribution-System Protection*, Cooper Industries, 3rd Edition, 1990.
- [25] *IEEE Recommended Practice for Protection and Coordination of Industrial and Commercial Power Systems*, IEEE Std. 242-1986.
- [26] Institute of Electrical Engineers, *Power System Protection*, vol. 1-4, Second Edition, London, UK, 1995.
- [27] S. Chaitusaney and A. Yokoyama, "Impact of protection coordination on sizes of several distributed generation sources," in *Proc. 7th Intl. Power Engineering Conf.*, vol. 2, pp 669-674, Dec. 2005.
- [28] K. Maki, S. Repo, P. Jarventausta, "Methods for assessing the protection impacts of distributed generation in network planning activities," in *Proc. IET 9th Intl. Conf. on Developments in Power System Protection*, pp. 484-489, Mar. 2008.
- [29] M. T. Doyle, "Reviewing the impacts of distributed generation on distribution system protection," in *Proc. IEEE Power Engineering Soc. Summer Meeting*, vol. 1, pp. 103-105, Jul. 2002.
- [30] K. Kauhaniemi, L. Knmpnlained, "Impact of distributed generation on the protection of distribution networks," in *Proc. Intl. Conf. on Developments in Power System Protection*, vol. 1, pp. 315-318, Apr. 2004.

- [31] Y. W. Li, D. M. Vilathgamuwa, and P. C. Loh, "Design, analysis, and realtime testing of a controller for multibus MicroGrid system," *IEEE Trans. on Power Electronics*, vol. 19, no. 5, pp. 1195-1204, Sep. 2004.
- [32] H. Karimi, H. Nikkhajoei and R. Iravani, "Control of an electronically-coupled distributed resource unit subsequent to an islanding event," *IEEE Trans. on Power Delivery*, vol. 23, no. 1, pp. 493-501, Jan. 2008.
- [33] M. B. Delghavi and A. Yazdani, "A Control strategy for islanded operation of a distributed resource (DR) unit," in *Proc. IEEE Power and Energy Soc. General Meeting*, pp. 1-8, Jul. 2009.
- [34] M. B. Delghavi and A. Yazdani, "Islanded-mode control of electronically coupled distributed-resource units under unbalanced and nonlinear load conditions," *IEEE Trans. on Power Delivery*, vol. 26, no. 2, pp. 661-673, Apr. 2011.
- [35] N. Pogaku, M. Prodanović and T. C. Green, "Modeling, analysis and testing of autonomous operation of an inverter-based microgrid," *IEEE Trans. on Power Electronics*, vol. 22, no. 2, pp. 613-625, Mar. 2007.
- [36] J. C. Vasquez, J. M. Guerrero, A. Luna, P. Rodriguez and R. Teodorescu, "Adaptive droop control applied to voltage-source inverters operating in grid-connected and islanded modes," *IEEE Trans. on Industry Applications*, vol. 56, no. 10, pp. 4088-4096, Oct. 2009.
- [37] R. Majumder, B. Chaudhuri, A. Ghosh, R. Majumder, G. Ledwich and F. Zare, "Improvement of stability and load sharing in an autonomous microgrid using supplementary droop control loop," *IEEE Trans. on Power Systems*, vol. 25, no. 2, pp. 796-808, May 2010.
- [38] R. Majumder, G. Ledwich, A. Ghosh, S. Chakrabarti and F. Zare, "Droop control of converter-interfaced microsources in rural distributed generation," *IEEE Trans. on Power Delivery*, vol. 25, no. 4, pp. 2768-2778, Oct. 2010.
- [39] Y. Li, D. M. Vilathgamuwa and P. C. Loh, "Microgrid power quality enhancement using a three-phase four-wire grid-interfacing compensator," *IEEE Trans. on Industry Applications*, vol. 41, no. 6, pp. 1707-1719, Nov./Dec. 2005.

- [40] Y. W. Li, D. M. Vilathgamuwa and P. C. Loh, "A grid-interfacing power quality compensator for three-phase three-wire microgrid applications," *IEEE Trans. on Power Electronics*, vol. 21, no. 4, pp. 1021-1031, Jul. 2006.
- [41] M. Prodanović and T. C. Green, "High-quality power generation through distributed control of a power park microgrid," *IEEE Trans. on Industrial Electronics*, vol. 53, no. 5, pp. 1471-1482, Oct. 2006.
- [42] T. C. Green and M. Prodanović, "Control of inverter-based micro-grids," *Intl. Journal of Electric Power Systems Research*, vol. 77, issue 9, pp. 1204-1213, Jul. 2007.
- [43] M. Prodanović, T. C. Green and H. Mansir, "A survey of control methods for three-phase inverters in parallel connection," in *Proc. IEE intl. Conf. on Power Electronics and Variable Speed Drives*, no. 475, pp. 472-477, Sep. 2000.
- [44] M. S. Khan and R. Iravani, "Supervisory hybrid control of a micro grid system," in *Proc. IEEE Electrical Power Conf.*, pp. 20-24, Oct. 2007.
- [45] S. Mizani and A. Yazdani, "Design and operation of a remote microgrid," in *proc. 35th IEEE Conf. on Industrial Electronic*, pp. 4299-4304, Nov. 2009.
- [46] R. Majumder, A. Ghosh, G. Ledwich, S. Chakrabarti and F. Zare, "Improved power sharing among distributed generators using web based communication," in *Proc. IEEE Power and Energy Soc. General Meeting*, pp. 1-8, Jul. 2010.
- [47] C. A. Plet, M. Graovac, T. C. Green and R. Iravani, "Fault response of grid-connected inverter dominated networks," in *Proc. IEEE Power and Energy Soc. General Meeting*, pp. 1-8, Jul. 2010.
- [48] P. Rodrigues, A. V. Timbus, R. Teodorescu, M. Liserre and F. Blaabjerg, "Flexible active power control of distributed power generation systems during grid faults," *IEEE Trans. on Industrial Electronics*, vol. 54, no. 5, pp. 2853-2592, Oct. 2007.
- [49] A. V. Timbus, R. Teodorescu, M. Liserre, and P. Rodriguez, "PLL Algorithm for Power Generation Systems Robust to Grid voltage Faults," in *Proc. IEEE 37th Power Electronic Specialists Conf.*, pp. 1-7, Jun. 2006.
- [50] A. V. Timbus, P. Rodriguez, R. Teodorescu, M. Liserre and F. Blaabjerg, "Control strategies for distributed power generation systems operating on faulty grid," in *Proc. IEEE International Symp. on Industrial Electronics*, pp. 1601-1607, Jul. 2006.

- [51] F. Katiraei, M. R. Iravani and W. Lehn, "Micro-grid autonomous operation during and subsequent to islanding process," *IEEE Trans. on Power Delivery*, vol. 20, no. 1, pp. 248-257, Jan. 2005.
- [52] S. M. Brahma and A. Girgis, "Microprocessor-based reclosing to coordinate fuse and recloser in a system with high penetration of distributed generation," in *Proc. IEEE Power Engineering Soc. Winter Meeting*, vol. 1, pp. 453-458, Jan. 2002.
- [53] G. Tang and M. R. Iravani, "Application of a fault current limiter to minimize distributed generation impact on coordinated relay protection," in *Proc. Intl. Conf. Power Systems Transients*, pp. 1-6, Jun. 2005.
- [54] W. El-Khattam and T. S. Sidhu, "Restoration of directional overcurrent relay coordination in distributed generation systems utilizing fault current limiter," *IEEE Trans. on Power Delivery*, vol. 23, no. 2, pp. 576-585, Apr. 2008.
- [55] S. M. Brahma and A. A. Girgis, "Development of adaptive protection scheme for distribution systems with high penetration of distributed generation," *IEEE Trans. on Power Delivery*, vol. 19, no. 1, pp. 5663, Jan. 2004.
- [56] H. Wan, K. K. Li, and K. P. Wong, "A multi-agent approach to protection relay coordination with distributed generators in industrial power distribution system," in *Proc. 40th Industrial Application Soc. Annu. Meeting*, pp. 830836, Oct. 2005.
- [57] B. Hadzi-Kostova and Z. Styczynski, "Network protection in distribution systems with dispersed generation," in *Proc. Transmission Distribution Conf.*, pp. 16, May 2006.
- [58] B. Li, Y. Li, Z. Bo, and A. Kilmek, "Design of protection and control scheme for microgrid systems," in *Proc. 44th Intl. University Power Engineering Conf.*, pp. 15, Sep. 2009.
- [59] M. Dewadasa, R. Majumder, A. Ghosh and G. Ledwith, "Control and protection of a microgrid with converter interfaced micro sources," in *Proc. 3rd Intl. Conf. on Power Systems*, pp. 1-6, Dec. 2009.
- [60] E. Sortomme, G. J. Mapes, B. A. Foster and S. S. Venkata, "Fault analysis and protection of a microgrid," in *Proc. 40th North American Power symp.*, pp. 1-6, Sep. 2008.

- [61] H.H. Zeineldin, E. F. El-Saadany and M. M. A. Salama, "Distributed generation micro-grid operation: control and protection," in *Proc. Power System Conf.*, pp. 105-112, Mar. 2006.
- [62] E. Sortomme, S.S. Venkata and J. Mitra, "Microgrid protection using communication-assisted digital relays," *IEEE Trans. on Power Delivery*, vol. 25, no. 4, pp. 2789-2796, Oct. 2010.
- [63] R. M. Tumilty, M. Brucoli and T. C. Green, "Approaches to network protection for inverter dominated electrical distribution systems," in *Proc. 3rd IET Intl. Conf. on Power Electronics, Machines, and Drives*, pp. 622-626, Apr. 2006.
- [64] H. Al-Nasseri, M. Redfern and F. Li, "A voltage based protection for micro-grids containing power electronic converters," in *Proc. IEEE Power Engineering Society General Meeting*, pp. 1-7, Jun. 2006.
- [65] M. A. Redfern and H. Al-Nasseri, "Protection of micro-grids dominated by distributed generation using solid state converters," in *Proc. 9th Intl. IET Conf. on Developments in Power System Protection*, pp. 670-674, Mar. 2008.
- [66] T. Loix, T. Wijnhoven and G. Deconinck, "Protection of microgrids with a high penetration of inverter-coupled energy sources," in *Proc. IEEE PES/CIGRE Symp.*, pp. 1-6, Jun. 2009.
- [67] N. Jayawarna, C. Jones, M. Barnes and N. Jenkins, "Operating microGrid energy storage control during network faults," in *Proc. IEEE Intl. Conf. on System of Systems Engineering*, pp. 1-7, Apr. 2007.
- [68] N. Jayawarna, N. Jenkins, M. Barnes, M. Lorentzou, S. Papathanassiou and N. Hatziargyriou, "Safety analysis of a microgrid," in *Proc. the Intl. Conf. on Future Power Systems*, pp. 1-7, Nov. 2005.
- [69] PSCAD/EMTDC V. 4.2, Manitoba HVDC Research Center, Winnipeg, MB, Canada
- [70] M. H. J. Bollen, *Understanding Power Quality Problems: Voltage Sags and Interruptions*, New York, NY: IEEE Press, 2000.

- [71] G. Yalcinkaya, M. H. J. Bollen and P. Crossley, "Characterization of Voltage Sags in Industrial Distribution Systems", *IEEE Trans. on Industry Applications*, vol. 34, no. 4, pp. 682-688, Jul./Aug. 1998
- [72] L. Zhang and M. H. J. Bollen, "Characteristic of Voltage Dips (Sags) in Power Systems", *IEEE Trans. on Power Delivery*, vol. 15, no. 2, pp. 827-832, Apr. 2000
- [73] H. Song and K. Nam, "Dual current control scheme for PWM converter under unbalanced input voltage conditions," *IEEE Trans. on Industrial Electronics*, vol. 46, no. 5, pp. 953-959, Oct. 1999.
- [74] A. Yazdani and M. R. Iravani, "A unified dynamic model and control for the voltage source converter under unbalance grid condition," *IEEE Trans. on Power Delivery*, vol. 21, no. 3, pp. 1620-1629, Jul. 2006.
- [75] S. K. Chung, "A phase tracking system for three phase utility interface inverters," *IEEE Trans. on Power Electronics*, vol. 15, no. 3, pp. 431-438, May 2000.
- [76] *IEEE Application Guide for IEEE Standard for Interconnecting Distributed Resources with Electric Power Systems*, IEEE Std. 1547.2-2008.
- [77] K. Strunz, R. H. Fletcher, R. Campbell and F. Gao, "Developing benchmark models for low-voltage distribution feeders", in *Proc. IEEE Power and Energy Soc. General Meeting*, pp. 1-3, Jul. 2009.
- [78] S. Papathanassiou, N. Hatziargyriou and K. Strunz, "A benchmark low voltage microgrid network," *CIGRE Symposium*, pp. 1-8, Apr. 2005.
- [79] S. Chiniforoosh, J. Jatskevich, A. Yazdani, V. Sood, V. Dinavahi, J. A. Martinez and A. Ramirez, "Definitions and applications of dynamic average models for analysis of power systems," *IEEE Trans. on Power Delivery*, vol. 25, no. 4, pp. 2655-2669, Oct. 2010.
- [80] *IEEE Recommended Practices and Requirements for Harmonic Control in Electrical Power Systems*, IEEE Std. 519-1992.
- [81] *IEEE Recommended Practice for Industrial and Commercial Power System Analysis*, IEEE Std. 399-1997.

- [82] S. Santoso and T. A. Short, "Identification of fuse and recloser operations in a radial distribution systems," *IEEE Trans. on Power Delivery*, vol. 22, no. 4, pp. 2370-2377, Oct. 2007.
- [83] *IEEE Standard Inverse-Time Characteristic Equations for Over-current Relays*, IEEE Std. C37.112-1996, Sep. 1996.
- [84] *ABB Group Inc.*, ABB PCD Control Protection Curves, online available: <http://www.abb.com>.
- [85] T. S. M. Rao, *Power System Protection: Static Relays with Microprocessor Applications*, 2nd Edition, New Delhi: Tata Mc. Graw-Hill, 1989.
- [86] T. Gonen, *Electric Power Distribution System Engineering*, 2nd Edition, Boca Raton, FL: CRC press, 2008.
- [87] Westinghouse Electric Corporation, *Electric Utility Engineering Reference Book: Distribution Systems*, vol. 3, East Pittsburgh, PA, 1965.
- [88] R. Calvas and B. Lacroix, *System Earthing in LV*, Schneider Electric, Cahier Technique no. 172, 2000.
- [89] E. Lakervi and E. J. Holmes, *Electricity Distribution Network Design*, IEE Power Engineering Series 21, Peter Peregrinus Ltd., 2nd Edition, London, UK, 1995.
- [90] *British Standard Fuses BS 1361-3*, online available: [http://en.wikipedia.org/wiki/BS\\_1362](http://en.wikipedia.org/wiki/BS_1362), & [http://en.wikipedia.org/wiki/Fuse\\_electrical](http://en.wikipedia.org/wiki/Fuse_electrical).
- [91] *Ferraz Shawmut*, LV Fuse Link and Holder Catalogues, online available: <http://us.ferrazshawmut.com>.
- [92] *IEEE Recommended Practice for Monitoring Electric Power Quality*, IEEE Std. 1159-2009.
- [93] R. C. Christie, H. Zadehgol and M. M. Habib, "High impedance fault detection in low voltage networks", *IEEE Trans. on Power Delivery*, vol. 8, no. 4, pp. 1829-1836, Oct. 1993.
- [94] B. M. Aucoin and B. D. Russell, "Distribution high impedance fault detection utilizing high frequency current components", *IEEE Trans. on Power Apparatus and Systems*, vol. 101, no. 6, pp. 1596-1606, Jun. 1982.



- [95] D. I. Jeerings and J. R. Linders, "Unique aspects of distribution system harmonics due to high impedance ground faults", *IEEE Trans. on Power Delivery*, vol. 5, no. 2, pp. 1086-1094, Apr. 1990.
- [96] *General Electric Multilin Inc.*, Instruction Manual for D60 Line Distance Protection System, online available: <http://www.gedigitalenergy.com>.
- [97] J. Roberts and A. Guzman, "Directional element design and evaluation", in *Proc. 21st Annual Western Protective Relay Conf.*, pp. 1-27, 1994.
- [98] Qual-Tech Engineers Inc., Overcurrent Coordination Guidelines for Industrial Power Systems, online available: <http://www.qualtecheng.com/PDF/QT-608-1009.pdf>
- [99] *CEE Relays Ltd.*, Connection and Setting of Neutral Voltage Displacement (NVD) Relays, online available: <http://www.ceerelays.co.uk/RelayFAQs/NVD.htm>.
- [100] A. T. Johns and S. K. Salman, *Digital Protection for Power Systems*, IEE Power Engineering Series 15, Peter Peregrinus Ltd., London, UK, 1995.
- [101] *Schweitzer Engineering Laboratories*, SEL-751A Feeder Protection Relay, online available at: [www.selinc.com/WorkArea/DownloadAsset.aspx?id=2822](http://www.selinc.com/WorkArea/DownloadAsset.aspx?id=2822).
- [102] *IEEE Standard for Electrical Power System Device Function Numbers, Acronyms, and Contact Designations*, IEEE Std. C37.2-2008.
- [103] B. Jianguang, D. Xinzhou, G. Yongji and B. Zhiqian, "Research on non-communication protection of distribution lines based on fault components," in *Proc. Intl. Conf. on Power System Technology*, pp. 1151-1155, Oct. 2002.
- [104] J. D. Glover and M. S. Sarma, *Power System Analysis and Design*, 3rd Edition, Pacific Grove, CA: Brooks/Cole, 2002.
- [105] G. Benmouyal and J. Roberts, "Superimposed quantities: Their true nature and applications in relays," *Schweitzer Engineering Laboratories, Inc.*, pp. 1-18, 1999.
- [106] M. R. Iravani and M. Karimi-Ghartemani, "Online estimation of steady state and instantaneous symmetrical components," *IET Journal on Generation, Transmission & Distribution*, vol. 150, no. 5, pp. 616-622, Sep. 2003.

- [107] Z. Q. Bo, "Adaptive non-communication protection for power lines BO scheme1-The delayed operation approach," *IEEE Trans. on Power Delivery*, vol. 17, no. 1, pp. 85-91, Jan. 2002.
- [108] Z. Gan, X. Z. Dong, Z. Q. Bo, B. R. J. Counce and D. Montjean, "A new protection scheme for high impedance fault using adaptive trip and reclosure technique," in *Proc. Intl. Conf. on Power system Technology*, pp. 295-299, Oct. 2002.
- [109] Y. C. Lee, "Effects of Unbalanced Voltage on the Operation Performance of a Three-phase Induction Motor," *IEEE Trans. on Energy Conversion*, vol. 14, no. 2, pp. 202-208, Jun. 1999.
- [110] LONGO Inc., *Unbalanced voltages and electric motors: causes and consequences*, online available: <http://www.elongo.com/pdfs/voltages.PDF>.
- [111] B. Meyer, "Directional ground and sensitive ground fault settings," *Cooper Power Systems*, Cooper industries, pp. 1-17, Feb. 2004.
- [112] P. P. Parikh, M. G. Kanabar and T. S. Sidhu, "Opportunities and challenges of wireless communication technologies for smart grid applications", in *Proc. IEEE Power and Energy Society General Meeting*, pp. 1-7, Jul. 2010.
- [113] *IEEE Standard for Information Technology, Telecommunications and Information Exchange between Systems, Local and Metropolitan Area Networks*, IEEE Std. 802.11-2007.
- [114] *AFAR Communications Inc.*, Outdoor long range industrial wireless Ethernet Bridge, online available: <http://www.afar.net/wireless/ethernet-bridge/>.
- [115] S. Ekles, *Detecting High-Impedance Faults*, El-Paso Electric Inc., online available: <http://www.pennenergy.com/index/power/display/341599/articles/utility-automation-engineering-td/volume-13/issue-10/features/detecting-high-impedance-faults.html>
- [116] P. Kundur, *Power System Stability and Control*, McGraw Hill, 1994.
- [117] W. F. Horton, S. Goldberg and C. A. Volkmann, "The failure rates of overhead distribution system components," in *Proc. Power Engineering Society Transmission and distribution Conf.*, pp. 713-717, Sep. 1991.

- [118] J. C. Cebrian and N. Kagan, "Hybrid method to assess sensitive process interruption costs due to faults in electric power distribution networks," *IEEE Trans. on Power Delivery*, vol. 25, no. 3, pp. 1686-1696, Jul. 2010.
- [119] F. Roos and S. Lindah, "Distribution system component failure rates and repair times-An overview," in *Proc. Distribution and Asset Management Conf.*, pp. 1-6, Aug. 2004.
- [120] Y. M. Atwa and E. F. El-Saadany, "Reliability evaluation for distribution system with renewable distributed generation during islanded mode of operation," *IEEE Trans. on Power Systems*, vol. 24, no. 2, pp. 572-581, May 2009.
- [121] *Canadian Wind Energy Association*, Online available: <http://www.canwea.ca>.
- [122] *SIEMENS Product Brochure*, online available: [http://www.energy.siemens.com/hq/pool/hq/power-generation/renewables/wind-power/6\\_MW\\_Brochure\\_Jan.2012.pdf](http://www.energy.siemens.com/hq/pool/hq/power-generation/renewables/wind-power/6_MW_Brochure_Jan.2012.pdf).
- [123] *Canadian Wind Energy Atlas*, online available: <http://www.windatlas.ca/en/maps.php>.
- [124] F. A. Bhuiyan and A. Yazdani, "Multimode control of a DFIG-based wind-power unit for remote applications," *IEEE Trans. on Power Delivery*, vol. 24, no. 4, pp. 2079-2089, Oct. 2009.
- [125] J. G. Sloomweg, H. Polinder and W. L. Kling, "Representing wind turbine electrical generating systems in fundamental frequency simulations," *IEEE Trans. on Energy Conversion*, vol. 18, no. 4, pp. 516-524, Dec. 2003.
- [126] S. Chaitusaney and A. Yokoyama, "Prevention of reliability degradation from recloser-fuse miscoordination due to distributed generation," *IEEE Trans. on Power Delivery*, vol. 23, no. 4, pp. 2545-2554, Oct. 2008.
- [127] A. F. Naiem, Y. Hegazy, A. Y. Abdelaziz and M. A. Elsharkawy, "A classification technique for recloser-fuse coordination in distribution systems with distributed generation," *IEEE Trans. on Power Delivery*, vol. 27, no. 1, pp. 176-185, Jan. 2012.
- [128] M. Kim, S. Lim and J. Kim, "Improvement of recloser-fuse operations and coordination in a power distribution system with SFCL," *IEEE Trans. on Applied Superconductivity*, vol. 21, no. 3, pp. 2209-2212, Jun. 2011.

# Curriculum Vitae

**Name:** Mohammad Amin Zamani

**Post-Secondary Education and Degrees:** University of Western Ontario  
London, ON, Canada  
2009 - 2012, Ph.D. in Electrical Engineering

Shahid Chamran University  
Ahvaz, Iran  
2003 - 2005, M.Sc. in Electrical Engineering

Iran University of Science and Technology  
Tehran, Iran  
1999 - 2003, B.Sc. in Electrical Engineering

**Honours and Awards:**

- Queen Elizabeth II Graduate Scholarships in Science and Technology, 2012.
- Western Graduate Research Scholarship, since Jan. 2009.
- First Award for the best presentation in the Western Graduate Symposium, 2012 & 2011 (twice).
- University Teaching Award of Excellence, Azad University of Abadan, 2007.
- University Excellent Researcher Award, Shahid Chamran University, 2005.
- Ranked 1st in the Power Systems Engineering Group, Shahid Chamran University, 2005.
- Excellent Student Award in 3 semesters (out of 8), Iran University of Science and Technology.

**Related Work Experience:**

- Research and Teaching Assistant, University of Western Ontario, 2009-2012.
- Teaching Assistant, University of Waterloo, Summer 2011.
- Faculty Member and Head of the Electrical Engineering Department, Azad University of Abadan, Iran, 2005-2009.
- Consulting Engineer, National Iranian Oil Company, Iran, 2008-2009.
- Adjunct Instructor, Petroleum University of Technology, Iran, 2008-2009.
- Instructor, University of Applied Science and Technology, Iran, 2004-2005.

**Publications:****Peer-Reviewed Journals:**

- M. A. Zamani, A. Yazdani and T. S. Sidhu, "A communication-assisted protection strategy for inverter-based medium-voltage microgrids," *accepted for publication in IEEE Trans. on Smart Grid*, 12 pages, Nov. 2012.
- M. A. Zamani, A. Yazdani and T. S. Sidhu, "A control strategy for enhanced operation of inverter-based microgrids under transient disturbances and network faults," *IEEE Trans. on Power Delivery*, vol. 27, no. 4, pp. 1737-1747, Oct. 2012.
- M. A. Zamani, T. S. Sidhu and A. Yazdani, "A protection strategy and microprocessor-based relay for low-voltage microgrids," *IEEE Trans. on Power Delivery*, vol. 26, no. 3, pp. 1873-1883, Jul. 2011.

**Referred Conferences:**

- M. A. Zamani, A. Yazdani and T. S. Sidhu, "Investigations into the operation of an existing medium-voltage distribution feeder as a microgrid," in *Proc. IET Renewable Power Generation Conf.*, 6 pages, Sep. 2011.
- M. A. Zamani, T. S. Sidhu and A. Yazdani, "A strategy for protection coordination in radial distribution networks with distributed generators," in *Proc. IEEE Power and Energy Society General Meeting*, 8 pages, Jul. 2010.
- M. A. Zamani, M. Joorabian and A. Yazdani, "C-type filter design based on power factor correction for 12-pulse HVDC converters," in *Proc. 34th Annual Conf. of the IEEE Industrial Electronics Society*, pp. 3039-3044, Nov. 2008.
- M. Moghaddasian, M. A. Zamani and R. Kiani, "A direct torque control method for dual three phase induction motors using an adaptive Neuro-Fuzzy controller," in *Proc. 40th North American Power Symp.*, 6 pages, Sep. 2008.
- M. Mohseni, M. A. Zamani and M. Joorabian, "Harmonic components identifications through the Adaline with Fuzzy learning parameters," in *Proc. 33rd Annual Conf. of the IEEE Industrial Electronics Society*, pp. 2515-2520, Nov. 2007.
- M. A. Zamani and M. Mohseni, "Damped-type double tuned filters design for HVDC systems," in *Proc. 9th International Conf. on Electrical Power Quality and Utilization*, 6 pages, Oct. 2007.
- M. Joorabian, S. G. Seifossadat and M. A. Zamani, "An algorithm to design harmonic filters based on power factor correction for HVDC system," in *Proc. IEEE International Conf. on Industrial Technology*, 6 pages, Dec. 2006.